

Cellular trafficking disruption in amyotrophic lateral sclerosis

Submitted by

Vinod Sundaramoorthy

Masters in Biotechnology and Bioinformatics

**A thesis submitted in total fulfilment
of the requirements for the degree of
Doctor of Philosophy**

**Department of Biochemistry
La Trobe Institute of Molecular Science**

**La Trobe University
Bundoora, Victoria 3086**

February, 2015

Abbreviations.....	II
Abstract.....	VIII
Declaration.....	IX
Acknowledgements.....	X
List of publications.....	XII
Table of contents.....	XIII

Abbreviations

ADARB2	adenosine deaminase ribonucleic acid B2
ALS	Amyotrophic lateral sclerosis
AMPA	α -amino-3-hydroxy-5-methyl-4-isoxazolepropionic acid
AMPK	adenosine monophosphate activated protein kinase
ANOVA	analysis of variance
AOA2	ataxia ocular apraxia 2
APS	ammonium persulfate
Arp1	actin related protein 1
ASK1	apoptosis signal-regulating kinase 1
ATF4	activating transcription factor 4
ATF6	activating transcription factor 6
ATP	adenosine triphosphate
BCA	bicinchoninic acid
BIM	BCL2 interacting mediator of cell death
BiP	immunoglobulin binding protein
BMAA	β -N-methylamino-L-alanine
BMC	1,2-bis(mercaptoacetamido)cyclohexane
BSA	bovine serum albumin
Ca ²⁺	calcium ions
cDMEM	complete Dulbecco's modified Eagle's medium
cDNA	complementary DNA
CDK	cyclin dependent kinase
CHMP2B	charged multivesicular body protein 2B

CHOP	CCAAT/enhancer binding protein (C/EBP) homologous protein
CMA	Chaperone-mediated autophagy
CMT	Charcot-Marie-Tooth disease
COP	coat protein complex
CSF	cerebrospinal fluid
<i>C9ORF72</i>	Chromosome 9 open reading frame 72 gene
C9orf72	Chromosome 9 open reading frame 72 protein
DAPI	4',6-diamidino-2-phenylindole
DENN	differentially expressed in normal and neoplastic cells
DMEM	Dulbecco's modified Eagle's medium
DMSO	dimethyl sulphoxide
DNA	deoxyribonucleic acid
dNTPs	deoxynucleoside triphosphates
<i>E. coli</i>	<i>Escherichia coli</i>
EAAT2	excitatory amino acid transporter 2
EDTA	ethylenediaminetetraacetic acid
eIF2 α	eukaryotic translation initiation factor 2 subunit α
ERAD	ER-associated degradation pathway
ES cells	embryonic stem cells
ESCRT	endosomal sorting complex required for transport
FACS	fluorescence-activated cell sorting
F-actin	filamentous actin
FCS	fetal calf serum
FDA	food and drugs administration
FTD	frontotemporal dementia
FTLD	frontotemporal lobar degeneration

FUS	fused in sarcoma
GADD34	growth arrest and DNA damage-inducible 34
GDI	GDP dissociation inhibitor
GDP	Guanosine diphosphate
GEF	Guanine nucleotide exchange factor
GGT	geranylgeranyl transferase
GRP94	glucose regulated protein 94
GTP	Guanosine triphosphate
GWAS	genome-wide association studies
HDAC6	Histone deacetylase 6
HEPES	(4-(2-hydroxyethyl)-1-piperazineethanesulfonic acid)
hnRNP	heterogenous nuclear ribonucleoprotein
HSC-70	heat-shock cognate-70
HSP	hereditary spastic paraplegia
IBMPFD	inclusion body myopathy associated with Paget disease of bone and FTD
IgG	Immunoglobulin G
IPSCs	Induced pluripotent stem cells
IRE1	inositol-requiring kinase 1
JNK	c-Jun N-terminal kinase
Kan	kanamycin
KAP3	kinesin associated protein 3
kDa	Kilodalton/s
KIFAP3	kinesin-associated protein 3
KLF4	Kruppel-like factor 4
LAMP	lysosome associated membrane glycoprotein

LB	Luria-Bertani
LC3	Microtubule-associated protein 1A/1B-light chain 3
MAPK	mitogen-activated protein kinase
MND	motor neuron disease
MNs	motor neurons
mRNA	messenger RNA
MW	molecular weight
NFL	neurofilament light chain
NIH	National institutes of health
NLS	nuclear localization signal
NMDA	N-methyl-D-aspartate
<i>OCT4</i>	octamer-binding transcription factor 4 gene
<i>OPTN</i>	optineurin gene
PAGE	polyacrylamide gel electrophoresis
PBS	phosphate buffered saline
PCR	polymerase chain reaction
PDI	protein disulphide isomerase
PDIA1	PDI family A member 1
p62	Nucleoporin p62
PERK	protein kinase RNA-like endoplasmic reticulum kinase
PFA	paraformaldehyde
PLL	poly-L-lysine
PLS	primary lateral sclerosis
PMA	progressive muscular atrophy
POAG	primary open-angle glaucoma
PON	paraoxonase

PUMA	p53-upregulated modulator of apoptosis
RAN	repeat-associated non-ATG
REP	Rab escort protein
RFP	red fluorescent protein
RNA	ribonucleic acid
ROS	reactive oxygen species
RPL7	ribosomal protein L7
RRMs	RNA recognition motifs
sALS	sporadic ALS
SCF	SKP1-cullin-F-box
SDS	sodium dodecyl sulfate
SEM	standard error of the mean
siRNA	small interfering RNA
SMA	spinal muscular atrophy
SMN	survival motor neuron
SNPs	single-nucleotide polymorphisms
SOD1	superoxide dismutase 1
SP1	specificity protein 1
S1P	site-1 protease
S2P	site-2 protease
SPG	spastic paraplegia
TAE	tris-acetic acid-EDTA
TBK1	TANK-binding kinase 1
TBS	tris buffered saline
TDP-43	transactive response DNA binding protein of 43 kDa
TLS	translocated in sarcoma

TN	Tris-NaCl
TNFR	tumor necrosis factor receptor
TRAF2	TNFR-associated factor 2
TrKB	tropomyosin receptor kinase B
TUBA4A	tubulin, alpha 4a
ULK	autophagy-related 2 (Atg1)-Unc51-like kinase
UPR	unfolded protein response
UPS	ubiquitin proteasome system
UTR	untranslated region
VAPB	vesicle associated membrane protein-associated protein B
VCP	valosin containing protein
VSVG	vesicular stomatitis virus glycoprotein
VTCs	vesicular-tubular aggregates
WB	western blot
WT	wildtype
XBP1	X-Box binding protein-1
YIF1A	Yip1-interacting factor homologue A

Abstract

Amyotrophic lateral sclerosis (ALS) is a fatal neurodegenerative disease, which causes degeneration and death of motor neurons. Currently there is no effective treatment and understanding the cellular and molecular mechanisms of neurodegeneration is essential for designing an effective therapeutic strategy. Several distinct pathological mechanisms are associated with motor neuron death, but the link between these mechanisms remains unclear. ALS begins in a focal region and appears to spread contiguously throughout the motor neurons in the brain, brain stem and spinal cord, and it remains unclear how the spread of pathology is mediated. Another interesting feature of ALS is that motor neurons are specifically targeted by ubiquitously expressed pathogenic proteins. Disruption of intracellular trafficking processes is one mechanism associated with neurodegeneration in ALS, and this may underlie the specific vulnerability of motor neurons, which have large cell bodies and long axons. The overall aim of this thesis was to examine the role of disruption to intracellular trafficking in neurodegeneration in ALS. The thesis firstly presents an already published study, which demonstrates that uptake of extracellular misfolded wildtype or mutant superoxide dismutase 1 (SOD1) disrupts trafficking from the Endoplasmic reticulum (ER) to Golgi apparatus, induces Golgi fragmentation, ER stress and triggers apoptotic cell death in neuronal cells, providing novel insights into pathogenic mechanisms linked to the ER-Golgi compartments and the mechanism of spread of neurodegeneration in ALS. In the second study (currently under peer review), mechanisms of neurodegeneration linked to optineurin were investigated. Optineurin interacts with the molecular motor myosin VI and it was demonstrated here that this interaction is impaired in both sporadic and familial ALS. This leads to inhibition of optineurin-myosin VI mediated cellular trafficking and autophagy, thus describing novel insights into the pathology induced by optineurin in ALS. This thesis also examines a novel protein associated with ALS. Mutations in *CCNF*, which encodes a E3 ubiquitin ligase; cyclin F were recently described in familial ALS and expression of this mutant in neuronal cells induced ER stress, recruitment to stress granules and apoptosis. Finally this thesis examines the normal cellular function of C9orf72 (chromosome 9 open reading frame 72), which is associated with most cases of familial ALS. Depletion of C9orf72 led to impairment of endocytosis and autophagy, implying that the normal function of C9orf72 is related to cellular trafficking. In conclusion this thesis provides further evidence that disruption of cellular trafficking processes trigger neurodegeneration in ALS.

Declaration

Except where reference is made in the text of this thesis, this thesis contains no material published elsewhere or extracted in whole or part from a thesis submitted for the award of any other degree or diploma.

No other person's work has been used without due acknowledgement in the main text of the thesis. Contributions from other persons if any are acknowledged in the preface at the beginning of each chapter.

This thesis has not been submitted for the award of any degree or diploma in any other institution.

Where applicable, research procedures were carried out in accordance with relevant La Trobe University ethics committee (HEC # FHEC10/R4).

Vinod Sundaramoorthy Signed: 

Date: ...27/02/2015.....

Acknowledgements

Thanks goes to numerous people who have helped and encouraged me during my PhD. First of all, I would like to thank my supervisor Julie Atkin for her immense support and guidance all through the years from my Masters to PhD. You have always supported and improved my ideas, which I believe has tremendously helped to develop my talents and I truly appreciate the time you have spent in expanding my knowledge in science. I am greatly privileged to have worked under your supervision. A 'big thank you' to my unofficial co-supervisor Adam Walker. You have always been a great inspiration and have motivated to extend myself further. Thanks for the hands-on mentoring when I first started to work in lab and for your long emails providing valuable suggestions for my experiments and manuscripts.

Thanks to Manal Farg, for all her moral support and guidance. Your technical expertise has immensely helped in perfecting a number of experiments. I will always be grateful for your assistance and scientific suggestions during my PhD. Thanks also to Kai Ying Soo for being a nice person, for company in the lab and for your valuable inputs into my projects.

I could not go without mentioning Peter Cartwright for bringing me into science. Without our first meeting in India, I would have never selected this path. Thanks for guiding me in the right direction. Thanks to Damian Spencer for supervising my Masters year and for your support, constructive criticisms and friendly discussions all through my PhD.

All these intense years as a PhD student wouldn't have been so enjoyable without my dearest friends, who were with me to share all the joyful as well as the stressful moments. Particularly Dave for being more than a friend, and for being a big influence in my life. Mark for sharing great philosophies about life and accompanying during the long nights and weekends of performing experiments in the lab. Sonam and Jess for the great friendship in and out of lab. Mike and Jelena for sharing the fun part of my PhD life. Thanks to the honours students Brooke, Emma and Catalina for being true friends and making the lab such a great place to work.

Thanks to all the patients, their families and the Victorian Brain Bank Network (VBBN), for providing spinal cord tissues samples, which were important for key findings presented in the thesis. I sincerely hope that these findings could contribute to finding the cure for this deadly disease. Thanks to Co-operative Research Centre for Biomarker Translation (CRC-

BT) for the PhD Top-up scholarship and to the MND Association of Victoria for scholarship to attend the 2013 ALS/MND symposia and funding our projects. To our collaborators Dr Ian Blair and Dr Justin Yerbury for providing reagents, constructs and valuable discussions.

Last but the most important, my family. To Mom and Dad, a simple thanks does not suffice for the huge sacrifices in life that you have made to make me the person I am today. I am grateful for your unconditional love and affection. Finally, to my love, krithika, words cannot express how much your love and support has enabled me to cross the hurdles in the final year of my PhD. I am very much delighted to have you as my wife and I am looking forward to face any exciting new challenges that the future holds for us.

Dedicated to my Mom, Bagyalakshimi Sundaramoorthy.

List of publications

The following publication is presented as chapter 3 of this thesis:

Vinod Sundaramoorthy, Adam K. Walker, Justin Yerbury, Kai Y. Soo, Manal A. Farg, Vy Hoang, Rafaa Zeineddine, Damian Spencer, and Julie D. Atkin. "Extracellular wildtype and mutant SOD1 induces ER–Golgi pathology characteristic of amyotrophic lateral sclerosis in neuronal cells." *Cellular and Molecular Life Sciences* 70, 21 (2013): 4181-4195.

The following publication is presented as chapter 4 of this thesis:

Vinod Sundaramoorthy, Adam K. Walker, Vanessa Tan, Jennifer A. Fifita, Emily P. McCann, Kelly L. Williams, Ian P. Blair, Gilles J. Guillemin, Manal A. Farg, and Julie D. Atkin. "Defects in optineurin and myosin VI mediated cellular trafficking in amyotrophic lateral sclerosis." *Human molecular genetics* 24, 13 (2015): 3830-46.

The data presented in chapter 6 contributed to the following publication:

Farg A. Manal, **Vinod Sundaramoorthy**, Jessica M. Sultana, Shu Yang, Rachel AK Atkinson, Vita Levina, Mark A. Halloran, Paul A. Gleeson, Ian P. Blair, Kai Y. Soo, Anna E. King and Julie D. Atkin. "C9ORF72, implicated in amyotrophic lateral sclerosis and frontotemporal dementia, regulates endosomal trafficking." *Human Molecular Genetics* 23, 13 (2014): 3579-3595.

The author has also contributed to the following publications the data of which are not covered by this thesis.

Adam K. Walker, Kai Y. Soo, **Vinod Sundaramoorthy**, Sonam Parakh, Yi Ma, Manal A. Farg, Robyn H. Wallace, Peter J. Crouch, Bradley J. Turner, Malcolm K. Horne and Julie D. Atkin. "ALS-associated TDP-43 induces endoplasmic reticulum stress, which drives cytoplasmic TDP-43 accumulation and stress granule formation." *PloS one* 8, no. 11 (2013): e81170.

Farg A. Manal, Kai Y. Soo, Sadaf T. Warraich, **Vinod Sundaramoorthy**, Ian P. Blair and Julie D. Atkin. "Ataxin-2 interacts with FUS and intermediate-length polyglutamine expansions enhance FUS-related pathology in amyotrophic lateral sclerosis." *Human molecular genetics* 22, no. 4 (2013): 717-728.

Table of contents

1. Chapter 1: General Introduction.....	1
1.1 Epidemiology of ALS.	2
1.2 Clinical features of ALS	3
1.3 Proposed environmental and lifestyle risk factors for ALS.	5
1.4 Genetic causes of ALS.....	6
1.4.1 <i>SOD1</i> mutations in ALS.....	9
1.4.2 <i>C9ORF72</i> hexanucleotide repeat expansion in ALS.....	10
1.4.3 <i>TARDBP</i> and <i>FUS</i> mutations in ALS	12
1.4.4 Current experimental models to study ALS pathogenesis.....	13
1.5 Pathogenic mechanisms associated with ALS.....	14
1.6 Protein misfolding and aggregation.	15
1.7 Autophagy defects in ALS	16
1.8 Glutamate excitotoxicity.....	18
1.9 Mitochondrial dysfunction	19
1.10 ER stress and unfolded protein response (UPR)	20
1.10.1 ER stress is an important pathogenic mechanism in ALS.....	22
1.11 Golgi fragmentation	25
1.12 Disrupted RNA homeostasis.....	26
1.13 Cellular trafficking disruption in ALS	28
1.13.1 Mutations in genes encoding cytoskeletal and motor proteins are present in ALS.....	28
1.13.2 Rab mediated cellular trafficking.....	30
1.13.3 Optineurin mediated vesicular trafficking.	32
1.13.4 ER-Golgi vesicular trafficking.....	34
1.13.5 Axonal transport	36
1.13.6 Cellular trafficking disruption in sporadic ALS.....	38
1.14 Cell to cell transmission of pathology in ALS	39
1.15 Aims of thesis.	40
2. Chapter 2: Materials and methods.....	42
2.1 Molecular biology	43

2.1.1	Luria-Bertani (LB) medium	43
2.1.2	Transformation of competent cells.....	43
2.2	Plasmid isolation	43
2.3	DNA quantification.....	44
2.4	DNA purification by ethanol/sodium acetate precipitation	44
2.5	Mutagenesis	44
2.6	DNA sequencing	45
2.7	Mammalian cell culture	46
2.7.1	Fetal Calf serum (FCS) heat inactivation	46
2.7.2	Cell maintenance.....	46
2.7.3	Transfection	47
2.7.4	Long-term storage of cell lines.....	47
2.7.5	Cell lysate preparation.....	47
2.7.6	Protein quantification	48
2.8	SDS-PAGE and Immunoblotting.....	48
2.8.1	Materials.....	48
2.8.2	SDS-PAGE procedure.....	50
2.8.3	Immunoblotting procedure.....	50
2.9	Immunocytochemistry.....	51
2.9.1	Materials.....	51
2.9.2	Immunocytochemistry procedure.....	51
2.10	Fixed imaging	53
2.10.1	Epifluorescence imaging	53
2.10.2	Confocal imaging.....	53
2.11	Live cell imaging.....	53
2.12	Software and statistical analysis	53
3.	Chapter 3: Extracellular wildtype and mutant SOD1 induces ER-Golgi pathologies characteristic of amyotrophic lateral sclerosis in neuronal cells	54
3.1	Preface.....	55
3.2	Manuscript 1.....	56
4.	Chapter 4: Defects in optineurin and myosin VI mediated cellular trafficking in amyotrophic lateral sclerosis	57
4.1	Preface.....	58
4.2	Manuscript 2.....	59
5.	Chapter 5: Cellular mechanisms induced by novel <i>CCNF</i> mutations in ALS.....	60

5.1	Preface.....	61
5.2	Introduction	62
5.3	Materials and Methods.	65
5.3.1	Plasmids and cloning.....	65
5.3.2	Subcellular fractionation	65
5.3.3	Stress granule analysis	66
5.3.4	Cell death assays.	66
5.4	Results	67
5.4.1	ALS mutant cyclin F is localised more in the cytoplasm than wildtype cyclin F in SH-SY5Y cells.	67
5.4.2	ALS-associated mutation in cyclin F accelerates its association with stress granules.	67
5.4.3	ALS mutant cyclin F induces ER stress	68
5.4.4	ALS mutant cyclin F induces apoptotic cell death.	68
5.5	Discussion	75
6.	Chapter 6: C9orf72 regulates endosomal trafficking	78
6.1	Preface.....	79
6.2	Introduction	80
6.3	Materials and Methods	82
6.3.1	C9orf72 Knockdown	82
6.3.2	Endocytosis trafficking assays.....	82
6.3.3	Live cell imaging.....	83
6.4	Results	83
6.4.1	C9orf72 is expressed in the nucleus and as cytoplasmic vesicles	83
6.4.2	C9orf72 regulates trafficking of Shiga toxin from the plasma membrane to Golgi apparatus	83
6.4.3	C9orf72 regulates endocytosis of TrkB receptor	84
6.4.4	C9orf72 associates with autophagosomes and lysosomes in neuronal cell lines.....	84
6.5	Discussion	90
7.	General discussion	93
7.1	Summary of main findings from the thesis	94
7.1.1	Extracellular misfolded wildtype and mutant SOD1 inhibits ER-Golgi trafficking and exhibits similar potential to spread ALS pathology.	94
7.1.2	Defects in optineurin/myosin VI mediated cellular trafficking links key pathogenic features in ALS.....	95

7.1.3	Novel mutation in <i>CCNF</i> induces ER stress and other features typical of ALS.....	95
7.1.4	Role of C9orf72 in endosomal trafficking	97
7.2	Prion-like propagation in ALS	97
7.3	Cellular trafficking disruption links key pathogenic mechanisms in ALS.....	103
7.3.1	Inhibition of ER-Golgi associated vesicular trafficking associates with ER stress and Golgi fragmentation in ALS.....	103
7.3.2	Disruption of cellular trafficking impairs autophagy in ALS.....	106
7.3.3	Cellular trafficking disruption relates to other pathogenic mechanism in ALS.....	107
7.4	Concluding remarks.....	109
8.	References.....	111
9.	Appendix	112

Chapter 1

1.General Introduction

1. General introduction

Amyotrophic lateral sclerosis (ALS), also known as motor neuron disease (MND), is a rapidly progressive, invariably fatal neurodegenerative disease affecting motor neurons. Motor neurons are located in the cortex, brain stem, and spinal cord and they control all the voluntary muscles of the body. In ALS degeneration of motor neurons gradually leads to muscle atrophy, fasciculation and complete paralysis and typically death results within 3-5 years after diagnosis [1]. Currently there is no effective treatment for ALS. Riluzole is the only pharmaceutical agent approved by US Food and Drugs Administration (FDA), widely used for treatment of ALS, but it delays disease progression only by few months. Hence there is an urgent need for more effective therapeutics. Whilst 90% of ALS cases are sporadic, without any known genetic mutations, 10% of cases are familial, caused by mutations in a multitude of genes which encode proteins with many different functions [2]. Interestingly, wildtype versions some of these proteins are also misfolded and aggregated in sporadic ALS tissues, suggesting that these wildtype proteins could play a role in the pathogenesis of ALS [3-6]. Another interesting feature of ALS is that these proteins are expressed ubiquitously, yet motor neurons are specifically targeted. Recent evidence has implicated defects in intracellular trafficking in ALS [7] and motor neurons, with their large cell body and long axons, could be particularly susceptible to intracellular trafficking defects. This thesis examines the cellular pathogenic mechanisms associated with SOD1, optineurin, C9orf72 and a novel protein linked to ALS, cyclin F, focusing on intracellular trafficking defects and how they are associated with other pathogenic mechanisms in ALS in each case.

1.1 Epidemiology of ALS.

The rate of occurrence of ALS varies worldwide, with a predicted incidence rate of approximately 0.4 to 4 people per 100,000 general population [8]. However as most epidemiological studies on ALS have involved only on the European and American population [9-12], studies from large parts of the world including India, Russia, Africa and South America, should be included in order to establish the exact rate of ALS incidence worldwide [13]. The overall lifetime risk of developing the condition is 1:350 for men and 1:400 for women [13-15], with a higher frequency of spinal-onset forms of ALS observed in men [14]. There is also evidence that a racial pre-disposition to ALS exists, as there is increased prevalence among the white population compared to the non-white population in

both Europe [16] and America [17]. The lifetime risk of developing ALS peaks at the age of 50-75 years. However recent studies suggest that the risk plateaus or even declines after 75 years, in contrast to other neurodegenerative disorders such as Alzheimer's Disease and Parkinson's Disease, where the risk constantly increases with age [1, 11-13].

1.2 Clinical features of ALS

The clinical manifestations of ALS vary depending on the site of onset and the degree of upper motor neuron and lower motor neuron involvement. The typical survival period for a patient with ALS is 3-5 years after the onset of the first symptoms [1], although the prognosis varies and heterogeneous clinical features exist in ALS [18]. Diseases affecting motor neurons can be classified into four clinical subtypes, based on the site of onset and the symptoms presented upon diagnosis (Table 1.1). In most cases, patients diagnosed with one of these clinical subtypes, eventually develop classical ALS, which involves the progressive degeneration of both the upper and lower motor neurons. The heterogeneity of the motor phenotype in ALS is attributed to the multi-focal onset of motor neuron degeneration, followed by the contiguous spread throughout other motor neurons in the brain, brain stem and spinal cord [18].

Disease	Clinical features	Median survival time
Classical ALS	Both upper and lower motor neurons are affected, characterized by limb muscle weakness and wasting during onset. Dysphagia and dysarthria also occurs at later stages. Most common form of ALS, also referred as MND.	3-5 years
Primary lateral Sclerosis	Pure upper motor neuron syndrome resulting in muscle spasticity and hyperreflexia. Patients eventually develop classical ALS with 3 – 4 years	Prognosis can exceed 10 years if the patients do not develop classical ALS
Progressive muscular atrophy	Pure lower motor neuron syndrome, manifested as generalized muscle wasting and weakness, absent reflexes and muscle twitching.	Typically 5 years, however a subset of patients also live for more than 10 years.
Progressive bulbar palsy	Affects the lower motor neurons in the bulbar region; glossopharyngeal nerve (IX), vagus nerve (X), and hypoglossal nerve (XII). Results in dysphagia and dysarthria.	2- 3 years. Often progresses to classical ALS.

Table 1.1 Clinical features of ALS, adapted from [1, 13, 19, 20]

Currently, there is no sensitive biomarker or single clinical investigation specifically to diagnose ALS. Diagnosis is based on clinical examination of patients presenting with the symptoms outlined in Table 1, along with electrophysiological examination, after ruling out other possible neurological dysfunction [20]. The El Escorial diagnostic criteria for ALS were proposed by the World Federation of Neurology in 1994, to standardize ALS diagnosis for research and clinical trial purposes [21]. To reduce the delay in diagnosis and false-positive rates, these guidelines have undergone a number of modifications [20] and the most recent guidelines are referred as the Awaji–Shima criteria [22, 23], which have improved diagnostic sensitivity [24].

Cognitive impairment and behavioural changes reminiscent of frontotemporal dysfunction have also been frequently reported in patients with ALS [25-27]. It is also estimated that up

to 20% of patients with ALS develop Frontotemporal dementia (FTD) [28]. FTD represents a vast clinical subgroup within the broad spectrum of neurological disorders that constitute Frontotemporal lobar degeneration (FTLD), the second most common form dementia in patients less than 65 years of age [29]. FTD pathology includes atrophy and neuronal loss in the frontal and temporal lobes of the brain [29]. Most common clinical symptoms of FTD primarily manifests as personality and behavioral changes with speech and language disabilities. In addition, patients may develop motor abnormalities resembling ALS [30, 31]. As clinical observations support a link between FTD and ALS, recent identification of common genetic causes for familial forms of ALS and FTD, including mutations in *FUS* (Fused in sarcoma), *TARDBP* (TAR-DNA binding protein 43 encoding gene) and hexanucleotide expansions in *C9ORF72* definitively linked these two neurological disorders [32-34]. These evidence further imply that ALS and FTD may share common neurodegenerative mechanisms and may be a part of a common spectrum of diseases.

1.3 Proposed environmental and lifestyle risk factors for ALS.

Many environmental and lifestyle aspects are hypothesized to be risk factors for ALS. This includes exercise, smoking, exposure to heavy metals, pesticides and viral infection [8, 13]. Smoking is considered as risk factor for ALS [35, 36], and is also observed to be an increased risk for women than men [37, 38], although was negatively correlated in another study [13]. Exercise is another lifestyle feature which is hypothesized to be a risk factor for ALS. ALS patients are found to be significantly leaner than healthier individuals and have displayed a higher level of athleticism before diagnosis [39, 40]. A study performed in 2013 [41], showed significantly increased level of leisure time physical activity among 636 sporadic ALS patients compared to 2,166 control population. Similarly a previous study has identified a 6.5 fold increased risk of developing ALS in Italian soccer players [42], linking ALS to certain form of high physical activity. While the possibility of exercise as a risk factor for ALS remains plausible, more stringent studies and specific mechanism for how high motor activity could trigger ALS needs to be established.

One well-studied environmental risk factor for ALS is a non-protein amino acid, β -N-methylamino-L-alanine (BMAA). BMAA was first isolated from the cycad plant, *Cycas micronesica* [43], which is produced by symbiotic cyanobacteria living in its roots. BMAA was proposed as a risk factor for ALS after an unusually high (50-100x) frequency of ALS

was reported in the native Chamorro people on the island of Guam [44], who have a high dietary intake of BMAA from the cycad seeds in their traditional diet. It is postulated that BMAA becomes biomagnified in flying foxes and pigs native to Guam, who feed on these cycad seeds [45, 46]. BMAA was elevated in the brains of ALS patients from Guam, supporting this hypothesis [47, 48], although other studies provided conflicting results [49, 50]. Recently BMAA was also found to be synthesized by cyanobacteria living on blue green algae commonly found in lakes throughout the world [51]. BMAA was further found to be misincorporated into human proteins, which may trigger protein aggregation [52], a hallmark feature of ALS.

Hence, in spite of a large number of studies, there is no single proven risk factor for ALS. The environmental and lifestyle risk factors combined with the genetic susceptibility are more likely to play a role in the occurrence of ALS.

1.4 Genetic causes of ALS.

Approximately 90% of ALS cases are sporadic, as they occur randomly throughout the population, with no previous family history. However approximately 10% of ALS cases are familial, caused by inherited genetic mutations [2]. Mutations in *SOD1* were the first to be identified as a cause of familial ALS, in a study based on a linkage analysis in autosomal dominant familial ALS pedigrees [53]. Currently *SOD1* mutations are estimated to account for approximately 12% of familial ALS and 1-2% of sporadic ALS cases [2]. TDP-43, a RNA/DNA binding protein, was found to be a major component of the ubiquitinated protein inclusions in ALS and FTD patients [5], which directly led to the discovery of mutations in the *TARDBP* gene in autosomal dominant ALS as well as FTD families [33]. Mutations in *TARDBP* are now estimated to account for approximately 4% of familial ALS cases [2]. Subsequently, mutations in another gene encoding an RNA-binding protein, *FUS* were also identified in familial ALS [34, 54]. A breakthrough in ALS genetics was the identification of hexanucleotide GGGGCC repeat expansions in *C9ORF72* as the cause of most familial cases of both ALS (40%) and FTD (7%) [55, 56]. This discovery has opened new avenues of research aimed at investigating how mutations in the intronic region of this gene cause neurodegeneration. Similarly, the normal cellular function of the *C9orf72* protein also remains unknown, thus raising new research questions. Several genes encoding proteins associated with cellular trafficking, have also been linked to ALS, as discussed later in this

thesis. These include optineurin, profilin, valosin containing protein (VCP), TUBA4A and p62. Recent advances in exome sequencing and genome-wide association studies (GWAS) have greatly increased our knowledge of the genetic etiology of ALS, and many genetic mutations linked with ALS were identified in recent years (Table 1.2) [2, 57]. Interestingly as well as FTD, these findings have implicated an overlap between ALS and other neurological disorders including muscular atrophy and ataxia (Table 1.2). Currently, the genetic etiology of two third of familial ALS and 11% of sporadic ALS has been identified [2]. Intriguingly as both sporadic and familial forms of ALS exhibit similar pathogenesis and appear clinically identical, understanding disease mechanisms associated with the familial mutations may unravel mechanisms of neurodegeneration in both forms of ALS.

Gene	Chromosome location	Protein encoded	Disease feature	Percentage of ALS		Reference
				fALS	sALS	
C9ORF72	9p21	C9ORF72	ALS, FTD, ALS with FTD	40	7	[32, 56]
SOD1	21q22	SOD1	ALS	12	1-2	[53]
TARDBP	1p36	TDP-43	ALS, FTD, ALS with FTD	4	1	[33]
FUS	16p11	FUS	ALS, FTD, ALS with FTD	4	1	[34, 54]
VCP	9p13	VCP	ALS, IBMPFD	1	1	[58, 59]
OPTN	10p13	optineurin	ALS, POAG	<1	<1	[60]
UBQLN2	Xp11	Ubiquilin2	X-linked ALS	<1	<1	[61]
PFN1	17p13	Profilin1	ALS	<1	<1	[62]
SQSTM1	5q35	P62	ALS, Paget's disease of bone	<1	<1	[63, 64]

Other rare gene mutations in ALS (<1% of both familial and sporadic ALS)

Gene	Chromosome location	Protein encoded	Disease feature	Reference
DCTN1	2p13	Dynactin	ALS, Perry syndrome, PMA	[65-67]
ALS2	2q33-2q35	Alsin	ALS, Juvenile PLS, infantile HSP	[68-70]
CHMP2B	3p11	(Charged multivesicular protein 2B) CHMP2B	ALS, FTD	[71]
VAPB	20q13	VAPB	ALS, SMA	[72, 73]
ALS9	14q11.2	Angiogenin	ALS with FTD and Parkinson disease	[74, 75]
SPG 11	15q15-21	Spatacsin	Juvenile ALS	[76, 77]
NEFH	22q12	Neurofilament heavy chain (NF-H)	ALS	[78]
ATXN2	12q24	Ataxin 2	sALS, ataxia	[79, 80]
FIG4	6q21	Phosphoinositide 5-phosphatase	ALS, CMT	[81, 82]
TUBA4A		Tubulin alpha 4A protein	ALS, FTD	[83]
PRPH	12q12	Peripherin	ALS, RP, macular dystrophy	[84-88]
ELP3	8p21	Elongator protein 3	sALS	[89]
SETX	9q34	Senataxin	Juvenile sALS and AOA2	[90]
SIGMAR1	9p13.3	Sigma-1 receptor	Juvenile ALS and FTD	[91]
HNRNPA2B1	7p15	hnRNPA2B1	Multisystem proteinopathy and ALS	[92]
HNRNPA1	12q13	hnRNPA1	Multisystem proteinopathy and ALS	[92]
PON1/2/3	7q21.3	Paraoxonase (PON) 1, 2 and 3	ALS	[93]
GRN	17q21.32	Progranulin	ALS, ALS-FTD and FTD	[94-96]

Gene	Chromosome location	Protein encoded	Disease feature	Reference
DAO	12q22-23	D-amino acid oxidase (DAO)	ALS	[97]
CHCHD10	22q11.23	coiled-coil helix coiled-coil helix protein	ALS-FTD	[98]
MATR3	5q31.2	Matrin 3	ALS	[99]
TAF15	17q12	TATA-binding protein-associated factor 2N	ALS	[100, 101]
SS18L1/CREST	20q13.33	Synovial sarcoma translocation gene on chromosome 18-like 1 (SS18L1)	sALS	[102]
TBK1	12q14.2	TANK-Binding Kinase 1 (TBK1)	ALS	[103]

Table 1.2: Genetic causes of ALS. Abbreviations: sALS, sporadic ALS; fALS, familial ALS; IBMPFD, inclusion body myopathy with Pagets disease and fronto temporal dementia; POAG, Primary open-angle glaucoma; PMA, progressive muscular atrophy; PLS, primary lateral sclerosis; HSP, hereditary spastic paraplegia; CHMP2B, charged multivesicular body protein 2B; SMA, spinal muscular atrophy; CMT, Charcot-Marie-Tooth disease; AOA2, ataxia with oculomotor apraxia type 2; RP, retinitis pigmentosa

Mutations in four genes (*C9ORF72*, *SOD1*, *TARDBP*, and *FUS/TLS*) are estimated to account for over 50% of all familial ALS cases and hence are the most common ALS-linked genetic mutations. The section below provides brief description of each of these ALS-linked gene mutations.

1.4.1 *SOD1* mutations in ALS

SOD1 is the first gene identified to be mutated in ALS and accounts for about 20% of familial ALS cases [53]. *SOD1* is an abundant, ubiquitous antioxidant enzyme that exists as a stable 32 kDa homodimer comprising two 153 amino acid residue subunits [104, 105]. *SOD1* is an antioxidant metalloenzyme which controls the steady state concentration of superoxide ions [105]. *SOD1* catalyses the degradation of superoxide radicals via reduction and oxidation of its active site copper ion [105]. Over 140 different mutations have so far been identified throughout the structure of *SOD1* [106]. When mutations were first identified

in SOD1, initial predictions suggested a loss of function mechanism [53]. However the identification of wide distribution of mutations over the entire primary sequence and tertiary structure of the protein, and the finding that transgenic SOD1 knockout animals do not develop ALS, indicated that loss of SOD1 function is not the cause of mutant SOD1-linked ALS [107, 108]. This was further supported by the lack of correlation between disease progression and the level of dismutase activity of SOD1 mutants. Functionally inactive SOD1 H46R mutant associated with a slowly progressive disease whereas the catalytically active SOD1 G93A mutation, resulted in a classic rapidly progressing disease in patients [109, 110]. Hence a gain of toxic property by mutant SOD1 is likely to be involved in the pathogenesis of ALS. Mutant SOD1 has an increased propensity to misfold and aggregate, forming high molecular weight oligomeric and aberrantly disulphide-bonded SOD1 species, which are biochemically detectable in cell culture and transgenic mice models [111, 112]. Large protein inclusions containing SOD1 are also detected in the motor neurons of human ALS patient carrying SOD1 mutations [113]. Interestingly sporadic and SOD1-linked familial ALS cases are clinically indistinguishable and share similar pathogenic features. In recent years, misfolded wildtype SOD1 is implicated as a toxic species in sporadic ALS. Wildtype non-mutated SOD1 also has an intrinsic property to misfold and aggregate, which can be triggered in pathogenic conditions [4]. Misfolded wildtype SOD1 have been identified in sporadic ALS patient motor neurons, using specific antibodies developed against SOD1 epitopes exposed only when misfolded [3, 4, 6]. Wildtype SOD1 is also shown to misfold when overexpressed in neuronal cells [114]. Interestingly mice overexpressing human wildtype SOD1 developed ALS-like phenotype, with accumulation of SOD1 aggregates in the brain and spinal cord [115]. These findings suggest that a more general involvement of both wildtype and mutant SOD1 in the pathogenesis of ALS.

1.4.2 ***C9ORF72* hexanucleotide repeat expansion in ALS**

Mutations in *C9ORF72* that causes ALS and FTD are GGGGCC nucleotide repeat in the non-coding region, between two transcription initiation sites exon 1a and 1b (Figure 1.3) [32, 56]. This G₄C₂ sequence is also found in normal individuals, however the sequence is repeated mostly between 2-5 times and never exceeds 30 repeats [116]. In *C9ORF72*-linked FTD and ALS patients the G₄C₂ sequence is abnormally expanded. Although the exact number of abnormal repeats required to cause disease is not known, general observation is that, G₄C₂ sequence is repeated several hundreds to even thousands in ALS and FTD

cases [117]. In some rare cases expansion of just 20-22 repeats in *C9ORF72* is also linked with FTD [118]. Identifying the mechanism of toxicity of these repeat expansion in *C9ORF72* is now a key area of research in ALS and FTD. The expansion of short repeats regions have been previously identified in other genetically inherited neurodegenerative disorders including Huntington disease, various forms of ataxia and myotonic dystrophies [119, 120]. The repeat expansions in neurodegenerative diseases, now including ALS and FTD are generally believed to exhibit toxicity through three main mechanisms: gain of RNA toxicity from repeat expansion, decreased translation and protein levels (haploinsufficiency), and creation of repeat associated toxic proteins [119, 120]. Upon discovery of repeat expansion in *C9ORF72*, the group also found RNA foci formed from G₄C₂ repeat containing RNA present in frontal cortex and spinal cord of repeat expansion carriers [32]. These results have since been replicated by a number of studies [121-124] and in addition RNA foci formed from antisense transcripts were also reported [122, 123, 125]. The generation of repeat length dependent RNA foci were further found to be toxic in SH-SY5Y cells and Zebrafish embryos [124]. These RNA foci were also found to sequester specific RNA-binding proteins, including Pur-alpha, hnRNPH and Adenosine deaminase RNA-specific B2 (ADARB2), and is expected to disrupt RNA homeostasis [121, 126-128]. The G₄C₂ expanded repeats associated with *C9ORF72* were shown to undergo repeat-associated non-ATG (RAN) translation [129, 130] an unconventional mode of translation that occurs in the absence of an initiating ATG and in all possible reading frames [131]. RAN translation of G₄C₂ repeats is expected to generate poly(GA), poly(GP) and poly(GR) proteins, whereas RAN translation of antisense C₂G₄ transcripts could generate poly(PR), poly(PG) and poly(PA) proteins [132]. These RAN translated peptides are found to be accumulated in the brain of ALS and FTD patients with *C9ORF72* repeat expansion [129, 133-136] and are shown to exhibit neurotoxicity in dorsophila models [128, 137]. Another possible mechanism of toxicity for repeat expansion in *C9ORF72* is haploinsufficiency of the normal protein product. The repeat expansion in *C9ORF72*, is transcribed in exon 1a (variant 1, NM_145005.5; variant 3, NM_001256054.1) and will be located in the promoter region (variant 2, NM_018325.3) if exon 1b is used [132]. Hence the repeat expansion is expected to control the expression of C9orf72 protein. Consistent with this notion, decreased levels of C9orf72 variants were observed in ALS/FTD patients [130, 138-141]. In addition C9ORF72 mRNA expression is also shown to be reduced epigenetically by repeat associated histone trimethylation, followed by transcriptional silencing [138]. Hence it is possible that the *C9ORF72* associated repeat expansion may induce toxicity by the loss of protein

expression. However the function of C9orf72 protein is unknown, and establishing its function, is the next important step to understand how haploinsufficiency of C9orf72 could induce neurodegeneration.

1.4.3 ***TARDBP* and *FUS* mutations in ALS**

Discovery of genetic mutations in TDP-43 and FUS were the first indications of disrupted RNA metabolism in ALS. TDP-43 and FUS share similar structural and functional properties and is involved in various RNA processing steps [142]. In particular, these proteins belong to family of heterogeneous ribonucleoproteins (hnRNPs) which function in regulation of RNA metabolism and bind to RNA through their RNA recognition motifs (RRMs) [142, 143]. TDP-43 was identified major constituent of cytoplasmic and intranuclear inclusions in neurons and glia of patients with sporadic and familial forms of ALS and FTD [5], followed by which more than 40 different mutations in *TARDBP* gene encoding TDP-43 were found in sporadic and familial ALS [33, 142, 144]. Majority of mutations in TDP-43 are clustered at the C-terminal region with harbors a putative prion-like domain [142]. Almost immediately mutations in FUS were identified in familial and sporadic ALS [34, 54]. Most of the mutations in FUS are clustered at the extreme C-terminus, in and around the nuclear localisation signal (NLS) [142]. Together TDP-43 and FUS mutations account for about 10% of familial ALS cases [145]. Both FUS and TDP-43 appear to be nuclear in most cells at steady state, although they shuttle between the nucleus and cytoplasm, as required [146, 147]. FUS is also normally localized in the dendritic spines of neurons in addition to be in the nucleus [148]. However mutant forms of TDP-43 are distributed both in the nucleus and cytosol of neurons and glia, with several pathological modifications such as abnormal phosphorylation, ubiquitination and truncation into C-terminal fragments [5, 149]. Analysis of brain and spinal cords from patients with FUS mutations also revealed FUS cytoplasmic aggregations in neurons [34, 54], indicating mutation associated cytoplasmic redistribution similar to TDP-43, although other pathological modifications such as hyperphosphorylation and truncation have not been identified with FUS [150]. Even in the absence of mutation, cytoplasmic TDP-43 accumulation and/or aggregation can be found in the majority of ALS patients (estimated as 97% [145]) with the exception of patients with SOD1 mutations [151, 152] and is reported to be indistinguishable from patients with TDP-43 mutations [153]. Interestingly FUS-immunopositive and TDP-43-immunopositive aggregates are mutually exclusive of each other, indicating distinct pathologies [150, 154, 155]. Some studies have also suggested that

TDP-43 acts upstream of FUS in the induction of ALS pathology [156, 157]. Loss of nuclear TDP-43 and FUS in ALS, suggest a loss of their nuclear function, however the presence of cytoplasmic inclusions suggests gain of toxic properties. Thus the pathogenic mechanisms for TDP-43 and FUS are not clear in ALS, however it is likely to be a combination of both loss of function and gain of toxic properties [145].

1.4.4 Current experimental models to study ALS pathogenesis.

Although majority ALS cases are sporadic, without any known genetic mutations, they exhibit similar pathogenesis as familial ALS. Hence to understand the pathogenesis of ALS cell culture or animal models expressing mutant forms of genes linked with familial ALS are used. The first transgenic mice model of ALS was developed by expressing approximately 20-24 copies of the human SOD1 gene carrying the G93A mutation [158]. This transgenic SOD1 mice recapitulates many features of ALS, including progressive neuromuscular dysfunction, gliosis and motor neuron loss [158]. Similarly other transgenic mice and rat models expressing human SOD1 mutants have been developed [159]. Although vast amount of information about the pathogenesis of ALS has been gained, no therapeutic interventions from SOD1-linked animal models have proved beneficial in ALS patients [113]. Furthermore the most widely mutant SOD1 (G93A, D90A) mice models were also reported to show non-physiological, increased (100 fold) loading of SOD1 into mitochondria due to high expression of disulphide-reduced mutant SOD1 [160]. More recently overexpression of wildtype SOD1 at similar levels to mutant G93A SOD1 mice, have been shown to develop ALS-like phenotype [115]. Wobbler mice with a spontaneous recessive mutation (Q967L) in vacuolar protein sorting 54 (*Vps54*) gene, encoding a vesicular transport protein develops upper and lower motor denegeneration and exhibits a phenotype closely resembling human ALS, and has been used as a model to study ALS [161]. With the discovery of TDP-43 and FUS mutations, a number of attempts have been made to develop rodent models based on these genes. Homozygous deletion of *TARDBP* in mice is embryonically lethal, while the heterozygous deletion develop some motor deficits [162]. Similar deletion of FUS in mice has been either lethal or develop phenotype unrelated to neurodegeneration [163, 164]. Developing a valid rodent model for ALS, by overexpressing wildtype or mutant forms of TDP-43 and FUS have also proven difficult with no current model recapitulating all features of ALS [165-172].

Several yeast (*Saccharomyces cerevisiae*), roundworm (*Caenorhabditis elegans*), fly (*Drosophila melanogaster*) and zebrafish (*Danio rerio*) models for ALS have also been developed expressing mutant forms of SOD1, TDP-43 or FUS, in which greater abnormalities are observed compared to overexpression of wildtype protein [173-182]. However the ability of these models in reproducing the upper and lower motor signs of ALS remains questionable [183]. The identification of hexanucleotide repeat expansion associated with *C9ORF72* has provided new challenges in developing animal models to study repeat associated toxicity. *Drosophila* and zebrafish models have been recently developed overexpressing disease-related hexanucleotide expansions in *C9ORF72* [124, 128, 137, 184]. These models have been highly useful in identifying various repeat associated toxic mechanisms such as RNA foci formation, sequestration of RNA binding proteins and toxicity of RAN translated peptides [185]. Zebrafish models with depleted *C9orf72* also serves as a valuable model to study loss of protein function and indeed was shown to develop locomotion deficits with reduced axon lengths of motor neurons [139]. Recent advancement in stem cell research has allowed the reprogramming of patient's somatic cells, such as skin fibroblasts or endothelial cells, to the pluripotent state, similar to that of an embryonic stem (ES) cell, following artificial expression of four genes: *KLF4*, *SOX2*, *OCT4*, and *c-MYC* [186, 187]. These induced pluripotent stem cells (iPSCs) display the unlimited proliferative potential and the ability to differentiate into all cell types of the body. Such iPS cells derived from ALS patients can be reprogrammed into motor neurons or glial cells which currently serves as a robust model to study ALS pathology directly from patients [188, 189]. Such iPS cell derived from sporadic [190] or familial ALS patients carrying SOD1 [191, 192], TDP-43 mutations [193, 194] or *C9ORF72* associated repeat expansions [121, 195] are developed recently, which are being increasingly used to study disease pathogenesis and serves as an efficient system for large scale screening of therapeutic agents [196].

1.5 Pathogenic mechanisms associated with ALS.

Although the etiology of ALS remains unknown, several pathogenic mechanisms are implicated in neurodegeneration in ALS. This includes protein misfolding and aggregation, ER stress, Golgi fragmentation, disruption of RNA homeostasis, excitotoxicity and mitochondrial dysfunction (Figure 1.1) [7, 145, 197-199]. The initial trigger for each of these diverse mechanisms remains unknown. Furthermore, recent evidence suggests that these

mechanisms may be inter-linked and that disturbances in one cellular pathway can result in a domino effect, inducing other pathogenic mechanisms associated with ALS, eventually resulting in motor neuron dysfunction [116, 200].

It is unclear why motor neurons are specifically targeted by ubiquitously expressed pathogenic proteins in ALS. Motor neurons differ from most other type of neurons in the central nervous system in that they are exceptionally large, with extremely long axons, up to 1 metre in length in an adult human. Based on their unique morphology, motor neurons are expected to rely heavily on efficient cellular transport processes. Efficient cellular trafficking is essential for many cellular functions, including normal functioning of the ER, Golgi [201, 202] and mitochondria [203] and it is also essential for proteostasis by regulating pathogenic protein clearance pathways such as autophagy and ubiquitin-proteasome system [204-206]. Furthermore, there are also links to other pathogenic pathways linked to ALS such as axonal transport [207, 208]. Hence disturbances in this finely regulated, complex trafficking system may therefore perturb cellular viability and ultimately trigger motor neuron dysfunction. This section explains key cellular mechanisms associated with the pathogenesis of ALS.

1.6 Protein misfolding and aggregation.

Like other neurodegenerative disorders, a central pathological hallmark of ALS is the accumulation of intracellular inclusions containing misfolded protein aggregates, that can even be seen by light microscopy [198, 209, 210]. The protein inclusions found in ALS patients are identified as Lewy body-like hyaline inclusions or skein-like inclusions [211, 212]. These aggregates appear as clumps of randomly arranged filaments covered by fine granular structures [210]. In addition, small eosinophilic inclusions known as bunina bodies are observed in ALS patients [198]. Bunina bodies contain cystatin-C and round hyaline inclusions composed of neurofilaments. While it has been postulated that the protein aggregates maybe a simple cellular response to stress, increasing evidence suggests that these aggregates may be directly toxic by acting as a seed, triggering further protein aggregation [213], and indirectly toxic by recruiting key proteins essential for cellular viability [198]. The aggregates may also perturb intracellular trafficking pathways [200, 214] and protein clearance mechanisms in the cell [145, 198]. However, the biochemically defined, smaller misfolded forms of the misfolded proteins are more likely than the large macroscopic aggregates (ie the inclusions) to be toxic in ALS [215-217].

Interestingly, while mutant forms of ALS-linked proteins including TDP-43, SOD1, FUS and optineurin are found as a component of ubiquitinated protein inclusions in familial ALS patients, wildtype, non-mutated forms of the same proteins are recruited into the inclusions in sporadic ALS patients [3, 5, 198, 218]. This implicates wildtype ALS-linked proteins in the etiology of sporadic ALS. As discussed earlier (section 1.4.1) wildtype SOD1 has a demonstrated intrinsic ability to misfold and aggregate in response to pathogenic triggers such as oxidative stress [4]. These misfolded, oxidised forms of wildtype SOD1 inhibited axonal transport at a level similar to mutant SOD1 [3], suggesting that such misfolded forms of wildtype SOD1, found in sporadic ALS, may exhibit some toxic properties of mutant SOD1. Similarly wildtype TDP-43 as a major component of ubiquitinated proteins inclusions in almost all sporadic ALS cases, is mislocalized from nucleus and trapped in cytoplasmic inclusions, suggesting a loss of function [5]. However a gain of toxic function by aggregated TDP-43 is also possible due to its established propensity to seed further aggregation [219]. FUS is also present as a component of the cytoplasmic inclusions in a proportion of sporadic ALS cases, suggesting a similar possible mechanisms of toxicity as TDP-43 [218]. Optineurin is a key component of ubiquitinated protein aggregates in OPTN mutation carrying familial ALS patient as well as sporadic ALS patients [220]. Furthermore wildtype optineurin is also present within pathogenic aggregates found in other neurodegenerative disorders, including Alzheimer's, Parkinson's, Huntington's, and Creutzfeld-Jacob diseases and multiple system atrophy [221, 222], hence implicating a general role of optineurin in neurodegenerative mechanisms.

1.7 Autophagy defects in ALS

Autophagy is an evolutionary conserved process involving vacuolar acidic lysosome mediated degradation of substrates [223]. There are three different forms of autophagy classified according to which cargo is delivered to the lysosomes [224, 225]: Chaperone-mediated autophagy (CMA), where proteins containing a pentapeptide KFERQ-like sequence is specifically recognised by a cytosolic heat-shock cognate 70 (HSC70) chaperone, which then associates with the integral lysosome membrane protein LAMP-2A, followed by internalisation into lysosome. Microautophagy is a non-selective autophagy process where small quantities of cytoplasmic components in proximity with the lysosomal membrane enter the lysosome for degradation through invagination, protrusion or septation of lysosomal membrane [226]. Finally macroautophagy is a process of self-degradation,

characterised by the formation of double-membrane delivery vesicles, called autophagosomes, that engulf unwanted/defective proteins and organelles [227]. These autophagosomes then fuse with acidic lysosomes for degradation. Autophagy is an essential process in post-mitotic cells such as neurons, which are highly susceptible to the accumulation of defective organelles and proteins. Autophagy is also an important cellular mechanism to eliminate protein aggregates [228, 229] and autophagy dysfunction is increasingly implicated in the pathogenesis of ALS. Autophagy is initiated during cellular stress conditions including starvation of specific amino acids, growth factors, ATP (adenosine triphosphate), the presence of protein aggregates or ER stress [229, 230]. The selective binding of ubiquitin-interacting proteins such as p62 and histone deacetylase (HDAC6) to protein aggregates could also activate autophagy [231].

Autophagosome formation is initiated by altering the phosphorylation states of individual components of autophagy-related 2 (Atg1)-Unc51-like kinase (ULK) complex (Atg1-ULK), consisting of ULK1, ULK2, Atg13, FIP200 and Atg10 proteins [232, 233]. The initial step of ULK1 phosphorylation is controlled either by the mTOR complex 1 (TORC1), or by AMP-activated protein kinase (AMPK) [234]. The phosphorylation of ULK1 triggers the formation of a cup-shaped isolation membrane or pre-autophagosome, by a multiprotein complex containing beclin-1 and class III phosphoinositide 3-kinase (PI3K CIII or Vps34) [229]. The elongation of the autophagosome membrane is then regulated by two type of ubiquitylation-like modifications, Atg12 conjugation and lipidation of microtubule-associated protein 1A/1B-light chain 3 (LC3). Atg12 conjugation with Atg5 results in the formation of the Atg12-Atg5-Atg16 complex, activating the covalent attachment of phosphatidylethanolamine to LC3 [235]. The lipidated form of LC3, LC3 II, is then attached to the autophagosome membrane, marking the maturation of the autophagosome, which then fuses to the lysosome [236]. The execution of the complex processes involved in autophagy relies heavily on efficient cellular trafficking. The endosomes, premature autophagosomes, mature autophagosomes and lysosomes are all transported by a combination of microtubule and actin-based molecular motors including dynein, kinesin and myosin VI [237]. Similarly, several Rab proteins that regulate vesicular trafficking are also involved in autophagosome formation and maturation [238].

Autophagy is indeed a dynamic, complex process, and in many neurodegenerative disorders, this process goes awry at various points along the pathway, giving rise to distinct pathological patterns [229]. Similarly, defects in autophagy have been described in ALS, but

the nature and cause of the autophagy defects in ALS are not well characterised. Autophagosomes accumulate in ALS patient tissues [239] and the levels of LC3-II are elevated in spinal cords of mouse disease models, transgenic G93A [240] and H46R mutant SOD1 mice [241]. These findings indicate both an induction of autophagy in ALS as well as inhibition of clearance of autophagosomes. The importance of efficient autophagy in ALS is further understood from recent studies demonstrating that pharmacological induction of autophagy ameliorates disease pathology in cell culture and mice models of ALS. Activation of mTOR-dependent autophagy using rapamycin improved motor function in mice expressing TDP-43 [242], and induction of mTOR-independent autophagy using trehalose significantly prolongs life span and attenuates disease progression in G93A SOD1 transgenic mice [243, 244]. Activation of autophagy with novel compounds induced clearance of cytoplasmic TDP-43 and prevented TDP-43 mediated cell death in iPSC derived human motor neurons cells [245]. However in contradiction, treatment with rapamycin was reported to cause mitochondrial dysfunction and shorten lifespan of mutant G93A SOD1 mice [246]. Also attempts to treat ALS by inducing autophagy using lithium failed in human ALS patients in a large scale study [247]. These findings demonstrate that a simple induction of autophagy is not sufficient to treat ALS. Hence, there is a compelling need to understand the exact nature of autophagy dysfunction in ALS, in order to design more effective and specific therapeutic strategies. Recent identification of mutations in *TBK1* in familial ALS [103], encoding an autophagy related protein TANK-Binding kinase 1 further implicates autophagy disruption in the pathogenesis of ALS.

1.8 Glutamate excitotoxicity.

Glutamate excitotoxicity is another important pathological feature associated with motor neuron death in ALS. It is caused by over-stimulation of post-synaptic glutamate receptors, such as NMDA and AMPA type receptors, which triggers hyperpolarisation of the neuron [248]. This subsequently leads to an increased influx of calcium ions, activating enzymes such as phosphatases, proteases, lipases and endonucleases. This results in oxidative stress by generation of reactive oxygen species (ROS), mitochondrial damage, protein and lipid alterations in the cell membrane and impairment of glutamate transport in astrocytes [249, 250]. Excitatory amino acid transporter EAAT2, which is normally present on astrocytes and is responsible for rapid removal of glutamate from the synapse, is reduced in human patients and in mutant SOD1 transgenic mice models of ALS [251, 252].

Glutamate levels are also reported to be increased in the cerebrospinal fluid (CSF) of human ALS patients [253]. Hence reduced EAAT2 could be responsible for increased glutamate leading to excitotoxicity in ALS. Moreover, blocking of AMPA receptors reduced motor neuron loss in rat models of ALS, adding evidence for glutamate mediated excitotoxicity in ALS [254]. However a recent study has found that high excitability is protective for motor neurons [255]. It was observed that fast fatiguing (FF) MNs with low excitability that innervate hind leg muscles die first in ALS, followed by motor neurons with medium and high excitability, suggesting that excitation or hyperpolarisation could be protective for motor neurons in ALS [255]. Indeed, synaptic glutamate receptor activation can activate neuroprotective features in a biphasic dose responsive manner, which includes upregulation of neurotrophic factors, Ca^{2+} handling proteins, antioxidant systems, protein chaperones and DNA repair enzymes [256, 257]. Consistent with this notion, increased excitation of motor neurons by overexpression of glycine receptors is protective against mutant SOD1 induced pathology in mice models [255]. These results suggest that low levels of excitation are necessary to stimulate endogenous neuroprotective mechanisms in motor neurons, whereas higher levels of excitation may lead to degeneration [257].

1.9 Mitochondrial dysfunction

Mitochondria are critical cellular organelles with many important functions; including the synthesis of ATP, maintenance of calcium ion homeostasis and regulation of apoptosis. Morphological abnormalities and dysfunction of mitochondria are implicated in ALS pathogenesis. The first reports on mitochondrial pathology in ALS came from studies on post-mortem ALS patient brain tissues. Mitochondria accumulate in the dense neurofilamentous aggregates at presynaptic terminals in human ALS patients [258, 259]. Enlarged mitochondria and elevated calcium levels within the mitochondria were reported in muscle biopsies of ALS patients [260]. Dysregulation of the mitochondrial electron chain complex is also found in sporadic and familial ALS patient tissues [261]. Furthermore, mitochondria are fragmented, vacuolated and cluster in motor axons in transgenic mutant G93A SOD1 transgenic mice [262, 263]. However some mitochondrial abnormalities observed in transgenic SOD1 mice are also reported to be possible artefacts because of high expression of metal deficient and disulphide reduced G93A mutant SOD1, which is overloaded into mitochondria [160]. Cells expressing mutant SOD1 are also shown to exhibit mitochondrial abnormalities including decrease in the activities of complexes II and IV of

electron transfer chain and loss of calcium buffering capacity [264, 265]. There is evidence that mitochondrial-mediated apoptotic cell death is observed in ALS. Cytosolic release of cytochrome C, increased levels of pro-apoptotic Bad and Bax and decreased levels of anti-apoptotic Bcl-2 (B-cell lymphoma 2), are observed in brain and spinal cord tissues of ALS patients [266, 267]. Furthermore, mitochondrial mediated apoptosis is also shown to be activated by other signaling pathways such as ER stress in ALS [268].

1.10 ER stress and unfolded protein response (UPR)

The ER is an important cellular organelle with key roles in protein synthesis and secretion. Approximately one third of the human proteome is synthesized in the ER, and these proteins are then transported to the Golgi apparatus for transmembrane localization or secretion [269]. The ER is the primary site for the native folding of nascent proteins, and for post-translational modifications including N-linked glycosylation [270] and the formation of disulphide bonds [271]. The ER also acts as the cellular storage site for intracellular calcium ions [272], which are vital for neuronal synaptic transmission. The ER is also involved in the synthesis of lipids and sterols [273].

Various physiological and pathological factors affect protein folding within the ER, which can lead to accumulation of misfolded proteins within ER lumen, resulting in ER stress. ER stress is also triggered by chronic cellular stress conditions including impaired vesicular trafficking between ER and Golgi, nutrient deprivation, altered calcium homeostasis and defects in lipid biosynthesis [201, 274, 275]. Non-lethal levels of ER stress are also observed in cells with high secretory functions like lymphocytes and pancreatic β cells, due to their high work load [276]. When ER stress is activated, it leads to the activation of a complex signaling network termed the unfolded protein response (UPR). Initially UPR dynamically increases the protein folding and degradative capacity of the ER with the aim of reducing the load of misfolded proteins. However when the UPR is prolonged it activates apoptosis. The UPR is executed by stress sensors located at the ER membrane and a pool of downstream transcription factors that regulate gene expression, enabling quality control mechanisms or induction of apoptosis. ER stress also activates the ER associated degradation pathway (ERAD), in which misfolded proteins are translocated to the cytosol, where they undergo ubiquitylation and proteasome-mediated degradation. In addition, UPR signalling enhances autophagy [277].

The three main signaling sensors of the UPR located on the ER membrane are PERK (protein kinase RNA-like endoplasmic reticulum kinase), inositol-requiring enzyme 1 (IRE1) and activating transcription factor 6 (ATF6). In an unstressed state, the ER luminal chaperone immunoglobulin binding protein (BiP) binds to these UPR sensors and maintains each sensor in an inactivated state. Upon activation of ER stress, BiP titrates away from the UPR sensors, thus activating each individual signaling network. PERK induces an attenuation of global protein translation by phosphorylating ubiquitous eukaryotic translation initiation factor 2 α (eIF2 α). This arrest of protein translation process reduces the load of proteins within the ER lumen, with the aim of overcoming the stress. Phosphorylation of eIF2 α also favors specific translation of mRNAs that control expression of various genes involved in apoptosis, autophagy, ERAD and antioxidant responses, including that of activating transcription factor 4 (ATF4). IRE1 is a Serine/Threonine protein kinase and endoribonuclease that becomes activated by dimerization and auto-phosphorylation, which then triggers the most conserved UPR pathway. Activated IRE1 catalyzes unconventional processing of mRNA encoding the transcription factor X-Box binding protein-1 (XBP1) [276]. A 26-nucleotide intron within XBP1 mRNA is spliced and removed by IRE1 α , leading to an altered mRNA reading frame. The resulting spliced XBP1 is stable and it controls the upregulation of a pool of UPR-related genes involved in protein folding, protein entry to the ER, ERAD, biogenesis and expansion of ER and Golgi by enhancing phospholipid biosynthesis [278-282]. Apart from regulating the expression of spliced XBP1, activated IRE1 also directly initiates apoptosis upon prolonged ER stress. The cytosolic domain of activated IRE1 α recruits the adaptor protein TNFR-associated factor 2 (TRAF2), which then activates the apoptosis signal-regulating kinase 1 (ASK1) pathway [283]. ASK1 is a mitogen-activated protein kinase (MAPK) that relays the pro-apoptotic c-Jun N-terminal kinase (JNK) pathway [284]. Activated IRE1 also regulates the degradation of mRNAs of genes encoding ER proteins that are predicted to be difficult to fold under stress conditions [278, 285].

ATF6 has two Golgi localization signals which are masked by the binding of BiP in an unstressed state. Dissociation of BiP initiates translocation of ATF6 to the Golgi by a vesicular mediated process, where it is cleaved by two proteases, S1P and S2P (site-1 and site-2 protease). The resulting N-terminal cytosolic fragment then moves into the nucleus and induces transcription of XBP1 and other genes associated with ERAD [286]. ATF6 can also form heterodimers with XBP1 to regulate specific patterns of gene expression favoring

restoration of effective ER proteostasis [287]. During the initial stages of ER stress, BiP and other ER resident chaperones including glucose regulated protein 94 (GRP94), calreticulin, calnexin and protein disulphide isomerase (PDI) family members are upregulated by the combined action of spliced XBP1, ATF4 and ATF6.

Upon chronic or irreversible ER stress, apoptosis is triggered by a combination of distinct signaling pathways involving PERK and ATF6-mediated downstream signaling, and Ca^{2+} release from the ER [288, 289]. Persistent ER stress attenuates the pro-survival signaling mechanisms mediated by IRE1, and instead maintains PERK mediated signaling pathway, which triggers apoptosis [290]. PERK activation induces the transcription factor ATF4 which subsequently activates transcription of C/EBP-homologous protein (CHOP) and its target, growth arrest and DNA damage-inducible 34 (GADD34), as a key mechanism leading to apoptosis upon chronic ER stress [291]. CHOP is a regulator of pro-apoptotic and anti-apoptotic signals and it can inhibit the expression of survival protein BCL-2, and activate pro-apoptotic Bcl2-interacting mediator of cell death (BIM) and p53 upregulated modulator of apoptosis (PUMA) [292, 293]. This cascade of events results in the activation of mitochondrial BAX and BAK-mediated apoptotic cell death [289]. CHOP is also predicted to cause cell death by increasing protein synthesis in the ER, which increases the load of proteins within the ER, depletes ATP and induces oxidative stress [294]. Apart from regulating the expression of spliced XBP1, activated IRE1 also directly initiates apoptosis upon prolonged ER stress. The cytosolic domain of activated IRE1 α recruits the adaptor protein TNFR-associated factor 2 (TRAF2), which then activates the apoptosis signal-regulating kinase 1 (ASK1) pathway [283]. ASK1 is a mitogen-activated protein kinase (MAPK) that relays the pro-apoptotic c-Jun N-terminal kinase (JNK) pathway [284].

1.10.1 ER stress is an important pathogenic mechanism in ALS

ER stress and activation of the UPR is a well documented feature of ALS in human patients as well as in rodent and cell culture models of ALS [199]. Our group previously demonstrated the upregulation of UPR sensors IRE1, PERK, ATF-6 and cell death signals CHOP and caspase 3, 9, 12 in transgenic mice expressing mutant G93A SOD1 [295]. The chaperone PDI was also the most upregulated protein identified in a proteomic study of spinal cord extracts rats expressing mutant SOD1 [295]. An intriguing later study involving transcriptomic analysis of the motor neurons that specifically are targeted early in mutant

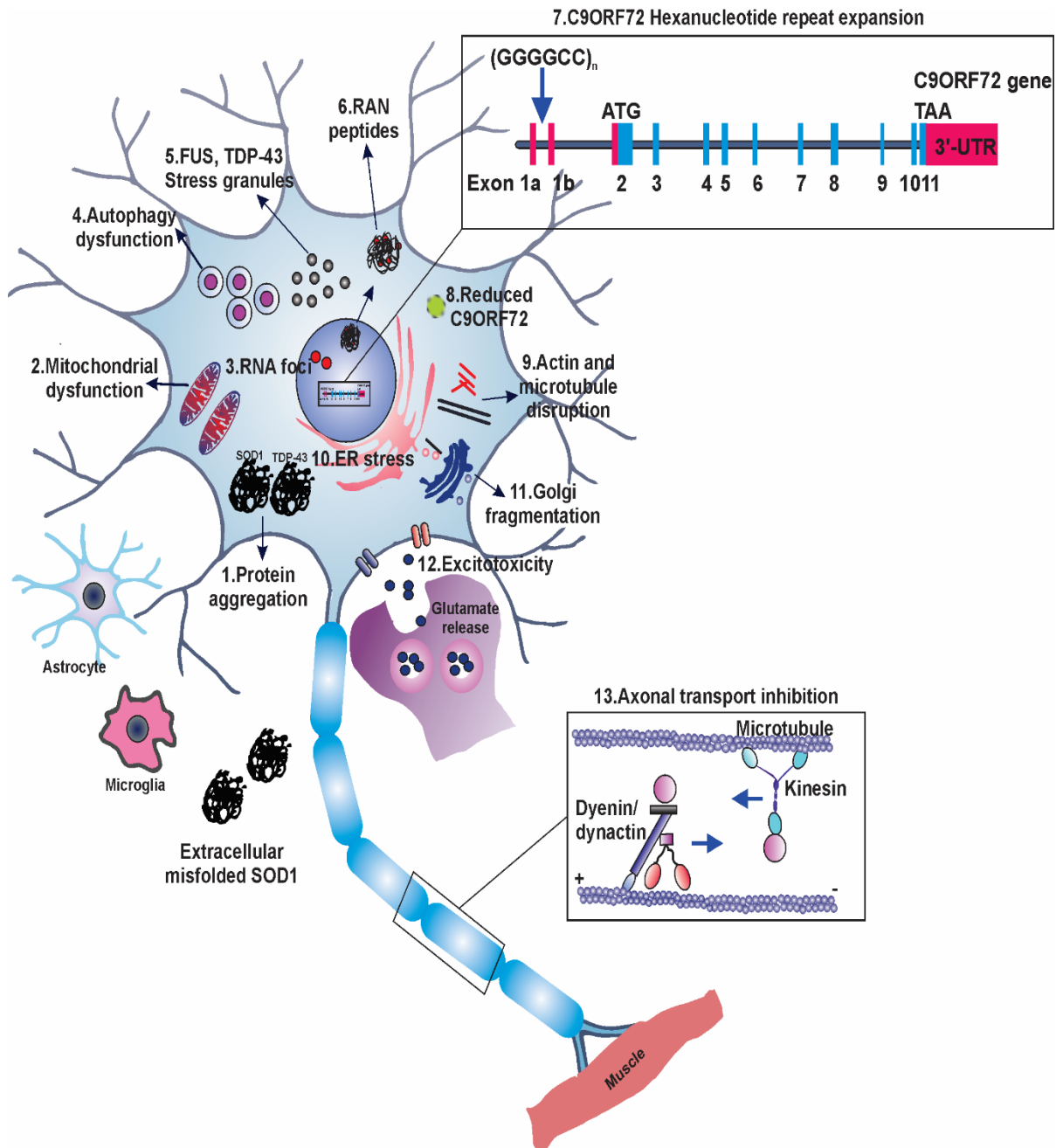


Figure 1.1 Pathogenic mechanisms associated with ALS, 1. Protein aggregation (representing SOD1 and TDP-43 aggregates found in both sporadic and familial ALS). 2. Mitochondrial dysfunction 3. *C9ORF72* repeat induced nuclear RNA foci formation 4. Autophagy dysfunction 5. Stress granules containing TDP-43 and FUS 6. *C9ORF72* repeat associated non-ATG translated proteins (nuclear and cytoplasmic) 7. GGGGCC repeat expansion in the non-coding region of *C9ORF72* gene. 8. Reduced expression of *C9orf72* protein 9. Actin and microtubule disruption associated with genetic mutations in profilin and TUBA4A 10. ER stress 11. Golgi fragmentation 12. Excitotoxicity 12. Axonal transport inhibition.

G93A SOD1 mice revealed that ER stress transcripts were the main molecular signature group different from motor neurons that are targeted later in this animal model [296]. Such specific upregulation of ER stress markers in most vulnerable motor neurons were also observed in other SOD1 mice models; low-copy number G93A and G85R mutant SOD1 mice. Moreover ER stress was first detected at postnatal day 5 in mutant G93A SOD1 mice, well before disease onset at p90 [296]. This evidence thus implicates ER stress as a key mechanism inducing the death of motor neurons early in ALS. Similarly, microarray analysis of motor neurons isolated by laser capture micro-dissection also revealed activation of ATF4 at disease onset and significant upregulation of CHOP at disease end stage in mutant G93A SOD1 mice, relating ER stress with disease progression [297]. Salubrinol, a small molecule inhibitor of ER stress, which blocks $\text{eIF}2\alpha$ phosphorylation reduced disease progression in mutant SOD1 mice [296]. Similarly, administration of Guanabenz, an anti-hypertensive drug which reduced ER stress and ameliorated neurodegeneration in worm and zebrafish models of ALS expressing mutant TDP-43 [298] and in transgenic G93A SOD1 mice [299].

UPR sensors, ER stress-activated chaperones and apoptotic effectors were also upregulated in human lumbar spinal cord tissue from sporadic ALS patients [300]. Similarly, in another study, enhanced phosphorylation of $\text{eIF}2\alpha$ and increased levels of PDIA1, Erp57, spliced XBP1 and ATF4 were detected in spinal cord of sporadic ALS patients [301]. Furthermore, S-nitrosylation of active site cysteine residues of PDI was detected in sporadic ALS patients, which would inactivate the enzymatic activity and thus contribute to disease progression [302]. In addition, several morphological changes to the ER have also been reported in human ALS patients. Ultrastructural investigation of sporadic ALS patient anterior horn cells using electron microscopy revealed fragmented ER cisternae and distended ER with detached ribosomes [303]. Such analysis also revealed the accumulation of abnormal dense material resembling bunina bodies within the ER of sALS patients [304]. Hence these findings implicate ER stress as a central feature of ALS pathogenesis common to both familial and sporadic forms.

Activation of ER stress has also been detected in cell culture in neuronal cells expressing mutant proteins associated with familial ALS; SOD1, FUS and TDP-43 [295, 305-307]. Overexpression of PD1 or treatment with 1,2-bis(mercaptoacetamido)cyclohexane (BMC), a small molecular mimic of the disulphide isomerase activity of PDI, reduced mutant SOD1 aggregation in Neuro2A cells [302]. Proapoptotic Bim is activated by ER stress in cells

expressing mutant SOD1. Knockdown of Bim reduced cytochrome c release into cytosol, but did not rescue ER stress mediated upregulation of CHOP [268], suggesting ER stress as an upstream trigger. Interestingly, ER stress is also activated by misfolded forms of wildtype SOD1 to a similar degree to the mutant forms, as described in this thesis in a published study (Chapter 3, [214]). Expression of mutant TDP-43 also upregulated UPR stress sensors and activated CHOP in neuroblastoma cells and pharmacological induction of ER stress drove cytoplasmic accumulation of mutant TDP-43 and stress granule formation [307]. Cytoplasmic mislocalisation of mutant FUS also correlated with activation of XBP1 and CHOP in NSC-34 cells [306], hence suggesting a possible role for ER stress in mutant TDP-43 and FUS mediated ALS pathology. Furthermore, mutations in VAPB, an ER membrane protein which interacts and inhibits the activity of ATF6, are present in familial ALS, and expression of mutant VAPB induces the UPR in NSC-34 cells and fly models of ALS [308-311]. Moreover neurotoxicity induced by the hexanucleotide repeat expansion in C9ORF72 is associated with the induction of ER stress in primary neurons. Expression of synthetically made poly(GA) RAN translated proteins induced CHOP and caspase 3 activation in primary neurons [312]. Additionally, treatment of primary neurons with ER stress inhibitors salubrinal and TUDCA, was protective against poly(GA)-induced ER stress and neurotoxicity, suggesting that ER stress is relevant pathogenic mechanism in C9orf72 ALS [312].

In conclusion these studies together imply that ER stress is a central and upstream feature of ALS pathogenesis, common to both familial and sporadic forms, and pharmacological inhibition of ER stress could be a potential therapeutic strategy for ALS. However it remains unclear how ER stress is triggered in ALS, as most mutated/misfolded proteins linked with ALS are not present in the ER lumen. This question is explored further in this thesis.

1.11 Golgi fragmentation

The Golgi apparatus is a highly dynamic organelle involved in the processing and sorting of both secretory, transmembrane proteins and lipids. Golgi morphology can become altered under a variety of normal, physiological conditions such as mitosis [313], and under pathological states, involving impaired ER function, disruption of intracellular transport, altered lipid metabolism, neuronal hyperexcitation, DNA damage, or activation of cell death pathways [314-317]. In normal cells, the Golgi apparatus is composed of a series of flattened, parallel, interconnected cisternae representing a ribbon-like network, organized

around the microtubule-organizing center in the perinuclear region of the cell. However in pathological conditions, fragmentation of Golgi occurs, which is characterised by the conversion of the Golgi stacks into smaller condensed, tubulovesicular punctate structures [318, 319]. Fragmentation of the neuronal Golgi apparatus is a prominent feature in ALS patients, which has been reported in 10-50% of motor neurons in sporadic patients [320-323] and up to 70% of motor neurons in familial ALS patients bearing either SOD1, FUS or Optineurin mutations [324-326]. In addition, Golgi fragmentation is observed in G93A SOD1 transgenic mice and cell culture models expressing SOD1 mutants [327, 328]. Interestingly, Golgi fragmentation precedes SOD1 inclusion formation, neuromuscular denervation and mitochondrial-mediated apoptosis in a low-copy number (8-10) G93A SOD1 transgenic mice, implicating Golgi dysfunction as an upstream event in ALS pathogenesis [323]. The motor neurons that display cytoplasmic mislocalisation of TDP-43 also display fragmented Golgi apparatus in sporadic ALS patients, suggesting a possible link between the two pathologies. Furthermore, Golgi fragmentation is also detected in cells expressing ALS-linked mutant forms of FUS and VAPB [329, 330]. In Chapter 4 of this thesis, Golgi fragmentation in cells expressing mutant optineurin is also described. However like many other pathologies in ALS, the trigger for Golgi fragmentation remains unclear. As the ER and Golgi compartments function in close association with each other, it therefore needs to be examined whether ER-Golgi abnormalities are induced together by a single trigger in ALS.

1.12 Disrupted RNA homeostasis.

Pathological and genetic association of RNA binding proteins TDP-43 and FUS with ALS and FTD [5, 33, 34, 54] suggested that defects in RNA processing may be an important pathogenic mechanism in both FTD and ALS. Both TDP-43 and FUS are involved in several steps of the regulation of gene expression including transcription, RNA splicing and RNA transport [331-334]. A key pathological feature associated with both TDP-43 and FUS in ALS is cytoplasmic mislocalisation. In the degenerating neurons and glial cells of ALS patients, both TDP-43 and FUS accumulate in the cytoplasm, where they form large aggregates [5, 34, 144, 218]. These aggregates further associate with stress granules in postmortem samples from ALS and FTD patients, as well as in cultured cells [179, 335-337]. Stress granules are formed under conditions of cellular stress to store mRNA temporarily and halt translation [338]. However, persistent TDP-43/FUS positive stress granules may be pathogenic by trapping mRNA transcripts, other RNA binding proteins and by providing a

seed for the formation of pathological inclusions in ALS [338, 339]. The recruitment of TDP-43 and FUS to stress granules also suggests loss of function of each protein under these conditions. Genome wide analysis has revealed that TDP-43 and FUS individually bind and regulate the transcription of nearly 30% of the transcriptome [333, 340], hence a loss of function of these proteins could be lethal. Furthermore cytoplasmic FUS is also shown to impede transcriptional regulation indirectly by nuclear depletion of protein arginine methyltransferase 1 (PRMT1) involved in histone acetylation [341]. Identification of mutations in other RNA binding proteins hnRNPA2B1, hnRNPA1 and TAF15 (Table 1.2) in familial and sporadic ALS patients, has provided further evidence for defective RNA processing in ALS. Furthermore there is also evidence that the hexanucleotide repeat expansion in *C9ORF72* disrupts RNA processing. Bidirectional transcription of these hexanucleotide repeats generates repeat length-dependent formation of nuclear RNA foci, which sequester specific RNA-binding proteins, including Pur-alpha, hnRNPH and Adenosine deaminase RNA-specific B2 (ADARB2) [126-128, 141]. This sequestration of RNA binding proteins has been demonstrated in brain sections of ALS patients bearing *C9ORF72* repeat expansions, as well as in pluripotent stem cells (iPSCs) derived from these patients [32]. *In vivo* studies using drosophila and zebrafish models expressing synthetic G₄C₂ repeats has also demonstrated repeat length dependent RNA toxicity [124, 128]. In a fascinating study, the G₄C₂ repeats were found to form G-quadruplexes, which are stacks of planar tetramers consisting of four guanines connected by Hoogsteen hydrogen bonds [342]. These G-quadruplex structures were found to determine repeat mediated RNA toxicity, by causing transcriptional abortion and recruiting RNA-binding proteins such as Nucleolin, hnRNPU, hnRNPF and ribosomal protein L7 (RPL7) in cell culture models [342]. Hence these studies suggest that *C9ORF72* hexanucleotide repeat mediated sequestration and functional depletion of RNA binding proteins contributes to disease progression by disturbing RNA homeostasis. A recent study has shown that RAN translated poly-PA dipeptides are more neurotoxic than RNA species generated from repeats [184]. However features of RNA processing defects such as decrease in RNA-processing bodies (P-bodies) and formation of cytoplasmic stress granules preceded cell death in neurons expressing poly-PA dipeptides [184] and hence suggesting that RNA homeostasis may also be perturbed by RAN translated peptides.

1.13 Cellular trafficking disruption in ALS

Cellular trafficking is essential for the viability of motor neurons by transporting variety of cargos including proteins, lipids, RNAs, neurotransmitters and mitochondria in their large cell body and axon. Furthermore cellular trafficking also plays an important role in maintaining proteostasis by transport of autophagosomes, endosomes, lysosomes and proteosomes. These variety of cargos usually in vesicular form are transported upon microtubule or actin cytoskeletal tracks, driven by distinct molecular motors. Dynein and kinesin motor complex serve as a major motor complex transporting multiple cargos towards the minus and plus end of microtubules in the cytoplasm and axon [343]. In addition myosin family of motor protein drive cargo trafficking upon filamentous actin (F-actin) network [344]. Then the Rab GTPases control distinct vesicular membrane trafficking steps along actin filaments or microtubules by recruiting motor adaptors or by binding directly to motors [345]. Several intracellular trafficking pathways including ER-Golgi vesicular trafficking, endocytosis, autophagosome/lysosomal trafficking and axonal transport, appear to be perturbed in ALS [7, 200, 346, 347]. Mutant forms of SOD1 and TDP-43 have been shown to impair distinct cellular trafficking processes [7, 148, 347]. Genetic mutations in proteins directly involved in cellular trafficking functions are also reported in ALS (Table 1.3). This section discusses genetic and pathological evidence indicating cellular trafficking disruption in ALS and describes ER-Golgi, Rab and optineurin/myosin VI mediated trafficking processes, which are related to studies presented in this thesis.

1.13.1 Mutations in genes encoding cytoskeletal and motor proteins are present in ALS

Many mutations that cause ALS have now been identified in genes encoding proteins that are directly involved in cellular trafficking functions (Listed in Table 1.3). Identification of mutations in genes encoding cytoskeletal and motor proteins in ALS, also suggest disruption of multiple cellular trafficking pathways which utilises these proteins. Mutations in the gene encoding the p150^{Glued} subunit of the dynein/dynactin complex have been reported in both sporadic and familial forms of ALS [67]. Expression of ALS mutant p150^{Glued} dynactin in mice results in selective motor neuron degeneration and reduced intracellular vesicular trafficking [348]. Similarly, recent findings of mutations in genes encoding cytoskeletal proteins have provided additional evidence for trafficking failure in ALS. Mutations in profilin 1, which mediates the conversion of soluble G-actin to functional F-actin, are present in familial ALS

cases [62]. ALS mutant profilin also inhibits axonal outgrowth in embryonic motor neurons [62]. Mutations in TUBA4A, an essential microtubule network protein, were recently reported in familial ALS, and these mutants were demonstrated to destabilise the microtubule network in cultured motor neurons [83].

ALS-linked Proteins	Cellular trafficking function	Reference
C9ORF72	Potential involvement in Rab-mediated membrane trafficking process. Predicted to function as Rab guanine nucleotide exchange factors (GEFs)	[349, 350]
TDP-43	Microtubule-dependent mRNA transport in neuronal axons	[347]
FUS	Axonal mRNA trafficking	[148]
Optineurin	Vesicular trafficking of secretory proteins, autophagosomes and lysosomes	[206, 351] Chapter 2
VCP	Secretory protein trafficking. Translocation of misfolded proteins from ER to cytoplasmic proteasome degradation	[352-354]
Profilin1	Polymerisation of actin cytoskeleton	[355]
VAPB	Vesicular ER-Golgi trafficking, dendritic membrane protein trafficking. Involved in microtubule organisation	[356, 357]
SQSTM1/p62	Mediates AMPA receptor trafficking at synapse and dynein-linked cellular trafficking	[358, 359]
Alsin	Function as a GEFs for Rab5 and Rac1. Involved in Rab5-endocytic trafficking and Rac1 regulation of actin cytoskeleton	[360, 361]
CHMP2B	Component of endosomal sorting complex required for transport-III (ESCRT-III), essential for endocytic trafficking	[362]
Dynactin	Mediates dynein and kinesin 2 driven intracellular and axonal trafficking on microtubules	[343, 363]
Neurofilament heavy chain	Essential for maintaining axon structure and function	[364]
TUBA4A	Component of microtubule cytoskeleton	[365]
Peripherin	Type III neuronal intermediate filament involved in peripheral axon outgrowth and regeneration	[366]
Spatacsin	Involved in axonal anterograde vesicular trafficking	[367]
Phosphoinositide 5 phosphatase	Associated with late endosome/lysosomal membrane trafficking pathways	[82, 368]
Sigma-1 receptor	Involved in lipid rafts associated transport of proteins and lipids to plasma membrane	[368, 369]

Table 1.3 List of proteins with cellular trafficking functions encoded by genes that are mutated in ALS

In addition to actin and microtubules, neurofilaments are an important component of neuronal cytoskeleton which provide structural support for axon [370] and mutation in neurofilament heavy chain is also linked with familial ALS [78]. Together these findings imply that defects in both motor proteins and cytoskeletal networks can induce motor neuron degeneration in ALS.

1.13.2 Rab mediated cellular trafficking

Rab proteins form a large family of small guanosine triphosphate (GTP)ases, with more than 60 members in humans that regulate vesicular trafficking at distinct cellular membrane compartments [371]. Rab proteins are involved in all steps of vesicular trafficking, such as vesicle formation, vesicle tethering, vesicle transport along actin and microtubule cytoskeletal networks, and fusion to the target compartments [345, 372]. Various Rabs mediate vesicular trafficking during ER-Golgi associated classical secretion [373-375], endocytosis and autophagy [238, 376]. Rabs act as molecular switches at specific membranes, by cycling from an inactive Guanosine diphosphate (GDP)-bound state to an active Guanosine triphosphate (GTP)-bound state, and vice versa [371, 377] (Figure 1.2). The newly synthesized Rab, in the GDP-bound inactive form, associates with a Rab escort protein (REP). The Rab-REP complex is post-translationally modified by Geranylgeranyl transferase (GGT) enzyme, which adds a geranylgeranyl group at one or two carboxy-terminal Cysteine residues of Rab. The GDP dissociation inhibitor (GDI), recognizes and binds to geranylgeranylated and GDP-bound inactive form of Rab in the cytosol. The Rab-GDI complex is then recruited to specific membrane by membrane-bound GDI displacement factor (GDF) [378]. Membrane binding of Rabs occur via hydrophobic geranylgeranyl groups at their carboxy terminal tails. Activation of membrane bound Rab is then catalysed by Guanine nucleotide exchange factors (GEFs), which facilitates the release of GDP from Rab, causing an immediate replacement with GTP, present at high concentrations in the cytosol [379]. Activated Rabs also then associates with their respective effector molecules which are either motor proteins or adaptors for motor attachment [345]. Rab-specific GTPase activating protein (GAP) inactivates the Rabs by catalyzing the hydrolysis of bound GTP to GDP, thus terminating the response [379].

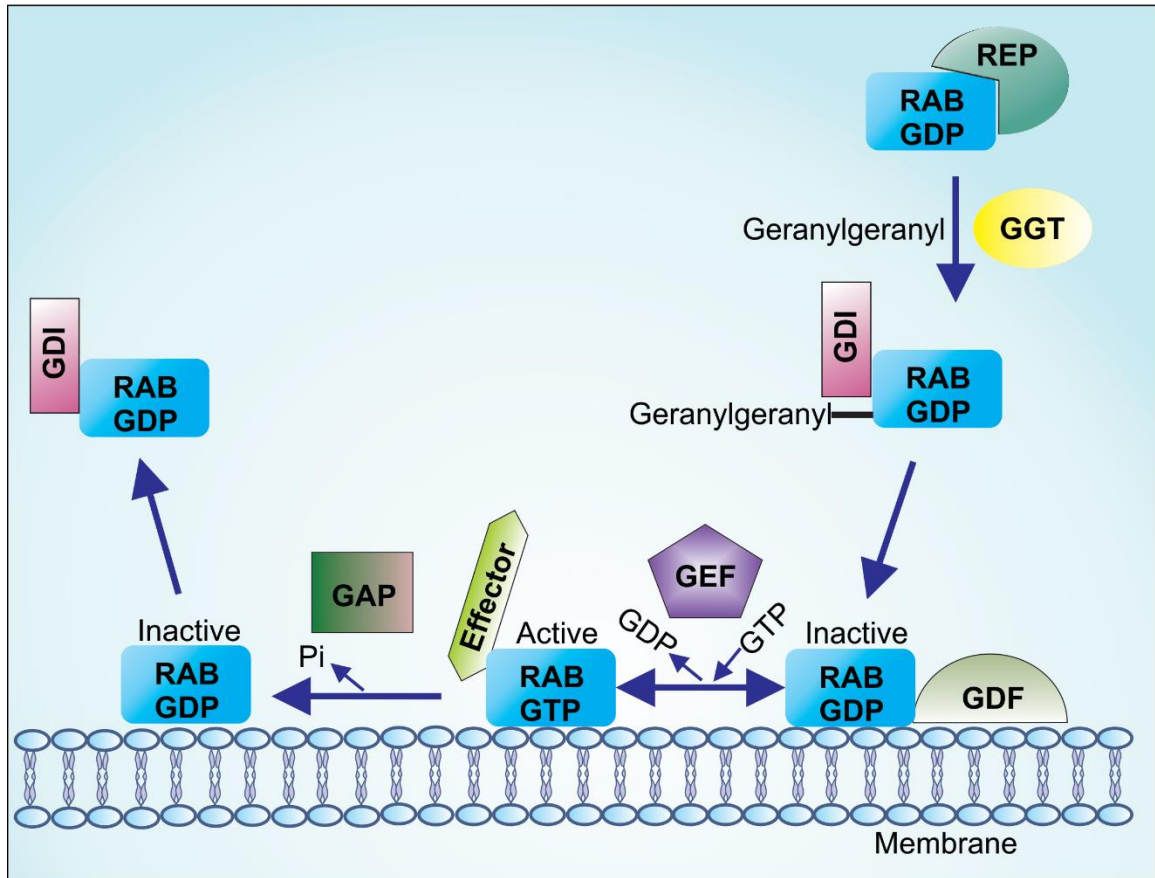


Figure 1.2 Membrane activation of Rab GTPases. GDP; Guanosine diphosphate. GTP; Guanosine triphosphate; REP; Rab escort protein. GGT; Geranylgeranyl transferase. GDI; GDP dissociation inhibitor. GEF; Guanine nucleotide exchange factor. GAP; GTPase activating protein.

Genetic mutations in proteins directly involved in Rab-mediated cellular trafficking have previously been reported in ALS. Deletion mutations in the *ALS2* gene, encoding the protein alsin, cause an autosomal recessive juvenile onset form of familial ALS [68, 380]. These deletion mutations, resulting in truncation of alsin, were predicted to result in loss of function [380]. In addition, mutations in *ALS2* have also been associated with infantile-onset hereditary spastic paraplegia [70, 381]. Initial bioinformatic analysis showed the presence of a putative RabGEF domain in alsin [68], which was then followed by experimental studies confirming the prediction [360, 361]. *In vitro* assays demonstrated that recombinant full length Alsин protein catalysed the dissociation of GDP from all three Rab isoforms; Rab5A, Rab5B and Rab5C but not from 11 other Rabs examined and hence showing Alsин as the specific RabGEF for Rab5 family of proteins [360]. Another study has also demonstrated that Alsин functions as a RabGEF for Rac1 [361], a small GTPase protein belonging to RAS

GTPase superfamily, which also function in membrane trafficking. ALS causing deletion mutations, truncates the carboxy-terminus of Alsin which harbors a VPS9 domain responsible for RabGEF function and endosomal localisation [360]. These deletion mutants of alsin were indeed shown to mislocalise from endosomes, and block the trafficking of lysosomes [360]. Similarly, mice with homozygous deletion of *ALS2* also displayed endosomal trafficking defects [382]. Hence a loss of RabGEF function could be linked with neurodegeneration in ALS. However the identification of repeat expansion in *C9ORF72*, has further linked Rab mediated cellular trafficking defects with ALS. Although the function of encoded C9orf72 protein is not known, recent bioinformatics studies have predicted a role for the C9orf72 protein in Rab-mediated membrane trafficking processes [349, 350]. A predicted DENN (differentially expressed in normal and neoplastic cells) domain was identified in C9orf72 protein structure, a key signature of RabGEFs protein. These studies suggested that C9orf72 could potentially function as RabGEFs because of the evolutionary conserved strong sequence and structural similarity to other DENN domain-containing RabGEFs. Whilst the hexanucleotide repeat expansion mutation in the *C9ORF72* gene is not present in the protein coding region, expression of the C9orf72 protein is reduced in ALS patients, leading to haploinsufficiency [32, 342]. Hence this could disrupt the potential function of C9orf72 in Rab-mediated trafficking pathways in ALS. However, the normal role of C9orf72 in Rab-mediated cellular trafficking is not clear, which is examined in this thesis (Chapter 6). Furthermore, the wobbler mouse, which develops features similar to ALS, shows abnormally enlarged Rab7-positive endosomes, suggesting Rab-mediated endosomal trafficking disruption, as a pathogenic mechanism in ALS [383].

1.13.3 Optineurin-mediated vesicular trafficking.

Optineurin is another important vesicular trafficking protein linked to ALS as well as other neurodegenerative disorders [221]. Optineurin is a multifunctional protein involved in autophagy, Golgi organisation, membrane trafficking and protein secretion [384]. Optineurin plays an important role in distinct cellular trafficking pathways, via its association with Rab8, huntingtin and myosin VI [384]. Optineurin is an established effector protein for Rab8, and is shown to bind only to the GTP-bound mutant of Rab8 (Q67L), but not to an inactive dominant-negative GDP-bound mutant (T22N) [385]. Optineurin associates with huntingtin and together with Rab8, optineurin/huntingtin/Rab8 complex mediates post-Golgi trafficking vesicular trafficking to lysosomes [386]. Furthermore optineurin as an adaptor for myosin VI

motor protein [351]. The binding of optineurin triggers dimerization and progressive movement of myosin VI motor on actin filaments [387]. Optineurin recruits myosin VI to Golgi apparatus and facilitates the transport of secretory proteins in complex with activated Rab8 [388]. Optineurin in association with myosin VI is also involved in the fusion of secretory protein at the plasma membrane [389]. Depletion of optineurin reduced the association of myosin VI with Rab8 and impaired the trafficking of secretory proteins from Golgi to plasma membrane [351]. Recently the optineurin/myosin VI complex was also demonstrated to mediate trafficking of autophagosomes on actin filaments [206]. Myosin VI in association with its adaptor proteins; NDP52, optineurin, T6BP and Tom1 was shown to be involved in maturation of autophagosomes and fusion with lysosomes [206]. Hence optineurin acts as an adaptor for myosin VI and links it to multiple cargos (Figure 1.3), playing an essential role in secretory pathway and autophagy related trafficking processes. Identification of familial ALS causing mutations in optineurin, suggest a possible disruption of its function in cellular trafficking which is examined further in this thesis (Chapter 4).

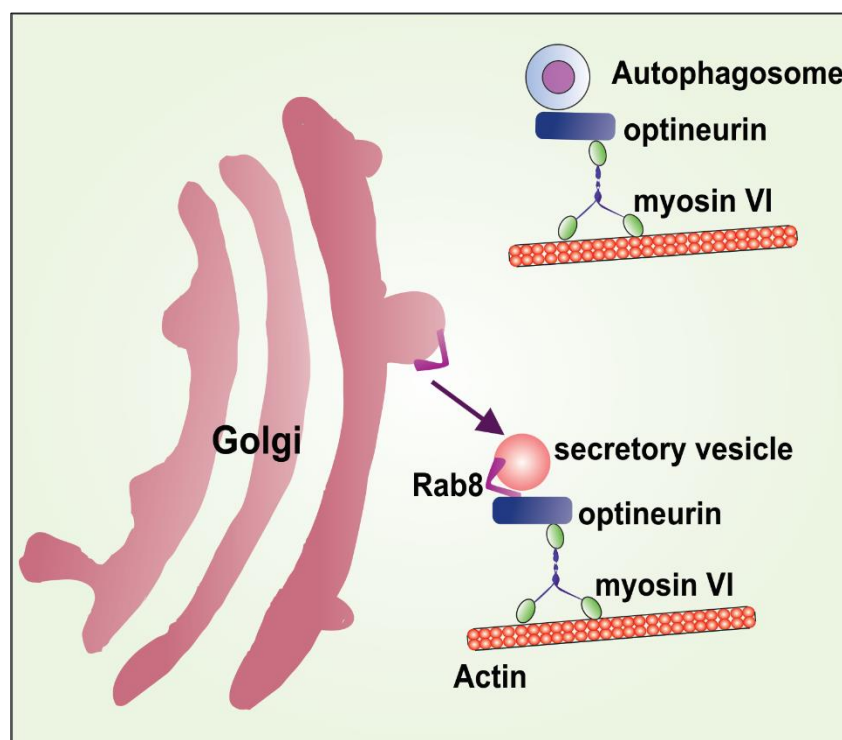


Figure 1.3 Optineurin regulates trafficking of secretory vesicles and autophagosomes. Optineurin links myosin VI motor with post Golgi secretory vesicles and autophagosomes, which are transported on actin filaments.

1.13.4 ER-Golgi vesicular trafficking

ER and Golgi organelles regulate the trafficking of secretory, transmembrane proteins and lipids. After synthesis and post-translational modifications in ER, proteins are transported in vesicles to Cis-Golgi compartments and subsequently to the trans-Golgi compartments, from which they are transported to distinct cellular and extracellular locations [390]. Inhibition of ER-Golgi associated classical secretory pathway, could result in accumulation of secretory protein in the ER lumen, triggering ER stress and UPR [201, 391]. The Golgi works in close association with the ER by the bidirectional vesicular transported system [392] and a block in ER-Golgi trafficking could also activate Golgi fragmentation [202]. The formation of Golgi stack requires continuous recycling of Golgi proteins to and from ER, via ER-Golgi vesicular transport [393]. Inhibition of protein export from ER disrupts Golgi organisation [394]. Furthermore, blockage of post Golgi vesicular trafficking could also result in accumulation of secretory proteins in ER and Golgi compartments subsequently activating ER and Golgi pathologies [316, 395]. Hence impairment of ER and Golgi associated vesicular trafficking, could activate two key pathogenic features observed in ALS; ER stress and Golgi fragmentation and thus warranting an examination of such trafficking defects in the pathogenesis of ALS.

The main mode for transport of secretory cargo from ER is via coat protein complex II (COPII), which is composed of five subunits: Sec23, Sec24, Sec13, Sec 31 (Figure 1.4), and the GTPase Sar1 [396, 397]. These COPII subunits soluble in the cytosol, associates with ER membrane to form coated vesicles which buds off from the ER. Sar1 is the first COPII subunit recruited to the ER. This binding and activation of Sar1 GTPase is mediated by Sec12, which acts as GEF at the ER membrane [398]. Activated Sar1 then subsequently recruits Sec23/Sec24 heterodimer and then the Sec13/Sec31 complex [399]. During COPII vesicle formation protein cargos are selectively recruited in COPII vesicles [400], while some proteins are also reported to flow into the vesicles unspecifically [401]. After budding from ER, COPII vesicles uncoated and fuse to each other to form the endoplasmic reticulum-Golgi intermediate compartment (ERGIC) or vesicular-tubular aggregates (VTCs) [402], which are then trafficked upon microtubules fuse with the Cis-Golgi compartment [403]. The Dynein/dynactin motor complex drives the transport of COPII vesicles on microtubules (Figure 1.4). Cytoplasmic dynein motor is linked to the cargo by associating with dynactin complex, composed of p150^{Glued}, p62, dynamin, actin related protein 1 (Arp1), CAPZ α and CAPZ β , p27 and p24. The Sec23 subunit of COPII complex was shown to interact directly

with the dynactin complex through the carboxy-terminal cargobinding domain of p150^{Glued} [404], and hence linking the COPII cargo with dynein motor. Rab1 has an established function in regulating budding, tethering and fusion of COPII vesicles during ER-Golgi transport [375, 405, 406]. Rab1 interacts with Sec23, Sec24 and Sec31 subunits to regulate COPII dynamics and function [405]. Activated form of Rab1, is shown to control the membrane association/dissociation dynamics of COPII [405].

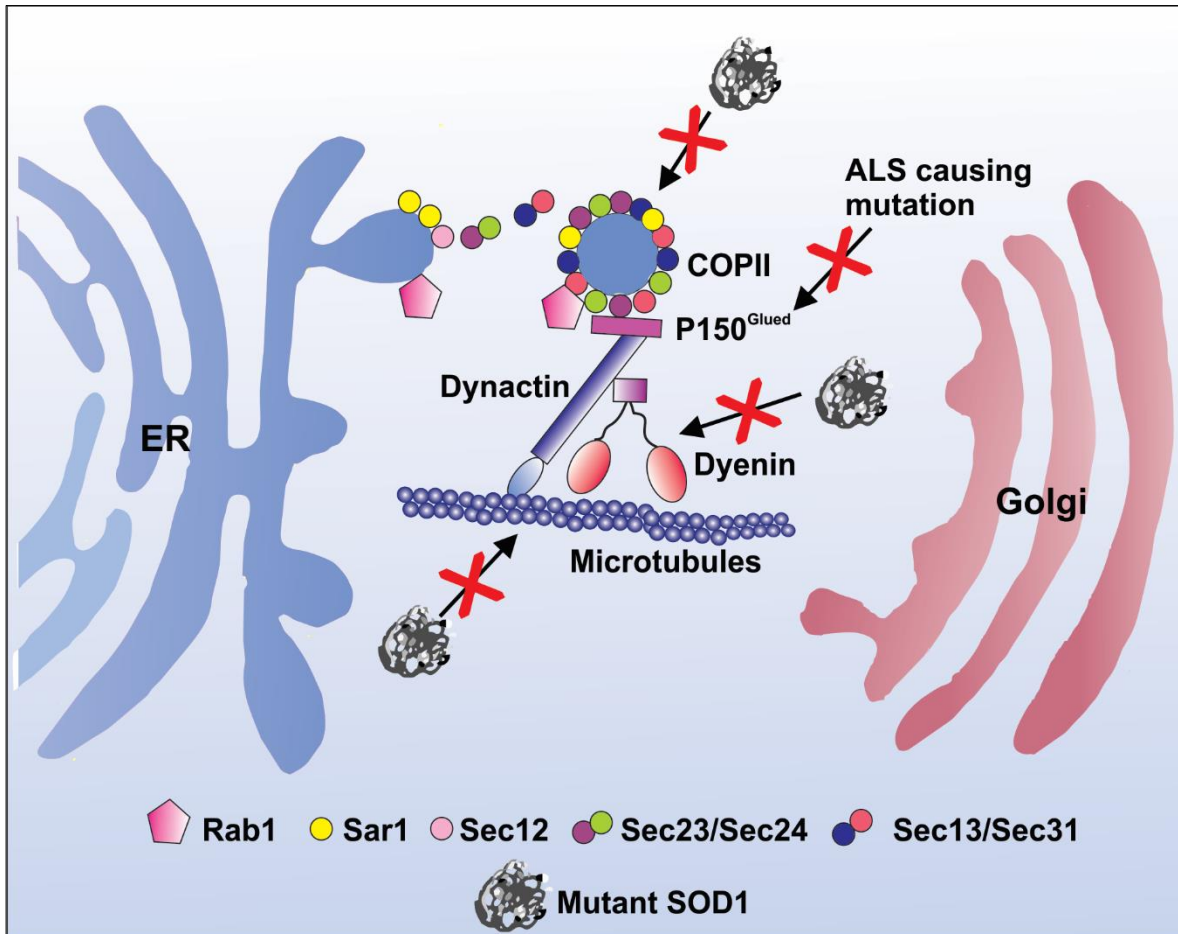


Figure 1.4 ER to Golgi vesicular trafficking and its possible disruption in ALS. COPII vesicles carrying the cargo from ER are transported on microtubules by dynein/dynactin motor complex. Rab1 plays a key role in dissociation of COPII vesicles from ER followed by tethering and fusion of COPII vesicles on microtubules. Mutant SOD1 aggregates block trafficking of COPII vesicles from ER to Golgi. Mutant SOD1 also inhibits microtubule organization and dynein functioning which could perturb ER-Golgi trafficking. Mutation in p150^{Glued} subunit which connects dynein/dynactin motor complex with COPII vesicles is also observed in familial ALS.

Previous evidence suggests that ER-Golgi trafficking pathway may be impaired in ALS. Mutation in the gene encoding p150^{Glued} causes familial ALS [67], and this mutation impedes the binding of p150^{Glued} with microtubules, resulting in dysfunction of dynactin [407]. VAPB is an ER transmembrane protein, which is involved in ER-Golgi vesicle transport in association with its binding partner, Yip1-interacting factor homologue A (YIF1A) [356]. In ALS, mutations in VAPB perturb its normal functioning, resulting in disruption of ER-Golgi vesicle transport [72]. In addition, mutant SOD1 has been shown to disrupt microtubule organisation and dynein motor functioning, which could affect ER-Golgi trafficking (Figure 1.4). Mutant SOD1 has also been demonstrated to interact with the dynein motor complex and recruit them into large cytoplasmic SOD1 aggregates, indicating disruption of dynein-mediated trafficking functions including ER-Golgi trafficking [408]. Similarly mutant but not wildtype SOD1 was also shown to aberrantly interact with tubulin and prevent tubulin polymerisation, disrupting microtubule organisation [409]. Furthermore, our laboratory recently demonstrated that mutant SOD1 inhibits vesicular trafficking between the ER and Golgi [200]. COPII was found to co-localise with mutant SOD1 inclusions in NSC-34 cells and mutant G93A SOD1 mouse tissues, providing a possible explanation for inhibition of ER-Golgi trafficking by mutant SOD1. Inhibition of ER-Golgi transport also preceded all the other cellular pathologies examined in this study in cells expressing mutant SOD1 including ER stress, Golgi fragmentation, protein aggregation, inclusion formation and apoptosis [200]. Hence ER-Golgi trafficking inhibition could be an upstream trigger for neurodegeneration in SOD1-linked familial ALS cases. These findings also warrants further examination of ER-Golgi trafficking defects by other pathogenic proteins linked with ALS.

1.13.5 Axonal transport

Motor neurons are highly dependent on efficient axonal trafficking, because of large axons which extend up to several meters [410]. Mutations in proteins involved in axonal trafficking are present in familial ALS, emphasizing the vulnerability of motor neurons to axonal trafficking disruption (Table 3). Mutations in genes encoding proteins essential for axonal structure and function such as neurofilament heavy chain [78] and peripherin [84, 86] have been reported in rare cases of ALS. ALS causing mutations in dynactin, induces swelling and denervation of axons in mice models [348], suggesting disruption of axonal trafficking. Consistently, profilin and TUBA4A mutations could also attenuate axonal trafficking by destabilising cytoskeletal network in axons. Recent studies have also demonstrated a role

for spatacsin [367] and p62 [358, 359] in axonal vesicular trafficking processes, suggesting further studies to examine whether ALS linked genetic mutations in these genes could impede axonal trafficking. Increasing evidence also suggests that both TDP-43 and FUS mediate trafficking of specific mRNA granules along the axon for local translation [148, 347, 411]. The mRNA's transported by TDP-43 and FUS encode proteins such as neurofilament light chain (NFL) and actin-stabilizing protein Nd1-L, which are involved in axon guidance and maintenance [148, 347]. Furthermore *in vitro* studies have demonstrated that ALS mutant TDP-43 reduces axonal mRNA trafficking, presumably by loss of function [200, 347].

Cellular trafficking pathways could also be disrupted by 'gain of toxic function' mechanisms in ALS. An increasing body of evidence also indicates that mutant SOD1 impairs retrograde and anterograde axonal trafficking [412, 413]. Axonal transport is primarily carried out by two major families of motor proteins; kinesin for anterograde transport, and the dynein/dynactin motor complex for retrograde transport [414]. In transgenic mouse models, mutant SOD1 impaired anterograde trafficking of neurofilaments and tubulin in the axon. Interestingly these defects were also observed prior to the onset of disease symptoms, indicating axonal transport defects are an upstream event triggered by mutant SOD1 [207, 415]. Misfolded SOD1 also inhibits anterograde axonal trafficking by directly interacting with KAP3 (kinesin associated protein 3), a component of kinesin-2 motor complex, in motor axonal lysates obtained from mutant G93A SOD1 mice [416]. Additionally, mutant SOD1 inactivates axonal kinesin-1 by activation of p38 mitogen-activated protein kinase (MAPKs), causing increased kinesin-1 phosphorylation [417]. Furthermore mutant SOD1 impairs dynein-mediated retrograde trafficking. Mutant but not wildtype SOD1 specifically interacts with dynein in G93A and G85R rodent spinal cord tissues. This interaction occurred before disease onset and correlated with disease progression [408]. Mutant SOD1 also alters the distribution of the dynein complex in axon of cultured motor neurons, impairing retrograde transport [418]. These data therefore provide evidence that mutant SOD1 disrupts distinct cellular trafficking processes by a gain of toxic function.

In addition to the reported loss of axonal mRNA trafficking function in ALS [347], mutant FUS and TDP-43 could also mediate axonal trafficking disruption through the formation of toxic stress granules and aggregates. [335, 337, 338]. NFL mRNA associates with TDP-43-positive stress granules in ALS patients, suggesting that this could limit the availability of neurofilament protein and thus disrupting axonal trafficking [116, 419]. Similarly ALS FUS mutants reduced the levels of survival motor neuron (SMN) in the axon, by sequestration of

SMN protein into cytoplasmic FUS aggregates [420]. SMN plays a key role in trafficking of mRNA in the axon [421, 422], which may therefore be impaired by interaction mutant FUS.

1.13.6 Cellular trafficking disruption in sporadic ALS.

There is also indirect evidence for cellular trafficking disruption in sporadic ALS [7, 300, 325, 423, 424]. As mentioned above, ER-Golgi pathologies are present in sALS patients [295, 320, 321], raising the possibility that ER-Golgi mediated trafficking is disrupted in sporadic ALS. Optineurin is recruited into motor neuronal inclusions in sporadic ALS patients [384], suggesting that this may reduce the levels of optineurin protein in these tissues, thus inhibiting optineurin-dependent trafficking functions in ALS. The levels of dynactin are reduced in sporadic ALS patient tissues, correlating with defective transport and accumulation of autophagosomes [424, 425]. Quantitative *in situ* hybridization has revealed 60% decrease in NFL mRNA in motor neurons of sALS patients compared to control cases [423]. In addition, axonal accumulation of neurofilament tangles, and disorganisation and swelling of the axon are common features in sporadic ALS patients [258, 259], suggesting disruption axonal functions. Consistent with this notion, accumulation of mitochondria and lysosomes in the proximal axon hillock, due to impairment of fast axonal transport, is observed in sporadic ALS [426]. NOGO-A, a myelin based axonal outgrowth inhibitor, is upregulated in the muscles of patients with ALS [427, 428].

Genome-wide association studies have also linked single-nucleotide polymorphisms (SNPs) in genes encoding cellular trafficking proteins with sporadic ALS. Reduced expression of kinesin-associated protein 3 (KIFAP3), a member of the kinesin motor complex, is associated with increased survival of sALS patients [389, 426]. Similarly, a SNP in the UNC13A gene, which encodes a protein involved in exocytic trafficking of synaptic vesicles [197], correlates with shorter survival of sporadic ALS patients [202, 429]. A more recent study has also identified genetic variations of the UNC13A gene as a risk factor for ALS [423]. Hence these data provide some evidence for disruption of cellular trafficking as a common pathological mechanism in sporadic and familial ALS.

1.14 Cell to cell transmission of pathology in ALS

A clinical feature of ALS is the multi-focal onset, followed by contiguous spread of pathology among surrounding upper and lower motor neurons. This spread of pathology also correlates with the progressive development of clinical features in the advanced stages of disease [18, 430] and it is also evident in other neurodegenerative disorders including Alzheimer, Parkinson and dementia with Lewy bodies [431]. Understanding individual pathogenic mechanisms in ALS emphasises the need to understand how the toxicity is progressively transmitted between motor neurons, in order to develop an effective therapeutic strategies [432-435]. Several possible mechanisms for propagation of disease have been proposed including, the release of toxic signals by dying neurons [436], and the chronic release of pro-inflammatory cytokines by neighbouring microglia and astrocytes [437]. However there is also evidence that a prion-like seeding and transmission mechanism is responsible for disease propagation in some neurodegenerative disorders [431, 438, 439]. This hypothesis would also explain the spread of pathogenic protein lesions over a long distance [431]. Prions are transmissible infectious proteins which causes neurodegenerative Creutzfeldt–Jakob disease in humans. The misfolded forms of prion protein (PrP^{Sc}) are ‘infectious’ which seeds aggregation of the native form (PrP^{C}) and thus misfolding is transmitted from cell to cell in human prion disease [440]. The term “prion-like” is used to describe the ability of a misfolded protein to seed further aggregation and spread pathology from one cell to another, mimicking the features of prion [441, 442]. Aggregates of A β (amyloid β), Tau and α -synuclein all exhibit prion-like seeding and transmission in *in vitro* models of disease [443-450]. Furthermore observation of α synuclein positive lewy bodies in the newly transplanted nigral neurons, suggest that pathological α -synuclein could be transmitted from the diseased striatal neurons to grafted neurons in parkinson’s patients, providing strong evidence for prion-like transmission in human patients [451, 452]. Hence this raises the question of whether a prion-like mechanism could explain the spread of pathology in ALS, similar to other neurodegenerative disorders [213, 453].

Recent studies have suggested that misfolded mutant proteins in ALS could exhibit a prion-like seeding mechanism. Aggregates prepared from recombinant H46R mutant SOD1 are taken up by Neuro2A cells, which subsequently induces aggregation of intracellular, soluble H46R SOD1[453]. Expression of SOD1 mutations G127X and G85R in human cell lines induced misfolding of natively folded wildtype SOD1, detected by misfolded SOD1 specific monoclonal antibodies [114]. Also overexpression of wildtype SOD1 is able to induce

misfolding of endogenous SOD1 in human cell lines, similar to mutant SOD1, thus implying that the ability to seed aggregation is common to misfolded forms of both wildtype and mutant SOD1 [114]. Studies based on yeast prion proteins have identified a distinctive 'prion domain' typically enriched in asparagine, glutamine, tyrosine and glycine residues, which is essential for the prion-ogenesis [454, 455]. Interestingly this prion-like domain has been identified in the C-terminus of TDP-43 and in the N-terminal domain of FUS [456], raising the intriguing possibility that TDP-43 and FUS could exhibit a prion-like mechanism in ALS. Recent findings of mutations in other RNA binding proteins that also contain prion-like domains, including hnRNPA2B1, hnRNPA1 and TAF15 (Table 1.2), further supports this hypothesis. Moreover, the C-terminal region of TDP-43, which contains the prion-like domain, was demonstrated to form the core of amyloid-like fibrillar aggregates generated *in vitro* from recombinant full length TDP-43 [219]. Transduction of fibrillar TDP-43 aggregates was also demonstrated to seed intracellular aggregation in HEK293T cells [219]. Additionally, *in vitro* studies have demonstrated that amyloid-like fibrillar aggregates produced from mutant G156E FUS can efficiently seed the aggregation of wildtype FUS [457]. Hence together these data suggest that misfolded/aggregated forms of SOD1, TDP-43 and FUS may exhibit a prion-like seeding mechanism in ALS. However it needs to be established whether the transmission of these proteins between cells can trigger specific ALS pathogenic mechanisms in the acceptor cells. This would therefore provide an explanation for how pathogenic mechanisms are spread from cell to cell in ALS.

1.15 Aims of thesis.

Multiple evidence implicate cellular trafficking disruption in the pathogenesis of ALS. However in order to completely understand the role of cellular trafficking disruption in the pathogenesis of ALS, the possible consequence of such defects should be examined. To examine how defects in distinct cellular trafficking pathways could be linked with key pathogenic mechanisms observed in ALS, each chapter of this thesis addresses specific aims as described below.

Chapter 2 Extracellular wildtype and mutant SOD1 induces ER-Golgi pathology characteristic of amyotrophic lateral sclerosis in neuronal cells.

The aims of the studies described in Chapter 1 were to examine whether extracellular misfolded wildtype and mutant SOD1 could be taken up by neuronal cells, and to analyse whether such an uptake could induce ALS specific pathogenic mechanisms as ER stress, Golgi fragmentation, leading to apoptotic cell death. This chapter is presented as a published manuscript.

Chapter 3 Defects in optineurin and myosin VI mediated cellular trafficking in amyotrophic lateral sclerosis

The aims of the studies described in Chapter 2 were to examine whether ALS causing mutations in optineurin could perturb its functions in cellular trafficking in association with myosin VI. The studies presented were also aimed to determine whether aberrant misfolding of optineurin in sporadic ALS patients, could alter its normal cellular localisation and interaction with myosin VI. This chapter is presented as a published manuscript.

Chapter 4 Cellular mechanisms induced by novel CCNF mutation in ALS

The aim of the studies described in Chapter 4 was to determine whether a novel ALS associated mutation in *CCNF* gene encoding cyclin F, altered protein subcellular localisation, formed stress granules, or induced ER stress and apoptotic cell death in neuroblastoma cells.

Chapter 5 C9orf72 regulates endosomal trafficking

The aim of the studies described in Chapter 4 was to determine the normal function of C9orf72 protein in Rab mediated endosomal trafficking.

Chapter 2

2.Materials and methods

2. Materials and methods

This section lists general materials and methods, specific methods of individual chapters are presented respectively.

2.1 Molecular biology

2.1.1 Luria-Bertani (LB) medium

Luria Bertani broth was used as the liquid culture medium to support growth of bacterial *Escherichia coli* (*E. coli*). LB broth was prepared by dissolving 10 g bacto-tryptone (Oxoid), 5 g yeast extract (Oxoid) and 10 g NaCl in 1 litre dH₂O, pH was then adjusted with 200 µl of 5 M NaOH. The broth was then autoclaved and stored in tightly closed containers in a sterile environment. Antibiotics ampicillin or kanamycin sulphate (Sigma) were added prior to usage. Stock antibiotic solutions were prepared at 100 mg/ml in dH₂O, filter sterilised and stored at -20°C. Antibiotics were added at a final concentration of 50 µg/ml for ampicillin and 100 µg/ml for kanamycin.

LB agar was the solid culture medium used to support growth of *E. coli* in petri dishes. LB agar was prepared by adding 20 g of bacteriological Agar (Oxoid) to LB broth prior to autoclaving. After autoclaving, either ampicillin or kanamycin antibiotic was added, while the LB agar was still warm, mixed, and then poured into sterile petri dishes. The plates were stored at 4°C or used immediately upon setting.

2.1.2 Transformation of competent cells

XLI Blue supercompetent cells (Stratagene) or TOP10 competent cells (Invitrogen) were thawed on ice. The cells were then aliquoted into 40-80 µl volumes and mixed with appropriate volume of DNA. Cells were incubated on ice for 30 mins, and then heat shocked at 42°C for 45 s. Cells were then immediately placed on ice for a further 2 mins, and 250 µl of SOC media (Invitrogen) was added. Tubes were then incubated for 1 h at 37°C in a shaking incubator, at ~300 rpm. Aliquots of 50 µl and 200 µl of each reaction were spread onto pre-warmed LB agar plates with appropriate antibiotics. Plates were then inverted and incubated at 37°C overnight.

2.2 Plasmid isolation

Small-scale DNA isolation was performed for mutagenesis screening, and initial mammalian cell transfection trials. Plasmids were isolated from bacterial cultures using QIAprep spin miniprep kits (Qiagen). Briefly, a single bacterial colony from an overnight (16 h) LB-agar plate was inoculated into ~4 ml LB medium with respective antibiotic and incubated at ~250

rpm, 37°C for 12-16 h. The cultures were processed according to the manufacturer's protocol, and the DNA from each spin tube was eluted with 50 µl of nuclease-free H₂O and stored at -20°C. DNA was then quantified by spectrophotometry. Large-scale DNA isolation was performed for all cell transfections using QIAGEN plasmid maxi kits with QIAGEN-tip 500 columns. Briefly, part of a single bacterial colony from an overnight (16 h) LB-agar plate was inoculated into ~2 ml LB medium with antibiotic and incubated at ~250 rpm, 37°C for 7-8 h. The starter culture was used to inoculate ~150 ml of LB medium with appropriate antibiotic, which was then incubated at ~250 rpm, 37°C for 12-16 h. The cultures were processed according to the manufacturer's protocol, and the air-dried DNA pellet from each QIAGEN-tip 500 was resuspended in 200-500 µl of nuclease-free H₂O and stored at -20°C. DNA was quantified by spectrophotometry and agarose gel electrophoresis, and analysed by restriction enzyme digestion where appropriate. DNA was diluted to 200 ng/µl working stocks with nuclease-free H₂O for use in transfection reactions.

2.3 DNA quantification

DNA concentration was quantified directly using a Nanodrop ND-1000 spectrophotometer. A conversion of $1.0 A_{260} = 50 \text{ ng/}\mu\text{L}$ was used to determine the original DNA concentration, and the A_{260}/A_{280} ratio was used to determine DNA purity, where $A_{260}<1.75/A_{280}<1.85$ was deemed sufficiently pure for transfection experiments.

2.4 DNA purification by ethanol/sodium acetate precipitation

DNA was purified or concentrated by precipitated after mixing with 1/10th volume of 3 M sodium acetate pH 5.2 and 2X volume of 100% ethanol (stored at -20°C). The reaction was kept at -20°C for 30 to 120 min and the precipitated DNA collected by centrifugation at 16,100 g for 15 min at 4°C. The DNA pellet was rinsed with 2X original volume of 70% ethanol and centrifuged at 16,100 g for 5 min at 4°C. The pellet was air-dried at room temperature for ~10 min or at 56°C for 2-3 min. Precipitated DNA was then resuspended in an appropriate volume of nuclease-free water.

2.5 Mutagenesis

Mutagenesis was performed using Stratagene QuikChange II site-directed mutagenesis kits (Agilent technologies) according the manufacturer's protocol, with primers shown in Table 2.1. Primers for mutagenesis were designed using the Stratagene QuikChange Primer Design Program (available at <http://www.stratagene.com/sdmdesigner>) or Primer3 program (available at <http://bioinfo.ut.ee/primer3-0.4.0/>). Primers for QuikChange mutagenesis were custom made and supplied by Sigma-Aldrich. Primers were dissolved at a stock

concentration of 1.0 µg/µl and a working concentration of 25 ng/µl in nuclease-free dH₂O. Included dNTPS were aliquoted as 5 µl aliquots. Primers, dNTPs and buffers are stored at -20°C to prevent degradation. Reactions were prepared containing 5 µl 10X reaction buffer, 2 µl (40 ng) plasmid DNA, 5 µl (125 ng) forward primer, 5 µl (125 ng) reverse primer, 1 µl dNTPs and 32 µl nuclease-free H₂O, mixed, and then 1 µl (2.5 U) PfuUltra DNA polymerase was added. Reactions were mixed and cycled on a Veriti thermal cycler (Applied Biosystems) as follows:

95°C 5 min

95°C 30 s

55°C 1 min x16-18 cycles

68°C 1 min/kDa plasmid length

Reactions were placed on ice to cool below 37°C and then parental DNA was digested by addition of 1 µl (10 U) DpnI with incubation at 37°C for 1 h. The DNA from the reactions were concentrated by ethanol/sodium acetate precipitation and were transformed into XL1-Blue supercompetent cells provided with the Stratagene QuikChange II kit and colonies screened for successful mutations by sequencing.

Primer Name	Primer Sequence
OPTN E478G For	5'-GTTCTGATTTTCATGCTGGAAGAGCAGCGAGAGAGAA-3'
OPTN E478G Rev	5'-TTCTCTCTCGCTGCTCTTCCAGCATGAAAATCAGAAC-3'
OPTN Q398X For	5'-GATGACACACAACAAGCTTCTTTAAGAACA TAATAATGCATTGA-3'
OPTN Q398X Rev	5'-TCAATGCATTATTATGTTCTTAAAGAAGCTTG TTGTGTGTCATC-3'
OPTN E50K For	5'-GAAAGAGCTCCTGACCAAGAACCACCAGCTGAA-3'
OPTN E50K Rev	5'-TTCAGCTGGTGGTCTTGGTCAGGAGCTCTTTC-3'

Table 2.1 Mutagenesis primers

2.6 DNA sequencing

Each of the purified plasmids were sequenced by multiple primers in separate reactions to produce overlapping regions in which all bases of the insert and flanking regions were covered. The primers used for sequencing were designed using Primer3 program are listed in Table 2.2. Samples with ~1 µg of plasmid and at least 2 µl of respective Primers each at a concentration of 5uM per reaction were submitted for sequencing to Applied Genetic

Diagnostics unit, Department of Pathology, University of Melbourne. Sequences results were analysed using ApE program.

Primer Name	Primer Sequence
OPTN Seq For 1	5'- GCCATGAAAGGGAGATTTGA-3'
OPTN Seq For 2	5' – GGAGACTGTTGGAAGCGAAG-3'
OPTN Seq For 3	5' – TTGATGGAGATGCAGAGTCG-3'
OPTN Seq Rev 1	5' – TCTGCTTCTCCTTCAGCCAT-3'
OPTN Seq Rev 2	5' - AACTTCCATCTGAGCCCTGA-3'

Table 2.2 Sequencing primers

2.7 Mammalian cell culture

2.7.1 Fetal Calf serum (FCS) heat inactivation

FCS purchased from Gibco was removed from -20°C, allowed to thaw and equilibrate to room temperature then suspended in a 60°C water bath. The FCS was allowed to equilibrate and then kept at 60°C for 30 mins with frequent mixing. The heat-inactivated FCS was aliquoted in 50 ml aliquots and stored at -20°C.

2.7.2 Cell maintenance

Human neuroblastoma SH-SY5Y, mouse motor neuron-like cell line NSC-34 (provided by Professor Neil Cashman, Vancouver Coastal Health ALS Centre, University of British Columbia) and Neuro2A mouse neuroblastoma cells were used throughout this study. SH-SY5Y neuroblastoma cells were developed from a bone marrow metastasis in a four year old girl [432]. Neuro2A cells were established from a spontaneous neuroblastoma tumour of a strain-A albino mouse [433]. NSC-34 cells are a hybrid mouse motor neuron-like cell line, which were developed by fusing mouse neuroblastoma (N18TG2) cells with motor neuron-enriched mouse embryonic spinal cord cells [434]. These cell lines were selected because of similarities with terminally differentiated neurons while being able to be cultured continuously. In the original studies, SH-SY5Y cells were tested positive for tyrosine hydroxylase and dopamine- β -hydroxylase, which is characteristic of catecholaminergic neurons [432], while Neuro2A cells displayed electrical excitability and acetylcholine sensitivity with the presence of neuron-specific protein 14-3-2, steroid sulfatase and glycosphingolipids [435]. NSC-34 cells were shown to resemble some characteristics of motor neuron including conduction of action potentials, expression of neurofilament triplet

proteins, and acetylcholine synthesis [434]. All these three cell lines were cultured strictly only up to 20 passages to maintain the neuronal characteristics. NSC-34 cells were obtained directly from Neil Cashman, hence we were confident that these cells maintain their original published characteristics. The cells were maintained in complete Dulbecco's modified Eagle medium (cDMEM) (Gibco), with 10% heat-inactivated FCS, 100 µg/ml penicillin and 100 µg/ml streptomycin. Cells were incubated at 37°C under 5% CO₂ and passaged nearing complete confluence. Passaging required treating cells with 1 ml of Trypsin-EDTA solution (Gibco) and incubating at 37°C for 2 min to detach cells from the plate. Cells were collected by the addition of cDMEM and centrifugation at 1200 rpm for 5 minutes. The cell pellet was resuspended in 1 ml DMEM with 10% FCS and concentration determined using an improved Neubauer haemocytometer. Briefly, 10 µl cell suspension were added to 90 µl DMEM and 100 µl trypan blue (Invitrogen) to give a 1:20 dilution. The number of viable (non-blue stained) cells in each of four 1 mm² areas (100 nl volume) were counted and the mean number of cells was multiplied by 20 (dilution factor) and 10⁴ to give cell number per ml. Cells were plated into 96- or 24-well plates as required, and subcultured into fresh T75 flasks at 1:10 dilution.

2.7.3 Transfection

Lipofectamine 2000 transfection reagent (Invitrogen) was used to transfect plasmid DNA into NSC-34, Neuro2A or SH-SY5Y cells, according to the manufacturer's protocol. Briefly, cells were plated at 0.5-2x10⁵ cells per well in 24-well plates in DMEM medium without antibiotics, 24h before transfection. DNA and lipofectamine mixture prepared in OptiMem medium (Invitrogen) were added to cells cultured. The medium is then replaced with fresh cDMEM medium with antibiotic, 5h after transfection.

2.7.4 Long-term storage of cell lines

Cells at low passage number were collected by trypsinisation in antibiotic-free DMEM with 20% FCS. Approximately 1-3x10⁶ cells were resuspended in this medium with 10% sterile DMSO in a final volume of 1 ml in cryotubes (Nunc). Cells were cooled to -80°C in an isopropanol-filled cryopreservative chamber, which causes a gradual decrease in temperature, and were then transferred to liquid nitrogen for long-term storage. Upon thawing, cells were rapidly warmed to 37°C and immediately plated in T75 flasks in DMEM with 10% FCS and 1% penicillin/streptomycin

2.7.5 Cell lysate preparation

Cell lysates were collected, by harvesting cells in Tris-NaCl (TN) buffer (50 mM Tris-HCl pH 7.5, 150 mM NaCl) with 0.1% (w/v) SDS and 1% (v/v) protease inhibitor cocktail (Sigma) and incubating on ice for 10 min. The supernatant (SDS-soluble fraction) was separated from the pellet fraction by centrifugation at 16,100 g for 10 min. The Pellet (SDS-insoluble fraction) was solubilised by sonicating with 250 µl of TN buffer containing 8M urea.

2.7.6 Protein quantification

Protein concentration of cell lysates was determined using the Pierce BCA Protein Assay Kit (Thermo-Scientific) following the manufacturers protocol. The procedure involved a 96-well plate, to which duplicate preparations of dilutions of bovine serum albumin (BSA) standards and lysates (1:10 dilution) were added to the plate in 10 µl volumes. The BCA working reagent (supplied by the kit) was then applied to the samples and incubated at 37°C for 20 mins. The plate analysed using the SpectraMax M2 Microplate Reader (Molecular Devices) at an absorbance of 562 nm. A standard curve was created from the BSA standards and the protein concentration of each sample was determined in accordance to the curve.

2.8 SDS-PAGE and Immunoblotting

2.8.1 Materials

SDS-PAGE resolving and stacking gel

Cell lysates were subjected to electrophoresis on 7.5%, 9.25% or 12.5% SDS-polyacrylamide gel. For two resolving gels, 30% acrylamide and H₂O were mixed with 2.82 ml resolving buffer and 150 µl 10% SDS according to percentage acrylamide required:

% Gel	Vol 30% acrylamide (ml)	Vol H ₂ O (ml)
7.5	3.75	8.25
9.25	4.625	7.3
12	6.0	6.0

To the above mixture, 120 µl 10% ammonium persulphate and 120 µl TEMED were added and the gel rapidly poured into the rig then overlayed with H₂O until set.

For two stacking, 1.125 ml of 30% acrylamide, 3.9 ml H₂O, 1.41 ml resolving buffer, 112.5 µl 10% SDS, 100 µl 10% APS and 100 µl TEMED were mixed and poured onto resolving gels. Appropriate comb was insert immediately to form wells.

5X SDS sample buffer

5X SDS sample buffer contained 250 mM Tris-HCl, pH 6.8, 10% SDS, 5% glycine, 0.025% bromophenol blue and 50% glycerol. To which 10% β-mercaptoethanol was added as a reducing agent upon immediate use.

SDS-PAGE Running Buffer

10X SDS-PAGE running buffer was prepared by dissolving 30 g Tris, 148 g glycine and 10 g SDS in 1 L dH₂O. It was then diluted 1 in 10 in dH₂O to prepare working solution with the final concentration of 0.12 M Tris, 0.1% SDS (g/L) and 0.96 M Glycine (g/L).

10X Tris-buffered saline (TBS)

12.1 g of Tris and 88 g of NaCl were dissolved in 1 L of dH₂O and stored at room temperature. To make up 1X working solution, the stock was diluted 1 in 10 in dH₂O with the pH adjusted to 8.0 with HCl. The resulting working solution contains 10mM Tris-HCl and 150 mM NaCl.

10X Tris-buffered saline with Tween-20 (TBS-T)

To each 1 L of 10X TBS, 5 ml of Tween-20 (polyoxyethylene sorbitol monolaureate, Sigma) was added. For 1X working solution, the stock was diluted 1 in 10 in dH₂O and the pH was adjusted to 8.0 with HCl. The working solution contains 10 mM Tris-HCl, 50 mM NaCl and 0.05% Tween-20.

10X Immunoblot Transfer Buffer

30 g Tris and 148 g glycine were dissolved in 1 L dH₂O, to make 10x transfer buffer, which is then diluted 1 in 10 with dH₂O, to make 1X working solution. Final 1X transfer buffer was comprised of 25 mM Tris, 190 mM Glycine and 20% Methanol.

Blocking Buffer

Blocking buffer consists of 5% Skim milk powder in TBS-T with 0.05% NaN₃ or 3% BSA in TBS-T with 0.05% NaN₃.

2.8.2 SDS-PAGE procedure

Cell lysates with 30-50 µg protein concentration were electrophoresed through 7.5%, 9.25% or 12% SDS-polyacrylamide gels. Samples were prepared in 5X SDS sample buffer (final concentration of 1X) and were heated at 95°C for 5 min. SeeBlue Plus 2 Pre-stained Markers (Invitrogen) was added to the first well of the gel then samples were then loaded, and electrophoresed for 1.5 h at 100 V. The gels were electrophoresed using the Mini-PROTEAN Tetra cell system (Bio-Rad).

2.8.3 Immunoblotting procedure

SDS-PAGE gels were transferred onto nitrocellulose membranes (Bio-Rad) in order to probing with antibodies to detect specific proteins within the cell lysate samples. A wet transfer method was carried out using the Mini-Trans blot cell system (Bio-Rad) for 1 h at 100 V. After the transfer, the membranes were incubated with the appropriate blocking buffer for 1 h at room temperature. The membranes were probed with the primary antibody which has been diluted in the blocking buffer in appropriate concentrations (Table 2.3) overnight at 4°C. The membrane were then washed once with TBS-T and then twice with TBS, followed by incubation for 1 h at room temperature with secondary antibodies (Chemicon): HRP-conjugated donkey anti-sheep/goat (#AB324P, 1:4000), goat anti-rabbit (#AB132P, 1:10,000), or goat anti-mouse (#AB326P, 1:4000).diluted in TBS-T (Table 2.3) for 1 hour at room temperature. The membrane is again washed three times as stated above. Lumi-Light Western blotting substrate (Roche) was applied to the membranes to allow detection of the bands and visualised using G:Box Chemi imager (SYNGENE) using GeneSys software. For subsequent re-blotting, the blots were then stripped with Re-Blot Plus solution (Chemicon) and were reprobed with another antibody as stated above.

Protein (antigen)	Dilution	Species	Manufacturer and Catalog Number
SOD1	1:1000	Sheep	Calbiochem; 574597
Optineurin (INT)	1:500	Rabbit	Cayman Chemical; 100002
Myosin VI	1:500	Rabbit	Santa Cruz; SC-50461
Myosin VI	1:500	Mouse	Sigma; M0691
Cyclin F	1:500	Rabbit	Santa Cruz; SC-953
BiP	1:4000	Rabbit	Stressgen; SPA-826
CHOP	1:400	Mouse	Santa Cruz; SC-7351 [B-3]

Xbp1	1:400	Rabbit	Santa Cruz; 7160
IRE1	1:600	Rabbit	Santa Cruz; 20790
LC3	1:1000	Rabbit	Novus Biological; NB100-2220
Sp1	1:1000	Rabbit	Santa Cruz; sc-14027
C9ORF72	1:500	Rabbit	Santa Cruz; sc-138763
GADPH	1:4000	Mouse	Ambion; AM4300
VSVG	1:1000	Rabbit	Sigma; V4888
FLAG	1:4000	Mouse	Sigma; F3165 [M2]
β-actin	1:2000	Mouse	Sigma; A5441 [AC-15]

Table 2.3 Primary antibodies used for Immunoblotting.

CHOP, optineurin, LC3 and C9orf72 were diluted in 5% skim milk in TBS-T, and the rest were diluted in 3% BSA in TBS-T.

2.9 Immunocytochemistry

2.9.1 Materials

4% W/V Paraformaldehyde

4 g of paraformaldehyde (PFA) in 100 ml dH₂O were mixed on a heated magnetic stirrer for 10 min at 60°C in a fume cupboard. One NaOH pellet was added, and once clear the solution was removed from heat and 500 ml 0.2 M phosphate buffer were added. The solution was adjusted to pH 7.4 with HCl and decanted to remove any debris.

Phosphate buffered saline (PBS)

5 PBS tablets (Sigma) were dissolved in 1 L dH₂O and stored at room temperature. The pH 7.4 solution contained 0.01 M phosphate buffer, 0.0027 M KCl and 0.137 M NaCl.

2.9.2 Immunocytochemistry procedure

For immunocytochemistry cells were plated on 24 well plates with coverslips (13 mm; MENZEL). The coverslips were sterilized by autoclaving and coated with approximately 150 μ L poly-L-lysine (PLL, diluted 1:20 in sterile H₂O from 0.01% stock, Sigma). Cells were then plated after washing thoroughly with 1X Phosphate buffered saline (PBS; Sigma). After transient transfection (24, 48 or 72 hrsrs), cells on coverslips were washed with PBS and fixed with 4% paraformaldehyde (PFA) for 10 min at room temperature.

Cells were washed twice with PBS and permeabilised with 0.1% Triton-X 100 in PBS for 10 min. Cells were washed again with PBS three times and were blocked with 1% BSA in PBS for 1 hour at room temperature. After blocking, cells were incubated with the appropriate primary antibody (Table 2.4) diluted in 1% BSA in PBS, overnight at 4°C. Cells were then washed twice with PBS and incubated with Alexa Fluor conjugated secondary antibody (Molecular Probes) diluted 1:250 in 1% BSA in PBS for 1 hour at room temperature. Secondary antibodies used were goat-anti-rabbit IgG AlexaFluor® 488, goat-anti-rabbit IgG AlexaFluor® 594, rabbit-anti-mouse IgG AlexaFluor® 594, rabbit-anti-mouse IgG AlexaFluor® 488, goat-anti-rabbit IgG AlexaFluor® 647 or rabbit-anti-mouse IgG AlexaFluor® 647 (all from Molecular Probes). After incubation, cells were washed twice with PBS and stained with 0.5 μ g/ml Hoescht 33342 for 5 min and coverslips were subsequently mounted onto glass slides, inverted, with fluorescent mounting medium (Dako).

Protein (antigen)	Dilution	Species	Manufacturer and Catalog Number
Optineurin (INT)	1:100	Rabbit	Cayman Chemical; 10002
Myosin VI	1:100	Rabbit	Santa Cruz; SC-50461
Myosin VI	1:50	Mouse	Sigma; M0691
Myosin VI	1:50	Rabbit	Abcam; ab11095
CHOP	1:50	Mouse	Santa Cruz; SC-7351 [B-3]
GM130	1:50	Mouse	BD Transduction; 610823
LAMP2	1:100	Rabbit	Abcam; ab37024
Calnexin	1:100	Rabbit	Abcam; ab75801
eIF2α	1:100	Rabbit	Santa Cruz; sc-11386

Table 2.4 Primary antibodies used for Immunocytochemistry

2.10 Fixed imaging

2.10.1 Epifluorescence imaging

Epifluorescence imaging experiments were performed using an Olympus 1X81 Epi-Fluorescence microscope (Nikon) and Analysis LS Research (Olympus). Images were acquired at $\times 40$ magnification.

2.10.2 Confocal imaging

Confocal imaging experiments were performed using a Zeiss LSM 780 Laser Scanning Confocal microscope using Zen BlackTM software (Zeiss). Images were acquired at $\times 100$ magnification.

2.11 Live cell imaging

Live cells expressing fluorescent tagged proteins were imaged directly Zeiss LSM 550 or Zeiss LSM 780 Laser Scanning Confocal microscope. In some cases, lysosomes were labelled with dyes: LysoTracker Deep Red (Invitrogen), by preincubation of the coverslip with 1ml of cDMEM containing 1 μ l LysoTracker Deep Red. The coverslip was relocated to a live cell imaging Sykes-Moore chamber (Bellco). The microscopy stage was kept at 37°C during all live cell imaging experiments.

2.12 Software and statistical analysis

For analysis and composition of microscopy images, ImageJ (NIH) was used. Data was presented as mean \pm SEM, unless otherwise stated. GraphPad Prism was used for statistical analysis and significance was analysed by One Way-ANOVA followed by Tukey's *post-hoc* test, the level of significance being $p < 0.05$ unless otherwise stated.

Chapter 3

3. Extracellular wildtype and mutant SOD1 induces ER-Golgi pathologies characteristic of amyotrophic lateral sclerosis in neuronal cells

3. Chapter 3

3.1 Preface

Chapter 3 is presented as it was published in *Cellular and Molecular Life Sciences*, 2013. The author performed all the work described, except where acknowledgements are made as below:

Recombinant expression and purification of wildtype and mutant SOD1 in *Escherichia coli* was performed by Dr Justin Yerbury (University of Wollongong). *In vitro* aggregation of recombinant SOD1 was performed by the author, according to the protocol provided by Dr Justin Yerbury.

The experiment examining the mode of uptake of recombinant wildtype and mutant SOD1 in NSC-34 cells (Figure S1) was performed by Rafaa Zeineddine (University of Wollongong).

The author also acknowledges valuable discussions regarding experimental design and manuscript preparation from Dr Adam Walker (University of Pennsylvania), Manal Farg and Dr Kai Ying Soo (La Trobe University). The author wrote the manuscript which was revised by principal supervisor Dr Julie Atkin (La Trobe University).

3.2 Manuscript 1

The following is the presentation of chapter 3 as a copy of the manuscript published in *Cellular and Molecular Life Sciences* (2013).

Extracellular wildtype and mutant SOD1 induces ER–Golgi pathology characteristic of amyotrophic lateral sclerosis in neuronal cells

Vinod Sundaramoorthy · Adam K. Walker · Justin Yerbury · Kai Ying Soo · Manal A. Farg · Vy Hoang · Rafaa Zeineddine · Damian Spencer · Julie D. Atkin

Received: 25 February 2013 / Revised: 3 May 2013 / Accepted: 23 May 2013
© Springer Basel 2013

Abstract Amyotrophic lateral sclerosis (ALS) is a fatal and rapidly progressing neurodegenerative disorder and the majority of ALS is sporadic, where misfolding and aggregation of Cu/Zn-superoxide dismutase (SOD1) is a feature shared with familial mutant-SOD1 cases. ALS is characterized by progressive neurospatial spread of pathology among motor neurons, and recently the transfer of extracellular, aggregated mutant SOD1 between cells was demonstrated in culture. However, there is currently no evidence that uptake of SOD1 into cells initiates neurodegenerative pathways reminiscent of ALS pathology. Similarly, whilst dysfunction to the ER–Golgi compartments is increasingly implicated in the pathogenesis of both sporadic and familial ALS, it remains unclear whether misfolded, wildtype SOD1 triggers ER–Golgi dysfunction. In this study we

show that both extracellular, native wildtype and mutant SOD1 are taken up by macropinocytosis into neuronal cells. Hence uptake does not depend on SOD1 mutation or misfolding. We also demonstrate that purified mutant SOD1 added exogenously to neuronal cells inhibits protein transport between the ER–Golgi apparatus, leading to Golgi fragmentation, induction of ER stress and apoptotic cell death. Furthermore, we show that extracellular, aggregated, wildtype SOD1 also induces ER–Golgi pathology similar to mutant SOD1, leading to apoptotic cell death. Hence extracellular misfolded wildtype or mutant SOD1 induce dysfunction to ER–Golgi compartments characteristic of ALS in neuronal cells, implicating extracellular SOD1 in the spread of pathology among motor neurons in both sporadic and familial ALS.

Electronic supplementary material The online version of this article (doi:10.1007/s00018-013-1385-2) contains supplementary material, which is available to authorized users.

V. Sundaramoorthy · A. K. Walker · K. Y. Soo · M. A. Farg · V. Hoang · D. Spencer · J. D. Atkin (✉)
Department of Biochemistry, Latrobe Institute for Molecular Science, La Trobe University, Bundoora, Melbourne, VIC 3086, Australia
e-mail: j.atkin@latrobe.edu.au

A. K. Walker
Center for Neurodegenerative Disease Research, School of Medicine, University of Pennsylvania, Philadelphia, PA 19104, USA

J. Yerbury · R. Zeineddine
School of Biological Sciences, University of Wollongong, Wollongong, NSW 2522, Australia

J. D. Atkin
Department of Florey Neuroscience, University of Melbourne, Parkville, VIC 3010, Australia

Keywords Extracellular · SOD1 · ALS · Endoplasmic reticulum · Golgi

Introduction

Amyotrophic lateral sclerosis (ALS) is a neurodegenerative disorder with focal onset followed by progressive spread throughout surrounding upper and lower motor neurons. The intercellular transfer of misfolded proteins has recently been demonstrated in several neurodegenerative diseases, including ALS [1–3], and it has been suggested that this mechanism is responsible for the progressive spread of pathology. Mutations in SOD1 (Cu/Zn-superoxide dismutase) cause 20 % of familial ALS, and these cases display similar clinical features and pathogenesis to sporadic ALS, which accounts for 90 % of all ALS cases. Misfolded and aggregated SOD1 is present in both familial and sporadic ALS, but its pathobiology remains unclear [4, 5].

However, endoplasmic reticulum (ER) stress and fragmentation of the Golgi apparatus are well-described features in human ALS patients as well as in animal and cellular disease models [6–9]. ER stress is triggered initially in the most vulnerable motor neurons during early disease stages in several lines of transgenic mutant SOD1 mice, thus implying an active role in neurodegeneration [8].

Wildtype SOD1 (SOD1^{WT}) misfolds upon pathogenic triggers such as oxidative stress, and misfolded SOD1^{WT} exhibits similar toxic properties to mutant SOD1 [4]. Oxidized, misfolded SOD1^{WT} is present in the intracellular inclusions in motor neurons of sporadic ALS patients [5, 10]. Furthermore, recently it was shown that transgenic overexpression of SOD1^{WT} causes ALS in mice [11]. Together these data suggest that misfolded SOD1^{WT} could play a similar role to mutant SOD1 in the pathogenesis of sporadic ALS. There is accumulating evidence that secreted, extracellular SOD1, which is misfolded either due to mutation or cellular stress, could be a toxic factor spreading neurodegeneration among motor neurons in ALS. SOD1 is secreted by neuronal cells [12, 13] and is present in the cerebrospinal fluid (CSF) of ALS patients [14, 15]. Aggregated mutant SOD1 can be taken up by cells via macropinocytosis which triggers subsequent aggregation of natively folded SOD1 [1]. Similarly, extracellular misfolded SOD1^{WT} induces cell death [16] and overexpression of SOD1^{WT} induces misfolding of natively folded SOD1 in human but not mouse neuronal cell lines, demonstrating species specificity in the transfer of misfolding [17]. Furthermore, therapeutic strategies targeting extracellular SOD1 using antibodies specific to misfolded SOD1, delay disease progression in mutant SOD1 transgenic mice [18–20]. However, there is currently no evidence to show that uptake of extracellular misfolded SOD1 into neuronal cells initiates neurodegenerative pathways reminiscent of ALS pathology. It also remains unclear if both natively folded and misfolded forms of SOD1^{WT} and mutant SOD1 can be taken up by neurons.

ER stress triggers the unfolded protein response (UPR), a set of signaling pathways that activate sensor proteins including inositol requiring kinase 1 (IRE1), activating transcription factor 6 (ATF-6) and x-box binding protein 1 (Xbp1) [21]. Activation of UPR leads to down-regulation of general protein expression and upregulation of specific ER chaperones including immunoglobulin binding protein (BiP) and protein disulfide isomerase (PD1). BiP plays a key role in regulating induction of ER stress [22]. This leads to the upregulation and activation of IRE1, which mediates the splicing of Xbp1. Whilst initially protective, prolonged ER stress initiates apoptosis by activating CHOP (C/EBP homologous protein) [21], a transcription factor which translocates to the nucleus upon activation. Whilst ER stress is now recognized as an important pathogenic

feature of ALS, the mechanism by which mutant SOD1 activates the UPR is not fully defined, but includes binding of mutant SOD1 to Derlin-1 at least by symptom onset in transgenic SOD1 mice [22]. Conventionally ER stress is triggered when misfolded proteins accumulate within ER, but SOD1 is predominately cytoplasmic [23]. However, ER stress can also be triggered by inhibition of protein transport between ER and Golgi apparatus [24, 25]. Inhibition of ER–Golgi transport implies disruption to the secretory pathway, and Golgi fragmentation is another pathological feature of ALS, observed in both human patients and cellular and animal disease models [9, 26]. Likewise, the Golgi apparatus can fragment due to defects in ER to Golgi trafficking [27].

In this study, we examined whether extracellular, misfolded SOD1^{WT} and mutant G93A SOD1 (SOD1^{G93A}) activate cellular events characteristic of ALS pathology after uptake into neurons. Aggregated SOD1^{WT} and SOD1^{G93A} proteins were taken up into mouse NSC-34 and human SH-SY5Y neuronal cells, leading to ER stress, Golgi fragmentation, and inhibition of ER–Golgi protein trafficking. Apoptotic cell death was also triggered in SH-SY5Y cells. Furthermore, natively folded SOD1^{WT} was taken up by both cell lines, demonstrating that uptake is not specific to mutation or misfolding of SOD1. Hence extracellular misfolded SOD1^{WT} and SOD1^{G93A} induce cellular pathology characteristic of ALS, providing evidence for cell-to-cell transfer of SOD1 mediated neurotoxicity.

Results

Uptake of extracellular SOD1^{WT} and SOD1^{G93A} by neuronal cells

In order to examine the cell-to-cell propagation of SOD1, we first analyzed the uptake of extracellular SOD1 by mouse (NSC-34) motor neuron-like cell lines. Wildtype human SOD1 (SOD1^{WT}) and ALS-linked human mutant SOD1^{G93A} proteins were expressed in bacteria and purified to homogeneity as previously described [28]. Both proteins were metallated to the extent that they were enzymically active [28]. Each protein was labeled with Alexa Fluor 488 dye and then added to the culture medium of NSC-34 cells at a concentration of 2 µg/mL. Using fluorescence microscopy, the uptake of both labeled SOD1^{WT} and SOD1^{G93A} was observed after 48 h (Fig. 1a), demonstrating that both SOD1^{WT} and mutant SOD1 can be taken up by neuronal NSC-34 cells. The formation of prominent inclusion-like structures was detected specifically after uptake of extracellular mutant SOD1 but not SOD1^{WT} in NSC-34 cells. Furthermore, inhibitors of

macropinocytosis [5-(*N*-ethyl-*N*-isopropyl)amiloride (EIPA) and rottlerin] blocked the uptake of both SOD1^{WT} and SOD1^{G93A} by NSC-34 cells, in contrast to inhibitors of clathrin mediated endocytosis [genistein and chlorpromazine hydrochloride (CPZ); Fig. S1]. This suggests that both SOD1^{WT} and SOD1^{G93A} are taken up by macropinocytosis into NSC-34 cells, as previously reported for aggregated mutant SOD1 [1].

We then examined the uptake of extracellular SOD1 prepared in a mammalian baculovirus expression system. We transiently expressed GST-tagged SOD1^{WT} and SOD1^{G93A} in Sf9 insect cells, which resulted in secretion of SOD1 into the medium due to the presence of the AKH signal peptide [29]. Expression and secretion of SOD1 was confirmed at 48 h post-transfection by immunoblotting of the conditioned Sf9 medium with an anti-GST antibody (Fig. S2A). Furthermore, zymography confirmed that both mutant and SOD1^{WT} retained enzymatic activity in the conditioned media, demonstrating that both proteins were in their metallated, native form (Fig. S2B). The Sf9 conditioned media was then applied to untransfected NSC-34 cells for 48 h. Immunocytochemistry using an anti-GST antibody revealed that GST-tagged SOD1^{WT} and SOD1^{G93A} were taken up by NSC-34 cells (Fig. 1b). However, there was no uptake in NSC-34 cells treated with conditioned medium from insect cells expressing GST only, demonstrating that there was some specificity in the uptake for SOD1. In cells treated with SOD1^{WT} conditioned medium, the fluorescence was uniform and dispersed throughout the cells. However, in cells treated with mutant SOD1^{G93A}, prominent fluorescent structures reminiscent of inclusions were present (Fig. 1b). Hence both natively folded SOD1^{WT} and SOD1^{G93A} present in insect cell conditioned media were taken up by NSC-34 cells, and the uptake of SOD1^{G93A} resulted in the formation of intracellular SOD1 inclusions.

Uptake of extracellular recombinant mutant SOD1 activates ER stress in mouse NSC-34 cells

We next examined whether the uptake of extracellular mutant SOD1 activates ER stress in NSC-34 cells. We first examined whether the early phase of the UPR is activated in cells treated with extracellular SOD1. Immunoblotting for UPR markers IRE1, BiP and Xbp1 revealed an upregulation of all three proteins in cells treated with mutant SOD1^{G93A} compared to untreated cells or those treated with SOD1^{WT} (Fig. 1c, d; threefold, $P < 0.01$). Hence the early phases of UPR are induced in cells treated with extracellular mutant SOD1^{G93A}. We then examined cells for the later, pro-apoptotic phase of UPR using immunocytochemistry for nuclear CHOP [30, 31]. After 72 h treatment, a significant increase in nuclear CHOP immunoreactivity was

observed in NSC-34 cells treated with SOD1^{G93A} compared to untreated and SOD1^{WT} treated cells (Fig. 1e, f; twofold, $P < 0.001$). Hence the pro-apoptotic phase of UPR was also triggered in mutant SOD1 treated cells. These findings were confirmed in NSC-34 cells treated with Sf9 cell conditioned media. A significant upregulation in nuclear CHOP immunoreactivity was detected on treatment with Sf9 medium from SOD1^{G93A} expressing cells compared to SOD1^{WT} and GST alone expressing cells (Fig. 1g; twofold, $P < 0.001$). Hence the uptake of extracellular mutant SOD1 expressed in either bacterial or a baculovirus system specifically induces ER stress, including pro-apoptotic CHOP, in NSC-34 cells.

Uptake of extracellular aggregated SOD1^{WT} and SOD1^{G93A} by SH-SY5Y human neuronal cells

We next asked whether uptake of aggregated/misfolded SOD1^{WT} could induce ALS-like pathology in neuronal cells. For this purpose a human neuroblastoma cell line (SH-SY5Y) was used due to the previously reported species specificity in seeding SOD1^{WT} aggregation [17]. Aggregated recombinant SOD1^{WT} and mutant SOD1^{G93A} proteins were prepared by treatment with 5 mM EDTA and 50 mM DTT to remove metal ions and reduce the native Cys57–Cys146 SOD1 disulfide bond, respectively, as described previously [28, 32–34]. The aggregated proteins (aggSOD1^{WT}, aggSOD1^{G93A}) and native SOD1^{WT} and SOD1^{G93A} were then labeled with Alexa Fluor 488 dye. Silver staining of non-denaturing native gel and denaturing SDS-PAGE gel revealed that both SOD1^{WT} and SOD1^{G93A} formed SDS-stable high molecular weight aggregates (Fig. 2a, b).

Labeled aggSOD1^{WT} and aggSOD1^{G93A}, and unaggregated SOD1^{WT} and SOD1^{G93A} for comparison were then added to the culture medium of SH-SY5Y cells at a concentration of 2 μ g/mL. Fluorescence microscopy revealed that 48 h after treatment, SH-SY5Y cells had taken up both aggregated and unaggregated SOD1^{WT} and SOD1^{G93A} from the culture medium (Fig. 2c). Differential interference contrast (DIC) microscopy revealed the formation of membrane ruffles in all cases, consistent with a macropinocytosis mechanism for uptake of SOD1, as previously reported for mutant SOD1 aggregates [1] (Fig. 2c). In cells treated with SOD1^{G93A}, aggSOD1^{WT} and aggSOD1^{G93A} intracellular fluorescent inclusions were formed (20–30 % of cells; Fig. 2d). Surprisingly, in a small proportion of cells (7 %) treated with unaggregated native SOD1^{WT}, inclusions were also present (Fig. 2d), which were never observed in murine NSC-34 cells (Fig. 1a, b). Intracellular higher molecular weight SOD1 aggregates were also present in cell lysates, which were harvested after 0.125 % trypsin treatment of the cells, to digest residual extracellular SOD1 aggregates

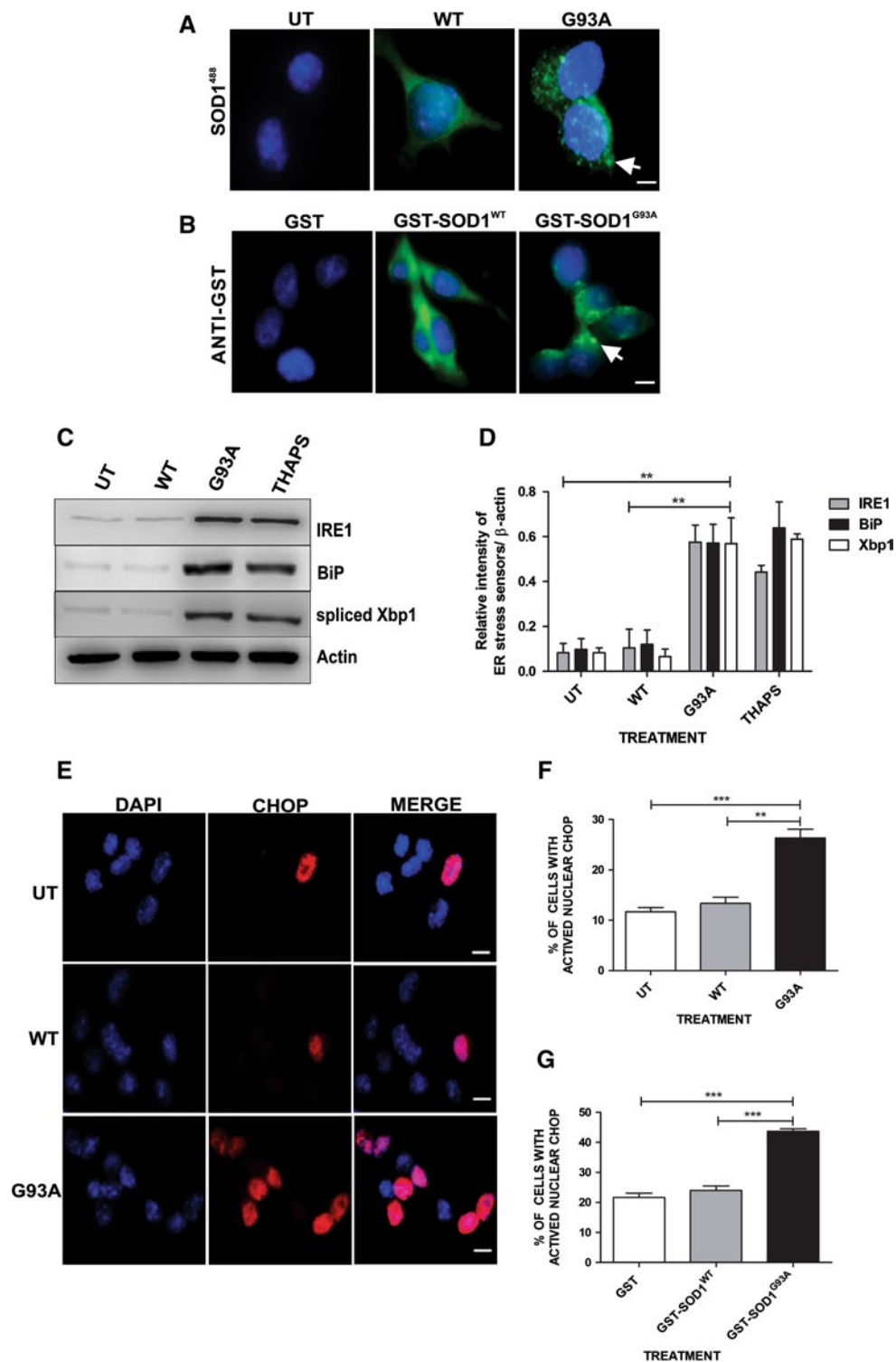


(Fig. 2e). Endogenous human SOD1 was clearly present in untreated cells (Fig. 2e). However, in all cells treated with extracellular SOD1, reduced levels of endogenous SOD1 was observed, and a corresponding increase in the levels of high molecular weight aggregates was detected. This finding implies that recruitment of endogenous SOD1

into higher molecular weight aggregates has occurred in cells treated with aggregated SOD1^{WT} and mutant SOD1. Also, consistent with the microscopy findings, in unaggregated SOD1^{WT} treated cell lysates, SOD1 aggregates were observed, although these aggregates ran at a faster mobility than those formed by mutant SOD1, suggesting they

Fig. 1 Uptake of extracellular mutant SOD1^{G93A} triggers ER stress in mouse NSC-34 cells. **a** Recombinant SOD1^{WT} and SOD1^{G93A} (2 µg/mL) labeled with Alexa Fluor 488 dye (green) are taken up by NSC-34 cells 48 h after addition to medium. Nuclei are stained with DAPI (blue). White arrows show the formation of inclusion-like structures in cells treated with extracellular SOD1^{G93A}. **b** Extracellular GST-tagged SOD1^{WT} and SOD1^{G93A} (GST-SOD1^{WT}, GST-SOD1^{G93A}) are taken up by NSC-34 cells. Insect cell (Sf9) conditioned medium containing GST-SOD1^{WT}, GST-SOD1^{G93A} or GST only control (100 µg total protein) was added to NSC-34 cells for 48 h. Cells were then fixed and immunostained with anti-GST antibody (green). No immunoreactivity was observed in cells treated with GST alone (GST) in contrast to GST-SOD1 treated cells. White arrow shows the formation of inclusion-like structures in cells treated with extracellular GST-SOD1^{G93A}. **c** Immunoblotting reveals upregulation of UPR markers IRE1, BiP, and spliced Xbp1 in NSC-34 cells 72 h after treatment with recombinant purified SOD1^{G93A}, in contrast to cells treated with recombinant SOD1^{WT} and untreated (UT) cells (20 µg/lane). As a positive control NSC-34 cells were treated with 10 µM thapsigargin to induce ER stress (THAPS) for 1 h before lysis. β-actin was used as a loading control. **d** Densitometric analysis of the immunoblots relative to β-actin intensity confirms upregulation of all three UPR markers in NSC-34 cells treated with recombinant SOD1^{G93A}. **e** Representative images showing increased nuclear immunoreactivity to pro-apoptotic, ER stress-specific CHOP (red) in NSC-34 cells treated with SOD1^{G93A} for 72 h. Nuclei are stained with DAPI (blue). **f** Quantification of NSC-34 cells containing nuclear immunoreactivity to CHOP 72 h after treatment with recombinant, purified SOD1 (SOD1^{WT}, SOD1^{G93A}) and untreated cells (UT). **g** Quantification of NSC-34 cells containing nuclear immunoreactivity to CHOP 72 h after treatment with Sf9 insect cell conditioned medium containing GST-SOD1 (GST-SOD1^{WT}, GST-SOD1^{G93A}) or GST alone. Results are expressed as mean ± SEM; *n* = 3; ***P* < 0.01, ****P* < 0.001 versus SOD1^{WT} and untreated cells (UT) (**f**) or SOD1^{WT} or GST treated cells (**g**) as indicated by one-way ANOVA with Tukey's post-test, *n* = 3. All scale bars represent 10 µm

are smaller than those in other cell populations. Hence misfolded/aggregated SOD1^{WT} and mutant SOD1 are taken up by human neuronal cells, leading to intracellular SOD1 aggregation and possible recruitment of endogenous SOD1. Induction of SOD1 aggregation by natively folded SOD1^{WT} was also detected in a small proportion of cells.

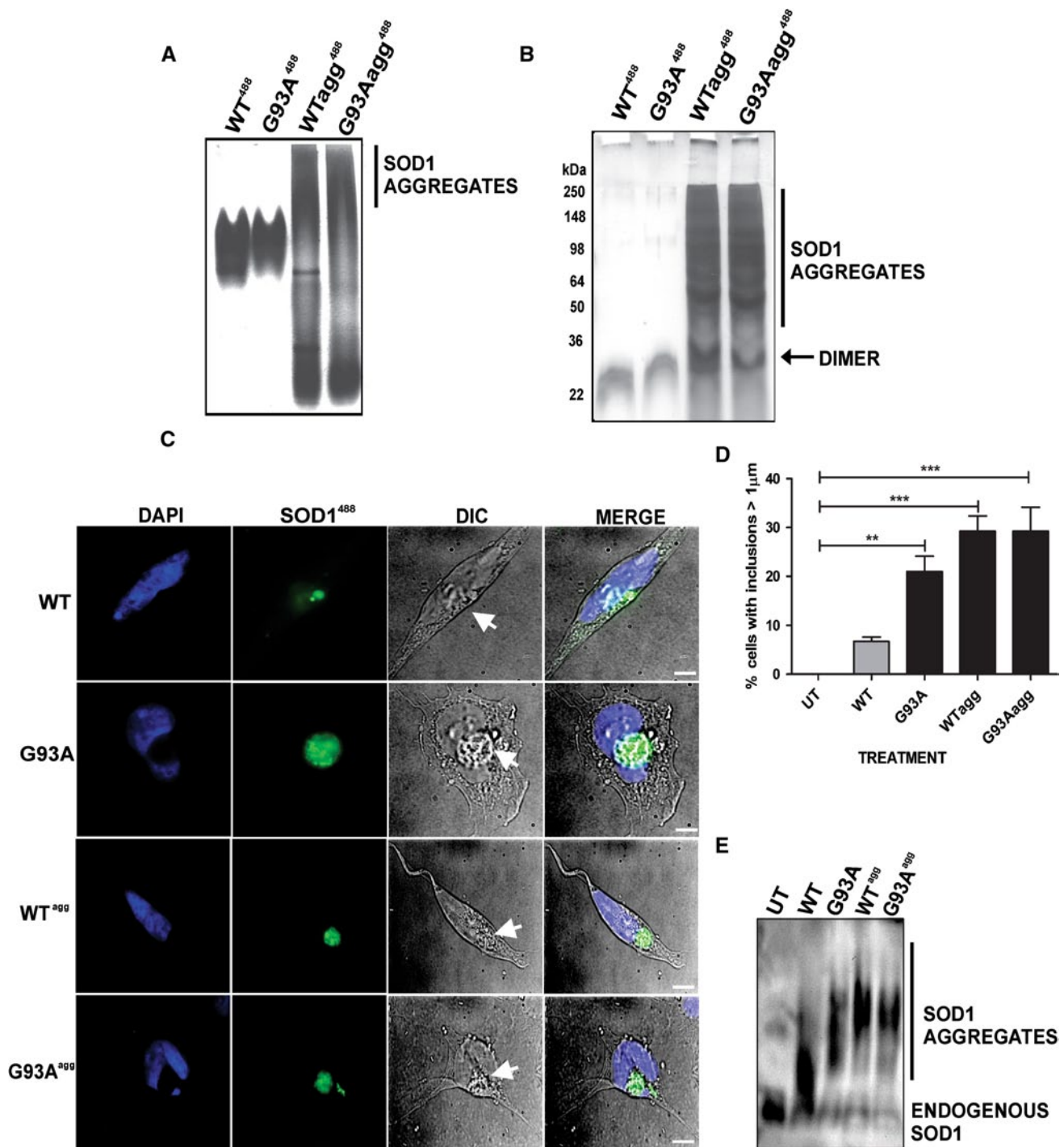
Uptake of extracellular aggregated SOD1^{WT} and SOD1^{G93A} activates ER stress in SH-SY5Y cells

We next examined whether ER stress is activated in SH-SY5Y cells treated with extracellular SOD1^{G93A}, aggSOD1^{WT} and aggSOD1^{G93A} for 72 h. Immunoblotting for IRE1, BiP and spliced Xbp1, revealed that the UPR was induced (Fig. 3a, b; twofold, *P* < 0.01) in SH-SY5Y cells treated with aggregated and unaggregated SOD1^{G93A} compared to untreated cells, consistent with the findings in NSC-34 cells. Furthermore, in cells treated with aggSOD1^{WT}, induction of the UPR was also observed, demonstrating that SOD1^{WT} can also trigger ER stress when misfolded. Surprisingly we also observed a slight but significant upregulation of Xbp1 (*P* < 0.05) in cells

treated with unaggregated SOD1^{WT} compared to untreated cells. Similarly, using immunocytochemistry, a significant increase in nuclear CHOP in SH-SY5Y cells treated with SOD1^{G93A}, aggSOD1^{WT} and aggSOD1^{G93A} treated cells compared to untreated cells was detected (Fig. 3c, d; three-fold, *P* < 0.001). Hence uptake of extracellular aggregated SOD1 induces the ER stress-specific pro-apoptotic phase of UPR in SH-SY5Y cells, similar to mutant SOD1. Consistent with the immunoblotting results, we observed a modest but significant increase in nuclear CHOP immunoreactivity in cells treated with unaggregated SOD1^{WT} (*P* < 0.05) compared to untreated cells. In contrast, neither bacterial nor baculovirus SOD1^{WT} induced ER stress in NSC-34 cells (Fig. 1c). Hence extracellular, native SOD1^{WT} induces ER stress in the SH-SY5Y human cell line but not the NSC-34 mouse neuronal cell line.

Extracellular aggregated SOD1^{WT} and SOD1^{G93A} inhibits ER to Golgi protein trafficking and induces Golgi fragmentation

We next examined whether extracellular misfolded or mutant SOD1 could also inhibit ER to Golgi protein trafficking. Vesicular stomatitis virus glycoprotein ts045 (VSVG-ts045) is a widely employed marker used to examine ER–Golgi transport [35]. VSVG-ts045 misfolds and is retained in the ER at 40 °C, but is transported to the Golgi apparatus at the permissive temperature of 32 °C [35]. We first examined ER–Golgi transport in SH-SY5Y cells transfected with SOD1 proteins linked to EGFP [6, 12] and VSVG-ts045 mCherry, to confirm that intracellular mutant SOD1 can inhibit ER–Golgi trafficking in this cell line. VSVG-ts045 was detected immunocytochemically using markers of the ER (calnexin) and Golgi (GM130) and its co-localization with each marker was quantified using Mander's coefficient [36]. At 32 °C, VSVG-ts045 was transported to the Golgi in untransfected cells and in cells expressing SOD1^{WT} (Fig. S3A). However, in cells expressing mutant SOD1 (Fig. S3A) most VSVG-ts045 remained in the ER and significantly less (~50 %) was transported to the Golgi (Fig. S3B; *P* < 0.01). Hence ER–Golgi trafficking is inhibited by intracellular mutant SOD1 in the SH-SY5Y cell line (Fig. S3A, S3B). We next examined ER–Golgi transport in cells treated with extracellular SOD1 proteins. SH-SY5Y cells were transiently transfected with VSVG-ts045 mCherry. At 24 h post-transfection, 2 µg/mL of purified, labeled SOD1^{WT}, SOD1^{G93A}, aggSOD1^{WT} and aggSOD1^{G93A} were added to the SH-SY5Y medium for another 48 h. Transport of VSVG-ts045 from the ER to Golgi was then examined using immunocytochemistry to calnexin and GM130 as above. Quantification of the degree of co-localization of VSVG-ts045 with ER and Golgi compartments using Mander's coefficient was then performed.



VSVG-ts045 was efficiently transported to the Golgi apparatus in untreated cells after 60 min at 32 °C. However, in cells treated with extracellular SOD1^{G93A}, aggSOD1^{WT} or aggSOD1^{G93A}, VSVG-ts045 was retained in the ER and significantly less was transported to the Golgi ($P < 0.001$) compared to untreated cells (Fig. 4a–c). Hence extracellular mutant SOD1 inhibits ER–Golgi transport similar to intracellular mutant SOD1. These findings were confirmed using NSC-34 cells treated with extracellular SOD1^{G93A}

(Fig. 4d). Furthermore, aggSOD1^{WT} also inhibited ER to Golgi protein trafficking in SH-SY5Y cells, to a level comparable to both SOD1^{G93A} and aggSOD1^{G93A}. Hence both mutant and aggregated SOD1 inhibit ER–Golgi transport. There was no significant difference in the transport of VSVG-ts045 from ER–Golgi in NSC-34 cells treated with native SOD1^{WT} compared to UT cells. A slight difference was observed in SH-SY5Y cells treated with native SOD1^{WT}, but this was not statistically significant

Fig. 2 Uptake and aggregation of extracellular mutant SOD1^{G93A} and aggregated SOD1^{WT} in SH-SY5Y cells. **a** Recombinant purified SOD1^{WT} and SOD1^{G93A} proteins were aggregated by treatment with 50 mM DTT and 5 mM EDTA at 37 °C for 72 h and labeled with Alexa Fluor 488 dye. The formation of aggregates was confirmed by 10 % native gel electrophoresis (1 µg/lane) followed by silver staining. **b** Silver stained SDS PAGE of SOD1 aggregates with 100 mM Iodoacetamide, revealed the presence of SDS stable higher molecular weight WTagg⁴⁸⁸ and G93Aagg⁴⁸⁸ aggregates, as indicated. **c** Native and aggregated SOD1^{WT} and SOD1^{G93A} labeled proteins were added to the SH-SY5Y cell culture medium at a concentration of 2 µg/mL. After 48 h treatment, the cells were fixed and examined by fluorescence microscopy (SOD1⁴⁸⁸, green), after staining the nuclei with DAPI (blue). Representative images show the uptake of extracellular protein in each case. Intracellular fluorescent SOD1 inclusions were abundant in mutant SOD1 and aggregated SOD1 treated cells, and were present in a small proportion of native SOD1^{WT} treated cells. DIC images (panel 3 from left, white arrows) show the formation of membrane ruffles characteristic of macropinocytosis in each case. All scale bars represent 10 µm. **d** Quantification of SOD1 inclusion formation in SH-SY5Y cells 48 h after treatment (UT, SOD1^{WT}, SOD1^{G93A}, SOD1^{WTagg}, SOD1^{G93Aagg}). SOD1 inclusions were defined as fluorescent, inclusion-like structures greater than 1 µm in diameter and were quantified using ImageJ. Results are expressed as mean ± SEM; *n* = 3; ***P* < 0.01, ****P* < 0.001 versus UT by one-way ANOVA with Tukey's post-test. **e** Following extracellular protein treatment for 48 h, SH-SY5Y cell lysates were collected after 0.125 % trypsin digestion of cells to remove the residual extracellular SOD1 inoculum and run on 10 % native PAGE. High molecular weight intracellular SOD1 aggregates were present in all lysates except UT cells as indicated. Endogenous human SH-SY5Y SOD1 can be seen in UT, but this band is reduced in cells treated with native SOD1^{WT}, indicating the recruitment of endogenous SOD1 into the high molecular weight aggregates. Similarly, this band is further decreased in cells treated with G93A, WT^{agg} and G93A^{agg} compared to both UT and SOD1^{WT}

(Fig. 4a–c). Consistent with these findings, extracellular mutant SOD1 did not co-localise with ER markers after uptake into NSC-34 cells (Fig S4). Hence these data suggest that extracellular SOD1 triggers ER stress from the cytoplasm following uptake into neuronal cells, by inhibiting the transport of secretory proteins from the ER to Golgi.

Inhibition of ER–Golgi transport implies disruption to the secretory pathway. Hence fragmentation of the Golgi apparatus was next examined in SH-SY5Y cells treated with extracellular SOD1, by immunostaining with anti-GM130 antibody. In untreated cells the Golgi apparatus mostly localized to a compact, perinuclear ribbon. In contrast, the Golgi apparatus fragmented into condensed punctate structures in 25–40 % of cells treated with SOD1^{G93A}, aggSOD1^{WT} and aggSOD1^{G93A} (Fig. 5a, c). Similarly, Golgi fragmentation was also detected in 25 % of NSC-34 cells treated with extracellular SOD1^{G93A} (Fig. 5b, d; *P* < 0.05). The Golgi was fragmented in a smaller but significant percentage of SH-SY5Y cells (*P* < 0.05) treated with native SOD1^{WT}, but not in NSC-34 cells treated with native SOD1^{WT} (Fig. 5c, d).

Uptake of extracellular aggregated SOD1^{WT} or mutant SOD1 induces cell death in SH-SY5Y cells

Prolonged ER stress and induction of CHOP implies that apoptotic cell death is triggered in cells treated with extracellular SOD1. Hence we next examined induction of apoptosis using Annexin V/propidium iodide (PI) staining by flow cytometry [37]. After 72 h treatment with extracellular SOD1, apoptotic cell death was quantified using FACS. In SH-SY5Y cells there was a significant increase (*P* < 0.05) in the percentage of cells undergoing apoptosis after treatment with aggSOD1^{WT}, SOD1^{G93A} and aggSOD1^{G93A} compared to untreated cells (Fig. 6a, b). Treatment with aggregated forms of SOD1^{WT} and SOD1^{G93A} induced apoptosis in a higher percentage of cells compared to the respective native forms (*P* < 0.05). Hence apoptosis is triggered by extracellular misfolded SOD1 proteins in SH-SY5Y cells. However, there were no significant differences in the percentage of cells undergoing apoptosis in NSC-34 cells after treatment with extracellular SOD1^{WT} and SOD1^{G93A} compared to the controls (Fig. 6c).

Discussion

This study provides clear evidence that the uptake of extracellular misfolded SOD1 into neuronal cells initiates neurodegenerative pathways reminiscent of ALS pathology. Misfolded SOD1^{WT} and mutant SOD1 were taken up by neuronal cells, inducing the formation of intracellular SOD1-positive inclusions. This triggered inhibition of transport from the ER to Golgi apparatus, ER stress, fragmentation of the Golgi and neuronal cell death, implying that extracellular SOD1 may be responsible for the spread of neurodegeneration among motor neurons in ALS. Moreover, both mutant SOD1 and aggregated SOD1^{WT} displayed a similar ability to induce these effects, thus providing clues into the pathology of both familial and sporadic ALS.

This study also demonstrates that the uptake of extracellular SOD1 does not depend on the presence of a mutation or aggregation. Extracellular SOD1^{WT} was taken up by murine NSC-34 cells, which did not induce pathology. A previous study demonstrated that extracellular, aggregated mutant SOD1 is taken up by macropinocytosis, a mechanism of non-selective endocytosis of macromolecules from the extracellular space [1]. The findings of our study are consistent with this mechanism because both natively folded and aggregates of SOD1^{WT} and mutant SOD1 were taken up to a similar degree. Also, inhibitors of macropinocytosis were able to block the uptake of SOD1^{WT} and SOD1^{G93A} into NSC-34 cells. Furthermore, membrane ruffles characteristic of macropinocytosis were present in SH-SY5Y cells after

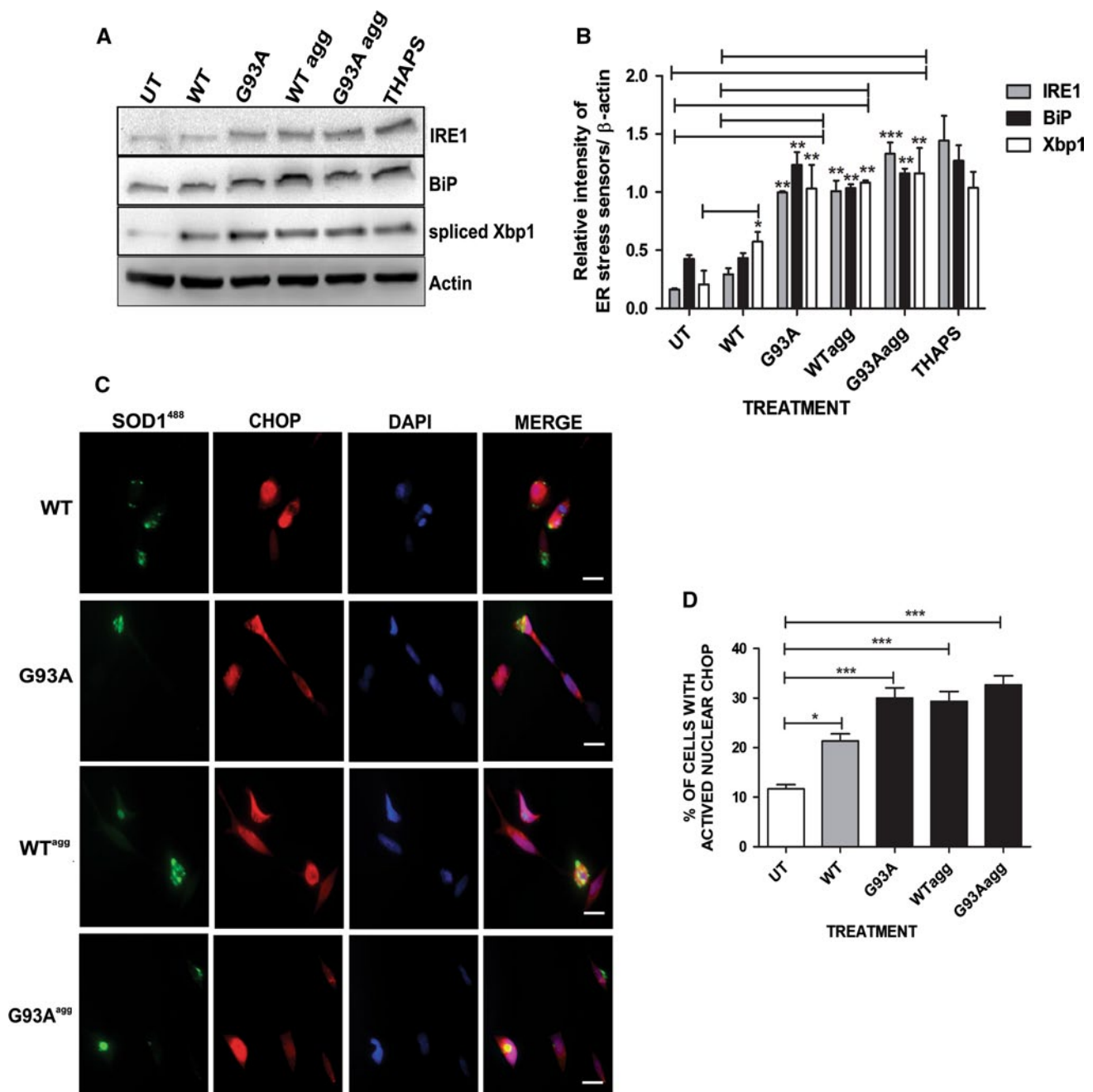


Fig. 3 Uptake of extracellular, aggregated SOD1^{WT} and mutant SOD1 activates ER stress in SH-SY5Y cells. **a** Immunoblotting of cell lysates from SH-SY5Y cells treated with extracellular proteins SOD1^{G93A}, WT^{agg}, and G93A^{agg} reveals upregulation of UPR markers IRE1, BiP, and spliced Xbp1 after 72 h treatment (20 μg/lane). As a positive control, cells were treated with 10 μM thapsigargin (THAPS) for 1 h before lysis to induce ER stress. β-actin was used as a loading control. **b** Densitometric quantification of immunoblots relative to β-actin intensity reveals upregulation of all three UPR markers in cells treated with SOD1^{G93A}, WT^{agg}, and G93A^{agg} compared to UT cells. Results are expressed as mean ± SEM; $n = 3$; * $P < 0.05$, ** $P < 0.01$,

*** $P < 0.001$ versus untreated cells or SOD1^{WT} treated cells as indicated, by one-way ANOVA with Tukey's post-test. **c** Representative fluorescent microscopy images demonstrate nuclear immunoreactivity to CHOP (red), indicating activation of CHOP and hence ER stress, 72 h after treatment with WT, G93A, WT^{agg}, G93A^{agg} SOD1. All scale bars represent 10 μm. **d** Quantification of the proportion of SH-SY5Y cells with nuclear CHOP immunoreactivity in (c), 72 h after treatment with WT, G93A, WT^{agg} and G93A^{agg}. Results are expressed as mean ± SEM; $n = 3$; * $P < 0.05$, *** $P < 0.001$ versus UT by one-way ANOVA with Tukey's post-test

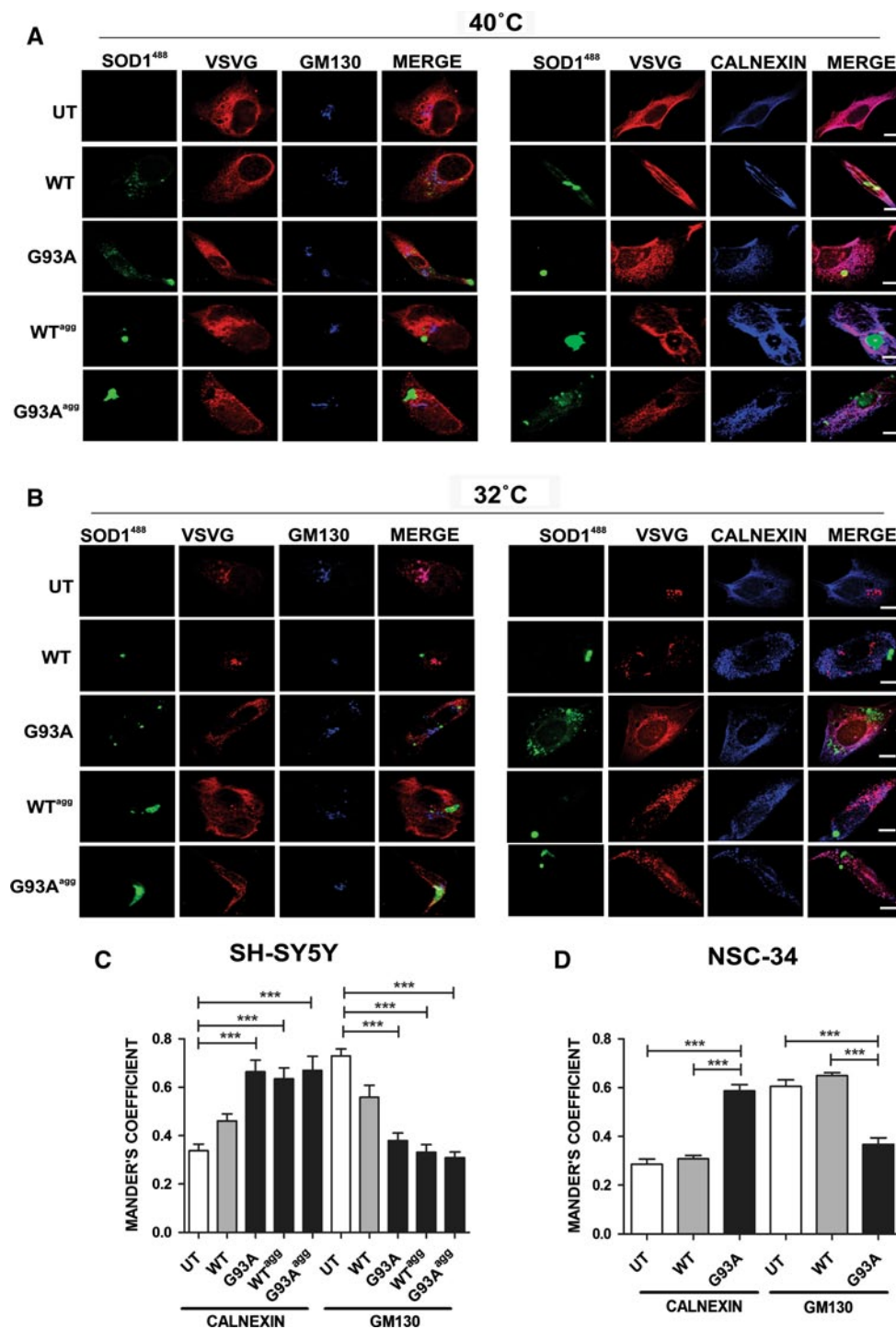
treatment with extracellular SOD1 [38–40]. Our findings imply that secretion or simple diffusion of misfolded SOD1 into CSF by affected cells (including astrocytes and microglia, as well as motor neurons) could be subsequently endocytosed by neighboring motor neurons, thus inducing neurodegeneration. As ALS is now considered as a multi-system disorder where there is an interplay between motor neurons and other neuronal cell types [41, 42], uptake of misfolded or mutant SOD1 by neuronal cells would therefore explain the neurospatial spread of pathology in human ALS. Consistent with this notion, misfolded SOD1 has been identified in the CSF of sporadic and familial ALS patients [14, 15]. Even low levels of misfolded SOD1 in CSF could seed intracellular aggregation after uptake [14], subsequently spreading pathology.

Aggregated forms of SOD1^{WT} induced similar cellular pathogenic effects to mutant SOD1 in this study. Furthermore, we observed the formation of inclusions in a small proportion of SH-SY5Y cells treated with native SOD1^{WT}, which were never present in NSC-34 cells. Metal-free forms of SOD1 have been proposed to be the toxic precursor preceding aggregation in familial ALS [43, 44]. The majority of ALS mutations affect the structural stability of SOD1, leading to the exposure of buried hydrophobic residues, thus resulting in aggregation [45]. Hence SOD1^{WT} has an intrinsic propensity to aggregate which is enhanced by mutation. Previous studies have demonstrated that misfolded, oxidized SOD1^{WT} is as pathogenic as mutant SOD1 [16]. However, we observed pathological effects induced by extracellular native SOD1^{WT} in human SH-SY5Y cells not previously observed in murine NSC-34 cells or by intracellular expression of SOD1^{WT}. The reason for this is unclear, but it is possible that native SOD1^{WT} recruits endogenous human SOD1 into aggregates after uptake in SH-SY5Y cells. This would explain the lower but significant inclusion formation, activation of ER stress and Golgi fragmentation in SH-SY5Y cells treated with unaggregated, extracellular SOD1^{WT}. Both recombinant, purified SOD1^{WT} from *Escherichia coli*, or Sf9 medium containing SOD1^{WT}, were taken up by NSC-34 cells, but neither induced ER stress, or aggregate/inclusion formation. Similarly, we detected apoptosis in SH-SY5Y cells but not NSC-34 cells treated with extracellular SOD1. These data are consistent with the notion that there is species specificity in the recruitment of SOD1 misfolding [17], thus implicating a gain of toxic function by SOD1^{WT} in the presence of human SOD1. Indeed, overexpression of SOD1^{WT} induces misfolding of endogenous SOD1 in the same cell line [17]. We also observed that the addition of extracellular SOD1 results in the rapid formation of intracellular SOD1 aggregates in the cytoplasm after uptake. This replicates the commonly described observation that

over-expression of mutant SOD1 in cell culture results in the rapid formation of aggregates. In contrast, aggregates appear much later in mouse ALS models based on transgenic over-expression of mutant SOD1, generally at the end stages of disease [11, 46], thus highlighting differences observed between animal and cellular disease models.

ER stress is now established as a key pathway to cell death in ALS [7, 8, 23, 31]. Mutant SOD1 induces ER stress [6] and Golgi fragmentation [26] in neuronal cell cultures, and we now show that aggregated SOD1^{WT} induces UPR and Golgi fragmentation similar to mutant SOD1. These findings are consistent with recent evidence for common pathogenic pathways shared by mutant SOD1 and SOD1^{WT}, and the presence of misfolded SOD1^{WT} in sporadic ALS tissues [4, 5]. It is unclear how ER stress is triggered in ALS because SOD1 is normally located in the cytoplasm and reports that it is found in microsomes [47] have been subsequently challenged [23]. However, it was previously proposed that ER stress in ALS is triggered by cytoplasmic SOD1 [23]. We show here that extracellular SOD1 does not co-localise with ER markers after uptake, consistent with the notion that ER stress is triggered from the cytoplasm. However, ER stress can be caused by failure of ER–Golgi trafficking [24, 25]. We also confirm here that intracellular mutant SOD1 inhibits the transport of VSVG-ts045 from the ER to Golgi in SH-SY5Y cells, and we show that extracellular forms of mutant and aggregated SOD1^{WT} also delay ER–Golgi traffic, thus providing one possible explanation for induction of ER stress. Similarly, Golgi fragmentation is also triggered by an imbalance between anterograde and retrograde traffic between ER and Golgi [26], highlighting a possible role for disruption to ER–Golgi traffic in both events. The activation of pro-apoptotic CHOP and increase in the proportion of cells undergoing apoptosis in cells treated with extracellular SOD1 provides a link between extracellular proteins and neurodegeneration and UPR-specific cell death. Hence this study also provides further evidence linking the disruption of ER–Golgi compartments to ALS and shows that extracellular misfolded proteins can induce dysfunction in these organelles.

In conclusion, this study establishes mechanisms of toxicity induced by extracellular SOD1 applicable to both sporadic and familial ALS. Our findings are consistent with a prion-like propagation of neurotoxicity in ALS, and they provide further evidence for common neurodegenerative pathways shared by mutant and SOD1^{WT} linked to the ER–Golgi compartments. The demonstration of specific, cellular pathways targeted by extracellular, misfolded SOD1 also provides novel targets for ameliorating the spread of neurodegeneration in ALS.



Materials and methods

Expression and purification of recombinant SOD1

Human SOD1^{WT} and SOD1^{G93A} were expressed and purified from *E. coli* as previously described [28, 48]. Briefly, *E. coli* cells were cultured at 23 °C with 3 mM CuSO₄ and

30 μM ZnSO₄ for metal loading. SOD1^{WT} and SOD1^{G93A} proteins were then purified from bacterial lysates, by heat denaturation, size exclusion chromatography (Superdex 75; GE Healthcare), and anion-exchange chromatography using a Q-Sepharose anion exchange column (GE Healthcare), and eluted with a salt gradient of 0–125 mM NaCl, pH 7.5 [28].

Fig. 4 Uptake of extracellular, aggregated WT and mutant SOD1 inhibits ER to Golgi protein trafficking in SH-SY5Y cells. Cells expressing VSVG-ts045 mCherry were treated with WT, G93A, WT^{agg}, G93A^{agg} at 24 h post transfection. After trapping VSVG-ts045 mCherry in the ER by incubation at 40 °C for 24 h, the temperature was shifted to 32 °C for 60 min or fixed immediately at 0 min. The cells were then stained with calnexin (blue), a marker of the ER, or GM130 (blue), a marker of the Golgi apparatus. **a** Representative fluorescent images of cells expressing VSVG-ts045 (red) treated with WT, G93A, WT^{agg}, G93A^{agg} SOD1 protein (green) and UT cells after incubation at 40 °C (0 min). **b** Representative fluorescent images after 60 min incubation at 32 °C. VSVG is co-localised with GM130 in cells treated with native SOD1^{WT} and UT cells in contrast to cells treated with WT^{agg}, G93A, G93A^{agg}, in which VSVG is still predominantly co-localised with calnexin, indicating an inhibition of VSVG-ts045 transport from ER to Golgi. All scale bars 10 µm. **c** Quantification of the degree of co-localisation of VSVG-ts045 with calnexin and GM130 at 60 min as in **b** using Mander's coefficient. Data are presented as mean ± SEM, ****P* < 0.001 versus UT by one-way ANOVA with Tukey's post-test, *n* = 3. **d** Uptake of extracellular mutant SOD1 inhibits ER to Golgi protein trafficking in NSC-34 cells. Cells expressing VSVG-ts045 mCherry were treated with recombinant, labelled SOD1^{WT} or SOD1^{G93A} at 24 h post transfection. After trapping VSVG-ts045 mCherry in the ER by incubation at 40 °C for 24 h, the temperature was shifted to 32 °C for 0 and 30 min. The degree of co-localisation of VSVG-ts045 with calnexin and GM130 was quantified using Mander's coefficient. Data are presented as mean ± SEM, ****P* < 0.001 versus SOD1^{WT} treated or UT cells as indicated by one-way ANOVA with Tukey's post-test, *n* = 3

Expression of SOD1 from Sf9 baculoviral system

Human SOD1^{WT} and SOD1^{G93A} constructs were generated by PCR and cloned into pIEX-3 plasmids using *Spe*I restriction sites. *Spodoptera frugiperda* (Sf9) cells were kindly provided by Dr. Mark Hulett, La Trobe University. The cells were cultured at 28 °C and transfected using GeneJuice transfection reagent (Invitrogen) as per the manufacturer's protocol. 48 h after transfection the culture medium was collected after centrifugation at 1200 rpm for 5 min and analyzed by immunoblotting.

Zymography–SOD1 activity assay

For zymography, SOD1 protein samples were electrophoresed on a 10 % native PAGE. The gel was then soaked in 2.45 mM nitro blue tetrazolium (Sigma) for 20 min, washed with dH₂O and soaked in developer solution containing 28 mM tetramethylethylenediamine (TEMED; BIO-RAD), 28 µM riboflavin, and 36 mM KH₂PO₄ (Sigma) for 15 min. The gel was illuminated for 5–15 min until sufficient contrast between achromatic zones and blue background was achieved.

Aggregation and labeling of SOD1^{WT} and mutant SOD1^{G93A}

In vitro SOD1 aggregation was performed as previously described [28]. Purified SOD1^{WT} and G93A SOD1 proteins

(1 mg/mL) dissolved in PBS were incubated with 50 mM dithiothreitol (DTT) and 5 mM ethylenediaminetetraacetic acid (EDTA) at 37 °C for 72 h whilst shaking and vortexed briefly to obtain a homogenous solution. Aggregated and native SOD1^{WT} and SOD1^{G93A} were then labeled using the Alexa Fluor 488 Microscale Protein Labeling Kit (Invitrogen). Protein (100 µg) was incubated with dye in the presence of 100 mM NaHCO₃ at room temp for 15 min. The unlabeled protein was then separated using Amicon Ultra 10 kDa centrifugal filters (Millipore).

Extracellular SOD1 treatment

Mouse motor neuron-like NSC-34 or human neuroblastoma SH-SY5Y cells were cultured on 24 well plates with or without 13 mm coverslips at 10⁵ cells/well. Purified recombinant SOD1 (2 µg/mL) expressed in bacteria was added to the culture medium 24 h after seeding, and 48 h later the cells were analyzed by immunocytochemistry or immunoblotting. For cells treated with Sf9 conditioned medium containing GST-SOD1 or GST-only control, medium containing 100 µg total protein was added to the NSC-34 culture medium to a final concentration of 0.2 mg/mL.

SOD1 uptake and inhibition

NSC34 cells were cultured on coverslips for 24 h before treatment with either 3 µM rottlerin D, 100 µM EIPA, 10 µM genistein or 5 µM chlorpromazine HCL for 30 min at 4 °C. These cells were then treated with SOD1^{WT} or SOD1^{G93A} or untreated at 4 °C for 30 min before being washed with PBS. The cells were then fixed with 4 % PFA and incubated with 0.5 % BSA in PBS for 20 min at room temperature. A 1:500 dilution of anti-human SOD1 sheep antiserum (Thermo Fisher Scientific) in PBS containing 0.1 % BSA and subsequent goat anti-sheep Alexa488 (Invitrogen) was used to detect internalized SOD1. SOD1 was visualized using a Leica SP5 scanning confocal microscope.

Immunocytochemistry

NSC-34 or SH-SY5Y cells grown on coverslips were washed with PBS and fixed with 4 % paraformaldehyde (PFA; Merck) in PBS for 10 min. Cells were permeabilized in 0.1 % Triton X-100 in PBS for 2 min, blocked for 30 min with 1 % BSA in PBS and incubated with the appropriate primary antibodies as follows for 16 h at 4 °C: anti-CHOP (1:50; Santa Cruz), anti-GM130 (1:50; BD Transduction Laboratories™), anti-Calnexin (1:100; Abcam) or anti-GST (MBB lab; La Trobe University). Secondary AlexaFluor-594 or 644 conjugated anti-mouse or anti-Rabbit antibodies (1:2000; Molecular Probes) were incubated for

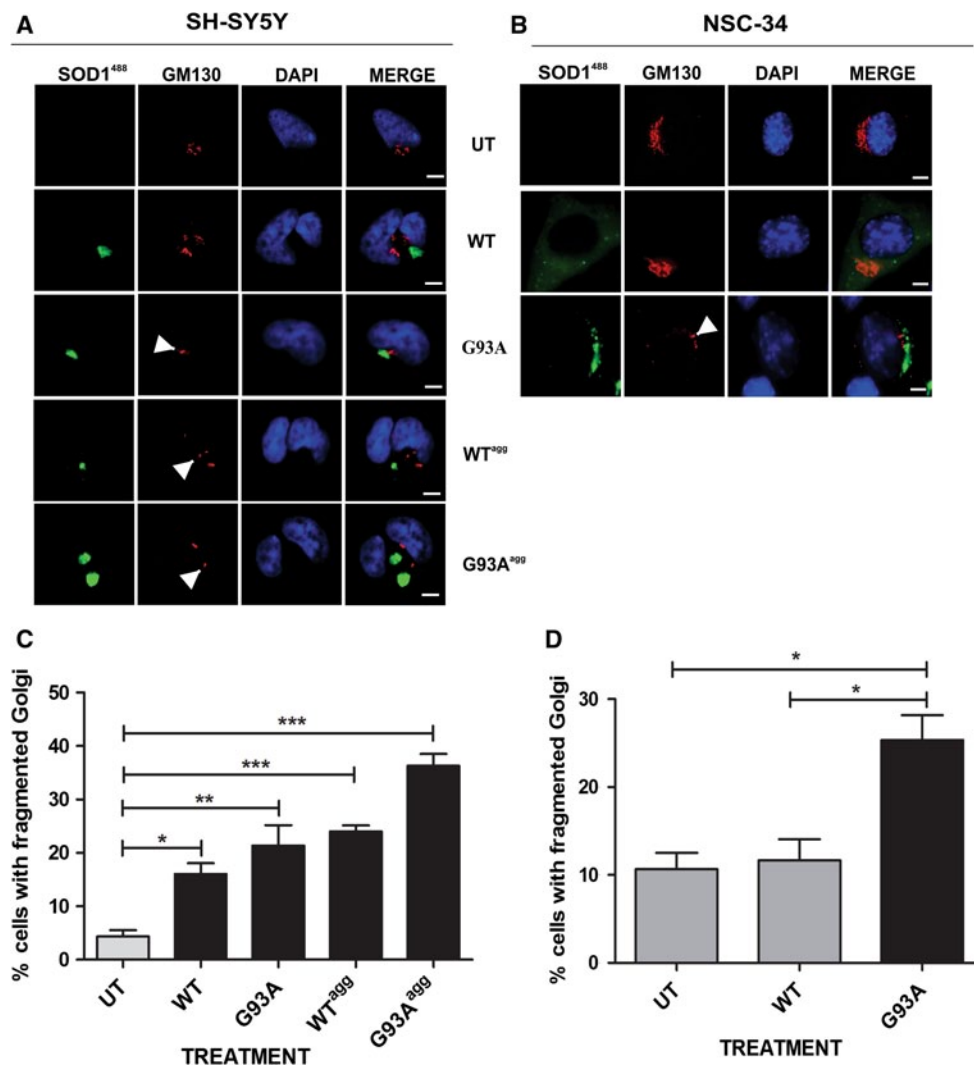


Fig. 5 Uptake of extracellular, aggregated SOD1^{WT} and mutant SOD1 induces Golgi fragmentation in SH-SY5Y and NSC-34 cells. SH-SY5Y cells treated with extracellular WT, G93A, WT^{agg}, G93A^{agg} SOD1 or NSC-34 cells treated with SOD1^{WT} and SOD1^{G93A} were fixed with 4 % PFA after 72 h treatment and immunostained with anti-GM130 antibody. **a** Representative images of SH-SY5Y cells treated with WT, G93A, WT^{agg}, G93A^{agg} SOD1 (green). Cells were stained with anti-GM130 antibody (red) and nuclei were stained with DAPI (blue). Arrows indicate fragmented Golgi, indicated by condensed punctate structures in contrast to intact Golgi (UT cells). **b** Representative images of NSC-34 cells stained with GM130 (red)

showing fragmented Golgi after treatment with mutant SOD1^{G93A}. All scale bars represent 10 μ m. **c** Quantification of cells with fragmented Golgi in SH-SY5Y cells upon treatment with extracellular WT, G93A, WT^{agg}, G93A^{agg} SOD1 for 72 h. **d** Quantification of cells with fragmented Golgi in NSC-34 cells 72 h after treatment with extracellular SOD1^{WT} and SOD1^{G93A}. There is no significant difference in the proportion of NSC-34 cells with fragmented Golgi in extracellular SOD1^{WT} treated cells compared to UT cells, in contrast to SH-SY5Y cells. Results are expressed as mean \pm SEM; $n = 3$; * $P < 0.05$, ** $P < 0.01$, *** $P < 0.001$ versus UT cells by one-way ANOVA with Tukey's post-test

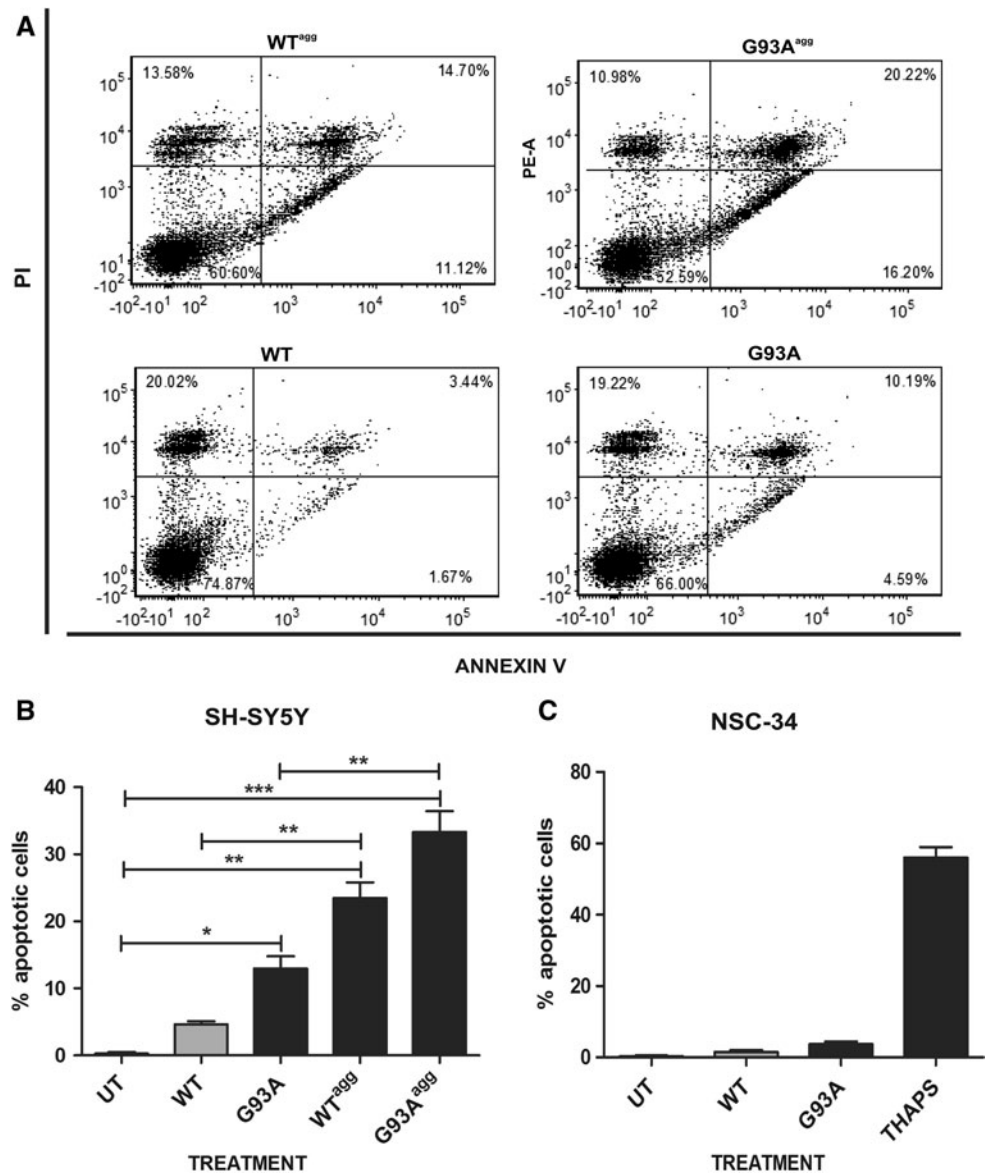
1 h at room temperature, cells were then treated with Hoechst 33342 (Invitrogen) and mounted on slides using fluorescent mounting medium (Dako). Images were acquired using constant gain and offset settings for CHOP using an Olympus fluorescence microscope at 40 \times magnification. Induction of ER stress was assessed by examining individual cells for nuclear immunoreactivity to CHOP. For each treatment, 100 cells from three different experiments were scored. Fragmentation of the Golgi apparatus was

determined by staining with the anti-GM130 antibody. The number of cells with fragmented Golgi per 100 cells from three different experiments was scored by fluorescence microscopy.

Protein extraction

The cells were washed with PBS and lysed with TN buffer (50 mM Tris-HCl pH 7.5, 150 mM NaCl, 0.1 % SDS) with

Fig. 6 Uptake of extracellular aggregated SOD1^{WT} and mutant SOD1 induces apoptotic cell death in SH-SY5Y cells but not NSC-34 cells. **a** SH-SY5Y cells treated with extracellular WT, G93A, WT^{agg} and G93A^{agg} SOD1 for 72 h were harvested, stained with PI/Annexin V and the percentage of cells in both early and late apoptotic phase was gated and scored by flow cytometry, as indicated by cells stained with both PI and Annexin V. **b** Percentage of apoptotic cells among cells treated with WT, G93A, WT^{agg} and G93A^{agg} and UT cells. Results are expressed as mean \pm SEM; $n = 3$; * $P < 0.05$, ** $P < 0.01$, *** $P < 0.001$ versus untreated cells by one-way ANOVA with Tukey's post-test, $n = 3$. **c** NSC-34 cells treated with extracellular SOD1^{WT} and SOD1^{G93A} for 72 h were stained with PI/Annexin V and analysed by flow cytometry. In contrast to SH-SY5Y cells, no significant percentage (>5 %) of apoptotic cells were identified in NSC-34 after treatment with SOD1^{G93A}. NSC-34 cells were treated with 10 μ M thapsigargin (THAPS) for 4 h before harvesting as a positive control



1 % protease inhibitor (Sigma), followed by incubation on ice for 10 min. The SDS soluble protein fraction was collected by centrifugation at 16 100 g for 10 min. For immunoblotting, the cells were also treated with 0.125 % trypsin for 2 min at room temperature before lysis, to remove residual extracellular SOD1.

Immunoblotting

Protein samples (20 μ g) electrophoresed through 10 % SDS–polyacrylamide gels or 10 % native PAGE (non-denaturing) gels and transferred to nitrocellulose membranes (Millipore). For the SDS-PAGE analysis of SOD1 aggregates, the samples were prepared in sample loading buffer (0.042 M Tris–HCl, 2 % SDS, 1 % glycine, 0.005 % bromophenol blue, 10 % glycerol, 100 mM iodoacetamide,

4 % freshly added β mercaptoethanol). Membranes were blocked with 3 % (w/v) bovine serum albumin (BSA; Sigma), pH 8.0 for 1 h. The appropriate primary antibodies were prepared in 1 % (w/v) BSA solution as follows: SOD1 (1:1000; Calbiochem), BiP (1:4000; Stressgen), Xbp1 (1:400; SC), IRE1 (1:600; SC) and β actin as a loading control (1:750; Sigma-Aldrich). All antibodies were incubated with membranes for 1 h at room temperature (RT). Blots were probed with HRP-conjugated donkey anti-sheep, goat anti-rabbit or goat anti-mouse antibodies at 1:2500 (Chemicon) for 1 h at RT and then developed using enhanced chemiluminescence (ECL) reagents (Roche). Quantification of band intensities was performed by densitometric analysis following subtraction of background using Image J (National Institutes of Health, Bethesda, MA, USA) and expressed relative to the corresponding signal for β -actin.

Blots were stripped using Reblot Plus solution (Chemicon) for 15 min, and then reprobed as above.

VSVG transport assay

SH-SY5Y or NSC-34 cells were plated on 24-well plates with 13 mm coverslips. After 24 h in culture, cells were transfected with VSVG-ts045 tagged with fluorescent mCherry (a kind gift from Dr. Jennifer Lippincott-Schwartz and Dr. George Patterson) and another 24 h later cells were treated with extracellular SOD1 protein [35]. Following treatment for 24 h, cells were incubated at 40 °C for 24 h to accumulate VSVG-ts045 in the ER. Cycloheximide (20 µg/mL) was then added, and cells were shifted to 32 °C for 60 min or immediately fixed at 0 min. At each time interval, cells were washed with ice-cold PBS and fixed with 4 % PFA. The ER and Golgi compartments were immunostained with rabbit polyclonal anti-Calnexin antibody (Abcam) and mouse monoclonal anti-GM130 antibody (BD Transduction Laboratories™) as described above. In each experiment 20 cells were scored, and all experiments were performed in triplicate. Image analysis was performed using Image J using the JACoP plugin to threshold and collect the Mander's coefficient [36] between the mCherry and far-red channels.

Annexin V binding assay to detect apoptotic cell death

SH-SY5Y cells cultured in six-well plates were treated with extracellular SOD1 protein as above. The cells were harvested after 72 h treatment by adding trypsin for 1 min at room temperature. The cells were then collected in PBS, centrifuged at 1200 rpm for 5 min, and resuspended in 200 µl of annexin V binding buffer (10 mM HEPES, 140 mM NaCl, 2.5 mM CaCl₂, pH 7.4). The cell suspension was treated with 3 µl of annexin V dye (Invitrogen) at room temperature for 15 min in the dark. Annexin V binding buffer (100 µl) was then added to the cell suspension, counter-stained with 5 µg/mL of propidium iodide (PI, Sigma) and analyzed by BD FACS Canto II flow cytometer.

Statistical analyses

Data are presented as mean \pm standard error of the mean (SEM) from at least three independent experiments and were analyzed by one-way ANOVA followed by Tukey's post hoc test using Prism 5.0 GraphPad Software. A value of $P < 0.05$ was considered significant.

Acknowledgments We thank Professor Neil Cashmann for the gift of NSC-34 cells, and we thank Dr Jennifer Lippincott-Schwartz and Dr George Patterson for the VSVG-ts045-mCherry construct. This

work was supported by National Health and Medical Research Council of Australia Project Grants [# 1006141, 1030513 to J.A.], Bethlehem Griffiths Research Foundation, Motor Neuron Disease Research Institute of Australia, Suzie Harris Memorial Fund MND Research Grant and Rosalind Nicholson MND Research Grant [to J.A.], a National Health and Medical Research Council CJ Martin Biomedical Early Career fellowship [1036835 to A.W.] and an Australian Postgraduate Award and Australian Rotary Health scholarship [to A.W.].

References

- Münch C, O'Brien J, Bertolotti A (2011) Prion-like propagation of mutant superoxide dismutase-1 misfolding in neuronal cells. *Proc Natl Acad Sci USA* 108:3548–3553
- Desplats P, Lee HJ, Bae EJ, Patrick C, Rockenstein E, Crews L, Spencer B, Masliah E, Lee SJ (2009) Inclusion formation and neuronal cell death through neuron-to-neuron transmission of α -synuclein. *Proc Natl Acad Sci USA* 106(31):13010–13015
- Clavaguera F, Bolmont T, Crowther RA, Abramowski D, Frank S, Probst A, Fraser G, Stalder AK, Beibel M, Staufenbiel M (2009) Transmission and spreading of tauopathy in transgenic mouse brain. *Nat Cell Biol* 11(7):909–913
- Bosco DA, Morfini G, Karabacak NM, Song Y, Gros-Louis F, Pasinelli P, Goolsby H, Fontaine BA, Lemay N, McKenna-Yasek D (2010) Wild-type and mutant SOD1 share an aberrant conformation and a common pathogenic pathway in ALS. *Nat Neurosci* 13(11):1396–1403
- Forsberg K, Jonsson PA, Andersen PM, Bergemalm D, Graffmo KS, Hultdin M, Jacobsson J, Rosquist R, Marklund SL, Brännström T (2010) Novel antibodies reveal inclusions containing non-native SOD1 in sporadic ALS patients. *PLoS ONE* 5(7):e11552
- Atkin JD, Farg MA, Turner BJ, Tomas D, Lysaght JA, Nunan J, Rembach A, Nagley P, Beart PM, Cheema SS (2006) Induction of the unfolded protein response in familial amyotrophic lateral sclerosis and association of protein-disulfide isomerase with superoxide dismutase 1. *J Biol Chem* 281(40):30152–30165
- Atkin JD, Farg MA, Walker AK, McLean C, Tomas D, Horne MK (2008) Endoplasmic reticulum stress and induction of the unfolded protein response in human sporadic amyotrophic lateral sclerosis. *Neurobiol Dis* 30(3):400–407
- Saxena S, Cabuy E, Caroni P (2009) A role for motoneuron subtype-selective ER stress in disease manifestations of FALS mice. *Nat Neurosci* 12(5):627–636
- Gonatas N, Stieber A, Mourelatos Z, Chen Y, Gonatas J, Appel S, Hays A, Hickey W, Hauw J (1992) Fragmentation of the Golgi apparatus of motor neurons in amyotrophic lateral sclerosis. *Am J Pathol* 140(3):731
- Guareschi S, Cova E, Cereda C, Ceroni M, Donetti E, Bosco DA, Trotti D, Pasinelli P (2012) An over-oxidized form of superoxide dismutase found in sporadic amyotrophic lateral sclerosis with bulbar onset shares a toxic mechanism with mutant SOD1. *Proc Natl Acad Sci USA* 109(13):5074–5079
- Graffmo KS, Forsberg K, Bergh J, Birve A, Zetterström P, Andersen PM, Marklund SL, Brännström T (2013) Expression of wild-type human superoxide dismutase-1 in mice causes amyotrophic lateral sclerosis. *Hum Mol Genet* 22(1):51–60
- Turner BJ, Atkin JD, Farg MA, Rembach A, Lopes EC, Patch JD, Hill AF, Cheema SS (2005) Impaired extracellular secretion of mutant superoxide dismutase 1 associates with neurotoxicity in familial amyotrophic lateral sclerosis. *J Neurosci* 25(1):108–117
- Gomes C, Keller S, Altevogt P, Costa J (2007) Evidence for secretion of Cu, Zn superoxide dismutase via exosomes from

- a cell model of amyotrophic lateral sclerosis. *Neurosci Lett* 428(1):43–46
14. Frutiger K, Lukas TJ, Gorrie G, Ajroud-Driss S, Siddique T (2008) Gender difference in levels of Cu/Zn superoxide dismutase (SOD1) in cerebrospinal fluid of patients with amyotrophic lateral sclerosis. *Amyotrophic Lateral Scler* 9(3):184–187
 15. Zetterström P, Andersen PM, Brännström T, Marklund SL (2011) Misfolded superoxide dismutase-1 in CSF from amyotrophic lateral sclerosis patients. *J Neurochem* 117(1):91–99
 16. Ezzi SA, Urushitani M, Julien JP (2007) Wild type superoxide dismutase acquires binding and toxic properties of ALS linked mutant forms through oxidation. *J Neurochem* 102(1):170–178
 17. Grad LI, Guest WC, Yanai A, Pokrishevsky E, O'Neill MA, Gibbs E, Semenchenko V, Yousefi M, Wishart DS, Plotkin SS (2011) Intermolecular transmission of superoxide dismutase 1 misfolding in living cells. *Proc Natl Acad Sci* 108(39):16398–16403
 18. Urushitani M, Ezzi SA, Julien JP (2007) Therapeutic effects of immunization with mutant superoxide dismutase in mice models of amyotrophic lateral sclerosis. *Proc Natl Acad Sci* 104(7):2495–2500
 19. Gros-Louis F, Soucy G, Larivière R, Julien JP (2010) Intracerebroventricular infusion of monoclonal antibody or its derived Fab fragment against misfolded forms of SOD1 mutant delays mortality in a mouse model of ALS. *J Neurochem* 113(5):1188–1199
 20. Takeuchi S, Fujiwara N, Ido A, Oono M, Takeuchi Y, Tateno M, Suzuki K, Takahashi R, Tooyama I, Taniguchi N (2010) Induction of protective immunity by vaccination with wild-type apo superoxide dismutase 1 in mutant SOD1 transgenic mice. *J Neuropathol Exp Neurol* 69(10):1044
 21. Ron D, Walter P (2007) Signal integration in the endoplasmic reticulum unfolded protein response. *Nat Rev Mol Cell Biol* 8(7):519–529
 22. Bertolotti A, Zhang Y, Hendershot LM, Harding HP, Ron D (2000) Dynamic interaction of BiP and ER stress transducers in the unfolded-protein response. *Nat Cell Biol* 2(6):326–332
 23. Nishitoh H, Kadowaki H, Nagai A, Maruyama T, Yokota T, Fukutomi H, Noguchi T, Matsuzawa A, Takeda K, Ichijo H (2008) ALS-linked mutant SOD1 induces ER stress-and ASK1-dependent motor neuron death by targeting Derlin-1. *Genes Dev* 22(11):1451–1464
 24. Preston A, Gurisik E, Bartley C, Laybutt D, Biden T (2009) Reduced endoplasmic reticulum (ER)-to-Golgi protein trafficking contributes to ER stress in lipotoxic mouse beta cells by promoting protein overload. *Diabetologia* 52(11):2369–2373
 25. Thayanidhi N, Helm JR, Nycz DC, Bentley M, Liang Y, Hay JC (2010) α -Synuclein delays endoplasmic reticulum (ER)-to-Golgi transport in mammalian cells by antagonizing ER/Golgi SNAREs. *Mol Biol Cell* 21(11):1850–1863
 26. Mourelatos Z, Gonatas NK, Stieber A, Gurney ME, Dal Canto MC (1996) The Golgi apparatus of spinal cord motor neurons in transgenic mice expressing mutant Cu, Zn superoxide dismutase becomes fragmented in early, preclinical stages of the disease. *Proc Natl Acad Sci* 93(11):5472–5477
 27. Lucocq J, Warren G, Pryde J (1991) Okadaic acid induces Golgi apparatus fragmentation and arrest of intracellular transport. *J Cell Sci* 100(4):753–759
 28. Roberts K, Zeineddine R, Corcoran L, Li W, Campbell IL, Yerbury JJ (2012) Extracellular aggregated Cu/Zn superoxide dismutase activates microglia to give a cytotoxic phenotype. *Glia* 61:409–419
 29. Olczak M, Olczak T (2006) Comparison of different signal peptides for protein secretion in nonlytic insect cell system. *Anal Biochem* 359(1):45–53
 30. Schröder M, Kaufman RJ (2005) ER stress and the unfolded protein response. *Mutat Res Fundam Mol Mech* 569(1):29–63
 31. Walker AK, Farg MA, Bye CR, McLean CA, Horne MK, Atkin JD (2010) Protein disulphide isomerase protects against protein aggregation and is S-nitrosylated in amyotrophic lateral sclerosis. *Brain* 133(1):105–116
 32. Furukawa Y, Kaneko K, Yamanaka K, O'Halloran TV, Nukina N (2008) Complete loss of post-translational modifications triggers fibrillar aggregation of SOD1 in the familial form of amyotrophic lateral sclerosis. *J Biol Chem* 283(35):24167–24176
 33. Durer ZAO, Cohlberg JA, Dinh P, Padua S, Ehrenclou K, Downes S, Tan JK, Nakano Y, Bowman CJ, Hoskins JL (2009) Loss of metal ions, disulfide reduction and mutations related to familial ALS promote formation of amyloid-like aggregates from superoxide dismutase. *PLoS ONE* 4(3):e5004
 34. Furukawa Y, Kaneko K, Yamanaka K, Nukina N (2010) Mutation-dependent polymorphism of Cu, Zn-superoxide dismutase aggregates in the familial form of amyotrophic lateral sclerosis. *J Biol Chem* 285(29):22221–22231
 35. Hirschberg K, Miller CM, Ellenberg J, Presley JF, Siggia ED, Phair RD, Lippincott-Schwartz J (1998) Kinetic analysis of secretory protein traffic and characterization of Golgi to plasma membrane transport intermediates in living cells. *J Cell Biol* 143(6):1485–1503
 36. Manders E, Verbeek F, Aten J (2011) Measurement of co-localization of objects in dual-colour confocal images. *J Microsc* 169(3):375–382
 37. Darzynkiewicz Z, Juan G, Li X, Gorczyca W, Murakami T, Traganos F (1997) Cytometry in cell necrobiology: analysis of apoptosis and accidental cell death (necrosis). *Cytometry* 27(1):1–20
 38. Doherty GJ, McMahon HT (2009) Mechanisms of endocytosis. *Annu Rev Biochem* 78:857–902
 39. Sun P, Yamamoto H, Suetsugu S, Miki H, Takenawa T, Endo T (2003) Small GTPase Rac/Rab34 is associated with membrane ruffles and macropinosomes and promotes macropinosome formation. *J Biol Chem* 278(6):4063–4071
 40. Grimmer S, van Deurs B, Sandvig K (2002) Membrane ruffling and macropinocytosis in A431 cells require cholesterol. *J Cell Sci* 115(14):2953–2962
 41. Phatnani HP, Guarnieri P, Friedman BA, Carrasco MA, Muratet M, O'Keeffe S, Nwakeze C, Pauli-Behn F, Newberry KM, Meadows SK (2013) Intricate interplay between astrocytes and motor neurons in ALS. *Proc Natl Acad Sci* 110(8):E756–E765
 42. Nagai M, Re DB, Nagata T, Chalazonitis A, Jessell TM, Wichterle H, Przedborski S (2007) Astrocytes expressing ALS-linked mutated SOD1 release factors selectively toxic to motor neurons. *Nat Neurosci* 10(5):615–622
 43. Brotherton TE, Li Y, Cooper D, Gearing M, Julien JP, Rothstein JD, Boylan K, Glass JD (2012) Localization of a toxic form of superoxide dismutase 1 protein to pathologically affected tissues in familial ALS. *Proc Natl Acad Sci* 109(14):5505–5510
 44. Banci L, Bertini I, Boca M, Girotto S, Martinelli M, Valentine JS, Vieru M (2008) SOD1 and amyotrophic lateral sclerosis: mutations and oligomerization. *PLoS ONE* 3(2):e1677
 45. Tiwari A, Hayward LJ (2003) Familial amyotrophic lateral sclerosis mutants of copper/zinc superoxide dismutase are susceptible to disulfide reduction. *J Biol Chem* 278(8):5984–5992
 46. Gurney ME, Pu H, Chiu AY, Dal Canto MC, Polchow CY, Alexander DD, Caliendo J, Hentati A, Kwon YW, Deng H-X (1994) Motor neuron degeneration in mice that express a human Cu, Zn superoxide dismutase mutation. *Science* 264(5166):1772–1775
 47. Kikuchi H, Almer G, Yamashita S, Guégan C, Nagai M, Xu Z, Sosunov AA, McKhann GM II, Przedborski S (2006) Spinal cord endoplasmic reticulum stress associated with a microsomal accumulation of mutant superoxide dismutase-1 in an ALS model. *Proc Natl Acad Sci* 103(15):6025–6030
 48. Lindberg MJ, Tibell L, Oliveberg M (2002) Common denominator of Cu/Zn superoxide dismutase mutants associated with amyotrophic lateral sclerosis: decreased stability of the apo state. *Proc Natl Acad Sci* 99(26):16607–16612

Supplementary Materials

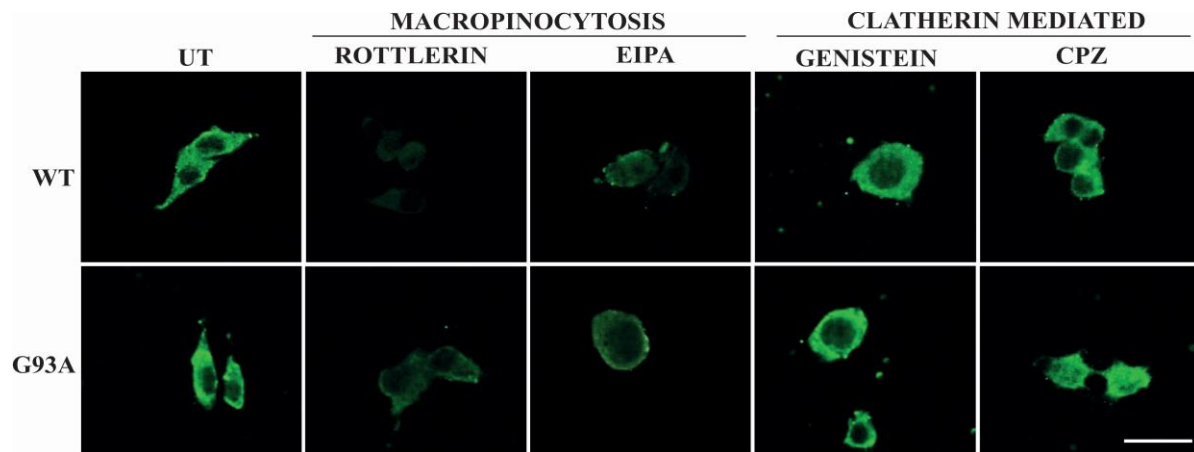


Fig.S1. SOD1 uptake is mediated by macropinocytosis. Scanning confocal micrographs of SOD1 proteins internalisation by NSC-34 cells. Cells were incubated with 20 μ g/mL of either SOD1^{WT} or G93A SOD1 for 30 minutes. At 30 minutes cells were fixed and stained for human SOD1. In some cases cells were pre- and co-treated with endocytosis inhibitors rottlerin, 5-(N-Ethyl-N-isopropyl)amiloride (EIPA), genistein or chlorpromazine hydrochloride (CPZ). Scale bar represent 10 μ m.

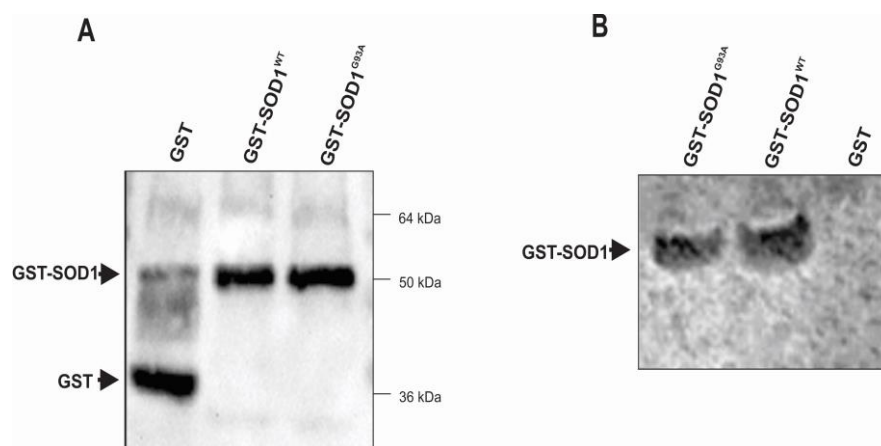
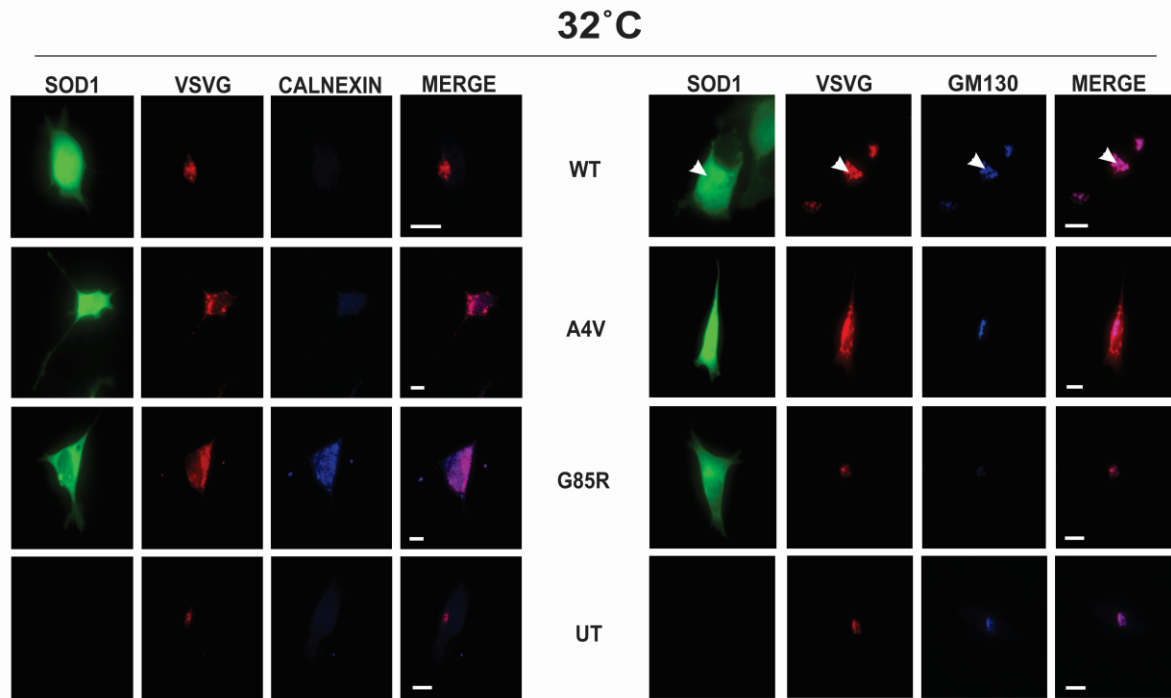


Fig.S2. Baculovirus expressed GST-labeled SOD1^{WT} and mutant SOD1 proteins are enzymically active in conditioned medium of insect Sf9 cells. (A) Insect Sf9 cells were transfected with pIEX-3 alone and pIEX-3 SOD1 WT and G93A constructs for 48 h. The conditioned cell culture medium was harvested, centrifuged at 1200 rpm for 5 min to remove cell debris and then analysed by immunoblotting with an anti-GST antibody (50 μ g/lane). The blot confirms the presence of GST, GST-SOD1^{WT} and GST-SOD1^{G93A} proteins, indicating secretion into Sf9 conditioned medium. (B) Zymography reveals SOD1

dismutase activity is present in the Sf9 conditioned medium of GST-SOD1^{WT} and GST-SOD1^{G93A} but not GST-only transfected cells.

A



B

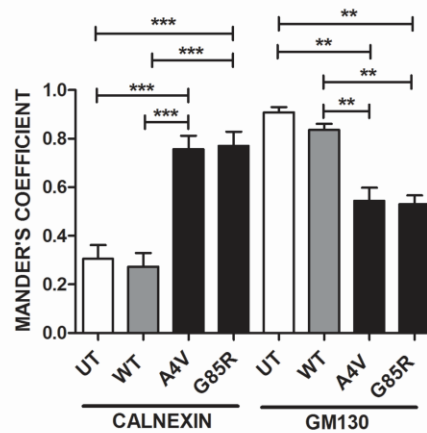


Fig.S3. ER to Golgi trafficking is inhibited in SH-SY5Y cells expressing intracellular mutant SOD1. Cells were transfected with VSVG-ts045 mCherry and either WT, A4V, or G85R SOD1-EGFP constructs for 24 h. After trapping VSVG-ts045 mCherry in the ER by incubation at 40°C for 24 h after transfection, the temperature was shifted to 32°C for 30 min or fixed immediately at 0 min. The cells were then fixed with 4% PFA and stained with calnexin (blue) or GM130 (blue). (A) Representative fluorescent images after 30 min incubation at 32°C. VSVG is co-localised with GM130 in cells expressing SOD1 WT and control untransfected (UT) cells. In contrast, in cells expressing mutant SOD1 A4V or G85R, VSVG-ts045 is still predominantly co-localised with calnexin. All scale bars 10 µm. (C) Quantification of the degree of co-localisation of VSVG with calnexin and GM130 at 60 min

as in (B) using Mander's coefficient. Data are presented as mean \pm SEM, *** $p < 0.001$, ** $P < 0.01$ versus SOD1^{WT} expressing cells or untransfected cells by one-way ANOVA with Tukey's post-test, $n=3$.

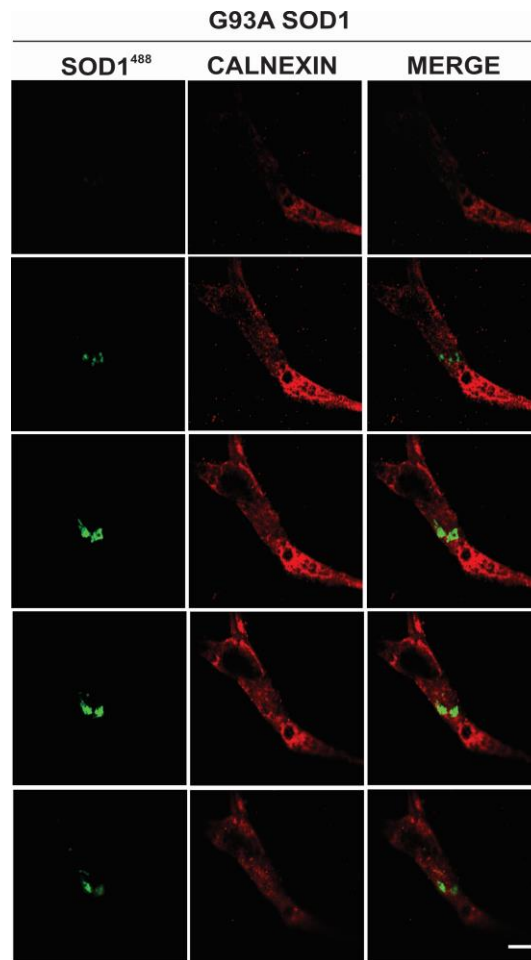


Fig.S4. Extracellular mutant G93A SOD1 does not localize in ER after uptake. NSC-34 cells treated with SOD1^{G93A} for 48 h was fixed with 4% PFA and stained with anti-calnexin antibody (red), ER marker. Series of Z stack images of NSC-34 cell bearing SOD1^{G93A} inclusions (green) are shown. Scale bar represent 10 μ m.

Chapter 4

4. Defects in optineurin and myosin VI mediated cellular trafficking in amyotrophic lateral sclerosis

4. Chapter 4

4.1 Preface

Chapter 4 is presented as a manuscript recently published at the journal *Human Molecular Genetics*. The previous versions of this manuscript were also peer reviewed after earlier submissions to *Brain* and *Acta Neuropathologica*. The current version is modified with additional data based on suggestions provided by the reviewers. The author performed all the work described here, except where acknowledgements are made as below:

Isolation, culture and fixation of human primary motor neurons was performed by Vanessa Tan (Macquarie University). These primary cells were then stained and analysed by the author (Figure 1a). Genomic sequencing was performed by members of Associate Professor Ian Blair's group (Macquarie University); Jennifer Fifta, Emily McCann and Dr Kelly Williams, using DNA samples extracted from sporadic patient tissue lysates by the author.

The author also acknowledges valuable discussions towards experimental design and manuscript preparation from Dr Adam Walker (University of Pennsylvania) and Manal Farg (La Trobe University). The author wrote the manuscript which was revised by principal supervisor Dr Julie Atkin (La Trobe University).

4.2 Manuscript 2

The following is the presentation of chapter 4 as a copy of the manuscript published in *Human Molecular Genetics* (2015).



ORIGINAL ARTICLE

Defects in optineurin- and myosin VI-mediated cellular trafficking in amyotrophic lateral sclerosis

Vinod Sundaramoorthy^{1,2}, Adam K. Walker^{2,†}, Vanessa Tan¹, Jennifer A. Fifta¹, Emily P. Mccann¹, Kelly L. Williams¹, Ian P. Blair¹, Gilles J. Guillemin¹, Manal A. Farg² and Julie D. Atkin^{1,2,*}

¹Department of Biomedical Sciences, Faculty of Medicine & Health Sciences, Macquarie University, NSW 2109, Australia and ²Department of Biochemistry, La Trobe Institute for Molecular Science, La Trobe University, Victoria 3086, Australia

*To whom correspondence should be addressed at: MND and Neurodegenerative Diseases Research Center, Australian School of Advanced Medicine, Macquarie University, NSW 2109, Australia. Tel: +61 298502772; Fax: +61 298502701; Email: julie.atkin@mq.edu.au

Abstract

Amyotrophic lateral sclerosis (ALS) is a fatal neurodegenerative disorder primarily affecting motor neurons. Mutations in optineurin cause a small proportion of familial ALS cases, and wild-type (WT) optineurin is misfolded and forms inclusions in sporadic ALS patient motor neurons. However, it is unknown how optineurin mutation or misfolding leads to ALS. Optineurin acts as an adaptor protein connecting the molecular motor myosin VI to secretory vesicles and autophagosomes. Here, we demonstrate that ALS-linked mutations p.Q398X and p.E478G disrupt the association of optineurin with myosin VI, leading to an abnormal diffuse cytoplasmic distribution, inhibition of secretory protein trafficking, endoplasmic reticulum (ER) stress and Golgi fragmentation in motor neuron-like NSC-34 cells. We also provide further insight into the role of optineurin as an autophagy receptor. WT optineurin associated with lysosomes and promoted autophagosome fusion to lysosomes in neuronal cells, implying that it mediates trafficking of lysosomes during autophagy in association with myosin VI. However, either expression of ALS mutant optineurin or small interfering RNA-mediated knockdown of endogenous optineurin blocked lysosome fusion to autophagosomes, resulting in autophagosome accumulation. Together these results indicate that ALS-linked mutations in optineurin disrupt myosin VI-mediated intracellular trafficking processes. In addition, in control human patient tissues, optineurin displayed its normal vesicular localization, but in sporadic ALS patient tissues, vesicles were present in a significantly decreased proportion of motor neurons. Optineurin binding to myosin VI was also decreased in tissue lysates from sporadic ALS spinal cords. This study therefore links several previously described pathological mechanisms in ALS, including defects in autophagy, fragmentation of the Golgi and induction of ER stress, to disruption of optineurin function. These findings also indicate that optineurin–myosin VI dysfunction is a common feature of both sporadic and familial ALS.

Introduction

Amyotrophic lateral sclerosis (ALS) is a neurodegenerative disorder affecting motor neurons in the brain, brainstem and spinal cord. While most ALS cases are sporadic, ~10% of cases are familial.

Mutations in the optineurin gene (OPTN) cause >1% of familial ALS cases and also primary open angle glaucoma, a neurodegenerative eye disorder (1,2). ALS is characterized by the accumulation of intracellular ubiquitinated protein inclusions in affected

[†] Present address: Center for Neurodegenerative Disease Research, Department of Pathology and Laboratory Medicine, Perelman School of Medicine, University of Pennsylvania, Philadelphia, PA 19104 USA.

Received: January 19, 2015. Revised: March 27, 2015. Accepted: April 7, 2015

© The Author 2015. Published by Oxford University Press. All rights reserved. For Permissions, please email: journals.permissions@oup.com

tissues in both familial and sporadic cases. Mutations in the genes encoding TAR DNA-binding protein 43 (TDP-43), fused in sarcoma (FUS) and Cu/Zn-superoxide dismutase (SOD1) also cause familial forms of ALS. However, in addition, wild-type (WT) forms of these proteins misfold and are present in inclusions in sporadic ALS motor neurons (3–5). Similarly, mutant optineurin co-localizes with ubiquitinated inclusions in OPTN mutation familial ALS cases (1), and WT optineurin is present in sporadic ALS motor neuron inclusions (6). WT optineurin is also present within pathogenic aggregates found in other neurodegenerative disorders, including Alzheimer's, Parkinson's, Huntington's and Creutzfeldt-Jacob diseases and multiple system atrophy (7,8).

The etiology of motor neuron dysfunction in ALS remains unclear. However, accumulation of misfolded protein aggregates, induction of endoplasmic reticulum (ER) stress, fragmentation of the Golgi apparatus and dysfunction in autophagy and intracellular trafficking are all implicated (9–13). Similarly, it is unknown how mutations in optineurin trigger ALS. Optineurin is a protein that functions in cellular trafficking and autophagy, a dynamic process involving the formation and trafficking of autophagic vacuoles that engulf misfolded proteins and defective organelles (14). Mature autophagosomes fuse with lysosomes, and the contents of the resulting autophagolysosome are then degraded by acidic components of the lysosome (15). These dynamic processes require efficient cellular trafficking to transport late endosomes to autophagosomes and then to drive fusion of autophagosomes with lysosomes. Autophagosomes were also recently linked to the ER-Golgi compartments, as the formation of autophagosomes occurs from the ER (16–18). Disruption to cellular trafficking can trigger ER stress and induce the unfolded protein response (UPR), a homeostatic response to the presence of intracellular misfolded proteins in the ER (19). ER stress is present in sporadic ALS patients, transgenic rodent models expressing mutant SOD1 and in neuronal cells expressing mutant forms of SOD1, FUS and TDP-43 (10,20–22). We recently demonstrated that cytoplasmic misfolded WT and mutant SOD1 disrupt ER-Golgi transport, and this is associated with ER stress in ALS (12,13). These findings raise the possibility that intracellular trafficking disruption is an important upstream event in ALS pathogenesis.

Myosin VI is involved in the intracellular transport of endocytic vesicles, secretory vesicles and autophagosomes (23,24). Adaptor proteins link myosin VI to specific cargoes by binding to the myosin VI globular tail/cargo binding domain (25). Optineurin is one such adaptor protein which co-localizes with myosin VI at the Golgi apparatus and plasma membrane (26). Binding of optineurin triggers dimerization of myosin VI, which allows unconventional processive movement toward the minus end of actin filaments (27). Optineurin is also an autophagy receptor that directly binds to protein aggregates and microtubule-associated protein 1A/1B-light chain 3 (LC3) (28,29). Furthermore, optineurin depletion using small interfering RNA (siRNA) inhibits autophagy (29) and exocytosis (26). Recently, myosin VI was shown to mediate the trafficking of autophagosomes on actin filaments, aiding their fusion with lysosomes (28). Simultaneous knockdown of optineurin together with other myosin VI-associated autophagy adaptors T6BP and NDP52 decreased autophagosome formation and prevented autophagosome-lysosome fusion, suggesting that these three adaptors mediate myosin VI-dependent autophagy trafficking (25). However, the role of these adaptors individually in autophagy has not been determined. Hence, it remains unclear exactly how optineurin, in conjunction with myosin VI, mediates autophagy trafficking and

whether optineurin/myosin VI also associate with lysosomes as well as autophagosomes, to promote autophagosome-lysosome fusion.

The majority of mutations in optineurin that cause ALS are present in the myosin VI binding site (1,30,31). Hence, we hypothesized that these mutations disrupt the normal association of optineurin with myosin VI and thus perturb myosin VI-dependent functions in trafficking and autophagy. Here, we demonstrate that in contrast to WT and a glaucoma-causing OPTN mutant (p. E50K, c.148G>A), two ALS-linked OPTN mutants (heterozygous p. E478G, c.1433A>G and homozygous p.Q398X, c.1192C>T) did not bind to myosin VI, form vesicles or co-localize with either autophagosomes or lysosomes in neuronal cells. Expression of the ALS mutants resulted in the accumulation of autophagosomes, suggesting a defect in lysosome fusion, inhibition of secretory protein transport from the Golgi to plasma membrane and a corresponding induction of ER stress and fragmentation of the neuronal Golgi apparatus. We also demonstrate that WT optineurin associates with lysosomes, thus providing an explanation for previous observations that optineurin-myosin VI mediates autophagosome/lysosome fusion (28). Moreover, examination of human spinal cord tissues revealed that in sporadic ALS patient motor neurons, optineurin did not bind to myosin VI or form vesicles, implying that loss of optineurin-myosin VI function occurs in sporadic ALS. Hence, we propose that optineurin and myosin VI defects are present in both familial and sporadic ALS, thus providing new insights into pathogenesis.

Results

ALS mutant optineurin mislocalizes from vesicles in neuronal cells

We next expressed four enhanced green fluorescent protein (EGFP)-tagged optineurin proteins in the NSC-34 motor neuron-like cell line; WT, ALS mutants E478G and Q398X (1) and a glaucoma mutant, E50K (2). As expected, the truncation mutant Q398X migrated at a lower apparent molecular weight (~72 kDa) compared with the other proteins (~90 kDa) (Supplementary Material, Fig. S1A). Immunoblotting revealed increased levels of insoluble optineurin in cells expressing the ALS mutants compared with WT and E50K ($P < 0.001$), indicative of protein misfolding or aggregation (Supplementary Material, Fig. S1A and B). Although both WT and E50K formed vesicular structures (defined as punctate structures of less than 3 μm in diameter, Supplementary Material, Fig. S1C) in 70–80% of cells, E478G and Q398X optineurin mutants were expressed in the cytoplasm in a diffuse, non-vesicular manner in most cells (~70%; Supplementary Material, Fig. S1C), with only <10% of cells bearing vesicles ($P < 0.0001$; Supplementary Material, Fig. S1D), consistent with previous observations (1). Similar findings were obtained when HA-tagged WT and Q398X mutant optineurin were expressed in NSC-34 cells, allowing us to rule out an aberrant effect of EGFP on the cellular distribution of optineurin (Supplementary Material, Fig. S1E and F).

Dissociation of ALS-linked mutant optineurin from myosin VI prevents vesicle formation

We investigated whether the ALS-linked optineurin mutations disturb myosin VI-optineurin function. First, immunocytochemistry of human primary motor neuron cultures revealed that optineurin was present as vesicular structures that co-localized with myosin VI in all cells examined (Fig. 1A), confirming that optineurin-myosin VI function together in human motor neurons.

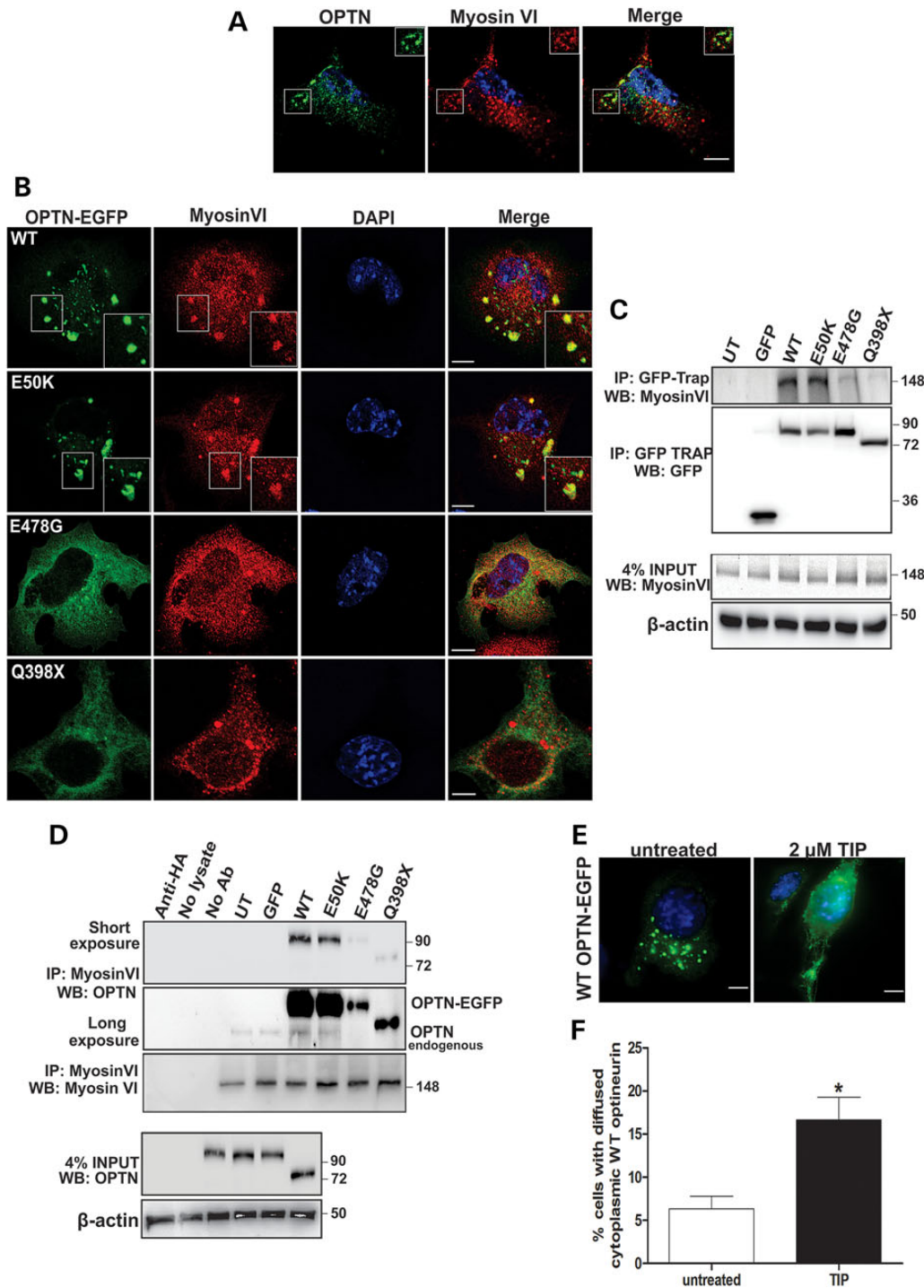


Figure 1. ALS optineurin mutants dissociate from myosin VI, which induces diffuse cytoplasmic distribution of optineurin. (A) Human primary motor neurons were stained with anti-optineurin (green) and anti-myosin VI (red) antibodies. Nuclei were stained with DAPI (blue). Scale bar, 10 μ m. (B) Immunofluorescence images of NSC-34 cells expressing optineurin-EGFP proteins (green), immunostained with an anti-myosin VI antibody (red). Optineurin-positive vesicles that co-localize with myosin VI were observed in WT and E50K expressing cells but not in ALS mutant expressing cells. Insets show higher magnification of the areas outlined. Scale bars, 10 μ m. (C) Co-precipitation of NSC-34 cell lysates expressing optineurin-EGFP proteins using GFP-Trap, followed by immunoblotting using an anti-myosin VI antibody. Less myosin VI precipitated with ALS mutant optineurin when compared with WT and E50K glaucoma mutant optineurin. 4% input control is shown: blot was re-probed for β -actin as a loading control. (D) Immunoprecipitation of NSC-34 lysates using an anti-myosin VI antibody followed by immunoblotting using an anti-optineurin antibody. Endogenous optineurin is observed at ~74 kDa upon long exposure. 4% input control is shown: blot was re-probed for β -actin as a loading control. Immunoprecipitation of similar levels of optineurin-EGFP or myosin VI are revealed by immunoblotting of the respective blots with anti-GFP or anti-myosin VI antibodies (C and D). Bottom panels show immunoblotting of 4% lysates as input with anti-myosin VI or anti-optineurin antibodies. β -Actin was used as a loading control. Approximate molecular weight markers are shown on the right in kDa. (E) Treatment of NSC-34 cells with 2 μ M of TIP for 60 min alters the morphology of WT optineurin-EGFP (green) from predominately vesicular to diffuse appearance. (F) Quantification of NSC-34 cells expressing WT optineurin-EGFP with a diffuse non-vesicular morphology, with and without TIP treatment. One hundred cells were scored from each experiment. Data are represented as the mean \pm SEM; * P < 0.05, using unpaired t-test, n = 3. Nuclei stained with DAPI (blue). Scale bars, 10 μ m.

We next examined the interaction between optineurin EGFP-tagged proteins and myosin VI. In transfected NSC-34 cells, WT and E50K optineurin co-localized with vesicular myosin VI, in contrast to E478G or Q398X optineurin mutants, which showed little co-localization with myosin VI (Fig. 1B). Furthermore, although myosin VI was immunoprecipitated by GFP-Trap in lysates prepared from WT and E50K optineurin expressing cells, little myosin VI was precipitated from E478G or Q398X expressing cells, revealing that the ALS mutants do not bind to myosin VI (Fig. 1C). This finding was confirmed by immunoprecipitation of cell lysates using an anti-myosin VI antibody: little E478G or Q398X co-precipitated with myosin VI in contrast to WT and E50K optineurin (Fig. 1D). Interestingly, endogenous optineurin was precipitated using an anti-myosin VI antibody, from untransfected cells or GFP, WT, E50K optineurin expressing cells, but not from cells expressing E478G or Q398X (Fig. 1D). This result suggests that the optineurin ALS mutants may act in a dominant negative manner to disrupt the interaction of endogenous optineurin with myosin VI. We then examined whether ALS mutant optineurin interacts with endogenous optineurin to disrupt its interaction with myosin VI. Co-precipitation using GFP-Trap showed that endogenous optineurin co-precipitated with WT, E50K and E478G ALS mutant optineurin, suggesting that ALS mutant optineurin associates with endogenous optineurin and disrupts its binding with myosin VI (Supplementary Material, Fig. S2A). Furthermore, we performed co-precipitation with GFP-Trap in cells expressing Q398X-HA ALS mutant optineurin with EGFP-tagged WT or E50K optineurin. HA-tagged Q398X optineurin was precipitated in cells expressing EGFP-tagged WT or E50K optineurin using GFP-Trap, suggesting that the ALS mutant optineurin interacts with WT and E50K optineurin (Supplementary Material, Fig. S2B). In addition, the interaction between WT and E50K optineurin with myosin VI was decreased in cells co-expressing Q398X ALS mutant optineurin (Supplementary Material, Fig. S2B). Hence, together these data suggest that ALS mutant optineurin acts in dominant negative manner to induce a loss of association with myosin VI.

We next hypothesized that the loss of binding to myosin VI was responsible for the non-vesicular localization of optineurin observed with the ALS mutants. To investigate this possibility, NSC-34 cells expressing WT optineurin were treated with 2,4,6-triiodophenol (TIP), a pharmacological inhibitor of myosin VI ATPase activity, which should therefore inhibit the functional interaction between myosin VI and optineurin (27,32). In TIP-treated cells, significantly fewer optineurin vesicles were formed compared with untreated cells ($P < 0.05$), and optineurin was localized diffusely throughout these cells, similar to ALS mutant expressing cells (Fig. 1E and F). Hence, a functional association between myosin VI and optineurin is necessary for the formation of optineurin vesicles. This implies that the loss of binding of optineurin to myosin VI in ALS is responsible for the loss of vesicular localization of optineurin.

ALS optineurin mutants inhibit secretory protein trafficking from the Golgi apparatus to the plasma membrane

Since optineurin is an adaptor for myosin VI in exocytosis (26,33,34), we next analyzed whether expression of E478G and Q398X ALS optineurin mutants in neuronal cells inhibits the classical secretory pathway. We used a temperature sensitive mutant of vesicular stomatitis viral glycoprotein ts045 (VSVG) as a secretory protein transport marker (35). VSVG misfolds and is retained within the ER at 40°C, but upon switching to the permissive

temperature of 32°C, it is transported to the Golgi apparatus by 30 min and to the plasma membrane by 120 min (35). Using biotinylation of cell surface proteins, followed by immunoprecipitation with streptavidin beads and immunoblotting, we found that significantly less VSVG ($P < 0.05$) reached the cell surface by 120 min in cells expressing E478G or Q398X compared with WT, E50K or EGFP alone (Fig. 2A and B). Similarly, when VSVG-positive vesicles were transported from the Golgi apparatus toward the plasma membrane at 60 min after changing to the permissive temperature, significantly fewer cells showed ($P < 0.0001$) VSVG co-localized with optineurin in E478G or Q398X expressing cells compared with WT and E50K expressing cells (Fig. 2C and D). Furthermore, live cell imaging at 60 min demonstrated that WT optineurin, but not E478G or Q398X, co-migrates with VSVG vesicles during transit from the Golgi to the plasma membrane (Supplementary Material, Videos S1–S3). In contrast, transport of VSVG in the early stages of the secretory pathway, from the ER to Golgi, was not inhibited in cells expressing E478G or Q398X at the time point examined (Supplementary Material, Fig. S3A and B). Hence, the optineurin ALS mutants specifically inhibit protein transport from the Golgi apparatus to the cell surface during exocytosis.

ALS-linked optineurin mutant proteins display decreased co-localization with autophagosomes and lysosomes

Since we observed decreased binding of the optineurin ALS mutants to myosin VI, we next examined whether the ALS mutations affect the association of optineurin with autophagosomes. In NSC-34 cells expressing WT or the E50K glaucoma mutant, optineurin co-localized with both myosin VI and LC3-DsRed-positive autophagosomes in 70–80% of cells (Fig. 3A and B). However, in cells expressing E478G or Q398X, optineurin co-localized with myosin VI and autophagosomes in significantly fewer cells (~20%; Fig. 3A and B; $P < 0.0001$). Similarly, live cell imaging showed that, although WT optineurin co-migrated with LC3-DsRed-positive autophagosomes, Q398X ALS mutant optineurin displayed little co-localization with autophagosomes and did not co-migrate (Supplementary Material, Videos S4 and S5). It remains unknown whether optineurin is an adaptor protein linking myosin VI to lysosomes. Hence, we examined this possibility in NSC-34 cells co-expressing optineurin with Lysosome Associated Membrane Protein (LAMP1)-tagged with red fluorescent protein (RFP), using serum starvation to induce autophagy. In cells expressing WT or E50K, optineurin co-localized extensively with LAMP1-positive lysosomes (Fig. 3C), implying that optineurin links myosin VI to lysosomes and hence that optineurin/myosin VI could mediate lysosomal trafficking. This was confirmed by staining for myosin VI in NSC-34 cells, co-expressing WT optineurin and LAMP1-RFP, where optineurin and myosin VI co-localized with lysosomes (Fig. 3E). Live cell imaging studies similarly showed that vesicles containing WT and E50K optineurin co-migrate with lysosomes stained by the pH-sensitive LysoTracker dye (Supplementary Material, Videos S6 and S7). In contrast, however, in cells expressing E478G or Q398X, optineurin rarely co-localized with LAMP1, indicating that the ALS mutants did not associate with lysosomes (Fig. 3C and D, $P < 0.0001$). This was confirmed using live cell imaging studies, in which E478G or Q398X optineurin did not co-migrate with LysoTracker-stained vesicles (Supplementary Material, Videos S8 and S9). In order to rule out the possibility that optineurin was recruited to lysosomes because of its overexpression in cell culture, we also performed immunocytochemistry of endogenous optineurin and endogenous LAMP2 in human primary motor neurons (Fig. 3F)

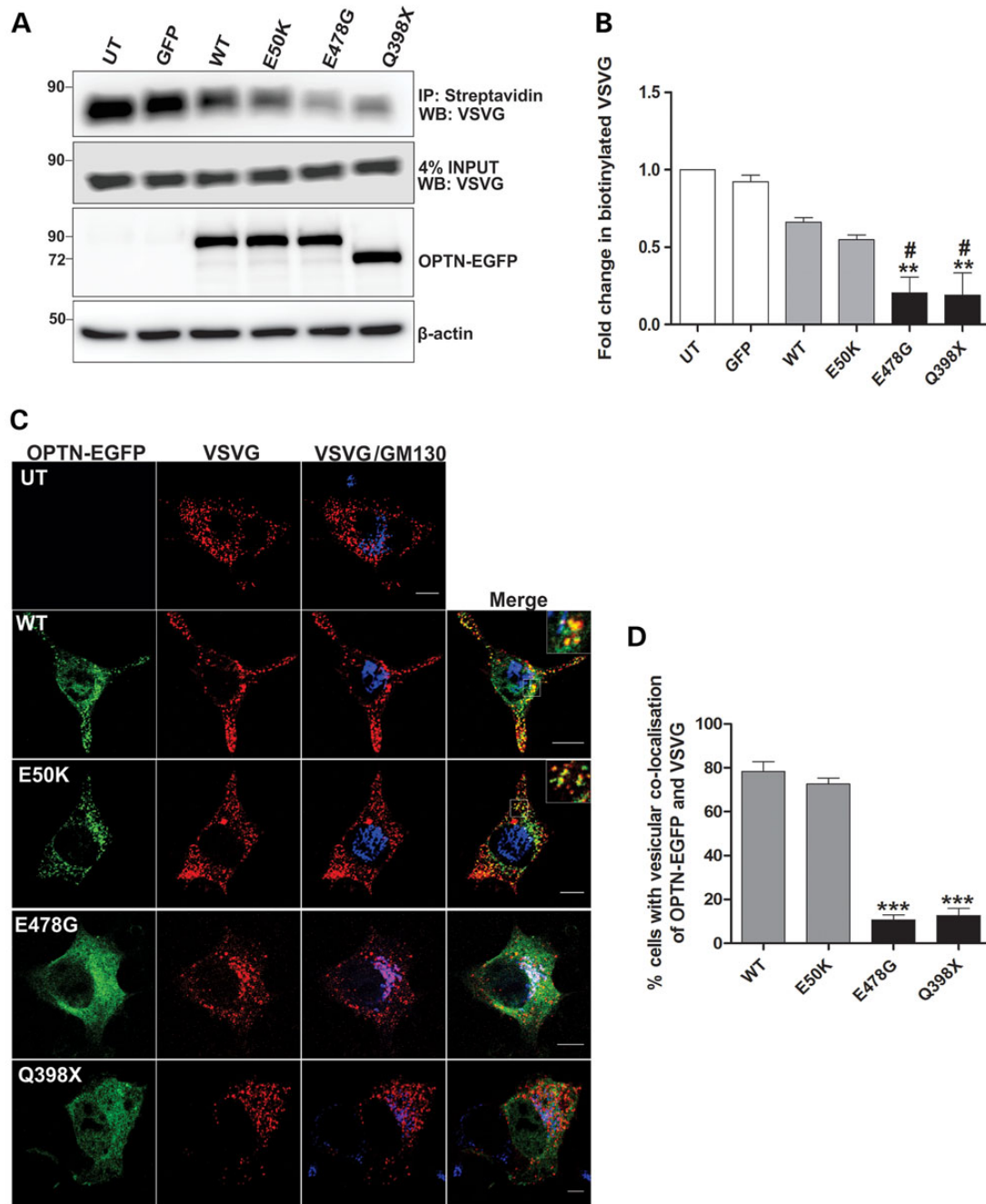


Figure 2. Expression of ALS mutant optineurin disrupts VSVG trafficking from the Golgi to the plasma membrane. NSC-34 cells co-expressing optineurin-EGFP and VSVG-ts04-mCherry were incubated at 40°C for 12 h, to entrap VSVG in the ER. The cells were then incubated at 32°C for 60 or 120 min to allow transport of VSVG to the cell surface. (A) Immunoprecipitation of NSC-34 cell lysates with streptavidin beads, followed by immunoblotting with anti-VSVG antibody, reveals decreased biotinylated VSVG in cells expressing ALS mutant optineurin. Bottom panel shows immunoblotting of 4% lysates with anti-VSVG antibody. β -Actin is shown as a loading control. The levels of optineurin-EGFP expression are shown by immunoblotting of NSC-34 lysates using anti-optineurin antibody. (B) Densitometric quantification of biotinylated VSVG [from immunoblots in (A)] reveals decreased transport of VSVG to the cell surface in ALS mutant optineurin expressing cells compared with GFP (*) and WT (#) optineurin expressing cells. Data are represented as the mean \pm SEM; ** P < 0.001, # P < 0.05 using ANOVA with Tukey's post hoc test, n = 3. The bands were quantified by normalizing to β -actin intensity and are shown relative to untransfected cells. (C) Immunocytochemistry reveals that after 60 min at 32°C, EGFP-tagged WT and E50K vesicles (green) co-localized with VSVG positive vesicular structures (red) that do not co-localize with GM130 (blue), indicating that they are post-Golgi. However, E478G and Q398X mutants do not form vesicles that co-localize with VSVG. Insets show higher magnifications of the areas outlined in the main images. Scale bars, 10 μ m. (D) Quantification of the percentage of cells displaying vesicular optineurin that co-localize with VSVG vesicles. Data are represented as the mean \pm SEM; *** P < 0.0001 compared with cells expressing WT optineurin using one-way ANOVA with the Tukey's post hoc test, n = 3.

and in NSC-34 cells (Fig. 3G) that were serum-starved to induce autophagy. These studies revealed that endogenous optineurin co-localized with LAMP2-stained lysosomes in all cells examined (Fig. 3F and G), confirming that optineurin associated with

lysosomes, unrelated to the protein expression level. Together these data indicate that WT optineurin normally associates with both autophagosomes and lysosomes, but this association is abrogated in ALS.

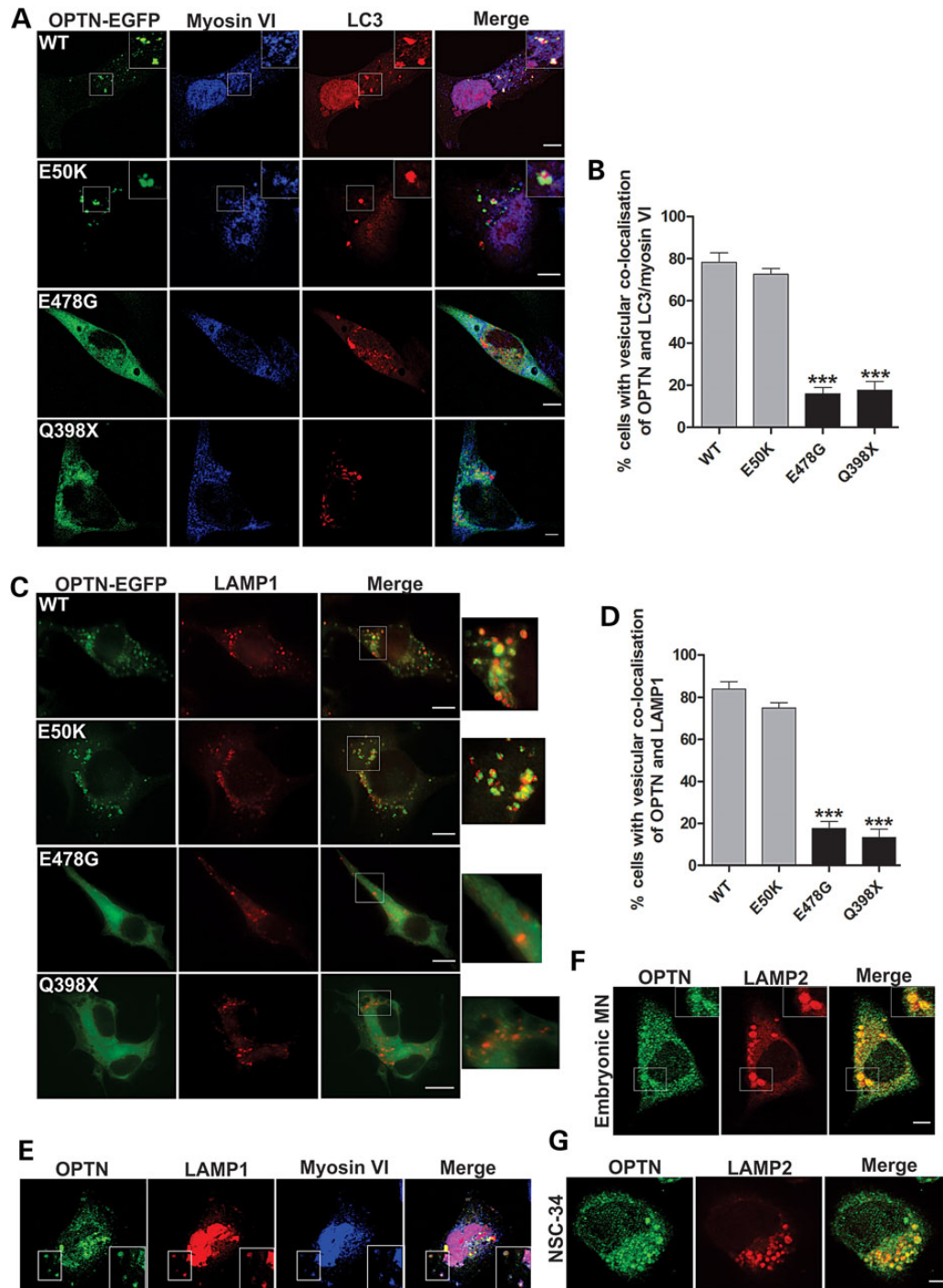


Figure 3. ALS-linked mutations decrease the co-localization of optineurin with autophagosomes and lysosomes. (A) NSC-34 cells co-expressing optineurin-EGFP and LC3-DsRed were fixed and immunostained with an anti-myosin VI antibody. WT and E50K mutant optineurin vesicles (green) co-localize with LC3-DsRed-positive autophagosomes (red) and myosin VI (blue). In contrast, ALS mutant optineurin is not vesicular and does not co-localize with either LC3 or myosin VI. (B) Quantification of the percentage of cells with co-localization of optineurin and both LC3/myosin VI structures. One hundred cells were counted for each cell type. Data are represented as the mean \pm SEM; *** P < 0.0001, using ANOVA with Tukey's *post hoc* test, n = 3. (C) NSC-34 cells co-expressing optineurin-EGFP and LAMP1-RFP were starved in serum-free medium for 6 h to induce autophagy. WT and E50K optineurin vesicles (green) co-localize with LAMP1-positive structures, indicating lysosomes (red), whereas E478G and Q398X mutants remain diffuse throughout cytoplasm. (D) Quantification of the percentage of cells with vesicular co-localization of optineurin and lysosomes. Data are represented as the mean \pm SEM; *** P < 0.0001, using ANOVA with Tukey's *post hoc* test, n = 3. (E) NSC-34 cells co-expressing WT optineurin and LAMP1-RFP were stained with anti-myosin VI, showing vesicular co-localization of optineurin and myosin VI with lysosomes. (F) Immunocytochemistry of human primary motor neurons with anti-optineurin (green) and anti-LAMP2 antibodies (red). (G) Immunocytochemistry of NSC-34 cells with anti-optineurin (green) and anti-LAMP2 antibodies (red). Images (F and G) show vesicular co-localization between endogenous optineurin and LAMP2-positive lysosomes. Insets show higher magnifications of the areas outlined in the main images. Scale bars, 10 μ m.

ALS-linked optineurin mutants inhibit autophagosome-lysosome fusion

The association of optineurin–myosin VI with autophagosomes and lysosomes (Fig. 3) and previous evidence demonstrating that optineurin depletion inhibits autophagy (29,36) implies that optineurin/myosin VI mediates the fusion of autophagosomes to lysosomes. We examined this notion by depletion of optineurin using siRNA in NSC-34 cells. siRNA treatment successfully depleted optineurin expression levels by 84% compared with control siRNA-treated cells (Fig. 4A). After serum starvation to induce autophagy, depletion of optineurin led to increased levels of lipidated LC3-II compared with control siRNA-treated cells, indicating accumulation of autophagosomes. Hence, this result indicates that optineurin is required for the clearance of autophagosomes (Fig. 4A and B). We then examined the fusion of autophagosomes to lysosomes by expressing tandem mCherry-LC3-GFP constructs (37,38), under conditions of serum starvation to induce autophagy (Fig. 4C). As the GFP signal is quenched in the acidic/lysosomal conditions of the lysosomal compartment, upon the expression of tandem mCherry-LC3-GFP construct, co-localization of both GFP and mCherry fluorescence indicates autophagosomes that has not fused with a lysosome; in contrast, mCherry signal without GFP corresponds to mature autolysosomes in which the autophagosomes have fused with lysosomes (38). Quantification of the percentage of mCherry-only positive puncta, in relation to total mCherry/EGFP puncta per cell, revealed that the proportion of mature autolysosomes is significantly decreased in cells treated with optineurin-targeted siRNA, compared with control siRNA-treated cells ($P < 0.001$, Fig. 4D). Therefore, fusion of autophagosomes with lysosomes is inhibited upon depletion of optineurin. These data indicate that optineurin is necessary for the clearance of autophagosomes by aiding the fusion of autophagosomes to lysosomes in neuronal cells.

We next investigated if the fusion of autophagosomes to lysosomes was altered in cells expressing optineurin ALS mutants. First, immunoblotting of cell lysates revealed a significantly increased intensity of LC3-II in cells expressing E478G and Q398X compared with WT and E50K optineurin ($P < 0.05$), indicating accumulation of autophagosomes, under basal conditions (Fig. 4E and F). There was no difference in LC3-II in cells expressing WT, E50K, E478G or Q398X in the presence of vacuolar-type H⁺-ATPase inhibitor bafilomycin A1 (Supplementary Material, Fig. S4), which blocks the fusion of autophagosomes and lysosomes, indicating that the increase in LC3-II in cells expressing E478G and Q398X mutant optineurin was specifically due to the accumulation of autophagosomes and not increased autophagosome biogenesis (28,37,39). Using fluorescent microscopy, we also observed a significant increase ($P < 0.0001$) in the proportion of E478G or Q398X optineurin-expressing cells containing LC3-DsRed-positive vesicles (>5) compared with WT or E50K expressing cells, indicating autophagosome accumulation in the ALS mutant cells under basal conditions (Fig. 4G). Furthermore, expression of HA-tagged ALS mutant Q398X caused a significant decrease in the proportion of fused autolysosomes per cell, detected by co-expression of tandem mCherry-LC3-GFP construct, under starvation-induced autophagy ($P < 0.0001$) compared with WT or untransfected cells (Fig. 4H and I). Together these data indicate that the fusion of autophagosomes to lysosomes was inhibited by expression of optineurin ALS mutants, leading to an accumulation of autophagosomes. Similar findings were obtained in cells depleted of optineurin (Fig. 4C and D), thus implying that the ALS mutations cause a loss of function of optineurin in mediating the fusion of autophagosomes with lysosomes.

ALS optineurin mutants cause Golgi fragmentation and induce ER stress

The inhibition of protein transport from the Golgi to plasma membrane and disruption of autophagosome–lysosome trafficking and fusion indicated that the ALS optineurin mutants trigger dysfunction to the secretory and endocytic compartments. As both ER stress and fragmentation of the Golgi apparatus occur in sporadic and familial ALS (9,10,20,21,40,41) and can result from dysfunction to the secretory pathway (12,19,42), we next examined whether these features were present in cells expressing ALS optineurin mutants. Immunoblotting for markers of ER stress, namely inositol requiring kinase 1 (IRE1) and spliced X-box binding protein 1 (Xbp1) (43), revealed greater activation of ER stress in cells expressing E478G and Q398X ($P < 0.05$) compared with WT or E50K (Fig. 5A and B). Similarly, expression of E478G and Q398X caused a significant increase ($P < 0.001$) in nuclear immunoreactivity to C/EBP homologous protein (CHOP), a pro-apoptotic transcription factor activated during the UPR, compared with WT or E50K optineurin expression (Fig. 5C and D). We also observed a small but significant up-regulation ($P < 0.05$) of CHOP in cells overexpressing WT and E50K optineurin compared with untransfected or GFP only cells (Fig. 5D), although IRE1 and spliced XBP-1 were not significantly increased (Fig. 5B). Similarly, immunocytochemistry for Golgi marker GM130 demonstrated that fragmented Golgi, indicated by the presence of condensed punctate structures, were present in a greater proportion of NSC-34 cells expressing E478G and Q398X compared with WT and E50K ($P < 0.05$) or GFP and untransfected cells ($P < 0.0001$), where the Golgi retained its characteristic perinuclear location (Fig. 5E and F). Consistent with previous studies (44,45), Golgi fragmentation was also detected in a small but significantly increased proportion of cells expressing WT optineurin and E50K compared with untransfected and GFP expressing cells (Fig. 5F). However, the ALS optineurin mutants induced ER stress ER stress and fragmentation of the neuronal Golgi apparatus in NSC-34 neuronal cells to a significantly greater extent than WT or E50K mutant optineurin.

Loss of optineurin association with myosin VI in sporadic ALS

The majority of ALS cases are sporadic without any known genetic mutations. Although mutations in optineurin cause a proportion of familial ALS cases (1,30), optineurin is also present in motor neuron inclusions in sporadic ALS patients (6). This suggests that the normal cellular function of WT optineurin might be perturbed in sporadic ALS. Therefore, we next analyzed the vesicular localization of optineurin in the motor neurons of ALS patient tissues. For this analysis, large neurons located in the ventral horn regions of spinal cord sections that stained positively using immunohistochemistry for SMI-32 were identified as motor neurons (Supplementary Material, Fig. S5D). Immunohistochemistry of lumbar spinal cord sections of sporadic ALS patients and control patients without neurological disease revealed that optineurin-positive vesicles were detected in most (~75%) motor neurons in control tissue, as expected (Fig. 6A). However, significantly fewer motor neurons in sporadic ALS patients contained optineurin-positive vesicular structures (21%, $P < 0.05$). In the ALS patient cells lacking optineurin-positive vesicles, optineurin was either expressed in a diffuse pattern (59%) or recruited to intracellular inclusions (41%) (Fig. 6B and C). In contrast, further immunohistochemistry studies revealed that the distribution of myosin VI was unchanged between control and sporadic patient motor neurons, in which it displayed a predominantly

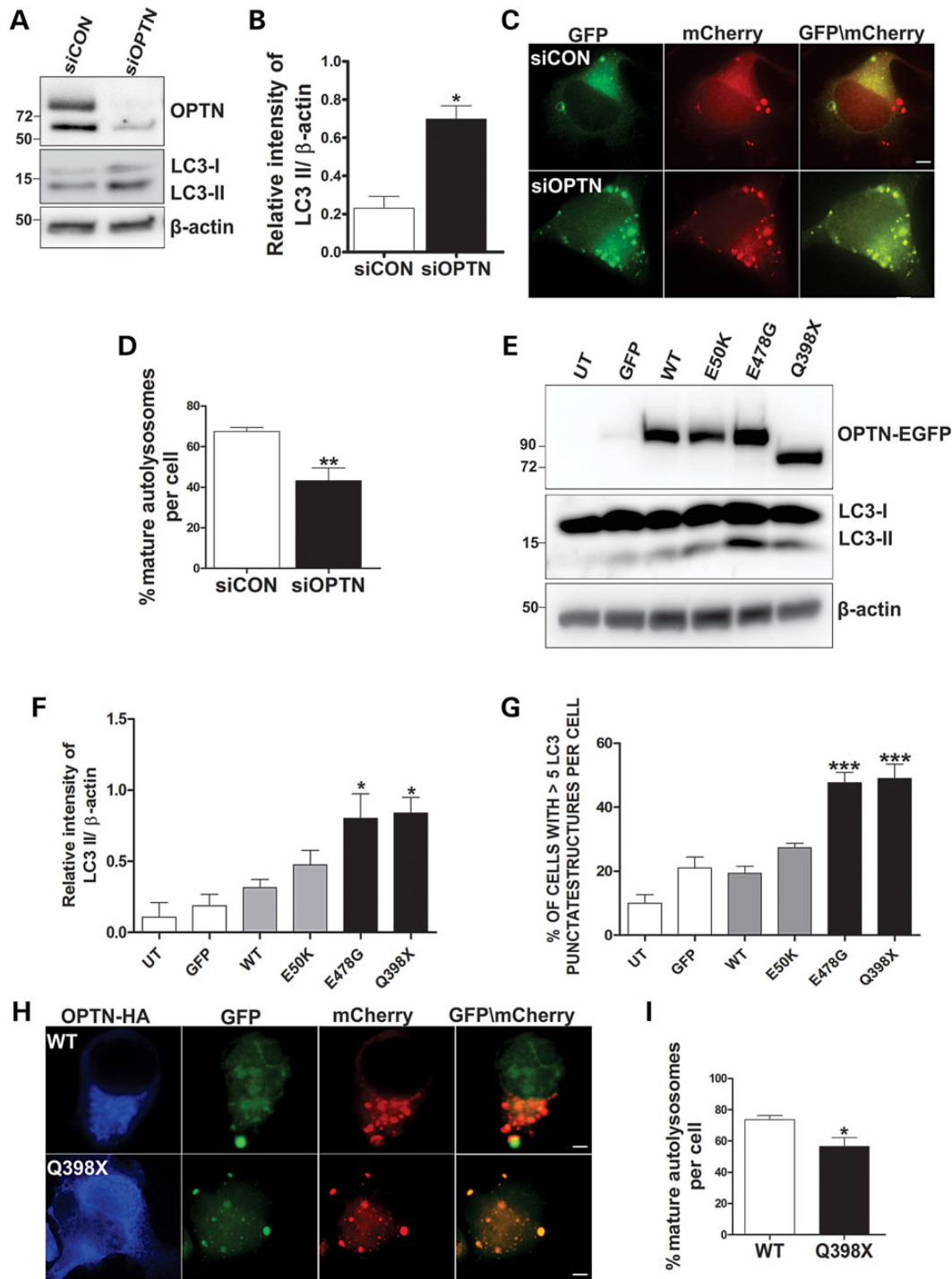


Figure 4. ALS optineurin mutations or optineurin knockdown block autophagosome-lysosome fusion, leading to accumulation of autophagosomes. (A) Immunoblotting of NSC-34 cell lysates treated with optineurin siRNA (siOPTN) and control siRNA (siCON) under serum-deprived conditions using anti-optineurin and anti-LC3 antibodies. β -Actin was used as a loading control. (B) Quantification of LC3-II intensity relative to β -actin. Data are represented as the mean \pm SEM; * $P < 0.05$, using ANOVA with Tukey's post hoc test, $n = 3$. (C) Optineurin siRNA-treated NSC-34 cells were transfected with mCherry-GFP-LC3 construct and serum-starved for 6 h to induce autophagy. In optineurin siRNA-treated cells, there is a decreased proportion of mCherry-positive mature autolysosomes without GFP, indicating that fusion between autophagosomes and lysosomes is inhibited. Scale bars, 10 μ m. (D) Quantification of the percentage of mCherry only positive autolysosomes relative to total puncta per cell. Data are represented as the mean \pm SEM; ** $P < 0.05$, *** $P < 0.0001$ using unpaired t-test compared with control siRNA-treated cells, $n = 3$. (E) Immunoblotting using anti-LC3 antibodies of NSC-34 lysates expressing optineurin-EGFP proteins. (F) Quantification of LC3-II intensity relative to β -actin. Data are represented as the mean \pm SEM; * $P < 0.05$, *** $P < 0.0001$ using ANOVA with Tukey's post hoc test, compared with cells expressing WT optineurin or GFP alone, $n = 3$. (G) Quantification of the percentage of cells with > 5 LC3-DsRed punctate structures in NSC-34 cells expressing optineurin-EGFP proteins under basal conditions, indicating accumulation of autophagosomes. (H) NSC-34 cells co-expressing optineurin-HA and mCherry-LC3-GFP were serum-starved for 6 h to induce autophagy. Representative images show the decreased proportion of mCherry only positive autolysosomes in cells expressing Q398X-HA mutant optineurin. (I) Quantification of the percentage of mCherry-positive autolysosomes without GFP, relative to total puncta per cell. Data are represented as the mean \pm SEM; *** $P < 0.0001$ using one-way ANOVA with Tukey's post hoc test, compared with cells expressing WT optineurin or untransfected cells, $n = 3$.

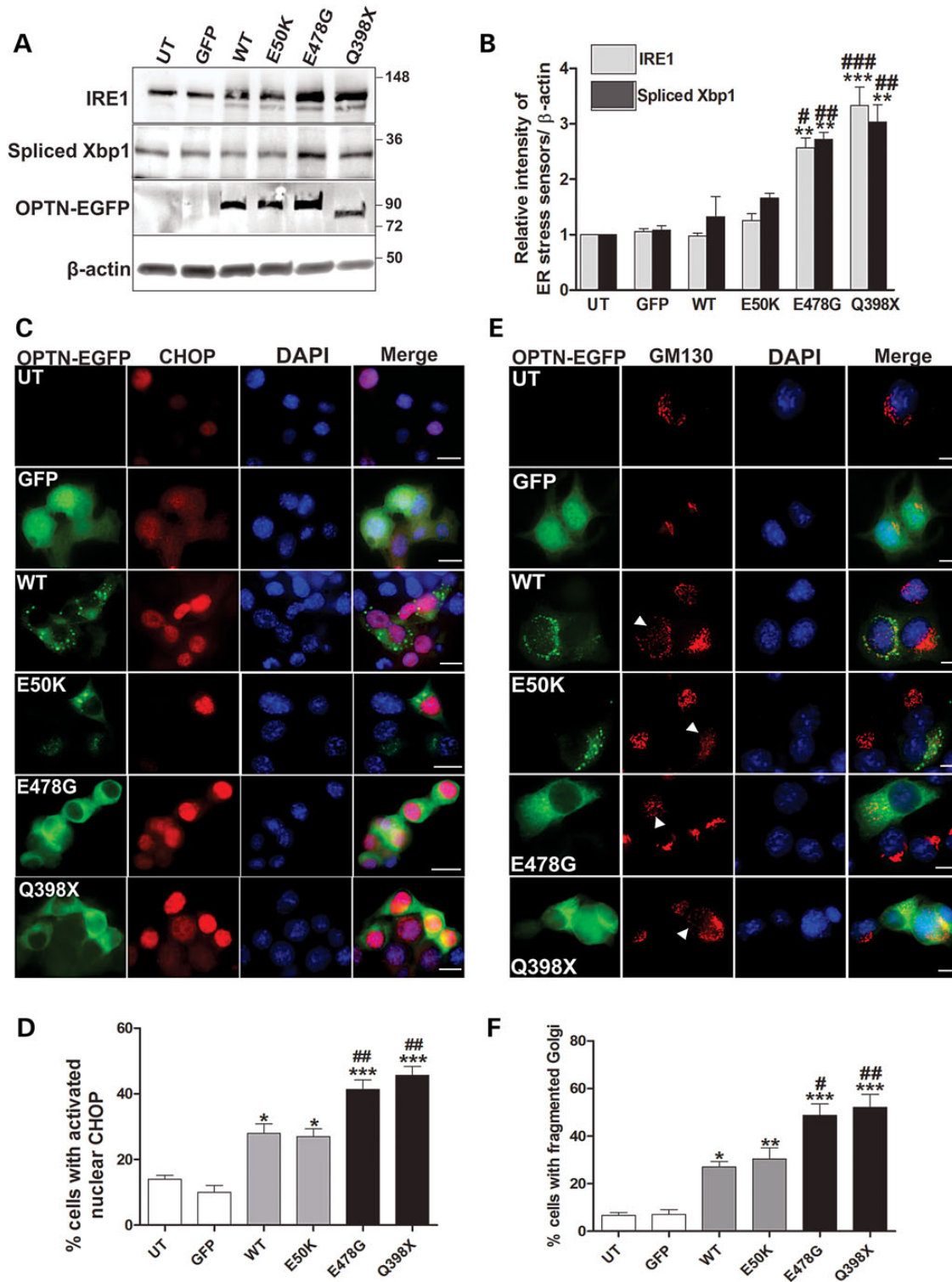


Figure 5. ALS mutant optineurin induces Golgi fragmentation and ER stress. (A) NSC-34 cell lysates expressing optineurin-EGFP proteins were analyzed by immunoblotting using anti-IRE1 and anti-Xbp1 antibodies as ER stress markers. Immunoblotting with anti-GFP antibody reveals similar expression of optineurin-EGFP proteins. β-Actin is shown as a loading control. (B) Densitometric quantification of IRE1 and Xbp1 intensity of blots in (A) relative to β-actin intensity and intensities from untransfected cells of the respective blot for each marker. (C) Representative images of NSC-34 cells show increased nuclear CHOP immunoreactivity in cells expressing E478G and Q398X ALS mutants, compared with untransfected cells or GFP expressing cells. (D) Quantification of percentage of the cells with activated nuclear CHOP in (C). (E) Immunocytochemistry of NSC-34 cells with anti-GM130 antibodies reveals fragmentation of Golgi in cells expressing optineurin-EGFP ALS mutants. Fragmented Golgi was identified by the formation of condensed punctate GM130-positive structures compared with a compact ribbon Golgi network in cells expressing GFP alone or in untransfected cells. Scale bars, 10 μm. (F) Quantification of cells with fragmented Golgi apparatus in (E). One hundred cells were scored per group from each experiment. Data are represented as the mean ± SEM; **P* < 0.05, ***P* < 0.001, ****P* < 0.0001 compared with GFP alone expressing cells or #*P* < 0.05, ##*P* < 0.001, ###*P* < 0.0001 compared with cells expressing WT optineurin using one-way ANOVA with Tukey's post hoc test, *n* = 3.

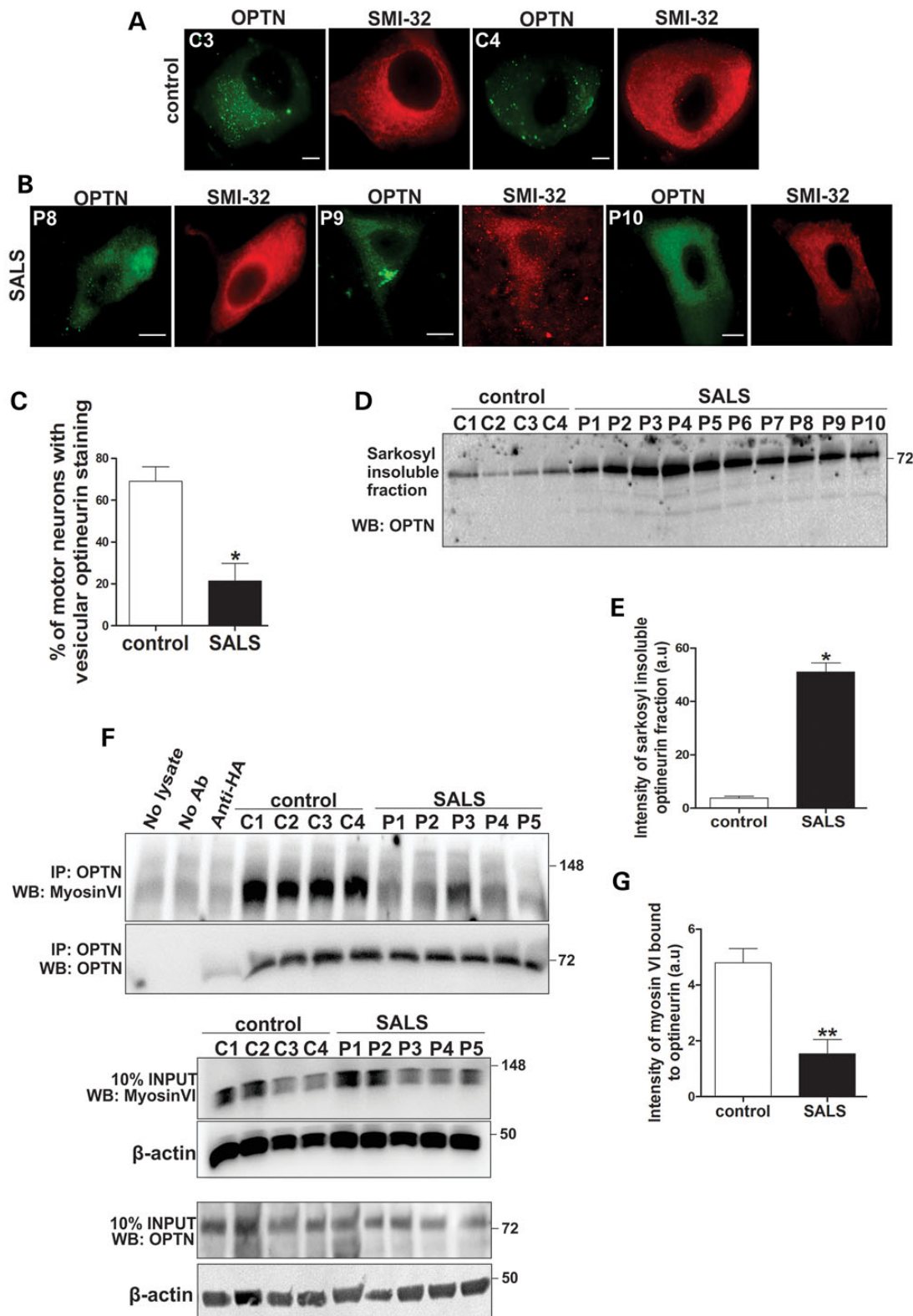


Figure 6. Optineurin dissociates from myosin VI in sporadic ALS patient spinal cord tissues. Immunohistochemistry of human spinal cord sections (from two non-neurological control patients and three sporadic ALS patients; patients details described in Supplementary Material, Table S1) using anti-optineurin and anti-SMI-32 antibodies. Motor neurons were identified as large cells located in the ventral horn regions of spinal cord sections that stained positively for SMI-32 (red) using immunohistochemistry. (B) In contrast, in sporadic ALS patients, optineurin is either diffuse and non-vesicular or rarely detected in intracellular aggregates. Scale bars, 10 μ m. (C) Quantification of motor neurons with vesicular optineurin in controls and sporadic ALS patients. Fifty motor neurons were scored from each patient. (D) Immunoblotting of sarkosyl insoluble, but SDS soluble fraction separated from human sporadic ALS and control patient spinal cord lysates, showing increased insoluble optineurin in sporadic ALS. (E) Quantification of insoluble optineurin intensity (expressed as arbitrary units a.u.) after immunoblotting with anti-optineurin antibody as shown in (D). (F) Immunoprecipitation of human patient spinal cord lysates using anti-optineurin antibodies followed by immunoblotting using anti-

vesicular pattern (Supplementary Material, Fig. S5E and F). This implies that loss of vesicular optineurin, but not myosin VI, is present in sporadic ALS patient tissues. We then examined whether the loss of vesicular appearance of optineurin could be due to aggregation of optineurin in sporadic ALS. We sequentially extracted the insoluble protein fraction from human spinal cord lysates using buffers with increasing salt and detergent concentrations and immunoblotted for optineurin. Such an analysis revealed higher levels of sarkosyl insoluble optineurin in sporadic ALS patient spinal cord lysate compared with controls (Fig. 6D and E). These results demonstrate that optineurin becomes misfolded in addition to losing its vesicular appearance in sporadic ALS.

The loss of the vesicular localization and misfolding of optineurin in human ALS was similar to the findings obtained from cells expressing ALS mutants E478G and Q398X, which displayed decreased binding to myosin VI (Fig. 1). Hence, we next examined the association between optineurin and myosin VI in sporadic ALS and control patient spinal cord lysates. Myosin VI co-precipitated using an optineurin antibody in control patient tissue lysates as expected. However, little myosin VI co-precipitated from sporadic ALS patient tissues, suggesting that myosin VI loses its association with optineurin in sporadic disease (Fig. 6F and G; additional patients shown in Supplementary Material, Fig. S1A; details of patients shown in Supplementary Material, Table S1). To confirm this finding, we co-immunoprecipitated optineurin using an anti-myosin VI antibody. Significantly less optineurin was co-precipitated with the anti-myosin VI antibody from sporadic patient tissues compared with non-neurological controls (Supplementary Material, Fig. S5B and C). Furthermore, to confirm that these ALS patients do not contain ALS mutations, we sequenced DNA extracted from patient tissues for common TDP-43, FUS and SOD1 mutations and the C9ORF72 repeat expansion. We found a known sporadic TDP-43 mutation, p.G294A, c.880G>C mutation (rs80356721) in patient P3 (46). We did not detect mutations in C9ORF72, TDP-43, FUS or SOD1 in any of the other patients. These patients are therefore most likely to be sporadic cases, given the lack of common disease-causative mutations and the lack of known family history. Together these data demonstrate that the association between myosin VI and optineurin is disrupted in sporadic ALS patients, implying that the function of optineurin as an adaptor for myosin VI is inhibited in both sporadic and familial ALS.

Discussion

This study describes novel pathogenic mechanisms associated with optineurin in sporadic and familial ALS. We demonstrate that optineurin mutations present in familial ALS inhibit the normal association of optineurin with myosin VI, which prevents the fusion of lysosomes to autophagosomes and inhibits the transport of secretory proteins from the Golgi to the plasma membrane. This results in accumulation of autophagosomes, ER stress and fragmentation of the Golgi apparatus. Furthermore, we also demonstrate that the association between optineurin and myosin VI is inhibited in human sporadic ALS, suggesting that disruption to optineurin function is not confined to rare

familial cases. Hence, optineurin–myosin VI dysfunction is associated with previously described pathogenic events in ALS and our findings imply that it is a common feature of both familial and sporadic disease.

Protein misfolding and aggregation is a key pathogenic feature of ALS. Autophagy is an important cellular mechanism to eliminate protein aggregates (47,48) and autophagy dysfunction is increasingly implicated in the pathogenesis of ALS. Autophagosomes are accumulated in ALS patient tissues (49) and LC3-II levels are elevated in spinal cords of commonly studied mouse models of ALS, including transgenic SOD1^{G93A} (50) and SOD1^{H46R} mice (51). Activation of mammalian target of rapamycin (mTOR)-dependent autophagy using rapamycin improved motor function in mice expressing TDP-43 (52), and induction of mTOR-independent autophagy significantly prolongs life span and attenuates disease progression in SOD1^{G93A} transgenic mice (53). Our findings of autophagy dysregulation by mutant optineurin in ALS are therefore consistent with these studies.

Although the heterozygous E478G optineurin mutation causes ALS in patients, only homozygous Q398X carriers develop disease. It remains unknown whether the optineurin mutations trigger an aberrant gain of function, a loss of normal optineurin function or a dominant-negative mechanism (1). The findings of our study indicate that expression of both the homozygous and the heterozygous mutant produce similar pathogenic events in neuronal cells, despite the presence of endogenous optineurin in these cells. Depletion of endogenous optineurin using siRNA and expression of the ALS mutants both triggered similar autophagy defects in the fusion of autophagosomes and lysosomes, suggesting that E478G and Q398X act in a dominant-negative manner when expressed in the presence of endogenous protein. Indeed, less endogenous optineurin was co-precipitated with myosin VI in cells expressing either E478G or Q398X optineurin compared with controls (Fig. 1D), suggesting that endogenous protein is sequestered from its normal binding partners by the mutant protein (Supplementary Material, Fig. S2A and B), leading to loss of normal cellular function. We cannot rule out the possibility that the Q398X mutant protein may not accumulate in human patients, since mRNA levels are decreased to only 13.8% of normal levels in homozygous Q398X mutation patient tissues, possibly due to non-sense-mediated mRNA decay (1). Indeed, two homozygous Q398X optineurin mutation patients were recently described without optineurin-positive pathology, despite TDP-43 accumulation and Golgi apparatus fragmentation in affected neurons (54). However, our results suggest that if the protein is expressed, it could cause similar pathogenic events as the E478G mutant protein. Finally, our findings also reveal that optineurin mutations are not required for optineurin dysfunction in disease, since sporadic ALS patients also showed changes in optineurin localization and solubility. These findings suggest that additional mechanisms, in addition to mutation, are involved in the development of optineurin-related cellular pathology. A previous study reported reduced optineurin levels in whole spinal cord lysates of sporadic ALS patient (55); however, our approach showed a specific increase in optineurin levels in the sarkosyl insoluble fraction sequentially extracted from sporadic ALS spinal cord sections (Fig. 6D and E), indicating optineurin

myosin VI antibodies. Control immunoprecipitations were negative: samples without spinal cord lysates, without antibody and using species matched non-specific anti-HA antibody. Input blot is also shown: 10% of lysates fraction used for immunoprecipitation was immunoblotted with anti-myosin VI and optineurin antibodies, demonstrating the myosin VI and optineurin levels in spinal cord lysates. β -Actin is shown as a loading control. (G) Quantification of myosin VI intensity (expressed as arbitrary units a.u.) after immunoprecipitation with anti-optineurin antibody from 10 sporadic ALS patients and 4 non-neurological control patients (patients details described in Supplementary Material, Table S1). Data are represented as the mean \pm SEM; * P < 0.05, ** P < 0.001 using unpaired t-test. Additional patients are shown in Supplementary Material, Figure S4.

aggregation in sporadic ALS. Furthermore, the loss of optineurin/myosin VI binding and optineurin misfolding in whole spinal cord lysates of sporadic patients suggests that the optineurin/myosin VI-related defects we describe here could be present in other cell populations in the spinal cord in addition to motor neurons in sporadic ALS patients.

Since the myosin VI-binding region of optineurin is located at residues 412–520 (26), both E478G and Q398X mutations are predicted to have decreased myosin VI binding, which may account for the alterations in mutant optineurin localization. We observed that treatment of cells with a myosin VI inhibitor caused WT optineurin to display a more diffuse, subcellular distribution (Fig. 1), similar to that seen in ALS patient motor neurons (Fig. 6). This implies that the interaction of myosin VI with optineurin is important to maintain normal optineurin localization and function. Overall, these findings suggest that a complex mechanism involving both loss of normal optineurin functions and mutation-specific functional changes exists in ALS. Consistent with our observations, a recent study demonstrated that depletion of optineurin induces an ALS-like phenotype in zebrafish (36). This result, together with our finding of decreased optineurin binding to myosin VI in sporadic ALS patients, implies that disturbance of optineurin function can trigger neurodegeneration in the absence of OPTN mutations. However, how optineurin function is disturbed in sporadic disease, what triggers misfolding of WT optineurin and its loss of association with myosin VI and what downstream functional impacts result from such disturbances remain to be determined.

Myosin VI was previously shown to drive classical exocytosis along actin filaments (33,56). Association of myosin VI with optineurin and other regulators of post-Golgi trafficking including Rab8 and Huntingtin (48) drive these processes. Recently, we demonstrated ER-Golgi protein trafficking disruption in cells expressing mutant SOD1 (12,13), which is consistent with increasing evidence for disruption to cellular trafficking in ALS (57–60). Here, we demonstrate that E478G and Q398X optineurin mutants inhibit exocytic transport from the Golgi to plasma membrane, consistent with this notion. Furthermore, motor neurons are particularly vulnerable to defects in intracellular trafficking because of their large cell bodies and long axons. However, in our study, the optineurin ALS mutants did not inhibit ER-Golgi transport at the time point examined, despite displaying decreased association with myosin VI. These data suggest that optineurin does not associate with myosin VI until later, post-Golgi stages of the classical secretory pathway (33). Consistent with this notion, myosin VI in association with optineurin was previously shown to mediate fusion of secretory vesicles at the plasma membrane, implicating a role for optineurin–myosin VI in post-Golgi protein trafficking (33,56). How disruption of different subcellular transport components by diverse dysfunctional proteins leads to motor neuron death in ALS remains to be clearly defined.

We also observed that ALS optineurin mutants induced Golgi fragmentation and ER stress to a much greater extent than either WT or the glaucoma mutant E50K. This implies that in ALS, dissociation of optineurin from myosin VI disrupts post-Golgi protein trafficking, inducing Golgi fragmentation and ER stress. Similar to this observation, previous studies have shown that inhibition of post-Golgi trafficking leads to accumulation of misfolded proteins in secretory compartments, consequently inducing Golgi fragmentation and ER stress (42,61,62). We also show here that overexpression of both WT and E50K optineurin induces Golgi fragmentation and activates CHOP, albeit to a lesser extent than the ALS mutants, indicating possible pathogenic effects upon overexpression of WT optineurin (63). Further

temporal delineation of the events triggered by ALS mutant optineurin will allow identification of the upstream triggering factors for these changes.

In this study, we also provide further insight into the function of WT optineurin as an autophagy receptor. Previously optineurin was identified along with two other adaptor proteins, NDP52 and T6BP, as mediators of myosin VI-dependent autophagosome formation and fusion to lysosomes (28). However, this previous study examined only the simultaneous depletion of all three adaptor proteins using siRNA. In the current study, we extend these findings and demonstrate that in complex with myosin VI, optineurin alone is required for autophagosome/lysosome fusion. We also demonstrate that optineurin and myosin VI associate with lysosomes, and either dissociation of optineurin from myosin VI or knockdown of optineurin blocked the fusion of lysosomes to autophagosomes. However, it remains unclear if optineurin physically binds to lysosomes or whether this is mediated by additional binding partners. Hence, these findings imply that optineurin links myosin VI to both lysosomes and autophagosomes, leading to their fusion during the final stages of autophagy.

Although previous studies have described tentative links between myosin VI and neurodegeneration, this study is the first to report dysfunction of myosin VI in ALS. Previously, myosin VI was shown to co-localize with tau fibrils in brains of both Alzheimer's disease mouse models and human patients (64), and myosin VI knockout mice develop astrogliosis in the brain (65). Our findings suggest that alterations in myosin VI function contribute to several pathways implicated in ALS pathogenesis, including intracellular transport disturbances, ER stress activation and Golgi fragmentation. Further studies of the broad role of myosin VI in ALS and other neurodegenerative disorders are therefore warranted.

In conclusion, this study demonstrates that dissociation of optineurin from myosin VI is associated with disturbances in autophagosome–lysosome fusion, activation of ER stress, Golgi fragmentation and dysfunction in protein secretion. We also demonstrate that optineurin displays altered subcellular distribution in sporadic ALS patient motor neurons, and we identify a decreased interaction between optineurin and myosin VI in sporadic ALS patient spinal cords. These findings implicate optineurin and myosin VI dysfunction as a possible upstream trigger of several pathogenic mechanisms, in both rare familial mutation carriers and the much more common sporadic ALS cases. These findings suggest new therapeutic avenues for ameliorating motor neuron demise in ALS based on optineurin function.

Materials and Methods

Constructs

The OPTN mutants used in this study are p.E50K (c.148G>A, NM_021980), p.E478G (c.1433A>G, NM_021980) and p.Q398X (c.1192C>T, NM_021980). A WT optineurin-EGFP expressing construct in pEGFP-C3 vector was kindly provided by Dr Ghanshyam Swarup, Centre for Cellular and Molecular Biology, Hyderabad, India (66). The WT optineurin-HA construct in pCVM5 vector was kindly provided by Dr Andrew Macdonald, University of Leeds, UK (67). Glaucoma and ALS mutant optineurin constructs were generated using QuikChange site-directed mutagenesis (Stratagene) with respective forward primers as listed below and its reverse complement.

E50K 5'-GAAAGAGCTCCTGACCAAGAACCACCAGCTGAA-3'

E478G 5'-GTTCTGATTTTCATGCTGGAAGAGCAGCGAGAGA-GAA-3'

Q398X 5'-GATGACACACAAGCTTCTTTAAGAACATAATAATG-CATTGA-3'

The LAMP1-RFP construct deposited by Dr Nathan M. Sherer was obtained from Addgene (Addgene plasmid #1817) (68). Similarly pBABE-puro mCherry-EGFP-LC3B deposited by Dr Jayanta Debnath was obtained from Addgene (Addgene plasmid #22418) (69).

Cell culture and transfection

Mouse NSC-34 cells (provided by Professor Neil Cashman, University of British Columbia) were maintained in Dulbecco's modified Eagle's medium with 10% fetal calf serum (FCS). Cells were transfected using Lipofectamine 2000 (Invitrogen) as per the manufacturer's protocol.

Optineurin siRNA knockdown

ON-TARGETplus SMARTpool siRNA duplexes (Dharmacon) targeting mouse optineurin or non-targeting control (20 nM each) were transfected using Lipofectamine reagent (Invitrogen) in serum-free opti-MEM medium (Gibco). Cells were lysed after 72 h and immunoblotted with anti-optineurin (INT) antibody (Cayman Chemical). To analyze the fusion of autophagosomes with lysosomes, 24 h after siRNA treatment, cells were transfected with mCherry-LC3-GFP constructs (0.5 µg each) using Lipofectamine (Invitrogen). A further 48 h later, cells were fixed with 4% paraformaldehyde (PFA) and analyzed by fluorescence microscopy.

Immunoblotting

Cell lysates were collected in TN buffer (50 mM Tris-HCl, pH 7.5, and 150 mM NaCl) with 0.1% sodium dodecyl sulphate (SDS) and 1% protease inhibitor cocktail (Sigma) by incubation on ice for 10 min. Cell lysates were then centrifuged at 15 000g for 15 min at 4°C to separate the insoluble and soluble fractions. The insoluble fractions were solubilized in 8 M urea and sonicated for 30 s. Both soluble and insoluble fractions were quantified using the BCA assay kit (Pierce). For analysis of optineurin aggregation, total insoluble fractions separated from equal volume of lysates were subjected to immunoblotting. Protein samples (20 µg) were electrophoresed through 10% SDS-polyacrylamide gels and transferred to nitrocellulose membranes (Millipore). Membranes were blocked with 5% skim milk for 1 h. The appropriate primary antibodies were prepared in 1% (w/v) bovine serum albumin solution as follows: optineurin (1:500, Cayman Chemical), rabbit anti-myosin VI (1: 500, Santa Cruz), mouse anti-myosin VI (1:1000, Sigma), rabbit anti-LC3 (1:1000, Novus Biological), rabbit anti-VSVG (1:1000, Sigma), rabbit anti-Xbp1 (1:400, SC), rabbit anti-IRE1 (1:600, SC) and mouse anti-β-actin as a loading control (1:2000, Sigma-Aldrich). All antibodies were incubated with membranes at 4°C overnight. Blots were probed with HRP-conjugated goat anti-rabbit or goat anti-mouse antibodies at 1:2500 (Chemicon) for 1 h at RT and developed using enhanced chemiluminescence reagents (Roche). Quantification of band intensities was performed by densitometric analysis following subtraction of background using Image J (National Institutes of Health, Bethesda, MD, USA). Blots were stripped using Re-blot Plus solution (Chemicon) for 15 min, and then reprobed as above.

Immunocytochemistry

Transfected NSC-34 cells grown on coverslips were washed with phosphate-buffered saline (PBS) and fixed with 4% PFA in PBS for

10 min. Cells were permeabilized in 0.1% Triton X-100 in PBS for 2 min, blocked for 30 min with 1% bovine serum albumin (Sigma) in PBS and incubated with the appropriate primary antibodies as follows for 16 h at 4°C; anti-CHOP (1:50, Santa Cruz), anti-GM130 (1:50, BD Transduction Laboratories), anti-Calnexin (1:100, Abcam), anti-myosin VI (1:100, SC). Secondary AlexaFluor-594 or 644 conjugated anti-mouse or anti-rabbit antibodies (1:2000, Molecular Probes) were incubated for 1 h at room temperature, cells were then treated with Hoechst 33 342 (Invitrogen) and mounted on slides using DaKo fluorescent mounting medium (Agilent Technologies). Images were acquired using constant settings for CHOP using an Olympus IX81 epi-fluorescence microscope (Olympus) at 40× magnification or using Zeiss LSM 510 laser scanning confocal microscope (Zeiss) at 100× magnification. Induction of ER stress was assessed by examining individual cells for nuclear immunoreactivity to CHOP (70). One hundred cells for each treatment from three different experiments were scored. Fragmentation of the Golgi apparatus was identified by condensed punctate structures when compared with perinuclear ribbon-like network in healthy cells after staining with anti-GM130 antibody. The number of cells with fragmented Golgi per 100 cells from three different experiments was scored by fluorescence microscopy.

Primary culture of human embryonic motor neurons

Spinal cords of therapeutically terminated embryonic fetuses (17–19 weeks) were removed and washed with cold HBSS (studies were approved by Macquarie University HREC # 5201300330). Motor neurons were then mechanically sheared and isolated by density centrifugation with Optiprep (Sigma). Cells were then plated into flasks pre-coated with poly-L-lysine (Cultrex) and laminin (Invitrogen) and grown in neurobasal media (Gibco) supplemented with 10% FCS, B27 (Gibco), antibiotic/antimycotic (Gibco), L-glutamine (Gibco), bone-derived neurotrophic factor (Alomone Labs) and ciliary neurotrophic factor (Peprotech). Cells were treated on DIV3 with selection media containing cytosine arabinoside (Sigma) to remove astrocytes for 2 days, before returning to media without FCS and cytosine arabinoside. Media was then changed every 2 days until neurite outgrowth was observed. The cells were fixed with 4% PFA and immunostained with anti-optineurin (INT) (1:20, Cayman Chemical), anti-myosin VI (1:20, Sigma) or anti-LAMP2 (1:20, Abcam) antibody as above.

VSVG transport assay

NSC-34 cells were co-transfected with VSVG-ts045 tagged with fluorescent mCherry (a kind gift from Dr Jennifer Lippincott-Schwartz and Dr George Patterson) and optineurin-EGFP constructs. After 24 h, cells were incubated at 40°C for 24 h to accumulate VSVG-ts045 in the ER. Cycloheximide (20 µg/ml) was then added, and cells were shifted to 32°C for 30, 60 or 120 min, respectively. At 30 and 60 min intervals, cells were washed with ice-cold PBS and fixed with 4% PFA. The ER and Golgi compartments were immunostained with anti-calnexin antibody (Abcam) and anti-GM130 antibody (BD Transduction Laboratories) as described above. Twenty cells were scored in each experiment and all experiments were performed in triplicate. Image analysis was performed using Image J using the JACoP plugin to threshold and collect the Mander's coefficient (71) between the mCherry and far-red channels with calnexin or GM130 staining. To detect cell surface VSVG, the cells were collected by trypsinization after incubation at 40°C for 120 min. The cells were then biotinylated

by incubating with 0.5 mg/ml biotin-NHS (Thermo Scientific) at 4°C for 30 min. The excess biotin was neutralized by incubating with 50 mM NH₄Cl for 2 min. The cells were then lysed with TN buffer with 0.1% SDS and biotinylated cell surface proteins were then precipitated with 10 µl of streptavidin-agarose beads (Cell Signalling) and immunoblotted with anti-VSVG antibody as above.

Live cell imaging

For live cell imaging, NSC-34 cells were grown on 13 mm coverslips. Forty-eight hours after transfection, the cells were shifted to a Skyes-Moore chamber (BELLCO) and imaged using Zeiss LSM 510 laser scanning confocal microscope (Zeiss) at 37°C with 5% CO₂. The videos were acquired for 60 cycles at an interval of 7 s. The images were analyzed using Imaris software (Bitplane).

Human tissue samples

Human lumbar spinal cord segments (L3–L5) from 10 patients who died of respiratory failure caused by ALS were provided by the MND Research Tissue Bank of Victoria (Supplementary Material, Table S1). The clinical diagnosis of ALS was confirmed at post-mortem. Control lumbar spinal cord segments were obtained from four individuals without evidence of neurological or psychiatric disease (Supplementary Material, Table S1). Studies were approved by La Trobe University Human Ethics Committee (HEC # FHEC10/R4). Spinal cord samples were homogenized in radioimmunoprecipitation assay (RIPA) buffer (50 mM Tris-HCl, pH 7.5, 150 mM NaCl, 0.1% (w/v) SDS, 1% (w/v) sodium deoxycholate and 1% (v/v) Triton X-100) with 1% (v/v) protease inhibitor cocktail (Sigma). After homogenization, the samples were centrifuged for 5 min at 15 000g, and the supernatant was then frozen at –80°C. Proteins were quantified using the BCA assay Kit (Pierce). Separation of insoluble fractions from the spinal cord sections were performed based on the method described earlier (72). The lumbar spinal cord segments (30 mg of each) were homogenized in high-salt (HS) buffer (50 mM Tris, 750 mM NaCl, 10 mM NaF, 5 mM EDTA, pH 7.4) with 1 mM phenylmethylsulfonyl fluoride and 1% phosphatase and protease inhibitor cocktails (Sigma). Samples were centrifuged at 90 000g at 4°C for 30 min and the supernatant was taken as HS soluble fraction. Pellets were re-extracted as before with HS buffer and the supernatant was discarded. The pellets were then homogenized with 3× volume per weight of pellet in HS buffer with 1% Triton X-100. Samples were then centrifuged at 90 000g for 30 min at 4°C, and the supernatant was collected as HS-Triton X-100 soluble fraction. The pellets were then re-extracted with 3× volume of HS buffer with 1% Triton X-100 and 30% sucrose, by centrifugation at 90 000g for 30 min at 4°C. The pellets were then sonicated in 2× volume of HS buffer with 1% sarkosyl. The samples were incubated with agitation for 1 h at room temperature and centrifuged at 90 000g for 30 min at 4°C. The pellets were then sonicated in SDS sample loading buffer (0.05% bromophenol blue, 0.1 M dithiothreitol, 10% glycerol, 2% SDS and 50 mM Tris, pH 6.8) and heated at 95°C for 5 min before immunoblotting was performed.

Human spinal cord lysate immunoprecipitation

For immunoprecipitation, 400 µg of total human spinal cord lysates was incubated with anti-optineurin (INT) antibody or anti-myosin VI antibody or irrelevant control antibody and 50% w/v protein A-Sepharose CL-4B beads (Amersham Biosciences) in RIPA buffer at 4°C overnight on a rotating wheel. The beads were centrifuged at 2000g for 2 min at 4°C, and the pellet was

washed thrice with RIPA buffer. The immunoprecipitate was then released by boiling with 1× SDS sample loading buffer for 5 min followed by centrifugation at 15 000g for 2 min.

Immunostaining human spinal cord sections

Paraffin embedded human lumbar spinal cord sections (14 µm) from non-neurological controls and ALS patients were obtained from Victorian Brain Bank Network (Supplementary Material, Table S1). Paraffin was removed from sections by washing with xylene twice for 5 and 2 min, respectively, followed by washing with 100% ethanol and 50% ethanol for 5 min each. The sections were then washed with distilled water and soaked in PBS. Antigen retrieval was performed by boiling the sections in sodium citrate buffer for 1 min. The sections were then incubated with blocking serum (3% goat serum, 0.3% Triton X-100 in PBS) for 30 min. The sections were then incubated with primary antibodies [rabbit anti-optineurin (INT) (1:20), Cayman Chemical], rabbit anti-myosin VI (1:20, SC), mouse anti-SMI-32 (1:400, Abcam) prepared in blocking serum, overnight at 4°C. The sections were washed thrice with 0.1% Tween 20 in PBS for 10 min each. Secondary AlexaFluor-488 or 594 conjugated anti-mouse or anti-rabbit antibodies (1:200, Molecular Probes) were added and incubated for 1 h at room temperature. Finally, the sections were washed with 0.1% Tween 20 in PBS and coverslips were mounted with DAKO fluorescent mounting medium.

Sequencing

Genomic DNA was extracted from tissue samples using QIAamp DNA mini Kit (QIAGEN). Analysis of the C9ORF72 repeat expansion was performed using the method described previously (73). Fragment analysis was performed on an ABI 3730XL DNA Analyzer. All SOD1 exons, TARDBP exon 6, FUS exon 15 and at least 50 bp of flanking DNA were amplified using the polymerase chain reaction (primers available on request). Amplified products were analyzed using Big-Dye terminator sequencing on an ABI 3730XL sequencer (Macrogen Inc.).

Statistics

Data are presented as the mean ± standard error of the mean (SEM) from at least three independent experiments and were analyzed by one-way analysis of variance followed by the Tukey's post hoc test using Prism 5.0 GraphPad Software (San Diego, CA, USA). A value of $P < 0.05$ was considered significant.

Supplementary Material

Supplementary Material is available at HMG online.

Acknowledgements

We thank Dr Jennifer Lippincott-Schwartz/Dr George Patterson for the VSVG-ts045-mCherry construct and Dr Peter Lock (La Trobe University) for expert guidance on live cell imaging and confocal microscopy. Tissues were received from the Victorian Brain Bank Network, supported by The Florey Institute of Neuroscience and Mental Health, The Alfred and the Victorian Forensic Institute of Medicine and funded in part by Australia's National Health & Medical Research Council and Parkinson's Victoria.

Conflict of Interest statement. None declared.

Funding

This work was supported by National Health and Medical Research Council of Australia Project grants [# 1006141, 1030513 to J.A.], Bethlehem Griffiths Research Foundation, Motor Neuron Disease Research Institute of Australia, Suzie Harris Memorial Fund MND Research Grant and Rosalind Nicholson MND Research Grant [to J.A.], a National Health and Medical Research Council CJ Martin Biomedical Early Career fellowship [1036835 to A.W.].

References

- Maruyama, H., Morino, H., Ito, H., Izumi, Y., Kato, H., Watanabe, Y., Kinoshita, Y., Kamada, M., Nodera, H. and Suzuki, H. (2010) Mutations of optineurin in amyotrophic lateral sclerosis. *Nature*, **465**, 223–226.
- Rezaie, T., Child, A., Hitchings, R., Brice, G., Miller, L., Coca-Prados, M., Héon, E., Krupin, T., Ritch, R. and Kreutzer, D. (2002) Adult-onset primary open-angle glaucoma caused by mutations in optineurin. *Science*, **295**, 1077–1079.
- Forsberg, K., Jonsson, P.A., Andersen, P.M., Bergemalm, D., Graffmo, K.S., Hultdin, M., Jacobsson, J., Rosquist, R., Marklund, S.L. and Brännström, T. (2010) Novel antibodies reveal inclusions containing non-native SOD1 in sporadic ALS patients. *PLoS One*, **5**, e11552.
- Mackenzie, I.R., Bigio, E.H., Ince, P.G., Geser, F., Neumann, M., Cairns, N.J., Kwong, L.K., Forman, M.S., Ravits, J. and Stewart, H. (2007) Pathological TDP-43 distinguishes sporadic amyotrophic lateral sclerosis from amyotrophic lateral sclerosis with SOD1 mutations. *Ann. Neurol.*, **61**, 427–434.
- Deng, H.X., Zhai, H., Bigio, E.H., Yan, J., Fecto, F., Ajroud, K., Mishra, M., Ajroud-Driss, S., Heller, S. and Sufit, R. (2010) FUS-immunoreactive inclusions are a common feature in sporadic and non-SOD1 familial amyotrophic lateral sclerosis. *Ann. Neurol.*, **67**, 739–748.
- Deng, H.X., Bigio, E.H., Zhai, H., Fecto, F., Ajroud, K., Shi, Y., Yan, J., Mishra, M., Ajroud-Driss, S. and Heller, S. (2011) Differential involvement of optineurin in amyotrophic lateral sclerosis with or without SOD1 mutations. *Arch. Neurol.*, **68**, 1057.
- Osawa, T., Mizuno, Y., Fujita, Y., Takatama, M., Nakazato, Y. and Okamoto, K. (2011) Optineurin in neurodegenerative diseases. *Neuropathology*, **31**, 569–574.
- Mori, F., Tanji, K., Toyoshima, Y., Yoshida, M., Kakita, A., Takahashi, H. and Wakabayashi, K. (2012) Optineurin immunoreactivity in neuronal nuclear inclusions of polyglutamine diseases (Huntington's, DRPLA, SCA2, SCA3) and intranuclear inclusion body disease. *Acta Neuropathol. (Berl.)*, **123**, 747–749.
- Mourelatos, Z., Gonatas, N.K., Stieber, A., Gurney, M.E. and Dal Canto, M.C. (1996) The Golgi apparatus of spinal cord motor neurons in transgenic mice expressing mutant Cu, Zn superoxide dismutase becomes fragmented in early, pre-clinical stages of the disease. *Proc. Natl Acad. Sci. USA*, **93**, 5472–5477.
- Atkin, J.D., Farg, M.A., Walker, A.K., McLean, C., Tomas, D. and Horne, M.K. (2008) Endoplasmic reticulum stress and induction of the unfolded protein response in human sporadic amyotrophic lateral sclerosis. *Neurobiol. Dis.*, **30**, 400–407.
- Chen, S., Zhang, X., Song, L. and Le, W. (2012) Autophagy dysregulation in amyotrophic lateral sclerosis. *Brain Pathol.*, **22**, 110–116.
- Atkin, J.D., Farg, M.A., Soo, K.Y., Walker, A.K., Halloran, M., Turner, B.J., Nagley, P. and Horne, M.K. (2013) Mutant SOD1 inhibits ER-Golgi transport in Amyotrophic Lateral Sclerosis. *J. Neurochem.*, **129**, 190–204.
- Sundaramoorthy, V., Walker, A.K., Yerbury, J., Soo, K.Y., Farg, M.A., Hoang, V., Zeineddine, R., Spencer, D. and Atkin, J.D. (2013) Extracellular wildtype and mutant SOD1 induces ER-Golgi pathology characteristic of amyotrophic lateral sclerosis in neuronal cells. *Cell. Mol. Life Sci.*, **70**, 4181–4195.
- Kraft, C., Peter, M. and Hofmann, K. (2010) Selective autophagy: ubiquitin-mediated recognition and beyond. *Nat. Cell Biol.*, **12**, 836–841.
- Jahreiss, L., Menzies, F.M. and Rubinsztein, D.C. (2008) The itinerary of autophagosomes: from peripheral formation to kiss and run fusion with lysosomes. *Traffic*, **9**, 574–587.
- Graef, M., Friedman, J.R., Graham, C., Babu, M. and Nunnari, J. (2013) ER exit sites are physical and functional core autophagosome biogenesis components. *Mol. Biol. Cell*, **24**, 2918–2931.
- Ge, L., Melville, D., Zhang, M. and Schekman, R. (2013) The ER-Golgi intermediate compartment is a key membrane source for the LC3 lipidation step of autophagosome biogenesis. *eLife*, **2**, e00947.
- Axe, E.L., Walker, S.A., Manifava, M., Chandra, P., Roderick, H. L., Habermann, A., Griffiths, G. and Ktistakis, N.T. (2008) Autophagosome formation from membrane compartments enriched in phosphatidylinositol 3-phosphate and dynamically connected to the endoplasmic reticulum. *J. Cell Biol.*, **182**, 685–701.
- Preston, A., Gurisik, E., Bartley, C., Laybutt, D. and Biden, T. (2009) Reduced endoplasmic reticulum (ER)-to-Golgi protein trafficking contributes to ER stress in lipotoxic mouse beta cells by promoting protein overload. *Diabetologia*, **52**, 2369–2373.
- Atkin, J.D., Farg, M.A., Turner, B.J., Tomas, D., Lysaght, J.A., Nunan, J., Rembach, A., Nagley, P., Beart, P.M. and Cheema, S.S. (2006) Induction of the unfolded protein response in familial amyotrophic lateral sclerosis and association of protein-disulfide isomerase with superoxide dismutase 1. *J. Biol. Chem.*, **281**, 30152–30165.
- Farg, M.A., Soo, K.Y., Walker, A.K., Pham, H., Orian, J., Horne, M.K., Warraich, S.T., Williams, K.L., Blair, I.P. and Atkin, J.D. (2012) Mutant FUS induces endoplasmic reticulum stress in amyotrophic lateral sclerosis and interacts with protein disulfide-isomerase. *Neurobiol. Aging*, **33**, 2855–2868.
- Walker, A.K., Soo, K.Y., Sundaramoorthy, V., Parakh, S., Ma, Y., Farg, M.A., Wallace, R.H., Crouch, P.J., Turner, B.J., Horne, M.K. et al. (2013) ALS-associated TDP-43 induces endoplasmic reticulum stress, which drives cytoplasmic TDP-43 accumulation and stress granule formation. *PLoS One*, **8**, e81170.
- Wells, A.L., Lin, A.W., Chen, L.-Q., Safer, D., Cain, S.M., Hasson, T., Carragher, B.O., Milligan, R.A. and Sweeney, H.L. (1999) Myosin VI is an actin-based motor that moves backwards. *Nature*, **401**, 505–508.
- Buss, F., Spudich, G. and Kendrick-Jones, J. (2004) Myosin VI: cellular functions and motor properties. *Annu. Rev. Cell Dev. Biol.*, **20**, 649–676.
- Tumbarello, D.A., Kendrick-Jones, J. and Buss, F. (2013) Myosin VI and its cargo adaptors-linking endocytosis and autophagy. *J. Cell Sci.*, **126**, 2561–2570.
- Sahlender, D.A., Roberts, R.C., Arden, S.D., Spudich, G., Taylor, M.J., Luzio, J.P., Kendrick-Jones, J. and Buss, F. (2005) Optineurin links myosin VI to the Golgi complex and is involved in Golgi organization and exocytosis. *J. Cell Biol.*, **169**, 285–295.
- Phichith, D., Travaglia, M., Yang, Z., Liu, X., Zong, A.B., Safer, D. and Sweeney, H.L. (2009) Cargo binding induces dimerization of myosin VI. *Proc. Natl Acad. Sci. USA*, **106**, 17320–17324.

28. Tumbarello, D.A., Waxse, B.J., Arden, S.D., Bright, N.A., Kendrick-Jones, J. and Buss, F. (2012) Autophagy receptors link myosin VI to autophagosomes to mediate Tom1-dependent autophagosome maturation and fusion with the lysosome. *Nat. Cell Biol.*, **14**, 1024–1035.
29. Wild, P., Farhan, H., McEwan, D.G., Wagner, S., Rogov, V.V., Brady, N.R., Richter, B., Korac, J., Waidmann, O. and Choudhary, C. (2011) Phosphorylation of the autophagy receptor optineurin restricts Salmonella growth. *Science*, **333**, 228–233.
30. Del Bo, R., Tiloca, C., Pensato, V., Corrado, L., Ratti, A., Ticozzi, N., Corti, S., Castellotti, B., Mazzini, L. and Soraru, G. (2011) Novel optineurin mutations in patients with familial and sporadic amyotrophic lateral sclerosis. *J. Neurol. Neurosurg. Psychiatry*, **82**, 1239–1243.
31. Belzil, V.V., Daoud, H., Desjarlais, A., Bouchard, J.-P., Dupré, N., Camu, W., Dion, P.A. and Rouleau, G.A. (2011) Analysis of OPTN as a causative gene for amyotrophic lateral sclerosis. *Neurobiol. Aging*, **32**, 555.e513–555.e514.
32. Heissler, S.M., Selvadurai, J., Bond, L.M., Fedorov, R., Kendrick-Jones, J., Buss, F. and Manstein, D.J. (2012) Kinetic properties and small-molecule inhibition of human myosin-6. *FEBS Lett.*, **586**, 3208–3214.
33. Bond, L.M., Peden, A.A., Kendrick-Jones, J., Sellers, J.R. and Buss, F. (2011) Myosin VI and its binding partner optineurin are involved in secretory vesicle fusion at the plasma membrane. *Mol. Biol. Cell*, **22**, 54–65.
34. Chibalina, M.V., Roberts, R.C., Arden, S.D., Kendrick-Jones, J. and Buss, F. (2008) Rab8-optineurin-myosin VI: analysis of interactions and functions in the secretory pathway. *Methods Enzymol.*, **438**, 11–24.
35. Hirschberg, K., Miller, C.M., Ellenberg, J., Presley, J.F., Siggia, E. D., Phair, R.D. and Lippincott-Schwartz, J. (1998) Kinetic analysis of secretory protein traffic and characterization of Golgi to plasma membrane transport intermediates in living cells. *J. Cell Biol.*, **143**, 1485–1503.
36. Korac, J., Schaeffer, V., Kovacevic, I., Clement, A.M., Jungblut, B., Behl, C., Terzic, J. and Dikic, I. (2013) Ubiquitin-independent function of optineurin in autophagic clearance of protein aggregates. *J. Cell Sci.*, **126**, 580–592.
37. Klionsky, D.J., Abdalla, F.C., Abeliovich, H., Abraham, R.T., Acevedo-Arozena, A., Adeli, K., Agholme, L., Agnello, M., Agostinis, P. and Aguirre-Ghiso, J.A. (2012) Guidelines for the use and interpretation of assays for monitoring autophagy. *Autophagy*, **8**, 445–544.
38. Kimura, S., Noda, T. and Yoshimori, T. (2007) Dissection of the autophagosome maturation process by a novel reporter protein, tandem fluorescent-tagged LC3. *Autophagy*, **3**, 452.
39. Rubinsztein, D.C., Cuervo, A.M., Ravikumar, B., Sarkar, S., Korolchuk, V., Kaushik, S. and Klionsky, D.J. (2009) In search of an “autophagometer”. *Autophagy*, **5**, 585–589.
40. Gonatas, N., Stieber, A., Mourelatos, Z., Chen, Y., Gonatas, J., Appel, S., Hays, A., Hickey, W. and Hauw, J. (1992) Fragmentation of the Golgi apparatus of motor neurons in amyotrophic lateral sclerosis. *Am. J. Pathol.*, **140**, 731.
41. Farg, M.A., Soo, K.Y., Warraich, S.T., Sundaramoorthy, V., Blair, I.P. and Atkin, J.D. (2013) Ataxin-2 interacts with FUS and intermediate-length polyglutamine expansions enhance FUS-related pathology in amyotrophic lateral sclerosis. *Hum. Mol. Genet.*, **22**, 717–728.
42. Zolov, S.N. and Lupashin, V.V. (2005) Cog3p depletion blocks vesicle-mediated Golgi retrograde trafficking in HeLa cells. *J. Cell Biol.*, **168**, 747–759.
43. Ron, D. and Walter, P. (2007) Signal integration in the endoplasmic reticulum unfolded protein response. *Nat. Rev. Mol. Cell Biol.*, **8**, 519–529.
44. Park, B., Ying, H., Shen, X., Park, J.-S., Qiu, Y., Shyam, R. and Yue, B.Y. (2010) Impairment of protein trafficking upon overexpression and mutation of optineurin. *PLoS One*, **5**, e11547.
45. Turturro, S., Shen, X., Shyam, R., Yue, B.Y. and Ying, H. (2014) Effects of mutations and deletions in the human optineurin gene. *SpringerPlus*, **3**, 1–16.
46. Sreedharan, J., Blair, I.P., Tripathi, V.B., Hu, X., Vance, C., Rogelj, B., Ackerley, S., Durnall, J.C., Williams, K.L. and Buratti, E. (2008) TDP-43 mutations in familial and sporadic amyotrophic lateral sclerosis. *Science*, **319**, 1668–1672.
47. Levine, B. and Kroemer, G. (2008) Autophagy in the pathogenesis of disease. *Cell*, **132**, 27–42.
48. Nixon, R.A. (2013) The role of autophagy in neurodegenerative disease. *Nat. Med.*, **19**, 983–997.
49. Sasaki, S. (2011) Autophagy in spinal cord motor neurons in sporadic amyotrophic lateral sclerosis. *J. Neuropathol. Exp. Neurol.*, **70**, 349–359.
50. Zhang, X., Li, L., Chen, S., Yang, D., Wang, Y., Wang, Z. and Le, W. (2011) Rapamycin treatment augments motor neuron degeneration in SOD1(G93A) mouse model of amyotrophic lateral sclerosis. *Autophagy*, **7**, 412–425.
51. Otomo, A., Kunita, R., Suzuki-Utsunomiya, K., Ikeda, J.-E. and Hadano, S. (2011) Defective relocalization of ALS2/alsin missense mutants to Rac1-induced macropinosomes accounts for loss of their cellular function and leads to disturbed amphisome formation. *FEBS Lett.*, **585**, 730–736.
52. Wang, I.-F., Guo, B.-S., Liu, Y.-C., Wu, C.-C., Yang, C.-H., Tsai, K.-J. and Shen, C.-K.J. (2012) Autophagy activators rescue and alleviate pathogenesis of a mouse model with proteinopathies of the TAR DNA-binding protein 43. *Proc. Natl Acad. Sci. USA*, **109**, 15024–15029.
53. Zhang, X., Chen, S., Song, L., Tang, Y., Shen, Y., Jia, L. and Le, W. (2014) MTOR-independent, autophagic enhancer trehalose prolongs motor neuron survival and ameliorates the autophagic flux defect in a mouse model of amyotrophic lateral sclerosis. *Autophagy*, **10**, 22–36.
54. Kamada, M., Izumi, Y., Ayaki, T., Nakamura, M., Kagawa, S., Kudo, E., Sako, W., Maruyama, H., Nishida, Y. and Kawakami, H. (2014) Clinicopathologic features of autosomal recessive amyotrophic lateral sclerosis associated with optineurin mutation. *Neuropathology*, **34**, 64–70.
55. Hortobágyi, T., Troakes, C., Nishimura, A.L., Vance, C., van Swieten, J.C., Seelaar, H., King, A., Al-Sarraj, S., Rogelj, B. and Shaw, C.E. (2011) Optineurin inclusions occur in a minority of TDP-43 positive ALS and FTLTDP cases and are rarely observed in other neurodegenerative disorders. *Acta Neuropathol. (Berl.)*, **121**, 519–527.
56. Tomatis, V.M., Papadopoulos, A., Malintan, N.T., Martin, S., Wallis, T., Gormal, R.S., Kendrick-Jones, J., Buss, F. and Meunier, F.A. (2013) Myosin VI small insert isoform maintains exocytosis by tethering secretory granules to the cortical actin. *J. Cell Biol.*, **200**, 301–320.
57. Laird, F.M., Farah, M.H., Ackerley, S., Hoke, A., Maragakis, N., Rothstein, J.D., Griffin, J., Price, D.L., Martin, L.J. and Wong, P.C. (2008) Motor neuron disease occurring in a mutant dynactin mouse model is characterized by defects in vesicular trafficking. *J. Neurosci.*, **28**, 1997–2005.
58. Teuling, E., van Dis, V., Wulf, P.S., Haasdijk, E.D., Akhmanova, A., Hoogenraad, C.C. and Jaarsma, D. (2008) A novel mouse model with impaired dynein/dynactin function develops

- amyotrophic lateral sclerosis (ALS)-like features in motor neurons and improves lifespan in SOD1-ALS mice. *Hum. Mol. Genet.*, **17**, 2849–2862.
59. Johnson, J.O., Mandrioli, J., Benatar, M., Abramzon, Y., Van Deerlin, V.M., Trojanowski, J.Q., Gibbs, J.R., Brunetti, M., Gronka, S. and Wu, J. (2010) Exome sequencing reveals VCP mutations as a cause of familial ALS. *Neuron*, **68**, 857–864.
 60. Alami, N.H., Smith, R.B., Carrasco, M.A., Williams, L.A., Winborn, C.S., Han, S.S., Kiskinis, E., Winborn, B., Freibaum, B.D. and Kanagaraj, A. (2014) Axonal transport of TDP-43 mRNA granules is impaired by ALS-causing mutations. *Neuron*, **81**, 536–543.
 61. Lucocq, J., Warren, G. and Pryde, J. (1991) Okadaic acid induces Golgi apparatus fragmentation and arrest of intracellular transport. *J. Cell Sci.*, **100**, 753–759.
 62. Uchiyama, K., Muramatsu, N., Yano, M., Usui, T., Miyata, H. and Sakaguchi, S. (2013) Prions disturb post-Golgi trafficking of membrane proteins. *Nat. Commun.*, **4**, 1846.
 63. Park, B., Shen, X., Samaraweera, M. and Yue, B.Y. (2006) Studies of optineurin, a glaucoma gene: Golgi fragmentation and cell death from overexpression of wild-type and mutant optineurin in two ocular cell types. *Am. J. Pathol.*, **169**, 1976–1989.
 64. Feuillette, S., Deramecourt, V., Laquerriere, A., Duyckaerts, C., Delisle, M.-B., Muraige, C.-A., Blum, D., Buée, L., Frébourg, T. and Campion, D. (2010) Filamin-A and myosin VI colocalize with fibrillary Tau protein in Alzheimer's disease and FTDP-17 brains. *Brain Res.*, **1345**, 182–189.
 65. Osterweil, E., Wells, D.G. and Mooseker, M.S. (2005) A role for myosin VI in postsynaptic structure and glutamate receptor endocytosis. *J. Cell Biol.*, **168**, 329–338.
 66. Nagabhushana, A., Chalasani, M.L., Jain, N., Radha, V., Rangaraj, N., Balasubramanian, D. and Swarup, G. (2010) Regulation of endocytic trafficking of transferrin receptor by optineurin and its impairment by a glaucoma-associated mutant. *BMC Cell Biol.*, **11**, 4.
 67. Mankouri, J., Fragkoudis, R., Richards, K.H., Wetherill, L.F., Harris, M., Kohl, A., Elliott, R.M. and Macdonald, A. (2010) Optineurin negatively regulates the induction of IFN β in response to RNA virus infection. *PLoS Pathog.*, **6**, e1000778.
 68. Sherer, N.M., Lehmann, M.J., Jimenez-Soto, L.F., Ingmundson, A., Horner, S.M., Cicchetti, G., Allen, P.G., Pypaert, M., Cunningham, J.M. and Mothes, W. (2003) Visualization of retroviral replication in living cells reveals budding into multivesicular bodies. *Traffic*, **4**, 785–801.
 69. N'Diaye, E.N., Kajihara, K.K., Hsieh, I., Morisaki, H., Debnath, J. and Brown, E.J. (2009) PLIC proteins or ubiquilins regulate autophagy-dependent cell survival during nutrient starvation. *EMBO Rep.*, **10**, 173–179.
 70. Walker, A.K., Farg, M.A., Bye, C.R., McLean, C.A., Horne, M.K. and Atkin, J.D. (2010) Protein disulphide isomerase protects against protein aggregation and is S-nitrosylated in amyotrophic lateral sclerosis. *Brain*, **133**, 105–116.
 71. Manders, E., Verbeek, F. and Aten, J. (1993) Measurement of co-localization of objects in dual-colour confocal images. *J. Microsc.*, **169**, 375–382.
 72. Walker, A.K., Daniels, C.M.L., Goldman, J.E., Trojanowski, J.Q., Lee, V.M.-Y. and Messing, A. (2014) Astrocytic TDP-43 pathology in Alexander disease. *J. Neurosci.*, **34**, 6448–6458.
 73. Renton, A.E., Majounie, E., Waite, A., Simón-Sánchez, J., Rollinson, S., Gibbs, J.R., Schymick, J.C., Laaksovirta, H., Van Swieten, J.C. and Myllykangas, L. (2011) A hexanucleotide repeat expansion in C9ORF72 is the cause of chromosome 9p21-linked ALS-FTD. *Neuron*, **72**, 257–268.

Supplementary Materials

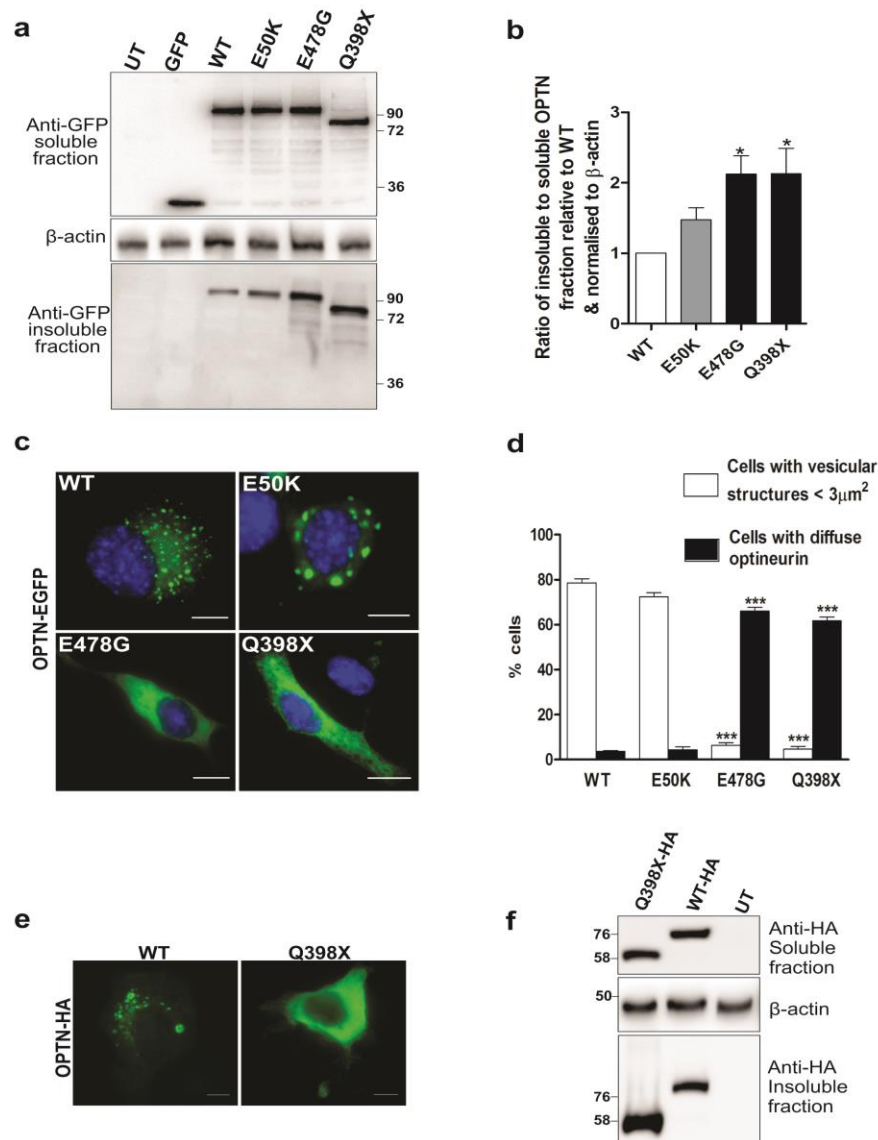


Figure S1 ALS optineurin mutants are mislocalised from vesicles in NSC-34 cells. (a) Immunoblot analysis of soluble and insoluble proteins collected from NSC-34 lysates transfected with optineurin-EGFP constructs, using anti-GFP antibody. β-actin is shown as a loading control for the soluble fraction. Approximate molecular weight markers are shown on the right in kDa. (b) Densitometric quantification of insoluble optineurin-EGFP protein fraction from NSC-34 cells, relative to soluble fraction, reveals decreased solubility of ALS mutants compared to WT or E50K optineurin. Data are represented as mean ± SEM; * $p < 0.05$, using one-way ANOVA with Tukey's post test, $n = 3$. (c) WT and E50K glaucoma mutant optineurin-EGFP are expressed as vesicular structures; whereas ALS mutants, E478G and Q398X are present diffuse throughout the cytoplasm of NSC-34 cells. Scale bar, 10 μm. (d) Quantification of NSC-34 cells with vesicular structures < 3 μm² and diffuse cytoplasmic optineurin that does not form vesicular structures. Data are represented as mean ± SEM; *** $p < 0.0001$, using one-way ANOVA with Tukey's post test, $n = 3$. (e) Expression of optineurin-HA constructs in NSC-34 cells. Fluorescence microscopy images of NSC-34 cells expressing HA tagged WT and Q398X optineurin. (f) Immunoblotting of NSC-34 lysates-soluble and insoluble fraction probed with an anti-HA antibody reveals increased insoluble protein, indicating aggregation in cells expressing Q398X-HA mutant construct. β-actin is shown as the loading control for the soluble fraction.

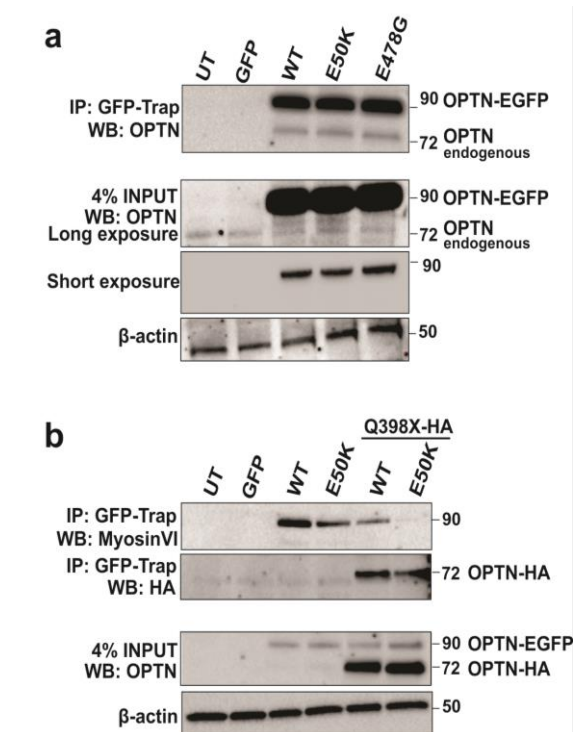


Figure S2 ALS mutant optineurin interacts with WT, E50K and endogenous optineurin and disrupts binding with myosin VI. (a) Co-precipitation of NSC-34 cell lysates expressing optineurin-EGFP proteins using GFP-Trap, followed by immunoblotting using anti-optineurin antibody. Endogenous optineurin band at ~72 kDa, is co-precipitated with EGFP tagged WT, E50K and E478G optineurin observed at ~90 kDa. 4% input control of lysates probed with anti-optineurin antibody displays endogenous optineurin and optineurin-GFP bands upon long exposure: blot was reprobed for β -actin as a loading control. (b) NSC-34 cell lysates expressing EGFP tagged WT and E50K optineurin with Q398X-HA were co-precipitated using GFP-Trap, and immunoblotted with anti-myosin VI antibody. The level of myosin VI co-precipitated is decreased in NSC-34 lysate co-expressing Q398X-HA optineurin, compared to WT and E50K optineurin alone expressing cells. Reprobe of the blot with anti-HA antibody, shows the interaction of Q398X-HA optineurin with EGFP tagged WT and E50K optineurin. 4% of input control probed with anti-optineurin antibody is shown and the blot was reprobed for β actin as a loading control.

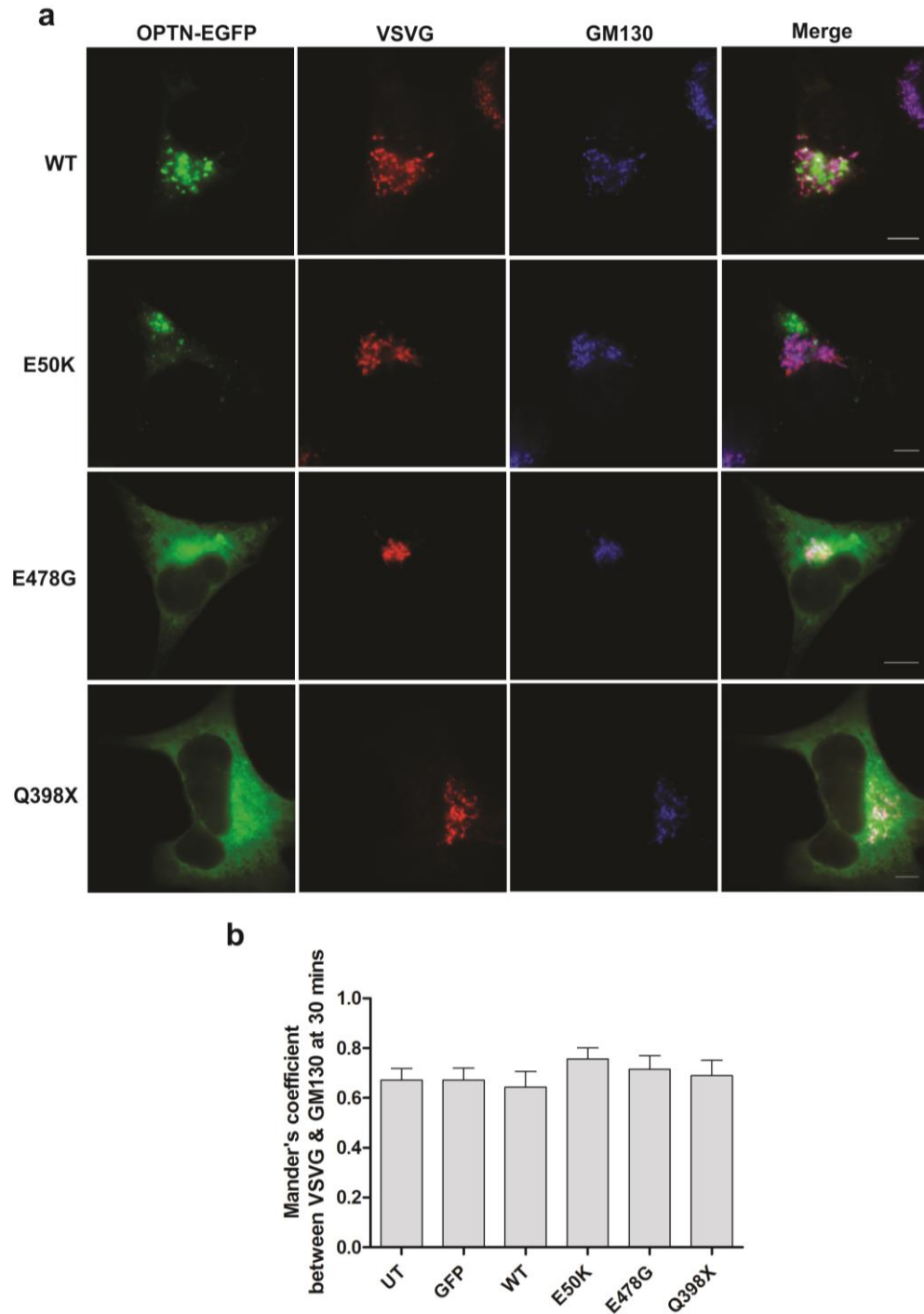


Figure S3 Expression of WT and mutant optineurin constructs does not affect VSVG trafficking from ER to Golgi.(a) NSC-34 cells co-expressing optineurin-EGFP (green) and VSVG-ts04 mCherry (red) were incubated at 40°C for 12 hrs to entrap VSVG in ER. The cells were then incubated at 32°C for 30 min, fixed and immunostained with an anti-GM130 antibody (blue). At 30 min, VSVG co-localizes with GM130 Golgi marker, indicating efficient transport from the ER to Golgi in cells expressing either WT or mutant optineurin proteins. Scale bars, 10 μ m. Analysis of co-localization of VSVG with GM130 using Mander's coefficient, after 30 min incubation at 32°C. Data are represented as mean \pm SEM using one-way ANOVA with Tukey post test, n=3.

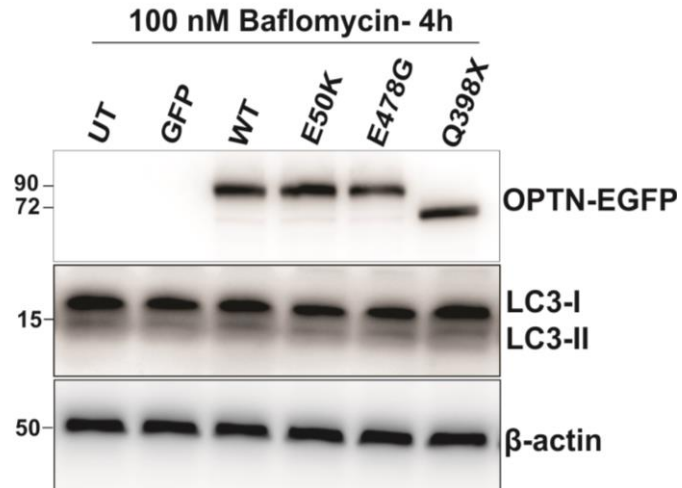


Figure S4 Baflomycin treatment of NSC-34 cells expressing optineurin constructs. Immunoblotting of NSC-34 cell lysates expressing optineurin-EGFP treated with baflomycin. Blot shows increased LC3-II intensity after treatment with 100 nM Baflomycin for 4hrs in all the cell lysates, indicating the increase in LC3-II in cells expressing E478G and Q398X mutant optineurin (observed in Fig 5f) was specifically due to the accumulation of autophagosomes and not increased autophagosome biogenesis. No difference was observed in the intensity of LC3-II between the ALS mutant optineurin and WT optineurin or untransfected cells. Expression of optineurin is revealed by immunoblotting with an anti-optineurin antibody. β -actin is shown as a loading control.

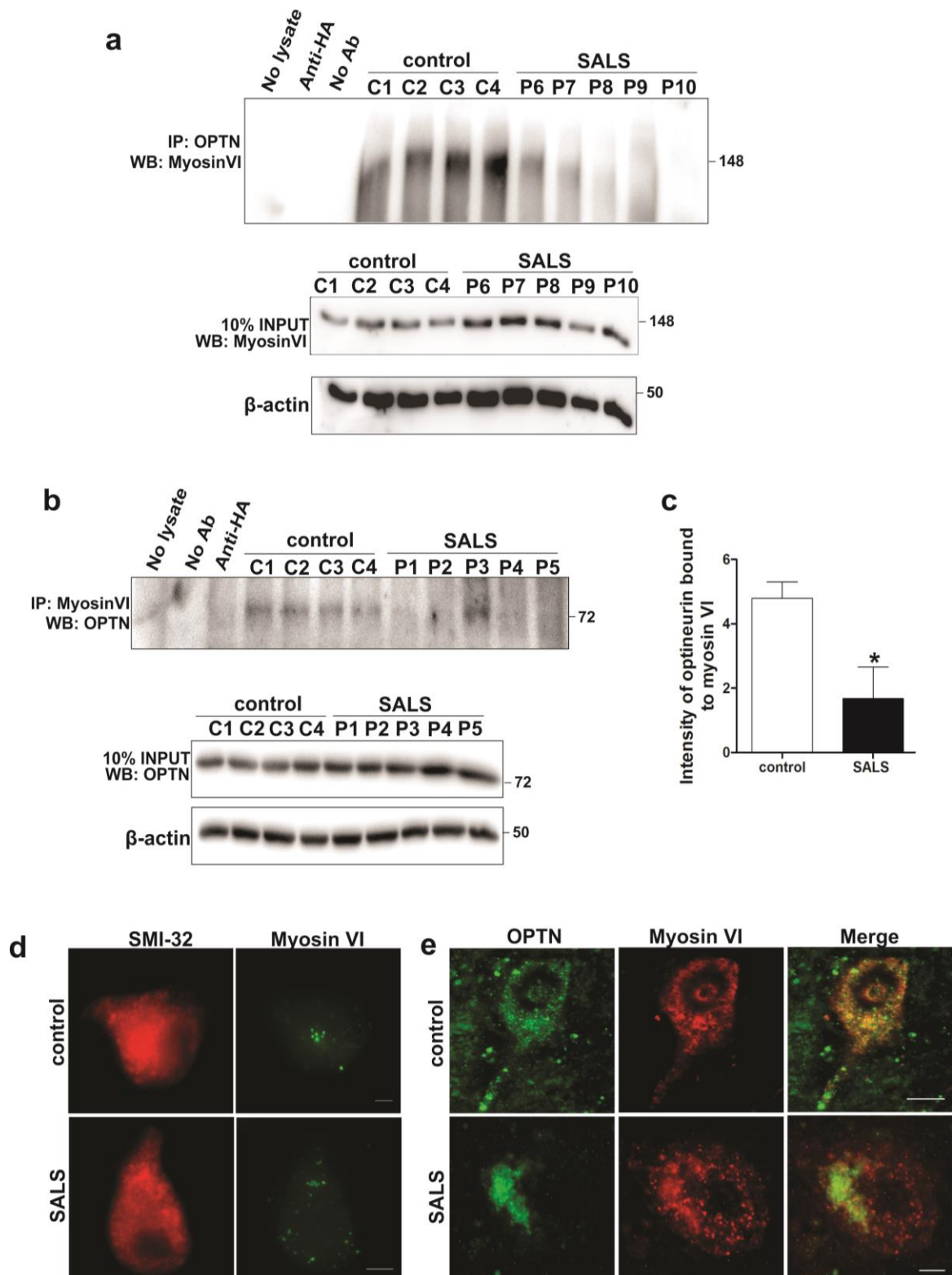


Figure S5 Optineurin dissociates from myosin VI in sporadic ALS patients (a) Immunoprecipitation using anti-optineurin antibodies of human patient spinal cord lysates followed by immunoblotting with an anti-myosin VI antibody (b) Immunoblotting using anti-optineurin antibody following immunoprecipitation using anti-myosin VI antibody of human patient spinal cord lysates. Control immunoprecipitations were negative: samples without spinal cord lysates, without antibody, or using species matched non-specific anti-HA antibody. Input blot is also shown: 10% of lysates fraction used for immunoprecipitation was immunoblotted with anti-myosin VI or anti-optineurin antibodies. β -actin is shown as loading control.

Figure S5 (c) Quantification of myosin VI expression after immunoprecipitation with anti-optineurin antibody (from immunoblots in (b)) from 5 sporadic ALS patients and 4 non-neurological control patients. Data are represented as mean \pm SEM; *, $p < 0.05$, using unpaired t test. (d) Immunohistochemistry of control and sporadic ALS patient lumbar spinal cord sections using anti-myosin VI (green) and anti-SMI32 (as a marker of motor neurons) antibodies, reveals there is no difference in the vesicular appearance of myosin VI between the samples. (e) Double immunostaining of control and sporadic ALS patient lumbar spinal cord sections using anti-optineurin and anti-Myosin VI antibody, showing the loss of vesicular optineurin but not myosin VI in sporadic ALS patient.

Supplementary videos are presented as attached media files.

Supplementary Video S1, S2, S3. NSC-34 cells co-expressing optineurin-EGFP (S1-WT, S2-E78G, S3-Q398X) and VSVG-mCherry proteins were incubated at 40°C for 12 h, followed by incubation at 32°C for 60 min. WT optineurin but not E78G or Q398X display co-migration with VSVG. The cells were imaged using a Zeiss LSM 510 confocal microscope at 37°C. The videos were captured for 60 cycles at an interval of 7 sec.

Supplementary Video S4, S5. NSC-34 cells co-expressing optineurin-EGFP (S4-WT, S5-Q398X) and LC3-DsRed proteins were imaged using a Zeiss LSM 510 confocal microscope at 37°C. The videos were captured for 60 cycles at an interval of 7 sec. WT optineurin but not Q398X display co-migration with LC3-DsRed positive autophagosomes.

Supplementary Video S6, S7, S8, S9. NSC-34 cells expressing optineurin-EGFP proteins (S6-WT, S7-E50K, S8-E78G, S9-Q398X) were stained with LysoTracker™ to visualize the lysosomes WT and E50K glaucoma mutant optineurin display tethering/trafficking with lysosomes stained by lysotracker dye. The cells were imaged using a Zeiss LSM 510 confocal microscope at 37°C. The videos were captured for 60 cycles at an interval of 7 sec.

Chapter 5

5. Cellular mechanisms induced by novel *CCNF* mutations in ALS.

5. Chapter 5

5.1 Preface

The study presented here as Chapter 5 was part of a collaborative study led by Associate Professor Ian Blair (Macquarie University). This study identified ALS associated mutations in the *CCNF* gene in familial ALS patients. The manuscript describing this genetic finding is presented in appendix 1. The author has performed all the work presented in this chapter, except where acknowledgements are made as below:

Expression constructs encoding wild type and mutant S621G *CCNF* cDNA, fused to N-terminal mCherry were generated by Associate Professor Ian Blair's group.

5.2 Introduction

Recent advancement in next-generation sequencing methods has over the last 10 years led to the identification of many novel genetic mutations that cause familial forms of ALS [13]. However the genetic causes for about one-third of ALS families and most cases (90%) of sporadic ALS still remains unknown [2]. Using genome-wide linkage analysis coupled with next generation sequencing, a collaborative study led by Associate Professor Ian Blair, Macquarie University, recently identified 10 novel missense mutations in the *CCNF* gene, in cohorts of familial and sporadic ALS and FTD cases from diverse geographic populations including Australia, Canada, Spain, Italy, the UK and US (Unpublished, currently under peer review and draft of the paper is presented in Appendix 1). *CCNF* mutations are present at frequencies ranging from 0.6 to 3.4% similar to those reported in TARDBP and FUS, in the populations examined. *CCNF* (also called *FBXO1*) is a 17 exon gene that encodes the 786 amino acid cyclin F protein. Cyclin F is a component of an E3 ubiquitin-protein ligase complex that is an integral part of the ubiquitin proteasome system (UPS). The aim of this study was to examine pathogenic mechanisms induced by the S21G novel *CCNF* mutations in ALS.

Cyclin F is the largest member of the cyclin protein family. It has a molecular weight of 87 kDa, but it migrates as a 100-110 kDa protein on SDS PAGE [458]. Cyclins are important regulators of cell cycle transitions through their ability to bind and activate cyclin-dependent protein kinases (CDK) [459, 460]. However unlike most cyclins, cyclin F does not bind or activate any known cyclin dependent kinase (CDK), making it an orphan protein of the family [461]. *CCNF* also belongs to the F-box protein family which is characterized by a 40 amino acid motif, the F-box [462]. The F-box proteins forms the SCFs (SKP1-cullin-F-box) complex, which constitute one of the four subunits of the E3 ubiquitin protein ligase complex [463]. The E3s complex mediate the ubiquitination and proteasomal degradation of target proteins and they are an integral component of the ubiquitin proteasome system (UPS). The ligase activity of the SCF complex catalyses the addition of multiple ubiquitin molecules to the target protein [464]. Cyclin F contains two nuclear localisation signals (NLS) [465] and a PEST sequence; short stretch of amino acids that are enriched in proline, glutamic acid, serine and threonine (Figure 5.1). The PEST sequence at the C-terminus of cyclin F, controls

the ubiquitination of regulatory short-lived proteins [466] and is also required for degradation of cyclin F through UPS-independent mechanisms [467].

Cyclin F regulates genomic integrity by ubiquitination and degradation of CP110, a protein essential for centrosome duplication [461]. Hence cyclin F is thought to function as an inhibitor of centrosome re-duplication. However cyclin F is expressed ubiquitously in all human tissues [458], and its role in UPS could be critical in long lived, post-mitotic cells like neurons, prone to accumulation defective proteins and damaged organelles [464]. E3 ubiquitin ligases also play a key role in selecting target proteins for degradation via the ERAD pathway. ERAD is an ER quality control mechanism, whereby terminally misfolded proteins in the ER translocate to the cytosol, where they are tagged with ubiquitin and subsequently degraded by the UPS [468, 469]. The F-box family of proteins which form the SCF complex specifically interact with and ubiquitinate typical substrates that translocate from the ER to cytosol by the ERAD pathway [470, 471]. Expression of mutant F-box family proteins Fbs1 and Fbs2, which lack the F-box domain, blocks the degradation of ERAD specific substrates, highlighting the functional importance of F-box proteins in the ERAD pathway [470, 471]. Cyclin F is predominantly localised in the nucleus and the localisation is mediated by the two NLS [458, 465]. Cyclin F also mediates the transport of cyclin B1 from the cytoplasm to the nucleus, suggesting a role for cyclin F in nucleo-cytoplasmic shuttling.

To determine whether mutations in *CCNF* are present in ALS and FTD patients, Associate Professor Blair's group and collaborators used targeted sequencing, whole exome sequencing, or whole genome sequencing in the following cohorts: index cases from 75 Australian ALS families, 159 UK ALS families, 108 US ALS families, 100 Canadian ALS families, 99 Italian ALS families, 30 Spanish ALS families, 16 Irish ALS families, 168 French-Canadian sporadic ALS cases, 26 US sporadic ALS cases, 49 US ALS trios, 43 Australian FTD families, and 29 Australian sporadic FTD cases. Ten missense variants in *CCNF* were identified and all the mutations are present in amino acids that are conserved across species (Figure 5.1). Three of the variants contain substitutions in the PEST rich sequence of cyclin F, and three others contain a single mutation in either the Fbox domain, cyclin domain or the NLS (Figure 5.1). The variants were examined in large control cohorts and datasets including: dbSNP; NHLBI ESP Exome Variant Server, 1000 Genomes Project, 947 Australian control exomes (of European ancestry) as well as other population-specific

controls from the UK, US, and Canada. None of the ten variants was present in genotyped controls. ALS/FTD variants in *CCNF* were present in the overall cohorts from these diverse geographic populations at frequencies ranging from 0.6 to 3.4%, which is comparable to the frequency of mutations in *TARDBP* and *FUS* in familial ALS cohorts [116]. In summary, seven *CCNF* mutations and three rare missense variants were identified from cohorts of familial and sporadic ALS and FTD cases from Australia, Canada, the UK, US, Spain and Italy. Associate Professor Blair's analysis demonstrated that each mutation was absent in large control cohorts including population-specific controls. Each variant showed conservation across species. The average age of disease onset in familial and sporadic ALS cases with *CCNF* mutations was 54.0 ± 6.9 and 54.8 ± 18.2 respectively.

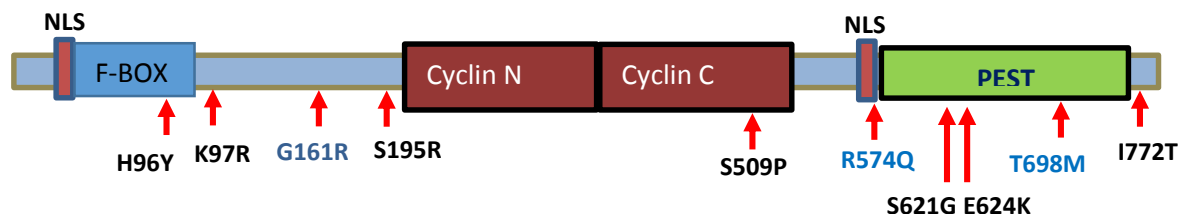


Figure 5.1 Representation of cyclin F protein domains and the location of mutations (black) and rare variants (blue). Cyclin F contains three functional modules within its protein structure; F-box domain forms a 'pseudocatalytic' module, the two cyclin domains form the substrate recruitment module and the C terminus containing both a nuclear localisation signal (NLS) and a PEST sequence (short stretch of amino acids enriched in proline, glutamic acid, serine and threonine) form the regulatory module

The genetic studies described above demonstrate that *CCNF* variants are present in familial ALS. However it remains unclear how these mutations trigger neurodegeneration in ALS. Accumulating evidence suggests that activation of ER stress is an upstream event in the pathogenesis of ALS. Furthermore ER stress is induced by genetic mutations in TDP-43, FUS, SOD1, optineurin and C9orf72 [295, 306, 307, 312]. The ERAD pathway is the primary mechanism for clearing misfolded protein accumulation in the ER lumen and a dysfunction in UPS and hence ERAD could activate ER stress [469, 472]. Translation and expression of cyclins including cyclin B1, a interacting partner of cyclin F, is controlled by stress granule formation and release [473]. In addition knockdown of TIA1, a key element for stress granule formation, substantially increased (2-fold) the levels of cyclin F, suggesting a possible association between cyclin F expression and stress granule formation [474]. Hence

investigation whether genetic mutations in cyclin F induce pathogenic mechanisms previously described in ALS, is therefore warranted. In this study we focussed on ER stress and stress granule accumulation because these mechanisms are relevant to cellular trafficking. We also wished to determine if these mutations also trigger apoptotic cell death, therefore providing evidence of a link to neurodegeneration.

In order to examine the consequences of expression of ALS causing mutations in cyclin F, SH-SY5Y human neuroblastoma cells were transiently transfected with plasmids expressing N-terminal mCherry-tagged WT or mutant S621G cyclin F. These cells were then analysed for cellular localisation, stress granule recruitment of cyclin F, ER stress activation and apoptotic cell death, in order to provide insights into the pathogenic mechanisms triggered by *CCNF* mutations.

5.3 Materials and Methods.

5.3.1 Plasmids and cloning

Expression constructs encoding wild type and mutant S621G *CCNF* cDNA fused to N-terminal mCherry were produced by collaborators from Associate Professor Blair's group using pmCherry-C1-*CCNF* (Addgene) encoding wildtype cyclin F. Site-directed mutagenesis was performed to generate S621G mutant using Q5® Site-Directed Mutagenesis Kit (NEB), according to the manufacturer's protocol.

5.3.2 Subcellular fractionation

SH-SY5Y cells transfected with cyclin F constructs for 48 hrs were lysed in subcellular fractionation buffer (250 mM Sucrose, 20 mM HEPES [pH-7.4], 10 mM KCl, 1.5 mM MgCl₂, 1 mM EDTA, 1mM EGTA, 1 mM DTT and 0.1% protease inhibitor cocktail [Sigma]). The pellet (pellet I) containing nuclear and cytoskeletal fraction was obtained by centrifugation at 720 g for 5 min and the supernatant was collected (supernatant I) to generate the cytoplasmic fraction. The pellet I was washed with subcellular fractionation buffer and lysed by passing 10 times through a 25 G needle. The lysate was centrifuged again at 720 g for 10 min. The supernatant was stored as supernatant II and the pellet was resuspended in Tris-NaCl buffer (50 mM Tris HCl [pH 7.6], 150 mM NaCl, 0.1% NP40, 0.1% SDS). The resulting lysate was collected as the nuclear fraction. The supernatants I & II were mixed and centrifuged at 100,000 g for 4 h to pellet the membrane fraction. The resulting

supernatant is collected as cytoplasmic fraction, which was then concentrated using Amicon Ultra 10 kDa centrifugal filters (Millipore).

5.3.3 Stress granule analysis

To induce the formation of stress granules, SH-SY5Y cells previously transfected with cyclin F constructs for 72 hrs were treated with 0.5 mM sodium arsenite for 30 min. The cells were then fixed with 4% PFA and stained with an anti-eIF2 α antibody. Images were acquired using an Olympus IX-81 inverted fluorescence microscope at 40X magnification. Cells displaying cytoplasmic cyclin F co-localised with eIF2 α positive stress granules were scored from three different experiments.

5.3.4 Cell death assays.

Sytox Blue staining: SH-SY5Y cells cultured in 6 well plates were transfected and harvested after 72 hrs treatment by adding trypsin for 1 min at room temperature. The cells were then collected in PBS, centrifuged at 1200 rpm for 5 min, and resuspended in 200 μ l of resuspension buffer (10mM HEPES, 140mM NaCl, 2.5mM CaCl₂, pH 7.4). The cell suspension was treated with 1 μ M Sytox Blue nucleic acid stain (Invitrogen) at room temperature for 10 min in the dark. The cell suspension was then analysed for SYTOX blue positive cells using flow cytometry, after gating for cells positive for mCherry fluorescence, using BD FACS Canto II flow cytometer.

Quantification of apoptotic nuclei: Cells grown on coverslips were co-transfected with 1 μ g DNA of wildtype (WT) and S621G mutant *CCNF* plasmid as indicated, using Lipofectamine 2000 (Invitrogen) according to the manufacturer's protocol. After 72 hrs cells were washed with PBS and fixed with 4% paraformaldehyde in PBS for 10 min. The cells were then treated with 0.5 μ g/ml Hoechst 33342 solution (5 mg/ml in stock, 1:10,000 dilution in water) prior to mounting in fluorescent mounting medium (Dako). Images were acquired using an Olympus IX- 81 inverted fluorescence microscope at 100x magnification. Apoptotic nuclei were defined as condensed (less than 5 μ m in diameter) or fragmented (containing multiple condensed Hoechst-positive structures in one cell). The quantification of apoptotic cells was calculated as a percentage of non-apoptotic cells from at least 100 cells expressing either WT or mutant cyclin F, in 3 independent experiments. Cells expressing displaying abnormal morphology or undergoing cell division were excluded from the analysis.

5.4 Results

5.4.1 ALS mutant cyclin F is localised more in the cytoplasm than wildtype cyclin F in SH-SY5Y cells.

TDP-43 and FUS are normally localised in the nucleus but they aggregate and mislocalise to the cytoplasm in ALS. In this study, the localisation of both WT and ALS mutant S621G cyclin F, whether nuclear or cytoplasmic, was examined after 48 hrs transfection in human neuroblastoma SH-SY5Y cells (Figure 5.2a). Quantification of microscopic images revealed that WT cyclin F was predominantly localised in the nucleus (~90% of cells), and was only expressing diffusely in the cytoplasm in ~10% of cells. However a significantly higher percentage of cells (~28%) expressing ALS mutant S621G expressed cyclin F in the cytoplasm (Figure 5.2b). This indicates that the ALS-associated mutation induces the redistribution of cyclin F from the nucleus to the cytoplasm. To confirm this observation, subcellular fractionation of lysates generated from SH-SY5Y cells expressing WT, S621G cyclin F or pmcherry-n1 alone was performed. The nuclear and cytoplasmic fractions were subjected to immunoblotting using anti-SP1 and anti-GAPDH antibodies to identify the nuclear and cytoplasmic fractions respectively. These analyses revealed that the two fractions were efficiently separated, with little cross contamination between the two (Figure 5.2c). The nuclear and cytoplasmic fractions were then probed with an anti-cyclin F antibody using immunoblotting. Quantification of these blots revealed that higher levels of cyclin F mutant S621G were present in the cytoplasmic fraction compared to the WT cyclin F (Figure 5.2c). Hence these data reveal that the ALS-associated mutation in cyclin F induces its mislocalisation to the cytoplasm.

5.4.2 ALS-associated mutation in cyclin F accelerates its association with stress granules.

Since an increased cytoplasmic localisation of ALS mutant cyclin F was observed (Figure 5.2) compared to wildtype cyclin F, it was next examined whether cytoplasmic cyclin F associates with stress granules. SH-SY5Y cells expressing cyclin F at 72 hrs post-transfection, were treated with 0.5 mM sodium arsenite for 30 min to induce stress granule formation. Immunocytochemistry followed by microscopic analysis revealed that approximately 90% of all the cells examined developed eIF2 α -positive stress granules following the treatment with sodium arsenite. ALS-associated mutant cyclin F co-localised with eIF2 α -positive stress granules in the cytoplasm, in a significantly higher ($p < 0.05$) percentage of cells (~30%) compared to WT cyclin F (Figure 5.3a, 5.3b). Hence this finding

implies that the S621G mutation in *CCNF* induces its recruitment to stress granules, pathology typical of ALS.

5.4.3 ALS mutant cyclin F induces ER stress

It was next examined whether mutant cyclin F induces ER stress. Lysates collected from SH-SY5Y cells expressing cyclin F proteins at 72 hrs post-transfection were probed for UPR sensor proteins IRE1 and the spliced form of xbp1 (Figure 5.4a, 5.4b). Both of these markers were significantly upregulated ($p < 0.001$) in cells expressing mutant cyclin F compared to WT, suggesting that ER stress is activated in these cells. It was then examined whether expression of mutant cyclin F also induces upregulation of ER stress pro-apoptotic factor, CHOP. Immunocytochemistry of cells expressing cyclin F using an anti-CHOP antibody revealed a significant activation ($p < 0.05$) of CHOP, as determined by the percentage of cells (58%) with nuclear immunoreactivity [302], in comparison to cells expressing WT cyclin F (Figure 5.4c, 5.4d). CHOP activation was also observed in a smaller percentage of cells (~30%) overexpressing WT cyclin F (Figure 5.4d), compared to cells expressing mCherry alone. In summary, these findings demonstrate that expression of the ALS-associated cyclin F mutant S621G induces ER stress, activating pro-apoptotic CHOP.

5.4.4 ALS mutant cyclin F induces apoptotic cell death.

Activation of ER stress and CHOP signalling in cells expressing mutant cyclin F implies that apoptotic cell death is triggered in these cells. Hence to examine this further, quantification of the percentage of dead cells was performed by flow cytometry after staining the cells with Sytox Blue, a general marker (apoptosis and necrosis) of cell death (Figure 5.5a, 5.5b). This analysis revealed a significantly higher percentage of dead cells in populations expressing mutant cyclin F compared to those expressing WT cyclin F ($p < 0.05$, 30% mutant; 21% WT). Similar to the results obtained for activation of CHOP (Figure 5.4d), a significant increase in the percentage of dead cells was also observed in populations expressing WT cyclin F compared to cells expressing mCherry ($p < 0.001$), as well as untransfected cells.

Apoptotic cell death was then quantified in these cell populations by examining nuclear morphology, where condensed nuclear morphology is indicative of apoptosis, in at least 100 cells per group per experiment [302]. Apoptotic nuclei were significantly more common in cells expressing mutant S621G cyclin F compared to WT cyclin F (Figure 5.5c, 5.5d; $p < 0.05$, 30% mutant; 18% WT). Hence these data show that ALS-associated mutant cyclin F activates apoptosis in SH-SY5Y human neuronal cells.

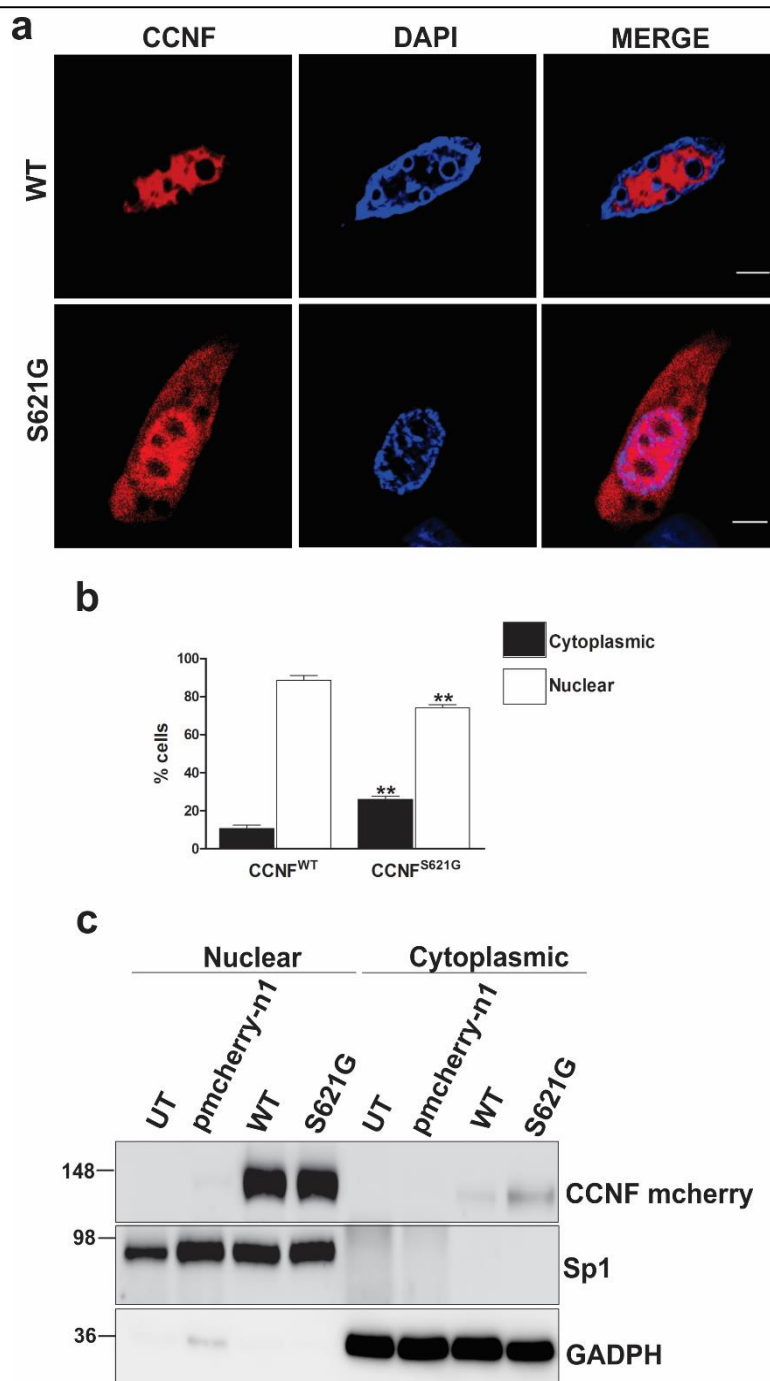


Figure 5.2 Mutant cyclin F displays a higher degree of cytoplasmic localisation than wildtype cyclin F in SH-SY5Y cells. SH-SY5Y cells transfected with cyclin F mCherry constructs (red) were fixed after 48 hrs and the nucleus was stained using DAPI (blue). **(a)** Representative images demonstrate that WT cyclin F displays predominantly nuclear staining and mutant cyclin F (S621G) displays both cytoplasmic and nuclear staining. **(b)** Quantification of staining indicating a significantly higher degree of cytoplasmic localisation of mutant cyclin F compared to WT cyclin F. Data represent mean \pm SEM. $n=3$; $**p<0.01$. Scale bar 10 μ m. **(c)** Western blots of subcellular fractions obtained from SH-SY5Y lysates transfected with cyclin F mCherry constructs demonstrate more cytoplasmic mutant S621G cyclin F than WT cyclin F. Anti-GADPH and Sp1 blots are shown as cytoplasmic and nuclear markers respectively.

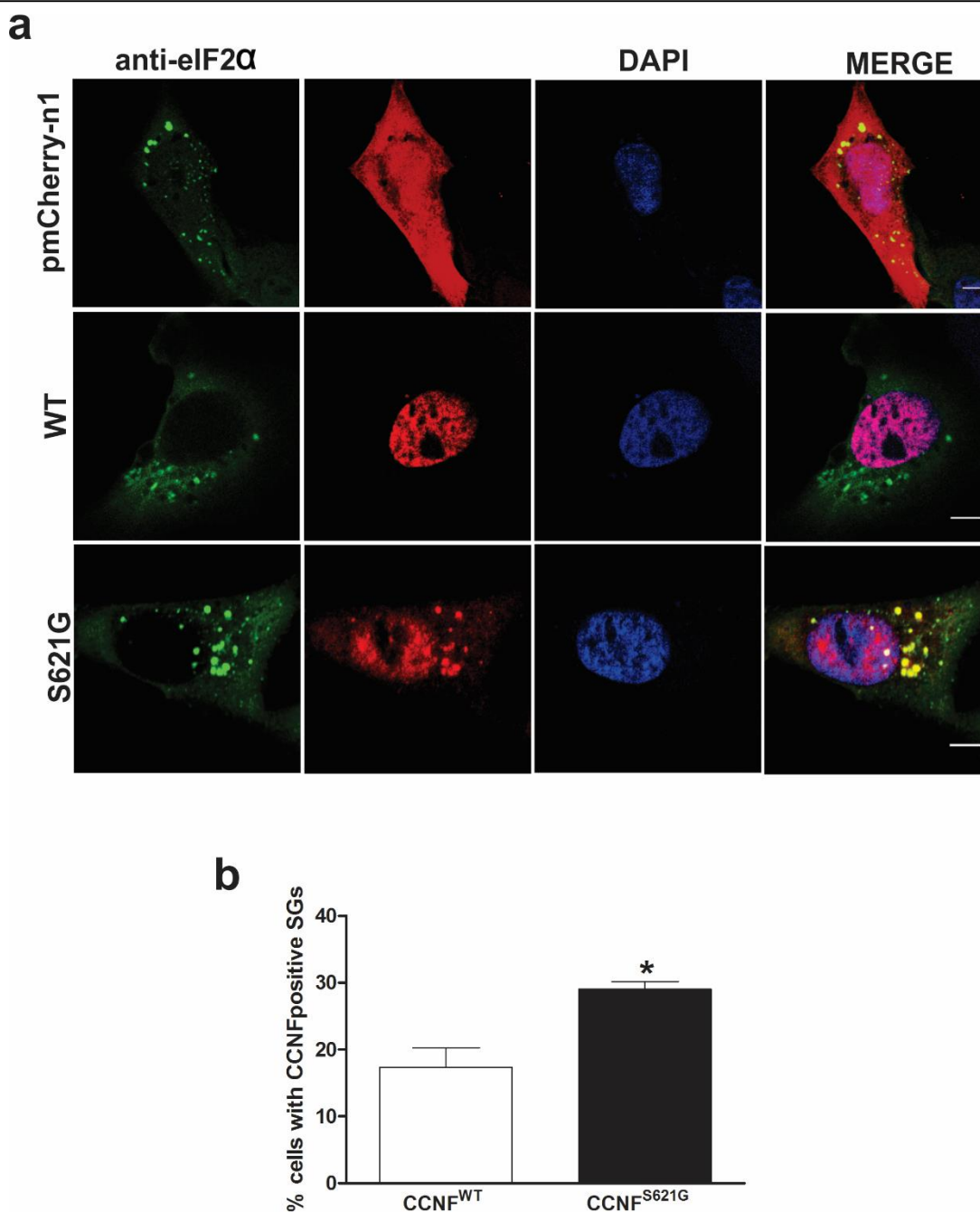


Figure 5.3 The S621G mutation promotes cyclin F recruitment into eIF2 α -positive cytoplasmic stress granules. SH-SY5Y cells transfected with cyclin F constructs for 72 hrs were treated with 0.5 mM sodium arsenite for 30 mins. The cells were then fixed and stained with anti-eIF2 α antibody (green), a cytoplasmic stress granule marker. **(a)** Representative images of SH-SY5Y cells showing recruitment of mutant cyclin F into eIF2 α positive stress granules, indicated by arrows. **(b)** Quantification of the percentage of cells displaying cyclin F positive stress granules after sodium arsenite treatment observed in **(a)**. Data represent mean \pm SEM. n=3; *p<0.05. Scale bar 10 μ m.

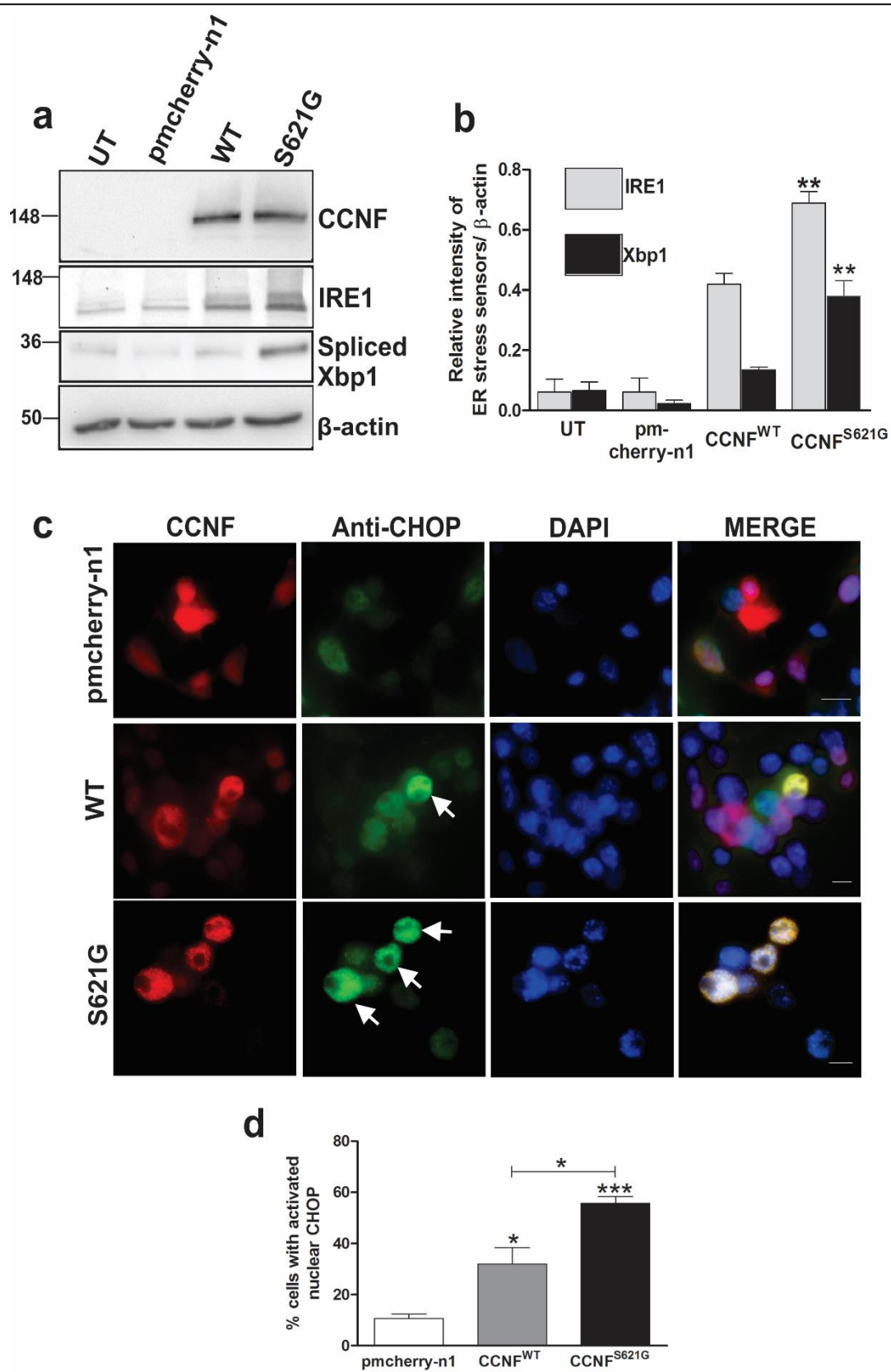


Figure 5.4 Induction of ER stress in SH-SY5Y cells expressing mutant cyclin D

Figure 5.4 SH-SY5Y cells were transfected with cyclin F constructs, and 72 hrs after transfection, the cells were lysed and immunoblotted for ER stress markers Xbp1 and IRE1. **(a)** Immunoblot demonstrating increased levels of spliced Xbp1 and IRE1 in cells expressing mutant cyclin F compared to wildtype. Expression of cyclin F is shown in the top panel. **(b)** Quantification of ER stress markers in **(a)** relative to β actin intensity. For analysis of CHOP activation, SH-SY5Y cells transfected with cyclin F constructs were fixed after 72 h and immunostained with anti-CHOP antibodies (red), DAPI (blue). **(c)** Representative images demonstrating increased nuclear CHOP immunoreactivity (indicated by arrows) in cells expressing WT and mutant cyclin F. **(d)** Quantification of nuclear CHOP immunoreactivity, indicating activation, reveals a significant increase in CHOP activation in cells expressing mutant cyclin F compared to wildtype cyclin F and vector alone transfected cells. Data represent mean \pm SEM. $n=3$; *** $p<0.001$, ** $p<0.01$, * $p<0.05$. Scale bar 10 μ m.

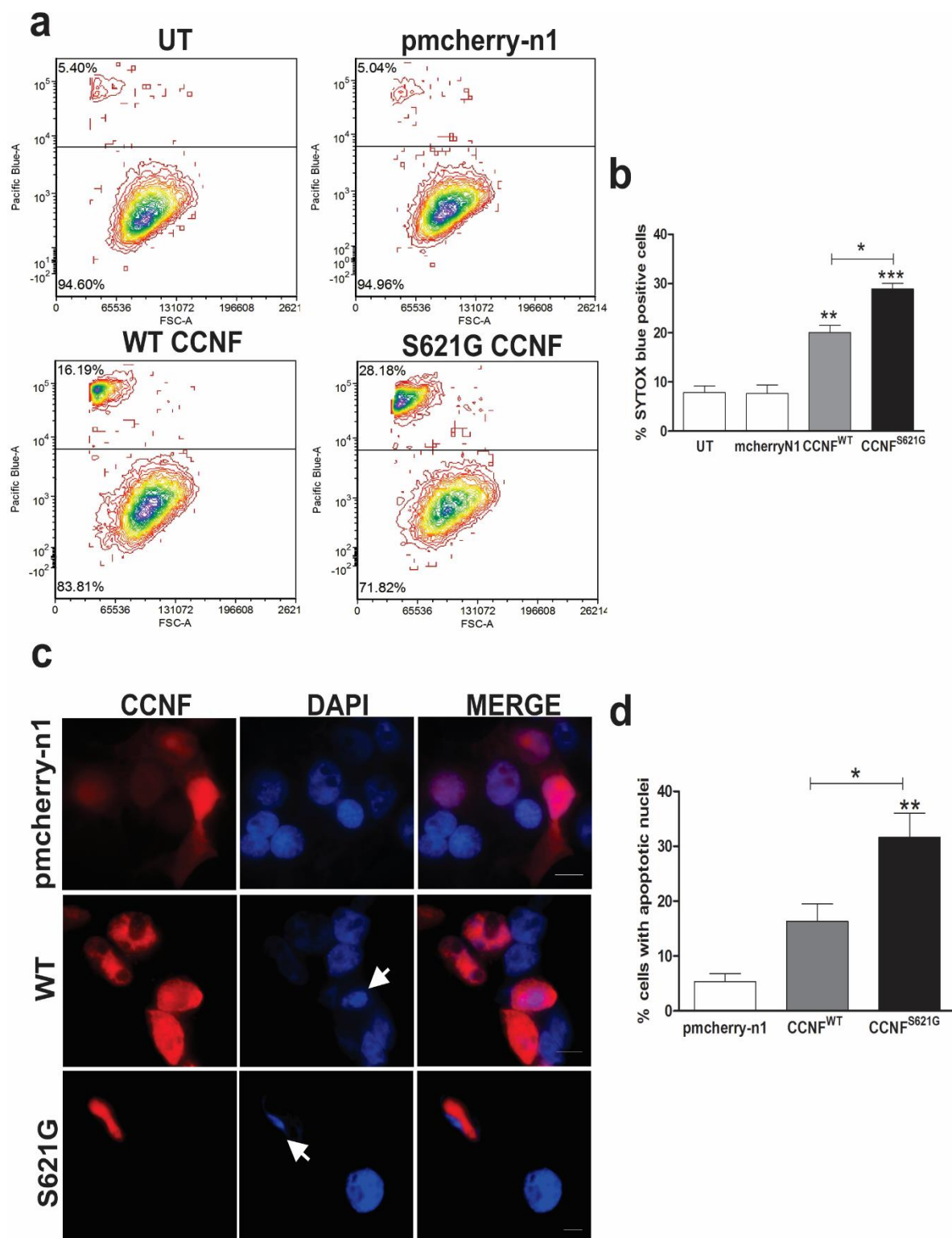


Figure 5.5 Higher percentage of cells undergo apoptosis in SH-SY5Y cells expressing mutant cyclin F compared to those expressing wildtype cyclin F. (a) Flow cytometry analysis of SH-SY5Y cells expressing cyclin F mcherry proteins after staining with Sytox Blue, a marker for cell death.

Figure 5.5 (b) Quantification of Sytox Blue positive cells at 72 hrs post transfection demonstrates a higher percentage of dead cells due to the expression of mutant cyclin F compared to WT. **(c)** SH-SY5Y cells transfected with cyclin F constructs were fixed after 72 hrs, the nuclei were stained using DAPI (blue) and the number of cells with condensed nuclei was quantified to determine the percentage of apoptotic cells. **(c)** Representative images showing apoptotic cells with condensed nuclei (indicated by arrows) in cells expressing cyclin F constructs. **(d)** Quantification of condensed nuclei demonstrates a significantly higher percentage of apoptotic cells due to expression of mutant cyclin F compared to WT cyclin F and vector alone transfected cells. Data represent mean \pm SEM. $n=3$; $**p<0.01$, $*p<0.05$. Scale bar 10 μm .

5.5 Discussion

This study demonstrates that the ALS-associated mutation in *CCNF*, S621G, induces cellular mechanisms and pathogenic features characteristic of familial and sporadic ALS. Mutant cyclin F displayed increased cytoplasmic localization, more recruitment into stress granules, and induced more ER stress and apoptosis, than cells expressing wildtype cyclin F. Hence these results provide *in vitro* evidence linking the cyclin F mutation S621G to ALS. In addition, this study provides additional evidence relating ER and stress granule pathologies to the etiology of ALS.

Increasing evidence links abnormal proteostasis, accumulation of misfolded protein aggregates and impairment of the UPS to the pathogenesis of ALS [198]. Mutations in the *UBQLN2* gene, which encodes ubiquilin 2, a protein that physically associates with ubiquitin ligases and proteasomes to mediate protein degradation, are present in familial ALS [61, 475]. Mutations in ubiquilin 2 also impair protein degradation mediated by the UPS [476]. In addition a recent study demonstrated that overexpression of wildtype or ALS mutant (P497H) ubiquilin 2 impairs ERAD and hence degradation of misfolded proteins by UPS, leading to the activation of ER stress [477]. Mutations in the ERAD-associated protein, VCP, have also been linked to familial ALS [59] and inclusion body myopathy with Paget's disease of the bone and frontotemporal dementia (IBMPFD) [478]. Expression of ALS mutant VCP impairs ERAD, resulting in increased accumulation of ubiquitinated proteins [478]. Furthermore, impairment of ERAD by mutant VCP activates ER stress and apoptotic cell death in *Drosophila* models [479]. Hence these data imply that impairment of ERAD and associated UPS induces ER stress in familial forms of ALS and FTD. Similarly in this study, a mutation in cyclin F, an integral component of UPS, in familial forms of ALS was demonstrated to induce ER stress. Whilst the mechanism for triggering the UPR is unknown, one likely possibility is impairment of ERAD. However future studies are needed to confirm the mechanism involved. It must also be considered that ER stress could be activated by inhibition of ER to Golgi trafficking. Cytoplasmic mutant SOD1 aggregates were previously shown to induce ER stress by inhibiting COPII mediated ER-Golgi trafficking [200]. Cytoplasmic accumulation of mutant cyclin F raises that possibility that mutant cyclin F may interfere with cellular trafficking pathways to induce ER stress. Hence future studies should also be aimed to examine such a possibility.

There is also evidence that defects in proteins functionally related to cyclin F are present in other neurodegenerative diseases and that this leads to impairment of UPS. Mutations in the related F-box only protein 7 gene (*FBXO7*) cause autosomal recessive, early-onset, parkinsonian-pyramidal syndrome, and lead to decreased stability of the *FBXO7* protein [480, 481]. Similar to cyclin F, the F-box motif of *FBXO7* interacts directly with Skp1 to form the SCF E3 ubiquitin-protein ligase complex [463]. Furthermore, around 10% of early onset Parkinson's disease cases are caused by mutations in *PARK2*, which encodes Parkin, an E3-ubiquitin ligase [482, 483]. Mutations in Parkin impair degradation of its normal substrates, leading to the accumulation of protein aggregates and eventually cell death [484, 485].

This is the first study to relate mutations in cyclin F to cellular pathogenic mechanisms implicated in ALS. Cyclin F is primarily considered to be a protein involved in cell cycle regulation, and it has been poorly studied in relation to other cellular processes including ERAD. The only known interactors of cyclin F are cyclin B1 [465], CP110 [461], NuSAP [486] and RRM2 [487], which are all its normal substrates, that become degraded during the normal cell cycle. It is therefore possible that abnormal cyclin F may contribute to ALS pathogenesis through dysregulation of the cell cycle. If terminally differentiated neurons re-enter the cell cycle, neuronal apoptosis is triggered instead of cell proliferation [488]. Cyclin F regulates nuclear translocation of the cyclin B1/cdc2 complex, a mitotic phase promoting factor [465]. Aberrant localisation and expression of the cyclin B1/cdc2 complex has been demonstrated in terminally differentiated and degenerating neurons in Alzheimer's disease [489]. In this study, ALS-associated mutant cyclin F was localised more in the cytoplasm than wildtype cyclin F (Figure 5.2). This suggests that in familial forms of ALS linked to cyclin F, loss of a nuclear transport function of cyclin F may be associated with pathogenesis, leading to neurotoxicity by mislocalisation of cyclin B1/cdc2 complex.

ALS mutant cyclin F also associated with stress granules at significantly higher levels than WT cyclin F in this study (Figure 5.3). Recent studies have demonstrated an association of cyclins with stress granules. Cyclin B1 mRNA association with stress granules controls the translation and expression of cyclin B1 protein [473]. The recruitment of cyclin B1, a mitotic phase factor, to stress granules is believed to be a part of the mechanism of cell cycle regulation, by halting the expression of cyclin B1 during the initial phases of cell cycle [473].

Similarly, expression of cyclin F is altered by the formation of stress granules, suggesting that cyclin F expression is controlled by stress granule recruitment [474]. In this study, while both WT and ALS mutant cyclin F were recruited to stress granules, ALS mutant cyclin F was retained in the stress granules at a higher rate than WT cyclin F, suggesting that mutant cyclin F cannot be released as readily from stress granules. It has been hypothesised that persistent stress granules containing FUS and TDP-43 are pathogenic by either initiating protein aggregation or halting the expression of key proteins essential for cellular viability [338, 455]. Hence it is possible that mutant cyclin F may be linked to pathogenesis by the accumulation of stress granules in ALS.

In summary, this study identifies pathogenic mechanisms induced by a novel cyclin F mutation recently described in familial forms of ALS. It also provides further evidence for a link between disruption to proteostasis, UPS dysfunction and activation of ER stress in the pathogenesis of ALS.

Chapter 6

6. C9orf72 regulates endosomal trafficking

6. Chapter 6

6.1 Preface

The work presented here formed part of the published manuscript presented in Appendix 2. This chapter describes only the experiments from this publication that were performed by the author. All the work presented here are performed by the author except where acknowledgements are made as below:

Manal Farg (La Trobe University) performed the culturing and co-transfection of SH-SY5Y cells without baflomycin treatment, which were then fixed and stained by the author, presented in Figure 6.3a. Manal Farg also assisted with image analysis and quantification presented in Figure 6.3c. The author also acknowledges the contributions of Manal Farg in designing the experiments for this study.

The data presented here was recently published in 'Farg *et al* 2014, *C9ORF72*, implicated in amyotrophic lateral sclerosis and frontotemporal dementia, regulates endosomal trafficking, *Human molecular genetics*, 2014: 23(13), 3579-3595.' This study was the first experimental investigation into the normal cellular function of C9orf72 protein [346] (presented in Appendix 2).

6.2 Introduction

Whilst hexanucleotide GGGGCC repeat expansions in the *C9ORF72* gene are the major cause of familial ALS (40%) and FTD (25%), the function of the C9orf72 protein remained unknown. Similarly, it remains unclear how *C9ORF72* repeat expansions trigger ALS pathology. Defining the cellular pathogenic mechanisms induced by *C9ORF72* is clearly essential to understand the pathogenesis of these two disorders.

Whilst the function of C9orf72 remains unknown, it is highly conserved throughout evolution and it is expressed in many tissues (including the cerebellum and cortex), implying that C9orf72 plays an important role in normal cellular function [32]. The repeat expansion is present within an intron, located between the first two exons (1a and 1b). Alternative splicing of C9orf72 results in three separate isoforms and the repeat expansion is predicted to inhibit expression of all three variants in a transcript-specific manner [132]. Consistent with this notion, decreased expression of C9orf72 variants was observed in the frontal cortex, motor cortex, cerebellum and cervical spinal cord of FTD/ALS patients [121, 130, 138, 139, 490], lymphoblast cell lines [139], and in neuronal cells differentiated from patient iPSC's [126, 141]. Together these data imply that reduced expression of C9orf72 protein is associated with pathogenesis, thus raising the possibility that loss of normal C9orf72 function is linked to neurodegeneration in ALS. Hence it is important to define the normal cellular function of C9orf72.

Two recent bioinformatics studies have predicted that C9orf72 is a novel homologue of DENN module-containing proteins [349, 350]. These proteins possess DENN domains and they function as GDP-GTP exchange factors (GEFs) for Rab GTPases. Rabs alternate between two conformational states: the activated GTP-bound form and the GDP-bound inactive form. Exchange of GDP with GTP is catalyzed by RabGEFs that act at specific membranes and facilitate GDP release, thus locally activating their targets [377]. DENN module containing proteins mostly function as RabGEFs for endocytotic Rabs [491]. The endolysosomal system is highly dynamic and endocytic trafficking is necessary for

regulating sorting and degradation of proteins, via autophagy or ubiquitin-proteasome system (UPS) [492]. Multiple Rabs have been implicated in autophagy including Rab5 and Rab7, Rab11, and Rab1 [238]. Disruption of autophagic clearance of misfolded proteins is increasingly implicated as a pathological feature of ALS [229, 493].

The DENN module is comprised of an N-terminal longin domain, followed by DENN and d-DENN domains [349]. A strong sequence and structural homology was observed between C9orf72 and the DENN family of proteins and the protein sequence of C9orf72 is predicted to form all the three modules of DENN domain [349, 350]. Furthermore the closest homologues of C9orf72 were identified as folliculin (FLCN), folliculin interacting protein 1 (FNIP1) and late secretory pathway protein AVL9 homolog, which belong to DENN-like superfamily of proteins, functioning as GEFs in late endosomal trafficking pathways [349]. This therefore raises the possibility that C9orf72 is a RabGEF, thus regulating Rab-dependent endocytic trafficking [349, 350].

The aim of this study was to examine whether the normal cellular function of C9orf72 is linked to Rab-mediated trafficking. Firstly, it was investigated whether C9orf72 regulates endocytosis. Human neuronal SH-SY5Y cells were treated with siRNA duplexes to silence human C9orf72 expression and the rate of endocytosis of two different substrates: Shiga toxin and Tropomyosin receptor kinase B (TrkB) receptor were measured by employing immunocytochemistry and biochemical techniques. Secondly it was further examined whether C9orf72 associates with lysosomes and autophagosomes, to determine whether C9orf72 functions in autophagy. This study describes a novel function of C9orf72 in Rab mediated cellular trafficking.

6.3 Materials and Methods

6.3.1 C9orf72 Knockdown

To knockdown endogenous C9orf72 protein, human SH-SY5Y cells were transfected with C9orf72 siRNA (Dharma; L-013341–01) or control scrambled siRNA, following the manufacturer's instructions. In some cases, the knockdown procedure was performed twice on the same cells at 24 h interval, to increase efficiency of C9orf72 knockdown.

6.3.2 Endocytosis trafficking assays

To examine endocytosis, SH-SY5Y cell were treated with C9orf72 and control siRNA for 24 h. Purified Shiga toxin conjugated to CY3 (SxTB-CY3) as previously described [494] was added to the medium of cells and incubated for 30 min. The medium was then refreshed and incubated for a further 60 min, to allow the trafficking of Shiga toxin from the plasma membrane to the Golgi apparatus. The cells were then fixed and examined by immunocytochemistry for co-localisation of Shiga toxin with Golgi marker GM130. Mander's overlap coefficients were calculated using JACoP image J plugin from at least 50 cells from each treatment.

The rate of endocytosis was measured by quantifying the internalization of TrkB receptor by cell surface biotinylation as described previously [495-497]. Briefly, SH-SY5Y cells were transfected with C9orf72 siRNA and 24 h later they were transfected again with siRNA to increase the efficiency of knockdown. The C9orf72 depleted cells were then transfected with a construct encoding FLAG-tagged TrkB receptor for 48 hrs (provided by Dr Simon Murray, University of Melbourne). Cells were then washed twice with ice-cold PBS, and incubated with 0.5 mg/ml biotin N-hydroxysuccinimide ester (biotin NHS; Thermo Scientific) in PBS for 30 min at 48°C to biotinylate all cell surface proteins. Unreacted biotin was quenched and removed with 50 mM NH₄Cl for 5 min. Biotinylated cells were then transferred to pre-warmed medium containing 50 ng/ml BDNF (Millipore) for 2 h to induce endocytosis of TrkB receptor. The cells were then immediately lysed in TN buffer with 0.1% SDS. Internalized, biotinylated TrkB receptor was then precipitated from cell lysates using 10 ml of streptavidin-agarose beads (Cell signaling). The levels of TrkB receptor were then quantified by immunoblotting with anti-FLAG antibody (Sigma).

6.3.3 Live cell imaging

Neuro2A cells transfected with C9orf72-GFP were stained for 20 min with 1 mM LysoTracker (L7528, Molecular Probes) and the movement of C9orf72 vesicles was examined by timelapse imaging. Images were acquired every 7 s for 15 min using a Zeiss LSM 510 confocal microscope.

6.4 Results

6.4.1 C9orf72 is expressed in the nucleus and as cytoplasmic vesicles

To characterise the function of C9orf72, the expression of endogenous C9orf72 in neuronal cell lines; murine neuro2a and human SH-SY5Y was examined. Immunofluorescence of C9orf72 was present diffuse in the nucleus and as cytoplasmic vesicles (Figure 1A and B, Appendix 2). Similarly, in cells transfected with a construct-encoding GFP-tagged C9orf72 (Figure 1C, Appendix 2), both nuclear protein and cytoplasmic vesicles were observed. Hence the expression of C9orf72 in cytoplasmic vesicles suggests a possible role in cellular trafficking, consistent with RabGEF function

6.4.2 C9orf72 regulates trafficking of Shiga toxin from the plasma membrane to Golgi apparatus

To examine if C9orf72 regulates endocytosis, human neuronal SH-SY5Y cells were treated with siRNA duplexes to reduce human C9orf72 expression. Using immunoblotting, C9orf72 levels were found to be depleted by 30%, without obvious off-target effects, as indicated by no change in the levels of β -actin (Figure 6.1a). Endocytosis was examined using Shiga toxin subunit B (STxB), an endocytosis marker conjugated to Cy3, which is transported from the plasma membrane to Golgi network via Rab GTPases including Rab5 [494]. Mander's overlap coefficient [498] was calculated to quantify colocalization between STxB and cis-Golgi marker GM130, detected by immunocytochemistry. In cells depleted of C9orf72, transport of STxB-Cy3 to the Golgi apparatus was inhibited by 18% (Figure 6.1b, 6.1c; $P < 0.001$) compared with cells treated with control siRNA. Hence, C9orf72 regulates an endocytotic pathway used by Shiga toxin to reach the cis-Golgi network.

6.4.3 C9orf72 regulates endocytosis of TrkB receptor

We next examined endocytosis using a second marker, TrkB receptor, to confirm the findings obtained using Shiga toxin. SH-SY5Y cells were depleted of C9orf72 by 80% using two successive siRNA transfections (Figure 6.2a) and then transfected with a construct encoding FLAG-tagged TrkB receptor for 48 hrs. C9orf72 depleted cells expressing FLAG-tagged TrkB were then biotinylated for 30 min at 48°C and endocytosis of biotinylated TrkB receptor was induced by incubation with BDNF ligand. Internalized TrkB receptor was precipitated with streptavidin beads and the levels of internalized receptor present in cell lysates was quantified by immunoblotting using an anti-FLAG antibody. In cells depleted of C9orf72 by 80%, endocytosis of TrkB was inhibited by 87% compared with control cells (Figure 6.2b, 6.2c; $P < 0.05$). Hence these data confirm that C9orf72 regulates endocytosis.

6.4.4 C9orf72 associates with autophagosomes and lysosomes in neuronal cell lines

As DENN proteins regulate both autophagy and endosomal trafficking, this study then examined if C9orf72 also regulates autophagy. Neuro2A cells were co-transfected with constructs encoding C9orf72-GFP and DsRed-tagged LC3, a marker for autophagosomes. GFP-positive C9orf72 was expressed as punctate structures in the cytoplasm, consistent with a role in vesicular trafficking, and diffusely in the cytoplasm. Vesicular cytoplasmic C9orf72 co-localise with LC3-DsRed in 23% of cells (counted from at least 100 cells), suggesting that C9orf72 associates with LC3-positive structures, indicative of autophagosomes, under basal conditions (Figure 6.3a). Cells were then treated with bafilomycin, which blocks fusion of the autophagosome to the lysosome and hence increases the number of autophagosomes. This resulted in a significantly increased proportion of cells in which C9orf72 co-localised with LC3-positive structures (73%, Figure 6.3b, 6.3c; $P < 0.05$), thus providing further evidence that C9orf72 associates with autophagosomes. It was next examined whether C9orf72 also associates with the lysosome using LysoTracker, a specific lysosomal marker. C9orf72-positive vesicles co-localised within every cell examined (Figure 6.3d), suggesting that C9orf72 is strongly associated with lysosomes. This was investigated further using live cell imaging studies, which revealed that C9orf72-positive vesicles co-migrated with LysoTracker-stained vesicles in every live cell examined, confirming that C9orf72 associates with lysosomes (Supplementary video 10). These data demonstrate that vesicular C9orf72 is associated with both lysosomes and autophagosomes, consistent with its predicted role as a DENN protein and hence RabGEF that regulates autophagy in association with Rab proteins.

This notion was investigated further by another member of the laboratory. Immunocytochemistry for Rab proteins revealed C9orf72 co-localised strongly with Rabs implicated in autophagy and endosomal transport: Rab1, Rab7, Rab5 and Rab11 (Figure 2A, Appendix 2). Similarly, C9orf72 co-immunoprecipitated with Rab1, Rab7 and Rab11 (Figure 2B, Appendix 2), suggesting a physical interaction between C9orf72 and Rab proteins. We further examined the expression of C9orf72 further in primary cortical neurons obtained from C57Bl/6 mice. C9orf72 was present both in the nucleus and in vesicles, similar to its expression in neuronal cell lines (Figure 3A, Appendix 2). Immunocytochemistry using Rab5, Rab7 and Rab11 antibodies revealed that C9orf72-positive vesicles frequently co-localised with Rab5, Rab7 and Rab11 (Figure 3B, Appendix 2). These findings were investigated further using immunohistochemistry of human spinal cord sections. Quantitative analysis of motor neurons in control patients revealed that C9orf72 co-localised with Rab5 (60%), Rab7 (70%) and Rab11 (60%), consistent with the findings obtained from cell lines (Figure 4A, 4B, Appendix 2), confirming that C9orf72 co-localises with Rab proteins. Quantitation of motor neurons from an ALS patient with the C9orf72 hrsexanucleotide repeat expansion revealed an increased proportion of cells with colocalization of C9orf72 with Rab7 or Rab11 compared with controls (Figure 4B, Appendix 2), suggesting possible dysregulation of endosomal trafficking in ALS patients with the C9orf72 hrsexanucleotide repeat expansion. In summary these findings suggest that C9orf72 associates with Rabs, consistent with the predicted RabGEF function.

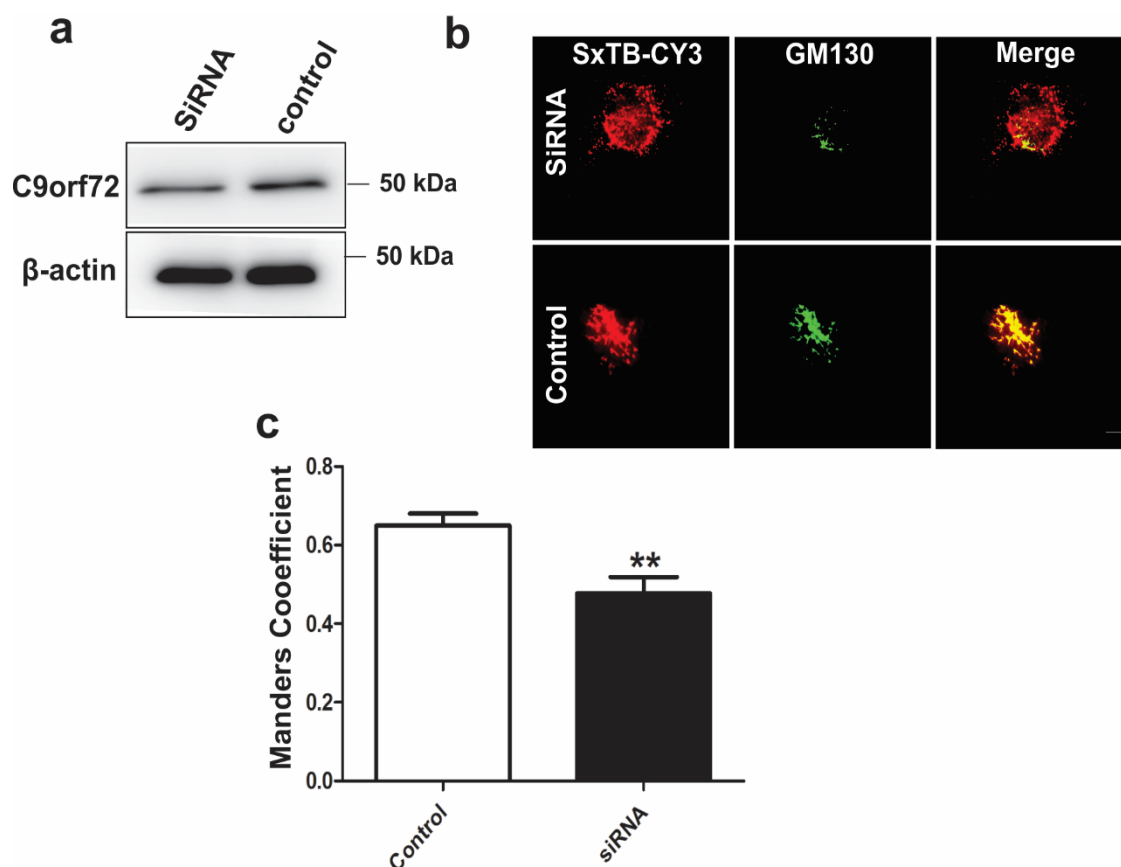


Figure 6.1 C9orf72 mediates endocytosis of Shiga toxin-CY3. (a) SH-SY5Y cells were transfected with C9orf72 targeted siRNA and control siRNA for 72 h. Cell lysates were harvested and immunoblotting followed by densitometry quantification revealed that C9orf72 expression was reduced by 30% in cells treated with C9orf72 siRNA compared with control siRNA-treated cells. (b) Purified Shiga toxin conjugated to CY3 (SxTB-CY3) (red) was added to the medium of cells treated with C9orf72 and control siRNA for 30 min. Endocytosis was examined after 60 min using immunocytochemistry for Golgi marker GM130 (green). Scale bar 10 μ m. (c) The colocalization between C9orf72 and GM130 was quantified using Mander's coefficient, revealing 18% inhibition of endocytosis of Shiga toxin in C9orf72-siRNA treated cells. For each of two replicate experiments, 50 cells were scored for each population. Data are represented as mean \pm SEM; ** $p < 0.001$, using unpaired t test, $n = 2$.

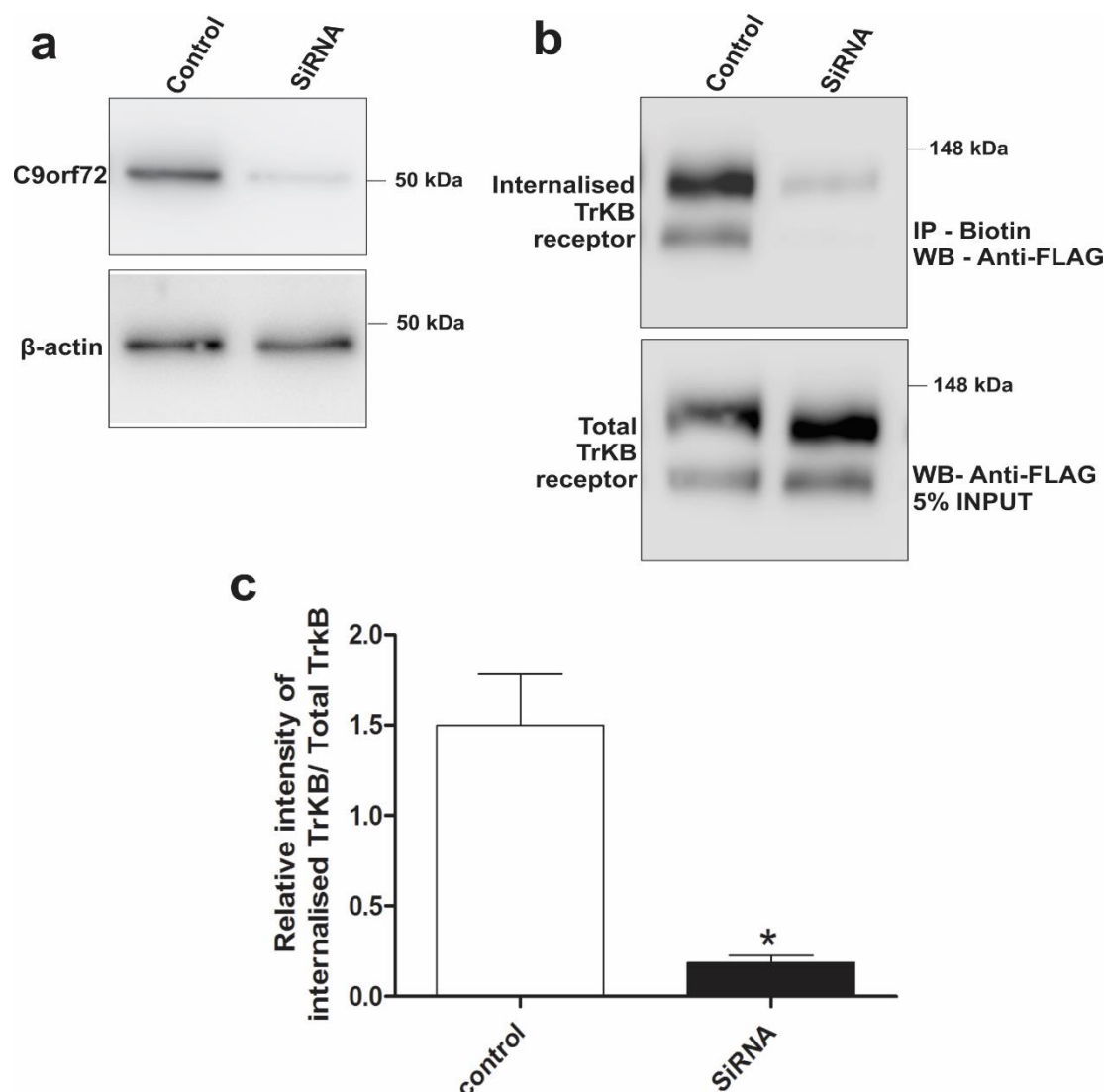


Figure 6.2 C9orf72 mediates endocytosis of TrkB receptor. SH-SY5Y cells were transfected with C9orf72 targeted siRNA and control siRNA followed by a second transfection 24 h later. **(a)** Immunoblotting followed by densitometry quantification revealed that C9orf72 expression was reduced by 80% compared with control siRNA-treated cells. **(b)** C9orf72 depleted and control cells expressing FLAG-tagged TrkB receptor were treated with biotin NHS at 4°C to biotinylate cell surface proteins. The cells were then incubated at 37°C and medium containing BDNF was added to induce endocytosis of TrkB receptor. The rate of TrkB receptor endocytosis was examined after 2 h by precipitating biotinylated and internalized TrkB receptor from cell lysates with streptavidin beads and immunoblotting with an anti-FLAG antibody. **(c)** Densitometric quantification of immunoblots reveals inhibition of endocytosis of TrkB receptor by 87% in cells depleted of C9orf72 compared with control cells. Biotin precipitation and immunoblotting were performed in triplicate. Data are represented as mean ± SEM; *p<0.05, using unpaired t test, n=3.

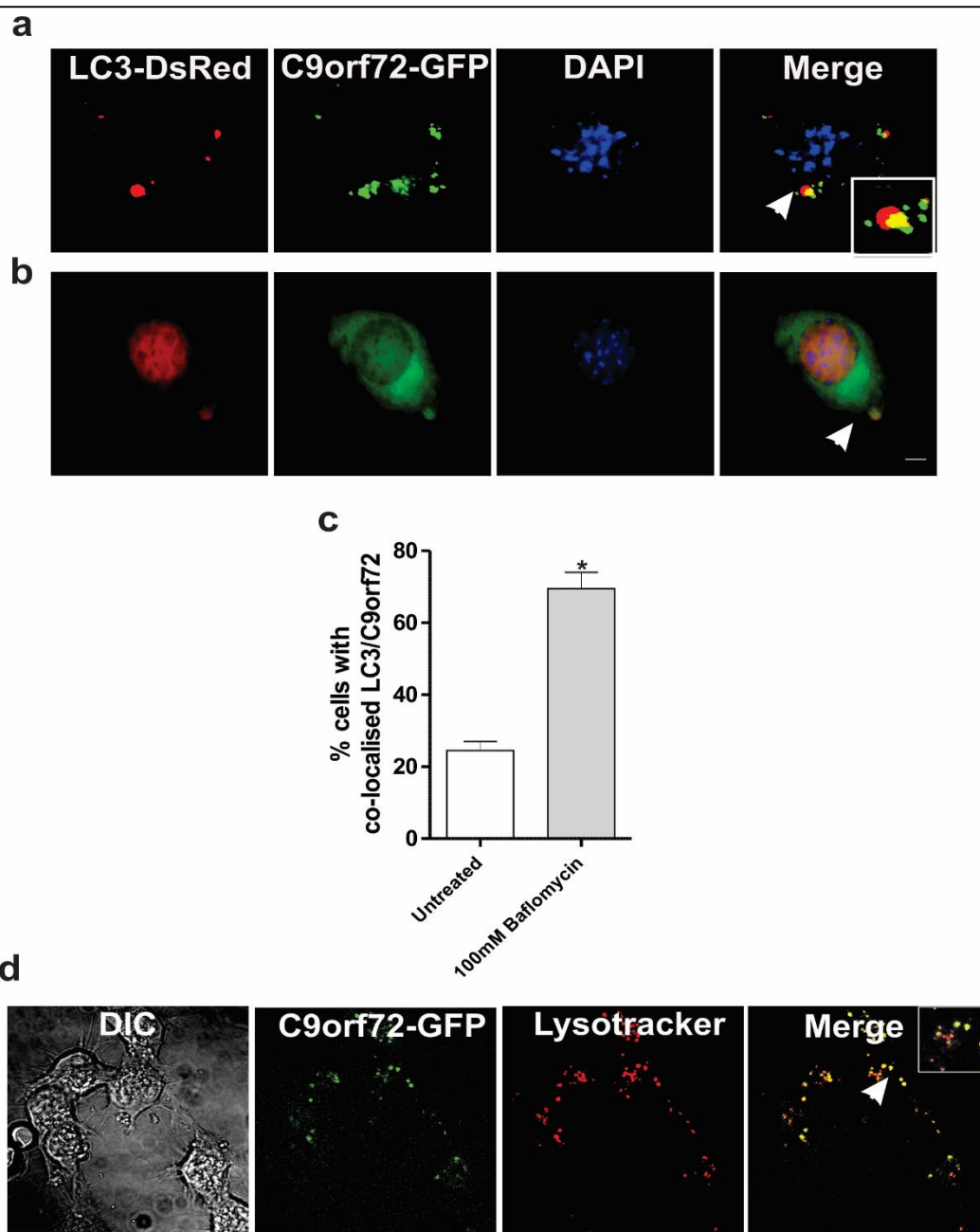


Figure 6.3 C9orf72 co-localises with autophagosomes and lysosomes. **(a)** Neuro2A cells were co-transfected with DsRed-LC3 for 48 hrs. Fluorescence microscopy revealed that C9orf72 appeared as punctate structures that co-localised with DsRed-LC3, indicating autophagosomes, inset demonstrates higher magnification (100x) of the areas highlighted to illustrate autophagosomes. **(b)** Cells were treated with 100 nM bafilomycin for 4 h to inhibit fusion of autophagosomes to the lysosome. White arrow represents C9orf72 co-localisation with autophagosomes. **(c)** Quantification of the percentage of cells in which C9orf72 co-localised with DsRed-LC3 revealed elevation in the numbers of LC3-positive structures, indicating autophagosomes, co-localising with C9orf72 in bafilomycin treated cells. Data are represented as mean \pm SEM; * $p < 0.05$, using unpaired t test, 50 cells were scored, $n = 2$. **(d)** C9orf72 is associated with lysosomes in Neuro 2A cells. Cells were transfected with C9orf72-GFP and treated with

Supplementary video S10 (presented as attached media files). Neuro2A expressing C9orf72-GFP were stained with LysoTracker for 20 min. C9orf72 displays tethering/trafficking with lysosomes stained by lysotracker dye. The cells were imaged using a Zeiss LSM 510 confocal microscope at 37°C. The images were captured for 15 min at an interval of 7 sec each.

6.5 Discussion

Despite the importance of C9orf72 in the pathogenesis of ALS and FTD, its normal cellular function remained undefined. This study is the first to provide experimental evidence for the involvement of C9orf72 in Rab mediated cellular trafficking of endosomes and autophagosome/lysosome compartments. Reduced expression of C9orf72 resulted in impaired endocytosis and trafficking of endocytic markers from the plasma membrane to the Golgi apparatus in SH-SY5Y neuronal cells. These results also raise the possibility that disruption to cellular trafficking is a possible mechanism of toxicity induced by haploinsufficiency in ALS patients. Endocytic trafficking is essential for autophagy. Autophagosome membrane originates from multiple endomembrane sources delivered through Rab mediated endocytosis [499, 500]. Inactivation of multiple Rabs by overexpression of respective RabGAPs was previously demonstrated to inhibit autophagy [499, 501], implicating that activated Rab functioning is essential of autophagy. The study presented here showed that C9orf72 regulates Rab mediated endocytosis presumably by its predicted RabGEF function, and hence loss of C9orf72 could impair autophagy. The co-localisation of C9orf72 positive vesicles with autophagosomes and co-migration with lysosomes (Figure 6.3), further suggests that C9orf72 functions in autophagy by regulating endolysosomal trafficking.

Indeed in further studies performed in our laboratory, immunoblotting for LC3 in human SH-SY5Y cells depleted of C9orf72 by 75% using siRNA (Figure 6E, Appendix 2), revealed that the LC3II:LC3I ratio was increased by 45% in C9orf72-siRNA treated cells, indicating dysregulation of autophagy. C9orf72 was also found to associate with multiple Rabs: Rab1, Rab5, Rab7, Rab11 that regulate various steps of autophagy (Figure 2, Appendix 2). Rab1 is essential for autophagosome formation by delivering membrane contents from the ER cisternae [502]. Rab5 is present within clathrin-coated vesicles, and it mediates the fusion of endocytic vesicles to form early endosomes [238, 503]. Rab7 coordinates traffic between late endosome and lysosome [504] and plays a critical role in the biogenesis of lysosomes [505] and maturation of autophagosomes [506]. Finally, Rab11 aids in the maturation of autophagosomes by regulating their fusion with multivesicular bodies (MVB) [507]. Hence the association of C9orf72 with these four Rabs implies that C9orf72 may have a broad role in regulating endolysosomal vesicular trafficking during autophagy. We also identified actin as an interacting partner of C9orf72 by mass spectrometry (Appendix 2). Actin plays a key

role in the early stages of autophagosome formation [508], and autophagosomes are surrounded by the actin filament network that is required for autophagosome/lysosome trafficking and fusion [206, 509]. Hence the interaction between C9orf72 and actin therefore provides additional evidence for a role for C9orf72 in autophagy.

Rabs function as molecular switches that alternate between two conformational states: the activated GTP-bound form and the GDP-bound inactive form. Rab GEFs mediate the exchange of GDP with GTP, which facilitates the release of GDP and thus activates the Rab protein [491]. Proteins with DENN domains act as Rab GEFs by physically interacting with Rab proteins in the appropriate cellular compartments [361, 377]. Consistent with this mechanism, C9orf72 co-localised and co-precipitated with four Rab proteins in both neuronal cell lines and primary cortical neurons. Hence, this study is consistent with two previous bioinformatics studies that reported the presence of a DENN domain in C9orf72, discovered as part of a previously undetected group of DENN proteins that mediate autophagy by vascular-vesicle interactions [349, 350]. The bioinformatics studies raised the possibility that C9orf72 functions as a RabGEF that regulates Rab-dependent intracellular trafficking. This study therefore provides the first experimental evidence to support this notion. However, more specific *in vitro* GEF assays [510], screening the GEF activity of recombinant C9orf72 protein against a library of Rabs would conclusively establish the RabGEF function of C9orf72.

Defects in Rab-mediated trafficking have been previously described in many neurodegenerative diseases, including ALS. Mutations in Rab7 cause Charcot-Marie-Tooth disease type 2B [511], and Rab7-positive endosome abnormalities impair trafficking in Wobbler mice [383]. Mutations in Alsln, a RabGEF for Rab5 [361], cause juvenile onset ALS and primary lateral sclerosis [68] and enlarged Rab5-positive endosomes are present in spinal ALS motor neurons [382]. Dysfunction in dynein, which powers endocytic trafficking, has been described in ALS [208] and depletion of dynein also results in endocytic Rab accumulation and endosomal pathology [512]. Overexpression of α -synuclein impairs Rab1 activity and decreases autophagosome formation in Parkinson disease models [513]. Mutant huntingtin disrupts Rab5 mediated autophagic clearance of pathogenic protein aggregates in cell and fly models of Huntington disease [514].

In conclusion, this study shows that C9orf72 regulates cellular trafficking, thus facilitating both endocytosis and autophagy. Further studies in this area are necessary in order to completely understand the normal cellular function of C9orf72 in association with Rab proteins. The role of C9orf72 in cellular trafficking pathways provides additional evidence that disruption to major cellular trafficking pathways are an important mechanism linked to neurodegeneration in ALS.

Chapter 7

7. General discussion

7. General discussion

7.1 Summary of main findings from the thesis

This thesis presents novel findings that increase our understanding of the role of cellular trafficking defects in the pathogenesis of ALS (Figure 7.1). These results imply that perturbation of cellular trafficking processes is linked to several pathogenic features observed in ALS. Cellular trafficking is important for proteostasis, and disruption to proteostasis is increasingly linked to the pathogenesis of ALS [145]. Autophagy is an important proteostatic mechanism and degradation of misfolded pathogenic proteins by autophagy is essential for cell survival in neurodegenerative diseases [515]. Furthermore protein degradation mechanisms including autophagy and UPS control stress granule formation and clearance [516, 517]. However the accumulation of protein aggregates in ALS suggests a broad role for disruption of proteostasis in the pathogenesis of ALS. Cellular trafficking processes play a key role in regulating protein degradation pathways as well as in stress granule dynamics [204, 518-520]. Abnormalities in the ER and Golgi compartments are observed early in the pathogenesis of ALS [296, 323], also implying that defects in cellular trafficking are linked to neurodegeneration. The findings presented in this thesis add weight to the notion that cellular trafficking defects are an upstream mechanism for triggering neurodegeneration in ALS.

7.1.1 Extracellular misfolded wildtype and mutant SOD1 inhibits ER-Golgi trafficking and exhibits similar potential to spread ALS pathology.

Chapter 3 presents a 2013 publication that describes novel molecular and cellular mechanisms to explain how extracellular, misfolded wildtype and mutant SOD1 spread pathology from cell to cell in ALS. This study demonstrated that NSC-34 and SH-SY5Y neuronal cells could uptake both recombinant, wildtype and mutant SOD1 from the culture medium. The uptake was non-specific for misfolded or mutant forms of SOD1 via macropinocytosis. The uptake of either mutant SOD1 or misfolded, wildtype SOD1 induced features reminiscent of ALS pathology in human neuronal cells, including intracellular SOD1 aggregation, ER stress, Golgi fragmentation and apoptotic cell death. It also demonstrated that misfolded SOD1 (mutant or misfolded wildtype) inhibited secretory protein transport between the ER and Golgi apparatus, thus providing an explanation for the induction of ER-Golgi pathologies by a cytoplasmic protein. Hence this study describes a specific ER-Golgi mechanism shared by extracellular forms of both misfolded, wildtype and mutant SOD1,

which could subsequently trigger several key pathological events in ALS. Both misfolded wildtype SOD1 and mutant SOD1 induced these features to a similar degree, demonstrating that misfolded wildtype SOD1 can behave in a similar way to mutant SOD1 in inducing pathogenic features of ALS.

7.1.2 Defects in optineurin/myosin VI mediated cellular trafficking links key pathogenic features in ALS.

The published study presented in chapter 4 demonstrates that loss of optineurin function in myosin VI mediated cellular trafficking is associated with pathogenic features typical of ALS. ALS causing mutations in optineurin was demonstrated to disrupt its association with myosin VI. The resulting loss of the optineurin/myosin VI complex led to accumulation of autophagosomes, inhibition of secretory protein trafficking from the Golgi apparatus to plasma membrane, ER stress, and fragmentation of the Golgi. Furthermore, less optineurin/myosin VI complex was formed in sporadic ALS patient tissues, implying that similar defects and disruption of optineurin/myosin VI trafficking is also present in sporadic ALS. In contrast to ALS-mutant optineurin, the optineurin-myosin VI complex formed normally in cells expressing an optineurin glaucoma-mutant, suggesting that optineurin/myosin VI dysfunction is a pathogenic mechanism specific to sporadic and familial ALS. The study presents a new information regarding the function of wildtype optineurin as an autophagy receptor. Optineurin/myosin VI associated with lysosomes in NSC-34 neuronal cells and in human primary motor neurons, and this association was necessary for the fusion of autophagosomes with lysosomes, because loss of the link between optineurin and myosin VI led to impaired clearance of autophagosomes in NSC-34 cells. Hence this study also provides clues as to the mechanism of how autophagy dysfunction occurs in sporadic and familial ALS, through the loss of optineurin/myosin VI cellular trafficking functions.

7.1.3 Novel mutation in *CCNF* induces ER stress and other features typical of ALS

The study presented in Chapter 5 describes novel cellular mechanisms induced by a newly discovered ALS-linked mutation in *CCNF*. Expression of mutant cyclin F altered its subcellular localization, promoted its recruitment into stress granules, and activated ER stress and apoptotic cell death in SH-SY5Y cells. Hence these results demonstrate that the pathogenic form of cyclin F induces cellular features typical of ALS, thus providing evidence

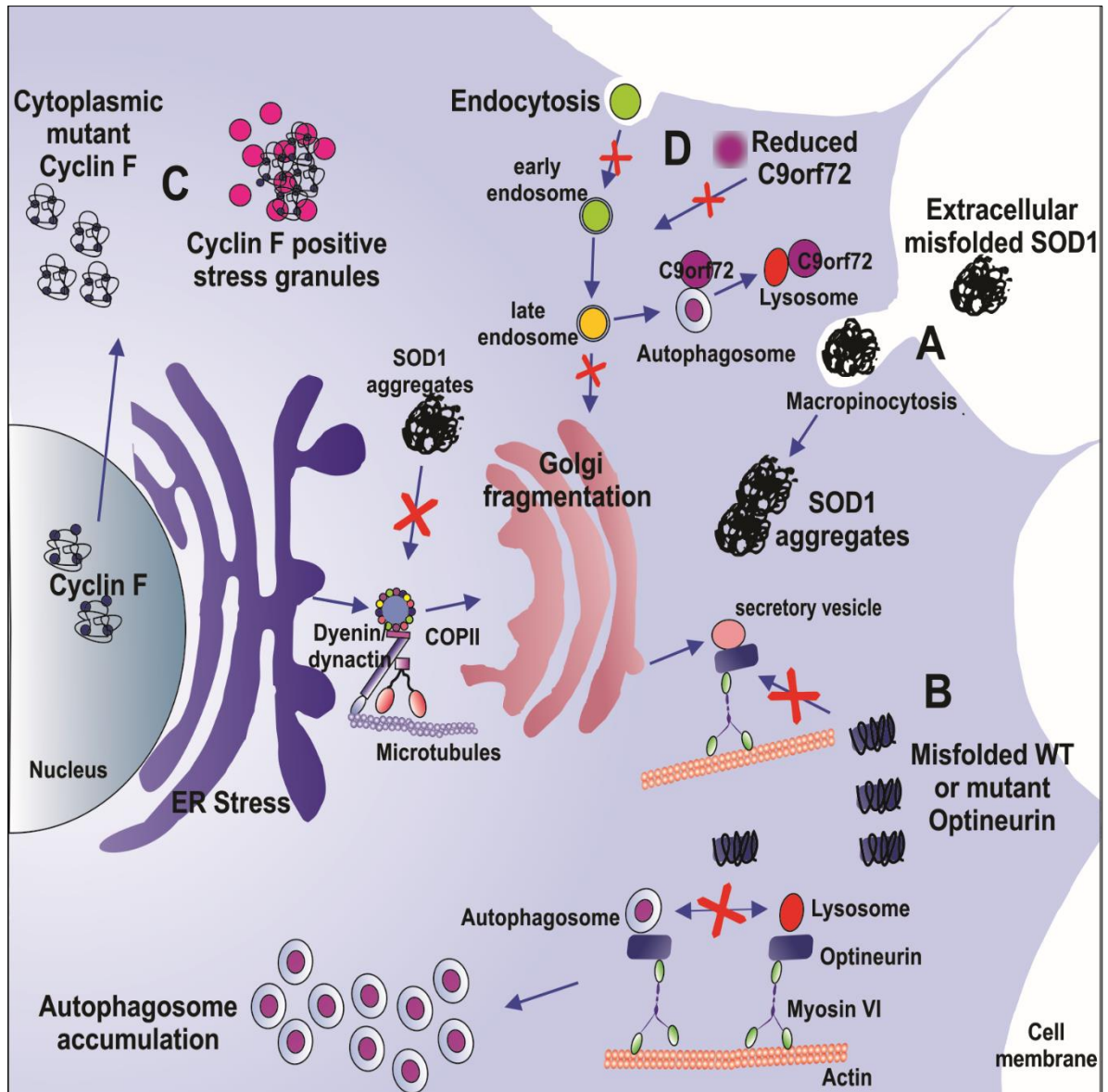


Figure 7.1 Representation of proposed ALS pathogenic mechanisms described in this thesis. **A.** Uptake of extracellular misfolded WT or mutant SOD1 via macropinocytosis forms intracellular SOD1 aggregates and inhibits ER-Golgi trafficking, resulting in ER stress and Golgi fragmentation. **B.** ALS mutations or misfolding of optineurin impede myosin VI-mediated transport of secretory vesicles, autophagosomes and lysosomes, resulting in accumulation of autophagosomes, ER stress and Golgi fragmentation. **C.** ALS-linked mutation in *CCNF* causes increased cytoplasmic accumulation and recruitment of cyclin F to stress granules, activation of ER stress, and apoptosis. **D.** C9orf72 mediates endocytosis and associates with autophagosomes and lysosomes. Reduced expression of C9orf72 inhibits autophagy and endocytosis and trafficking of endosomal substrates from the plasma membrane to the Golgi.

for mutant cyclin F in the pathogenesis of familial ALS. Induction of ER stress by mutant cyclin F raises the question of how ER stress is triggered, and whether this is linked to perturbation of ER-Golgi trafficking or impairment of ERAD similar to other mutant proteins linked to ALS. However future studies are required to examine in detail the mechanisms by which mutant cyclin F induces ER stress.

7.1.4 Role of C9orf72 in endosomal trafficking

The study presented in Chapter 6 formed part of a recent publication that provided the first experimental evidence to describe the normal function of C9orf72 and its role in cellular trafficking [346]. The results described in Chapter 6 demonstrate that C9orf72 regulates endocytosis in SH-SY5Y cells. Knockdown of C9orf72 using siRNA inhibited the transport of two endocytosis substrates, Shiga toxin and TrkB receptor, from the plasma membrane to the Golgi apparatus. Furthermore, C9orf72 co-localised with autophagosomes and co-migrated with lysosomes in live cells, consistent with a role for C9orf72 functions in endosomal trafficking. This study demonstrates that haploinsufficiency associated with the C9orf72 hexanucleotide repeat expansion in ALS may impair endosomal trafficking and lead to dysfunction of autophagy.

7.2 Prion-like propagation in ALS

Increasing evidence suggests that the spatiotemporal spread of pathology in ALS is a result of prion-like propagation of pathogenic proteins from cell-to-cell along the neuroanatomic axis. The published study presented in this thesis as Chapter 3, was the first report to demonstrate the uptake of wildtype as well as mutant SOD1 in neuronal cell cultures, suggesting a possible mechanism for cell-to-cell transmission in ALS. Furthermore, only one previous study [453] had demonstrated the uptake of mutant SOD1 from the culture medium. The results presented in Chapter 3 suggest that misfolded SOD1 released from affected neurons is taken up by neighbouring healthy neurons via macropinocytosis, and that this induces pathology in ALS. These findings also add strength to the hypothesis that aberrantly misfolded forms of WT SOD1 induce pathology in sporadic ALS, similar to mutant SOD1. Consistent with this notion, WT SOD1 has previously been shown to exhibit an enhanced propensity to aggregate *in vitro* and to mimic structural features of mutant SOD1 under cellular stress conditions, such as oxidative stress [521]. The oxidized and misfolded

forms of WT SOD1 isolated from sporadic ALS patient tissues have been shown to inhibit kinesin-based fast axonal transport in a manner similar to mutant SOD1 [4]. Denatured and misfolded forms of WT SOD1 also induced cell death similar to mutant SOD1 when administered exogenously [521, 522]. Moreover, mice overexpressing human WT SOD1 at levels similar to those present in mutant G93A SOD1 mice, developed a fatal ALS-like disease, implicating that SOD1 could be involved in the pathogenesis of ALS, even when it is not mutated [115].

After the study presented in Chapter 3 was published another study described similar findings to ours, demonstrating the uptake of misfolded, wildtype SOD1 aggregates from the medium via macropinocytosis [6]. This study also showed that transmission of misfolded SOD1 is mediated via cell-secreted vesicles that were identified as exosomes [6]. Both naked SOD1 aggregates by themselves or exosomes containing misfolded SOD1 were transmitted between cells, where they induced misfolding of native human SOD1 in the acceptor cells. This study further demonstrated the presence of misfolded, wildtype SOD1 in sporadic ALS patients [6], consistent with previous studies [3, 4]. In addition, this study estimated that misfolded SOD1 accounts for approximately 4% of total SOD1 in sporadic ALS patients [6].

Furthermore, another study by the same group has previously demonstrated that expression of cytoplasmic mutant FUS or TDP-43 induced misfolding of human WT SOD1 in cell culture studies [523], and misfolded SOD1 was detected in ALS patients with genetic mutations in FUS [523]. Together these data suggest that misfolded SOD1 may be a common pathogen causing the spread of pathology in all forms of ALS. Moreover, transmission of pathology by mutant SOD1 has also been recently demonstrated for the first time *in vivo*, in transgenic mice models [524]. Spinal cord homogenates from G93A SOD1 transgenic mice induced ALS phenotype when injected into genetically vulnerable G85R SOD1 mice [524]. Interestingly, spinal cord homogenates from this G85R SOD1 mice displaying an ALS phenotype, also transmitted the pathology when injected into newborn G85R mice. Hence these results strengthen the evidence for prion-like propagation of SOD1 as a valid mechanism leading to neurodegeneration in ALS. However the detection of misfolded SOD1 in sporadic ALS patients has also been dependent on the use of different misfolded-specific

SOD1 antibodies. While misfolded SOD1 in sporadic ALS tissues was detected by one group of misfolded SOD1 antibodies [6, 525], these findings were not replicated by using a misfolded SOD1 antibody developed in another study [526]. However it should be noted that the misfolded-specific antibodies used in these studies were not similar in that they were raised against different epitopes of SOD1, that were predicted to be exposed only upon misfolding. The SOD1 exposed dimer interface (SEDI) antibody was raised against residues 143–151 of the SOD1 sequence, which is normally sequestered in the SOD1 dimer interface and hence inaccessible in native SOD1 [527]. The SEDI antibody was shown to specifically recognize only the misfolded monomeric or non-native oligomeric forms of SOD1, in which the native dimer interface is exposed [527]. While this antibody did not show any immunoreactivity in a cohort of sporadic ALS patient tissues [526], disease specific epitope (DSE) SOD1 antibodies, 3H1 and 10C12, identified misfolded SOD1 in sporadic tissues as well as familial ALS cases without SOD1 mutations [6]. The 10C12 antibody was raised against SOD1 residues 145–151 similar to the SEDI antibody, although the epitope used to produce the antibody contained a cysteine residue at position 146 (Cys146) that had been replaced with cysteic acid [114, 528]. Substitution of this sulfonic acid derivative in the epitope was predicted to enable the detection of the sulfhydryl group of Cys146, which would be exposed by Cys57–Cys146 disulfide bond reduction in misfolded SOD1 [528]. The 3H1 antibody recognizes an epitope in the electrostatic loop of human SOD1 (between residues 125–142) that is normally buried in natively folded SOD1 [528]. Both 3H1 and 10C12 antibodies were demonstrated to specifically detect denatured, oxidized and disease-specific misfolded forms of SOD1 in previous studies [114, 528, 529]. The detection of misfolded SOD1 in sporadic ALS was also replicated in another study using antibodies generated against three different epitopes of misfolded SOD1, located at residues 24–39, 57–72 and 111–127 in the human SOD1 sequence [525]. All these three antibodies recognized misfolded WT SOD1 in the CSF of sporadic ALS patients. However the levels of misfolded SOD1 detected in the CSF was estimated to be at a much lower concentration than that sufficient to spread pathology [525]. Furthermore the C4F6 antibody, which was raised against the apo (metal-free) form of mutant G93A human SOD1, and was known to detect oxidized misfolded forms of WT SOD1, also detected misfolded WT SOD1 species in sporadic ALS patients [4]. Hence while misfolded SOD1 has been detected in sporadic ALS human tissues using the majority of misfolded-specific antibodies currently available, further studies are necessary to identify the specific misfolded form of WT SOD1 in sporadic ALS and its involvement in the spread of pathology in sporadic ALS.

However it is also important to consider that TDP-43 is a particularly important protein in ALS as it is a component of ubiquitinated inclusions in nearly 97% of sporadic ALS cases [5, 149, 530]. Furthermore both TDP-43 and FUS belong to a family of proteins with prion-like domains [338, 455], and both can seed protein aggregation *in vitro* [219, 457]. TDP-43 inclusions in a subset of ALS and FTD cases could be stained by thioflavin S, and hence these inclusions resembled an amyloid core, which could act as a seed for protein aggregation [211, 531]. It is therefore important to examine whether misfolded forms of TDP-43 can transmit misfolding when considering prion-like mechanisms and the link to neurodegeneration in ALS. The C-terminus of TDP-43 has a prion-like domain, and this is where majority of ALS causing mutations are located. These mutations directly accelerate TDP-43 misfolding [338]. In ALS, TDP-43 is abnormally cleaved, forming aggregate-prone C-terminal fragments that contain the prion-like domain [532-534]. Recombinant TDP-43 C-terminal fragments can also seed the formation of TDP-43 positive amyloid fibrils, *in vitro* and in cell cultures [219, 535]. An intriguing recent study [536] demonstrated that the addition of insoluble TDP-43 fractions, separated from the brains of ALS and FTD patients, seeded aggregation of overexpressed, wildtype TDP-43 in SH-SY5Y cells, implicating the prion-like mechanism in the aggregation of TDP-43 in ALS [536]. Interestingly, TDP-43 aggregates prepared from the brains of IBMPFD patients or from FTD patients bearing VCP mutations, did not seed intracellular TDP-43 aggregation [536]. This suggests that the prion-like propagation of misfolded TDP-43 is specific to ALS.

Furthermore, aggregated TDP-43 was also demonstrated to directly transmit from cell to cell *in vitro* [536]. Increased levels of TDP-43 were also detected in exosomal fractions prepared from cells treated with ALS patient brain fractions, indicating that TDP-43 transmission between cells may be mediated via exosomes [536]. However further studies are necessary to establish the mechanism of cellular release and uptake in the case of TDP-43. The evidence for propagation of TDP-43 aggregates also needs to be validated *in vivo*, to confirm these findings in a more physiologically relevant system. Interestingly, since TDP-43 is transported along the motor axons, it has been hypothesised that misfolded TDP-43 could spread along the motor network via axonal connections [430]. Consistent with this notion, the spread of other proteins linked to neurodegenerative diseases including tau [537, 538]

and α -synuclein [539, 540], are also thought to propagate via axonal pathways and neuronal networks.

FUS also harbors a predicted prion-like domain residues similar to TDP-43 in the N-terminus. Mutant FUS is capable of generating fibrillar amyloid seeds, which induce aggregation of wildtype FUS in-vitro [457]. However it remains to be examined whether FUS exhibits prion-like propagation, with cell to cell transmission seeding further aggregation, similar to TDP-43. Further studies are therefore necessary to examine this possibility. Table 7.1 summarises the available evidence for prion-like propagation of SOD1, TDP-43 and FUS in ALS.

Protein	Ability to Seed aggregation			Ability to spread cell to cell	Current mechanism of cellular release and uptake
	<i>In vitro</i>	Cell culture	Mice		
SOD1	Yes [541]	Yes [6, 214, 453]	Yes [524]	Yes [6, 214, 453]	Naked aggregates [214], exosomes [6], Uptake-Macropinocytosis [214, 453]
TDP-43	Yes [219]	Yes [536]	Not tested	Yes [536]	Possibly via exosome [536] Uptake-Not known
FUS	Yes [457]	Not tested	Not tested	Not tested	Not known.

Table 7.1 Summary of the evidence describing prion-like propagation in ALS

Hence in summary, a prion-like mechanism may be responsible for the spread of pathology in ALS, similar to that implicated in other neurodegenerative disorders. However the level of experimental evidence describing the prion-like activities of proteins implicated in ALS varies considerably [542] and further studies are needed to definitely establish such a mechanism in ALS. Misfolded mutant and wildtype SOD1 can spread from cell to cell and seed aggregation in the acceptor cell [6, 214]. However, future experiments examining the prion-like seeding ability of misfolded SOD1 isolated directly from brains/spinal cords of sporadic

and familial patients would further strengthen this evidence. Similarly, further studies are needed to define the mechanism of cellular release and uptake in the case of TDP-43 and FUS. It is important to understand why and how the misfolded proteins involved in ALS pathogenesis are secreted. It is necessary to examine in future studies whether secretion of these misfolded proteins is a cellular clearance mechanism to restore homeostasis during compromised proteostasis in ALS. Experiments studying such spread of pathology should also be extended using models other than cell culture or transgenic mice models overexpressing the candidate protein at a level higher than endogenous version. Use of patient derived iPSCs or fibroblast with endogenous levels of mutant SOD1, FUS or TDP-43 co-cultured with control cells could be used to study such cell-to-cell transmission and spread of pathology in future. Furthermore, it could be worthwhile to examine whether other pathogenic proteins associated with ALS including optineurin and *C9ORF72* RAN translated proteins could exhibit an ability to spread cell-to-cell.

Future studies should also be aimed towards defining the role of glial cells; microglia and astrocytes in prion-like spread of pathology in ALS. It is shown that expression of mutant SOD1 in both the motor neurons and glial cells is necessary to induce ALS in transgenic mice models, implicating that glial cells are involved in the degeneration of motor neurons [543]. Extracellular mutant SOD1 has previously been demonstrated to induce motor neuron toxicity indirectly by activating microglial cells [544, 545]. The activation of microglial cells by extracellular SOD1 is predicted to injure motor neurons by secretion of toxic mediators such as reactive oxygen species (ROS), proinflammatory cytokines and glutamate [546]. Furthermore protein aggregation and inclusions are also identified in astrocytes of ALS patients surrounding the motor neurons [547, 548], hence these cells could be a source of extracellular misfolded proteins which could then spread the pathology to motor neurons. Hence future studies are needed to describe the primary role of glial cells in the degeneration of motor neurons.

It is also worthwhile to identify the specific misfolded epitope of SOD1, TDP-43 and FUS, that forms the seed for prion-like propagation. This could facilitate future specific antibody-targeted therapies to arrest the spread of protein misfolding and seeding process. Targeted antibodies directed against misfolded α -synuclein can prevent both the uptake and

propagation of templated misfolding, in primary neuronal cultures and non-transgenic mice injected intrastrially with synthetic α -synuclein fibrils [549]. Administration of antibodies directed against different misfolded epitopes of SOD1 have also been beneficial in ameliorating disease in transgenic SOD1 mice models [550-552]. However more robust studies are needed to identify the optimal misfolded SOD1 epitope to be targeted. Since the spread of misfolded SOD1 has been demonstrated to be mediated by both exosomes and naked SOD1 aggregates, it would be essential to use antibodies that can recognise both these forms of extracellular SOD1 [6]. Similarly TDP-43 and FUS could be the next candidates for immunotherapeutic investigation. Clearly, the C-terminal regions of FUS and TDP-43 that harbour prion-like domains, are promising epitopes to be tested.

7.3 Cellular trafficking disruption links key pathogenic mechanisms in ALS.

Defects in cellular trafficking are increasingly implicated in ALS, consistent with disruption to proteostasis as an overarching mechanism of pathogenesis. However these pathways are not well defined and similarly, it remains unclear how these defects induce neurodegeneration. The studies presented in this thesis show that disruption of cellular trafficking pathways activates mechanisms linked to ALS pathogenesis, including ER stress, Golgi fragmentation and autophagy dysfunction and hence suggesting that cellular trafficking disruption could link several pathways associated with neurodegeneration in ALS.

7.3.1 Inhibition of ER-Golgi associated vesicular trafficking associates with ER stress and Golgi fragmentation in ALS.

The published study presented in this thesis (Chapter 3) showed that extracellular misfolded wildtype SOD1 and mutant SOD1 both inhibited transport from the ER to Golgi apparatus. This was the first study that described inhibition of ER-Golgi transport in ALS by pathogenic forms of SOD1. The study further showed that such inhibition of ER-Golgi transport was also accompanied with ER stress and Golgi fragmentation, suggesting a possible mechanism for induction of these pathologies in ALS.

The majority of ALS-linked proteins do not possess a classical secretory signal peptide and hence should not pass through the ER-Golgi compartments. Therefore it is unclear how

these proteins induce ER stress and Golgi fragmentation in ALS, without being physically present in these organelles. However, recent studies with mutant SOD1 provide possible insights as to how ER stress is activated and the Golgi is fragmented by cytoplasmic proteins in ALS [200] (Chapter 3). SOD1 is a cytoplasmic metalloprotein that is not normally present in the ER. Although some studies have described the presence of SOD1 in microsomal fractions, indicating possible ER localization [424, 425], other studies have argued against these findings [200, 423], suggesting that contamination of microsomal fractions by cytoplasmic SOD1 has led to erroneous results. Cytoplasmic mutant SOD1 has been shown to induce ER stress by interacting with Derlin-1, a key component of ERAD [423]. However the interaction between SOD1 and Derlin-1 was only detected after symptom onset in transgenic mutant SOD1 mice, indicating that other mechanisms of triggering ER stress must exist [426].

A major function of the ER and Golgi compartments is the transport of secretory proteins and lipids [269]. Hence it is possible that inhibition of ER-Golgi vesicular trafficking processes could activate ER stress and Golgi fragmentation by the accumulation of secretory proteins in these compartments [201, 202, 316, 395]. Consistent with this notion, in this study, mutant SOD1 induced ER stress and Golgi fragmentation as well as inhibited transport between ER and Golgi apparatus. In another study from our laboratory, inhibition of ER-Golgi trafficking occurred early, preceding ER stress, Golgi fragmentation, protein aggregation and apoptotic cell death, in cells expressing mutant SOD1 [200]. These data suggest that disruption to ER-Golgi trafficking is an upstream trigger of a pathogenic cascade of events [200]. Inhibition of ER-Golgi trafficking and ER stress are also observed in Parkinson's disease, in which mutant α synuclein induces ER stress by inhibiting ER-Golgi vesicular trafficking without affecting the ERAD pathway [553]. In addition, the published results presented in this thesis (Chapter 3), demonstrate that misfolded forms of wildtype SOD1 [3] also inhibits ER-Golgi trafficking, while activating ER stress and Golgi fragmentation [214]. Misfolded wildtype SOD1 is now widely implicated in pathogenesis of ALS. Misfolding of SOD1 can be induced by cytoplasmic FUS or TDP-43 [523] and is now identified in larger cohort of sporadic ALS patients [6]. Also overexpression of wildtype SOD1 has been to induce ALS phenotype in transgenic mice models [115], suggesting that misfolded wildtype SOD1 could be a central pathogenic species in ALS. Hence the identification of an ER-Golgi specific toxic mechanism exhibited by misfolded wildtype SOD1 has greatly implicated disruption to cellular trafficking in the pathogenesis of ALS.

These results imply that inhibition of ER-Golgi trafficking is a common mechanism triggering ER-Golgi pathologies in sporadic and SOD1-linked familial ALS cases. However further studies to define the relationship between trafficking inhibition and the subsequent events are required to define these pathways in more detail. Finding the exact mechanism of ER to Golgi trafficking inhibition by mutant and misfolded wildtype SOD1 is necessary. Future experiments should also examine ER-Golgi trafficking defects by misfolded or mutant SOD1 in models other than transient expression in cell culture. ER-Golgi trafficking inhibition and the subsequent cascade of events should be examined in primary motor neurons derived from transgenic SOD1 mice models and also directly in patient cells obtained from sporadic and familial ALS cases.

Optineurin in association with myosin VI mediates the trafficking of secretory proteins from the Golgi apparatus to the plasma membrane on actin filaments [351, 387, 389]. Prolonged inhibition of post-Golgi trafficking can also result in retention of secretory proteins in the Golgi and ER components, resulting in the activation of ER stress and fragmentation of the Golgi [202, 316, 395]. Similarly the results from this thesis (Chapter 4) demonstrate that ALS-linked mutations in optineurin induce ER stress and Golgi fragmentation as well as inhibit post-Golgi trafficking. Interestingly, loss of the optineurin/myosin VI complex was also observed in sporadic ALS patient spinal cord tissues. This raises the possibility that impairment of optineurin-mediated post Golgi trafficking is another possible trigger for ER stress and Golgi fragmentation in sporadic ALS. However, future studies are needed to examine whether the post Golgi trafficking defects induced by optineurin occur early, before ER and Golgi pathologies, are induced.

Chapter 6 of this thesis also demonstrates that reduced expression of C9orf72 impairs anterograde vesicular trafficking from the Golgi apparatus to plasma membrane and endocytosis. In another part of this published study, it was demonstrated that C9orf72 interacts and associates with Rab proteins, including Rab1. Together these data imply that C9orf72 could function in multiple Rab-mediated cellular trafficking processes. Rab1 regulates ER-Golgi trafficking by mediating the budding of COPII vesicles from the ER, as well as their delivery, tethering, and fusion to the Golgi [375, 406]. Rab1 further controls the

association and dissociation COPII vesicles from ER exit sites by interacting with COPII subunits: Sec23, Sec24 and Sec31 [405]. Depletion of Rab1 delays cargo sorting and exit from the ER, and expression of a dominant negative GTP-bound inactive mutant Rab1 (Rab1Q67L) alters COPII dynamics, suggesting the role of Rab1 in COPII mediated trafficking [405]. Rab1 is also essential for Golgi biogenesis and functioning [554]. The association of C9orf72 with Rab1 is mostly likely due to its predicted RabGEF function, and hence C9orf72 may therefore be essential for activation of Rab1. This raises the intriguing possibility that the reported reduced expression of C9orf72 in ALS patient tissues could block ER-Golgi vesicular trafficking by inhibiting Rab1 function. Hence future experimental studies are needed to examine this possibility further.

The results presented in Chapter 6 demonstrate that ER stress is induced as a result of expression of a novel ALS-associated cyclin F mutation in neuronal cells (Chapter 6). ER stress and Golgi fragmentation are also pathological features associated with mutant forms of FUS and TDP-43 [306, 307]. Furthermore, expression of poly(GA) RAN translated peptides from the *C9ORF72* repeat expansion induces ER stress in primary neurons [312]. Hence these studies provide further evidence that disruption to the ER-Golgi compartments is linked to the pathogenesis of ALS. However the mechanisms responsible for the induction of ER-Golgi pathologies by these proteins remains unknown. The findings presented in this thesis suggest that disruption of vesicular trafficking from the ER to Golgi triggers ER and Golgi abnormalities. Hence future studies examining whether cyclin F, TDP-43, FUS and the poly (GA) RAN translation peptides also inhibit ER-Golgi trafficking and thus induce ER stress by this mechanism, are therefore warranted. Aberrant cytoplasmic accumulation is observed with mutant forms of FUS, TDP-43, cyclin F and C9orf72 associated RAN peptides, thus raising the possibility that accumulation of these pathogenic proteins in the cytoplasm in ALS could interfere with cellular trafficking pathways. Hence future studies are needed to examine such a possibility.

7.3.2 Disruption of cellular trafficking impairs autophagy in ALS.

The highly dynamic process of autophagy is executed by an interplay between specific molecular motors and the cytoskeletal network [237]. Autophagy dysfunction is also increasingly implicated in ALS, and it has also become a target for therapeutic intervention in ALS in recent years [244, 247, 493]. However understanding the nature and cause of autophagy defects in ALS are essential to design effective and selective therapies based on

improving the autophagy process. The results described in Chapters 4 and 6 of this thesis demonstrate that disruption of cellular trafficking pathways impair the functioning of autophagy. Optineurin, in association with myosin VI, mediates the trafficking of autophagosomes on actin filaments. The results presented in chapter 4 also demonstrate a novel role for the optineurin/myosin VI complex in the trafficking of lysosomes, and mediating the fusion of autophagosomes and lysosomes. These data also demonstrate that the ALS associated mutations in optineurin disrupt its association with myosin VI, thus inhibiting fusion of the autophagosome with the lysosome. Furthermore, loss of optineurin/myosin VI complex is also observed in sporadic ALS patient spinal cord lysates. This finding raises the possibility that the optineurin-mediated defect in autophagosome/lysosome trafficking and fusion, may be responsible at least in part for the dysfunction of autophagy detected in sporadic ALS. Future studies examining the defects in optineurin-mediated trafficking and autophagy in sporadic patient cells, including fibroblasts or iPSC derived motor neurons, may add further evidence to this mechanism in sporadic ALS.

In addition, the evidence presented in Chapter 6 implies that C9orf72 has a role in the regulation of autophagy. Vesicular form of C9orf72 co-localised with autophagosomes and co-migrated with lysosomes, indicating that C9orf72 could mediate vesicular trafficking events during autophagy. Further studies from our group also demonstrated that reduced expression of C9orf72 dysregulated autophagy in SH-SY5Y cells [346]. Hence these results indicate that haploinsufficiency of C9orf72 in ALS patients may impede autophagy by disrupting Rab mediated vesicular trafficking. Indeed increased co-localisation of C9orf72 with Rab7 and Rab11 was observed in ALS patients bearing the C9orf72 repeat expansion in our study, suggesting possible disruption of endosomal trafficking in these patients [346]. Further experiments are necessary to examine the specific step in autophagy that is impaired by the loss of C9orf72 function. However, given the association of C9orf72 with multiple Rab proteins in our study, and its predicted broad acting RabGEF function, C9orf72 may function in many stages of autophagosome formation and clearance and may therefore have wide ranging activity in autophagy. Hence together these data imply that disruption of cellular trafficking is a possible trigger for autophagy dysfunction in ALS.

7.3.3 Cellular trafficking disruption relates to other pathogenic mechanism in ALS.

The evidence shown in this thesis therefore implicates disruption to cellular trafficking as a possible common trigger for induction of ER-Golgi pathologies and autophagy dysfunction in ALS. Hence restoring cellular trafficking therapeutically in ALS may have a beneficial effect in preventing these pathologies, and this possibility should be examined in future studies. In addition disruption of cellular trafficking pathways is also related to other pathogenic mechanism described in ALS including disruption to axonal transport, mitochondrial dysfunction and disruption of RNA homeostasis.

The ALS-causing mutations in FUS and TDP-43 as well as their pathological importance as components of the inclusions in sporadic ALS, has implicated disruption to RNA homeostasis in the pathogenesis of ALS [145]. Consistent with this notion, mutations in other hnRNPs have also been linked to familial ALS including hnRNPA1, hnRNPA2/B1, TAF15 and EWSR1 [338]. Both FUS and TDP-43 function in RNA metabolism by regulating transcription and splicing as well as RNA transport [142]. Transport of mRNA is essential for localised protein synthesis and for modulation of protein levels at distinct subcellular domains, particularly in the axon and dendrites [555]. TDP-43 and FUS are both transported along the axon and both are involved in axonal transport of mRNA granules. TDP-43 is involved in the bi-directional movement of RNA granules along microtubules, and this is impaired by the ALS associated-mutations in TDP-43 [347]. Similarly FUS mediates axonal transport of the mRNA encoding the actin-stabilizing protein Nd1-L [148]. However the exact mechanisms of how FUS and TDP-43 mediate the transport of mRNA is unknown. Further studies are required to examine whether FUS and TDP-43 associate with molecular motors or cytoskeletal proteins during their role in mRNA trafficking. The mechanism of how ALS mutations in TDP-43 affect axonal transport of mRNA granules also remains unknown. One possible explanation is that ALS mutant TDP-43 may lose its interaction with specific motor proteins responsible for axonal transport [347]. Hence the loss of mRNA trafficking in the motor neuronal axons could contribute to disrupted RNA homeostasis in ALS.

Mitochondrial dysfunction has also been implicated as a pathogenic mechanism in ALS [197, 429]. Mitochondrial dysfunction can be lethal in cells, especially for cells such as motor neurons that possess very long axons. The distribution of mitochondria in the axon is essential for local energy production and the regulation of calcium ion efflux [203]. Mitochondrial dynamics and function in neurons can be altered by impairment of axonal

trafficking [7, 325, 387, 426, 429]. While mitochondria are bi-directionally transported along the axon via microtubules, mediated by the dynein and kinesin families of motor proteins [203], myosin motor proteins also play a critical role in the docking of mitochondria on actin filaments along the axon, thus facilitating the local functioning of mitochondria [427]. Mutant SOD1 inhibits anterograde axonal transport of mitochondria, which results in depletion of the mitochondrial content of the axon [426]. Similarly, there is evidence that dynein/dynactin and kinesin motor proteins are also altered by being recruited to pathogenic inclusions in sporadic ALS [424-426], suggesting that there is deficient transport of axonal cargos including mitochondria in ALS. Inhibition of mitochondrial transport along axons may also be associated with the abnormal clustering of mitochondria in motor axons and the accumulation of mitochondria in the axon hillock of ALS patients [258, 426]. Hence disruption of axonal transport may impair the availability of mitochondria in the axon, resulting in the mitochondrial dysfunction of motor neurons. Since myosin VI is also involved in the axonal docking of mitochondria in the retrograde direction [427], further studies are needed to examine whether optineurin also associates with myosin VI during axonal transport and docking. Recently, mutations in two actin and microtubule cytoskeletal associated proteins were identified in familial ALS patients: profilin and TUBA4A, which adds further evidence for axonal transport defects in ALS [62, 83]. Apart from mitochondria, axonal transport also mediates transport of organelles such as autophagosome [556] and proteasome components [204] essential for maintaining local proteostasis in the axon. In addition transport of axonal proteins, neurotransmitters, lipids and synaptic vesicles also depend on axonal trafficking. Hence future studies are needed to examine whether defects in cellular trafficking system could impede the transport of axonal cargos and induce related ALS pathologies.

7.4 Concluding remarks

Over 140 years have passed, since ALS was first described in 1874. Since then, and particularly in the last 10 years, research has identified multiple genetic causes and pathogenic mechanisms associated with the disease. However the exact trigger for degeneration of motor neurons in ALS remains unclear, and developing an effective therapy for ALS would depend on identifying the upstream triggers. With nearly 384 cases of ALS diagnosed every day worldwide (International Alliance of ALS/MND Associations, www.alsmndalliance.org), there is a pressing need to find successful treatments for this

devastating disorder. The studies presented in this thesis provide novel insights into possible roles for defects in cellular trafficking pathways; ER-Golgi, Golgi-plasma membrane and autophagy in ALS. These pathways are integral to the maintenance of proteostasis and they are closely associated with other cellular mechanisms linked to neurodegeneration in ALS. Furthermore, the published study presented in this thesis provides novel insights into mechanisms underlying the cell-to-cell spread of pathology among motor neurons in ALS. These findings therefore increase our knowledge of the molecular and cellular mechanisms that trigger neurodegeneration in ALS. Future studies should now focus on validating these mechanisms *in vivo*, which may lead to the development of therapeutic strategies that target these mechanisms.

8. References

1. Hardiman, O., L.H. van den Berg, and M.C. Kiernan, *Clinical diagnosis and management of amyotrophic lateral sclerosis*. Nature Reviews Neurology, 2011. **7**(11): p. 639-649.
2. Renton, A.E., A. Chiò, and B.J. Traynor, *State of play in amyotrophic lateral sclerosis genetics*. Nature neuroscience, 2014. **17**(1): p. 17-23.
3. Richmond, J.E., W.S. Davis, and E.M. Jorgensen, *UNC-13 is required for synaptic vesicle fusion in C. elegans*. Nature neuroscience, 1999. **2**(11): p. 959-964.
4. Bosco, D.A., et al., *Wild-type and mutant SOD1 share an aberrant conformation and a common pathogenic pathway in ALS*. Nature neuroscience, 2010. **13**(11): p. 1396-1403.
5. Neumann, M., et al., *Ubiquitinated TDP-43 in frontotemporal lobar degeneration and amyotrophic lateral sclerosis*. Science, 2006. **314**(5796): p. 130-133.
6. Grad, L.I., et al., *Intercellular propagated misfolding of wild-type Cu/Zn superoxide dismutase occurs via exosome-dependent and-independent mechanisms*. Proceedings of the National Academy of Sciences, 2014. **111**(9): p. 3620-3625.
7. Soo, K.Y., M. Farg, and J.D. Atkin, *Molecular motor proteins and amyotrophic lateral sclerosis*. International journal of molecular sciences, 2011. **12**(12): p. 9057-9082.
8. Chio, A., et al., *Global epidemiology of amyotrophic lateral sclerosis: a systematic review of the published literature*. Neuroepidemiology, 2013. **41**(2): p. 118-130.
9. Chiò, A., et al., *Epidemiology of ALS in Italy A 10-year prospective population-based study*. Neurology, 2009. **72**(8): p. 725-731.
10. Donaghy, C., et al., *The epidemiology of motor neuron disease in Northern Ireland using capture-recapture methodology*. Amyotrophic Lateral Sclerosis, 2010. **11**(4): p. 374-378.
11. Huisman, M.H., et al., *Population based epidemiology of amyotrophic lateral sclerosis using capture–recapture methodology*. Journal of Neurology, Neurosurgery & Psychiatry, 2011. **82**(10): p. 1165-1170.
12. Pugliatti, M., et al., *Amyotrophic lateral sclerosis in Sardinia, insular Italy, 1995–2009*. Journal of neurology, 2013. **260**(2): p. 572-579.
13. Al-Chalabi, A. and O. Hardiman, *The epidemiology of ALS: a conspiracy of genes, environment and time*. Nature Reviews Neurology, 2013. **9**(11): p. 617-628.
14. Manjaly, Z.R., et al., *The sex ratio in amyotrophic lateral sclerosis: a population based study*. Amyotrophic Lateral Sclerosis, 2010. **11**(5): p. 439-442.
15. Johnston, C.A., et al., *Amyotrophic lateral sclerosis in an urban setting*. Journal of neurology, 2006. **253**(12): p. 1642-1643.
16. Cronin, S., O. Hardiman, and B.J. Traynor, *Ethnic variation in the incidence of ALS A systematic review*. Neurology, 2007. **68**(13): p. 1002-1007.
17. Mehta, P., et al., *Prevalence of amyotrophic lateral sclerosis-United States, 2010-2011*. MMWR Surveill Summ, 2014. **63**(suppl 7): p. 1-14.
18. Ravits, J.M. and A.R. La Spada, *ALS motor phenotype heterogeneity, focality, and spread Deconstructing motor neuron degeneration*. Neurology, 2009. **73**(10): p. 805-811.
19. Radunović, A., H. Mitsumoto, and P.N. Leigh, *Clinical care of patients with amyotrophic lateral sclerosis*. The Lancet Neurology, 2007. **6**(10): p. 913-925.
20. Brooks, B.R., et al., *El Escorial revisited: revised criteria for the diagnosis of amyotrophic lateral sclerosis*. Amyotrophic Lateral Sclerosis, 2000. **1**(5): p. 293-299.

21. Brooks, B.R., *El Escorial World Federation of Neurology criteria for the diagnosis of amyotrophic lateral sclerosis*. Journal of the neurological sciences, 1994. **124**: p. 96-107.
22. de Carvalho, M., et al., *Electrodiagnostic criteria for diagnosis of ALS*. Clinical neurophysiology, 2008. **119**(3): p. 497-503.
23. Nodera, H., Y. Izumi, and R. Kaji, [*New diagnostic criteria of ALS (Awaji criteria)*]. Brain and nerve= Shinkei kenkyu no shinpo, 2007. **59**(10): p. 1023-1029.
24. Costa, J., M. Swash, and M. de Carvalho, *Awaji criteria for the diagnosis of amyotrophic lateral sclerosis: a systematic review*. Archives of neurology, 2012. **69**(11): p. 1410-1416.
25. Phukan, J., N.P. Pender, and O. Hardiman, *Cognitive impairment in amyotrophic lateral sclerosis*. The Lancet Neurology, 2007. **6**(11): p. 994-1003.
26. Strong, M.J., et al., *Consensus criteria for the diagnosis of frontotemporal cognitive and behavioural syndromes in amyotrophic lateral sclerosis*. Amyotrophic Lateral Sclerosis, 2009. **10**(3): p. 131-146.
27. Strong, M.J., *The syndromes of frontotemporal dysfunction in amyotrophic lateral sclerosis*. Amyotrophic Lateral Sclerosis, 2008. **9**(6): p. 323-338.
28. Ringholz, G., et al., *Prevalence and patterns of cognitive impairment in sporadic ALS*. Neurology, 2005. **65**(4): p. 586-590.
29. Ferrari, R., et al., *FTD and ALS: a tale of two diseases*. Current Alzheimer Research, 2011. **8**(3): p. 273.
30. Cardarelli, R., A. Kertesz, and J.A. Knebl, *Frontotemporal dementia: a review for primary care physicians*. Am Fam Physician, 2010. **82**(11): p. 1372-7.
31. Lomen-Hoerth, C., T. Anderson, and B. Miller, *The overlap of amyotrophic lateral sclerosis and frontotemporal dementia*. Neurology, 2002. **59**(7): p. 1077-1079.
32. DeJesus-Hernandez, M., et al., *Expanded GGGGCC Hexanucleotide Repeat in Noncoding Region of C9ORF72 Causes Chromosome 9p-Linked FTD and ALS*. Neuron, 2011. **72**(2): p. 245-256.
33. Sreedharan, J., et al., *TDP-43 mutations in familial and sporadic amyotrophic lateral sclerosis*. Science, 2008. **319**(5870): p. 1668-1672.
34. Vance, C., et al., *Mutations in FUS, an RNA processing protein, cause familial amyotrophic lateral sclerosis type 6*. Science, 2009. **323**(5918): p. 1208-1211.
35. Armon, C., *Smoking may be considered an established risk factor for sporadic ALS*. Neurology, 2009. **73**(20): p. 1693-1698.
36. Das, K., C. Nag, and M. Ghosh, *Familial, environmental, and occupational risk factors in development of amyotrophic lateral sclerosis*. North American journal of medical sciences, 2012. **4**(8): p. 350.
37. Alonso, A., et al., *Association of smoking with amyotrophic lateral sclerosis risk and survival in men and women: a prospective study*. BMC neurology, 2010. **10**(1): p. 6.
38. Weisskopf, M., et al., *Prospective study of cigarette smoking and amyotrophic lateral sclerosis*. American journal of epidemiology, 2004. **160**(1): p. 26-33.
39. Scarmeas, N., et al., *Premorbid weight, body mass, and varsity athletics in ALS*. Neurology, 2002. **59**(5): p. 773-775.
40. Besson, H., et al., *Validation of the historical adulthood physical activity questionnaire (HAPAQ) against objective measurements of physical activity*. Int J Behav Nutr Phys Act, 2010. **7**: p. 54.
41. Huisman, M.H., et al., *Lifetime physical activity and the risk of amyotrophic lateral sclerosis*. Journal of Neurology, Neurosurgery & Psychiatry, 2013. **84**(9): p. 976-981.
42. Chiò, A., et al., *Severely increased risk of amyotrophic lateral sclerosis among Italian professional football players*. Brain, 2005. **128**(3): p. 472-476.

43. Vega, A. and E. Bell, *α -Amino- β -methylaminopropionic acid, a new amino acid from seeds of *Cycas circinalis**. *Phytochemistry*, 1967. **6**(5): p. 759-762.
44. Kurland, L.K. and D.W. Mulder, *Epidemiologic Investigations of Amyotrophic Lateral Sclerosis 1. Preliminary Report on Geographic Distribution, with Special Reference to the Mariana Islands, Including Clinical and Pathologic Observations*. *Neurology*, 1954. **4**(5): p. 355-355.
45. Banack, S.A. and P.A. Cox, *Biomagnification of cycad neurotoxins in flying foxes Implications for ALS-PDC in Guam*. *Neurology*, 2003. **61**(3): p. 387-389.
46. Cox, P.A., S.A. Banack, and S.J. Murch, *Biomagnification of cyanobacterial neurotoxins and neurodegenerative disease among the Chamorro people of Guam*. *Proceedings of the National Academy of Sciences*, 2003. **100**(23): p. 13380-13383.
47. Murch, S., et al., *Occurrence of β -methylamino-L-alanine (BMAA) in ALS/PDC patients from Guam*. *Acta Neurologica Scandinavica*, 2004. **110**(4): p. 267-269.
48. Pablo, J., et al., *Cyanobacterial neurotoxin BMAA in ALS and Alzheimer's disease*. *Acta Neurologica Scandinavica*, 2009. **120**(4): p. 216-225.
49. Montine, T.J., et al., *Lack of β -methylamino-L-alanine in brain from controls, AD, or Chamorros with PDC*. *Neurology*, 2005. **65**(5): p. 768-769.
50. Snyder, L., et al., *Lack of cerebral BMAA in human cerebral cortex*. *Neurology*, 2009. **72**(15): p. 1360-1361.
51. Cox, P.A., et al., *Diverse taxa of cyanobacteria produce β -N-methylamino-L-alanine, a neurotoxic amino acid*. *Proceedings of the National Academy of Sciences of the United States of America*, 2005. **102**(14): p. 5074-5078.
52. Dunlop, R.A., et al., *The non-protein amino acid BMAA is misincorporated into human proteins in place of L-serine causing protein misfolding and aggregation*. *PloS one*, 2013. **8**(9): p. e75376.
53. Rosen, D.R., et al., *Mutations in Cu/Zn superoxide dismutase gene are associated with familial amyotrophic lateral sclerosis*. *Nature*, 1993. **362**(6415): p. 59-62.
54. Kwiatkowski, T.J., et al., *Mutations in the FUS/TLS gene on chromosome 16 cause familial amyotrophic lateral sclerosis*. *Science*, 2009. **323**(5918): p. 1205-1208.
55. DeJesus-Hernandez, M., et al., *Expanded GGGGCC Hexanucleotide Repeat in Noncoding Region of C9ORF72 Causes Chromosome 9p-Linked FTD and ALS*. *Neuron*, 2011. **72**(2): p. 245-256.
56. Renton, A.E., et al., *A Hexanucleotide Repeat Expansion in C9ORF72 Is the Cause of Chromosome 9p21-Linked ALS-FTD*. *Neuron*, 2011. **72**(2): p. 257-268.
57. Chen, S., et al., *Genetics of amyotrophic lateral sclerosis: an update*. *Mol Neurodegener*, 2013. **8**(1): p. 28.
58. Watts, G.D., et al., *Inclusion body myopathy associated with Paget disease of bone and frontotemporal dementia is caused by mutant valosin-containing protein*. *Nature genetics*, 2004. **36**(4): p. 377-381.
59. Johnson, J.O., et al., *Exome Sequencing Reveals VCP mutations as a Cause of Familial ALS*. *Neuron*, 2010. **68**(5): p. 857-864.
60. Maruyama, H., et al., *Mutations of optineurin in amyotrophic lateral sclerosis*. *Nature*, 2010. **465**(7295): p. 223-226.
61. Deng, H.-X., et al., *Mutations in UBQLN2 cause dominant X-linked juvenile and adult-onset ALS and ALS/dementia*. *Nature*, 2011. **477**(7363): p. 211-215.
62. Wu, C.-H., et al., *Mutations in the profilin 1 gene cause familial amyotrophic lateral sclerosis*. *Nature*, 2012.
63. Fecto, F., et al., *SQSTM1 mutations in familial and sporadic amyotrophic lateral sclerosis*. *Archives of Neurology*, 2011. **68**(11): p. 1440-1446.

64. Laurin, N., et al., *Recurrent Mutation of the Gene Encoding sequestosome 1 (SQSTM1/p62) in Paget Disease of Bone*. The American Journal of Human Genetics, 2002. **70**(6): p. 1582-1588.
65. Farrer, M.J., et al., *DCTN1 mutations in Perry syndrome*. Nature genetics, 2009. **41**(2): p. 163-165.
66. Puls, I., et al., *Distal spinal and bulbar muscular atrophy caused by dynactin mutation*. Annals of neurology, 2005. **57**(5): p. 687-694.
67. Münch, C., et al., *Point mutations of the p150 subunit of dynactin (DCTN1) gene in ALS*. Neurology, 2004. **63**(4): p. 724-726.
68. Yang, Y., et al., *The gene encoding alsin, a protein with three guanine-nucleotide exchange factor domains, is mutated in a form of recessive amyotrophic lateral sclerosis*. Nature genetics, 2001. **29**(2): p. 160-165.
69. Panzeri, C., et al., *The first ALS2 missense mutation associated with JPLS reveals new aspects of alsin biological function*. Brain, 2006. **129**(7): p. 1710-1719.
70. Devon, R., et al., *The first nonsense mutation in alsin results in a homogeneous phenotype of infantile-onset ascending spastic paralysis with bulbar involvement in two siblings*. Clinical genetics, 2003. **64**(3): p. 210-215.
71. Skibinski, G., et al., *Mutations in the endosomal ESCRTIII-complex subunit CHMP2B in frontotemporal dementia*. Nature genetics, 2005. **37**(8): p. 806-808.
72. Nishimura, A.L., et al., *A mutation in the vesicle-trafficking protein VAPB causes late-onset spinal muscular atrophy and amyotrophic lateral sclerosis*. The American Journal of Human Genetics, 2004. **75**(5): p. 822-831.
73. Landers, J., et al., *New VAPB deletion variant and exclusion of VAPB mutations in familial ALS*. Neurology, 2008. **70**(14): p. 1179-1185.
74. van Es, M.A., et al., *Angiogenin variants in Parkinson disease and amyotrophic lateral sclerosis*. Annals of neurology, 2011. **70**(6): p. 964-973.
75. Greenway, M., et al., *A novel candidate region for ALS on chromosome 14q11. 2*. Neurology, 2004. **63**(10): p. 1936-1938.
76. Orlacchio, A., et al., *SPATACSIN mutations cause autosomal recessive juvenile amyotrophic lateral sclerosis*. Brain, 2010. **133**(2): p. 591-598.
77. Stevanin, G., et al., *Mutations in SPG11, encoding spatacsin, are a major cause of spastic paraplegia with thin corpus callosum*. Nature genetics, 2007. **39**(3): p. 366-372.
78. Figlewicz, D.A., et al., *Variants of the heavy neurofilament subunit are associated with the development of amyotrophic lateral sclerosis*. Human molecular genetics, 1994. **3**(10): p. 1757-1761.
79. Van Damme, P., et al., *Expanded ATXN2 CAG repeat size in ALS identifies genetic overlap between ALS and SCA2*. Neurology, 2011. **76**(24): p. 2066-2072.
80. Lee, T., et al., *Ataxin-2 intermediate-length polyglutamine expansions in European ALS patients*. Human molecular genetics, 2011. **20**(9): p. 1697-1700.
81. Chow, C.Y., et al., *Deleterious Variants of FIG4, a Phosphoinositide Phosphatase, in Patients with ALS*. The American Journal of Human Genetics, 2009. **84**(1): p. 85-88.
82. Chow, C.Y., et al., *Mutation of FIG4 causes neurodegeneration in the pale tremor mouse and patients with CMT4J*. Nature, 2007. **448**(7149): p. 68-72.
83. Smith, B.N., et al., *Exome-wide Rare Variant Analysis Identifies TUBA4A Mutations Associated with Familial ALS*. Neuron, 2014. **84**(2): p. 324-331.
84. Corrado, L., et al., *A novel peripherin gene PRPH mutation identified in one sporadic amyotrophic lateral sclerosis patient*. Neurobiology of aging, 2011. **32**(3): p. 552. e1-552. e6.

85. Leung, C.L., et al., *A pathogenic peripherin gene mutation in a patient with amyotrophic lateral sclerosis*. Brain pathology, 2004. **14**(3): p. 290-296.
86. Gros-Louis, F., et al., *A frameshift deletion in peripherin gene associated with amyotrophic lateral sclerosis*. Journal of Biological Chemistry, 2004. **279**(44): p. 45951-45956.
87. Goldberg, A.F. and R.S. Molday, *Defective subunit assembly underlies a digenic form of retinitis pigmentosa linked to mutations in peripherin/rds and rom-1*. Proceedings of the National Academy of Sciences, 1996. **93**(24): p. 13726-13730.
88. Felbor, U., H. Schilling, and B.H. Weber, *Adult vitelliform macular dystrophy is frequently associated with mutations in the peripherin/RDS gene*. Human mutation, 1997. **10**(4): p. 301-309.
89. Simpson, C.L., et al., *Variants of the elongator protein 3 (ELP3) gene are associated with motor neuron degeneration*. Human molecular genetics, 2009. **18**(3): p. 472-481.
90. Chen, Y.-Z., et al., *DNA/RNA helicase gene mutations in a form of juvenile amyotrophic lateral sclerosis (ALS4)*. The American Journal of Human Genetics, 2004. **74**(6): p. 1128-1135.
91. Al-Saif, A., F. Al-Mohanna, and S. Bohlega, *A mutation in sigma-1 receptor causes juvenile amyotrophic lateral sclerosis*. Annals of neurology, 2011. **70**(6): p. 913-919.
92. Kim, H.J., et al., *Prion-like domain mutations in hnRNPs cause multisystem proteinopathy and ALS*. Nature, 2013. **495**(7442): p. 467.
93. Ticozzi, N., et al., *Paraoxonase gene mutations in amyotrophic lateral sclerosis*. Annals of neurology, 2010. **68**(1): p. 102-107.
94. Sleegers, K., et al., *Progranulin genetic variability contributes to amyotrophic lateral sclerosis*. Neurology, 2008. **71**(4): p. 253-259.
95. Cruts, M., et al., *Null mutations in progranulin cause ubiquitin-positive frontotemporal dementia linked to chromosome 17q21*. Nature, 2006. **442**(7105): p. 920-924.
96. Baker, M., et al., *Mutations in progranulin cause tau-negative frontotemporal dementia linked to chromosome 17*. Nature, 2006. **442**(7105): p. 916-919.
97. Mitchell, J., et al., *Familial amyotrophic lateral sclerosis is associated with a mutation in D-amino acid oxidase*. Proceedings of the National Academy of Sciences, 2010. **107**(16): p. 7556-7561.
98. Bannwarth, S., et al., *A mitochondrial origin for frontotemporal dementia and amyotrophic lateral sclerosis through CHCHD10 involvement*. Brain, 2014. **137**(8): p. 2329-2345.
99. Johnson, J.O., et al., *Mutations in the Matrin 3 gene cause familial amyotrophic lateral sclerosis*. Nature neuroscience, 2014.
100. Ticozzi, N., et al., *Mutational analysis reveals the FUS homolog TAF15 as a candidate gene for familial amyotrophic lateral sclerosis*. American Journal of Medical Genetics Part B: Neuropsychiatric Genetics, 2011. **156**(3): p. 285-290.
101. Couthouis, J., et al., *A yeast functional screen predicts new candidate ALS disease genes*. Proceedings of the National Academy of Sciences, 2011. **108**(52): p. 20881-20890.
102. Chesi, A., et al., *Exome sequencing to identify de novo mutations in sporadic ALS trios*. Nature neuroscience, 2013. **16**(7): p. 851-855.
103. Cirulli, E.T., et al., *Exome sequencing in amyotrophic lateral sclerosis identifies risk genes and pathways*. Science, 2015: p. aaa3650.
104. Arnesano, F., et al., *The unusually stable quaternary structure of human Cu, Zn-superoxide dismutase 1 is controlled by both metal occupancy and disulfide status*. Journal of Biological Chemistry, 2004. **279**(46): p. 47998-48003.
105. Valentine, J.S., P.A. Doucette, and S. Zittin Potter, *Copper-zinc superoxide dismutase and amyotrophic lateral sclerosis*. Annu. Rev. Biochem., 2005. **74**: p. 563-593.

106. Lill, C.M., et al., *Keeping up with genetic discoveries in amyotrophic lateral sclerosis: the ALSod and ALSGene databases*. Amyotrophic Lateral Sclerosis, 2011. **12**(4): p. 238-249.
107. Cleveland, D.W. and J.D. Rothstein, *From Charcot to Lou Gehrig: deciphering selective motor neuron death in ALS*. Nature Reviews Neuroscience, 2001. **2**(11): p. 806-819.
108. Reaume, A.G., et al., *Motor neurons in Cu/Zn superoxide dismutase-deficient mice develop normally but exhibit enhanced cell death after axonal injury*. Nature genetics, 1996. **13**(1): p. 43-47.
109. Cudkovicz, M., et al., *Epidemiology of mutations in superoxide dismutase in amyotrophic lateral sclerosis*. Annals of neurology, 1997. **41**(2): p. 210-221.
110. Ogasawara, M., et al., *Mild ALS in Japan associated with novel SOD mutation*. Nature genetics, 1993. **5**(4): p. 323-324.
111. Turner, B.J., et al., *Impaired extracellular secretion of mutant superoxide dismutase 1 associates with neurotoxicity in familial amyotrophic lateral sclerosis*. The Journal of neuroscience, 2005. **25**(1): p. 108-117.
112. Johnston, J.A., et al., *Formation of high molecular weight complexes of mutant Cu, Zn-superoxide dismutase in a mouse model for familial amyotrophic lateral sclerosis*. Proceedings of the National Academy of Sciences, 2000. **97**(23): p. 12571-12576.
113. Turner, B.J. and K. Talbot, *Transgenics, toxicity and therapeutics in rodent models of mutant SOD1-mediated familial ALS*. Progress in neurobiology, 2008. **85**(1): p. 94-134.
114. Grad, L.I., et al., *Intermolecular transmission of superoxide dismutase 1 misfolding in living cells*. Proceedings of the National Academy of Sciences, 2011. **108**(39): p. 16398-16403.
115. Graffmo, K.S., et al., *Expression of wild-type human superoxide dismutase-1 in mice causes amyotrophic lateral sclerosis*. Human molecular genetics, 2012: p. dds399.
116. Robberecht, W. and T. Philips, *The changing scene of amyotrophic lateral sclerosis*. Nature Reviews Neuroscience, 2013. **14**(4): p. 248-264.
117. Dols-Icardo, O., et al., *Characterization of the repeat expansion size in C9orf72 in amyotrophic lateral sclerosis and frontotemporal dementia*. Human molecular genetics, 2014. **23**(3): p. 749-754.
118. Gómez-Tortosa, E., et al., *C9ORF72 hexanucleotide expansions of 20–22 repeats are associated with frontotemporal deterioration*. Neurology, 2013. **80**(4): p. 366-370.
119. Orr, H.T. and H.Y. Zoghbi, *Trinucleotide repeat disorders*. Annu. Rev. Neurosci., 2007. **30**: p. 575-621.
120. Todd, P.K. and H.L. Paulson, *RNA-mediated neurodegeneration in repeat expansion disorders*. Annals of neurology, 2010. **67**(3): p. 291-300.
121. Donnelly, C.J., et al., *RNA toxicity from the ALS/FTD C9ORF72 expansion is mitigated by antisense intervention*. Neuron, 2013. **80**(2): p. 415-428.
122. Gendron, T.F., et al., *Antisense transcripts of the expanded C9ORF72 hexanucleotide repeat form nuclear RNA foci and undergo repeat-associated non-ATG translation in c9FTD/ALS*. Acta neuropathologica, 2013. **126**(6): p. 829-844.
123. Lagier-Tourenne, C., et al., *Targeted degradation of sense and antisense C9orf72 RNA foci as therapy for ALS and frontotemporal degeneration*. Proceedings of the National Academy of Sciences, 2013. **110**(47): p. E4530-E4539.
124. Lee, Y.-B., et al., *Hexanucleotide repeats in ALS/FTD form length-dependent RNA foci, sequester RNA binding proteins, and are neurotoxic*. Cell reports, 2013. **5**(5): p. 1178-1186.
125. Mizielińska, S., et al., *C9orf72 frontotemporal lobar degeneration is characterised by frequent neuronal sense and antisense RNA foci*. Acta neuropathologica, 2013. **126**(6): p. 845-857.

126. Almeida, S., et al., *Modeling key pathological features of frontotemporal dementia with C9ORF72 repeat expansion in iPSC-derived human neurons*. Acta neuropathologica, 2013. **126**(3): p. 385-399.
127. Mori, K., et al., *hnRNP A3 binds to GGGGCC repeats and is a constituent of p62-positive/TDP43-negative inclusions in the hippocampus of patients with C9orf72 mutations*. Acta neuropathologica, 2013. **125**(3): p. 413-423.
128. Xu, Z., et al., *Expanded GGGGCC repeat RNA associated with amyotrophic lateral sclerosis and frontotemporal dementia causes neurodegeneration*. Proceedings of the National Academy of Sciences, 2013. **110**(19): p. 7778-7783.
129. Ash, P.E., et al., *Unconventional translation of C9ORF72 GGGGCC expansion generates insoluble polypeptides specific to c9FTD/ALS*. Neuron, 2013. **77**(4): p. 639-646.
130. Mori, K., et al., *The C9orf72 GGGGCC repeat is translated into aggregating dipeptide-repeat proteins in FTL/ALS*. Science, 2013. **339**(6125): p. 1335-1338.
131. Cleary, J.D. and L.P. Ranum, *Repeat-associated non-ATG (RAN) translation in neurological disease*. Human molecular genetics, 2013: p. ddt371.
132. Gendron, T.F., et al., *Mechanisms of toxicity in C9FTLD/ALS*. Acta neuropathologica, 2014. **127**(3): p. 359-376.
133. Zu, T., et al., *RAN proteins and RNA foci from antisense transcripts in C9ORF72 ALS and frontotemporal dementia*. Proceedings of the National Academy of Sciences, 2013. **110**(51): p. E4968-E4977.
134. Mackenzie, I.R., et al., *Dipeptide repeat protein pathology in C9ORF72 mutation cases: clinico-pathological correlations*. Acta neuropathologica, 2013. **126**(6): p. 859-879.
135. Mann, D., et al., *Dipeptide repeat proteins are present in the p62 positive inclusions in patients with frontotemporal lobar degeneration and motor neurone disease associated with expansions in C9ORF72*. Acta Neuropathol Commun, 2013. **1**(1): p. 68.
136. Mori, K., et al., *Bidirectional transcripts of the expanded C9orf72 hexanucleotide repeat are translated into aggregating dipeptide repeat proteins*. Acta neuropathologica, 2013. **126**(6): p. 881-893.
137. Mizielińska, S., et al., *C9orf72 repeat expansions cause neurodegeneration in Drosophila through arginine-rich proteins*. Science, 2014. **345**(6201): p. 1192-1194.
138. Belzil, V.V., et al., *Reduced C9orf72 gene expression in c9FTD/ALS is caused by histone trimethylation, an epigenetic event detectable in blood*. Acta neuropathologica, 2013. **126**(6): p. 895-905.
139. Ciura, S., et al., *Loss of function of C9orf72 causes motor deficits in a zebrafish model of Amyotrophic Lateral Sclerosis*. Annals of neurology, 2013. **74**(2): p. 180-187.
140. Fratta, P., et al., *Homozygosity for the C9orf72 GGGGCC repeat expansion in frontotemporal dementia*. Acta neuropathologica, 2013. **126**(3): p. 401-409.
141. Donnelly, C.J., et al., *RNA Toxicity from the ALS/FTD C9ORF72 Expansion Is Mitigated by Antisense Intervention*. Neuron, 2013. **80**(2): p. 415-428.
142. Lagier-Tourenne, C., M. Polymenidou, and D.W. Cleveland, *TDP-43 and FUS/TLS: emerging roles in RNA processing and neurodegeneration*. Human molecular genetics, 2010. **19**(R1): p. R46-R64.
143. Mackenzie, I.R., R. Rademakers, and M. Neumann, *TDP-43 and FUS in amyotrophic lateral sclerosis and frontotemporal dementia*. The Lancet Neurology, 2010. **9**(10): p. 995-1007.
144. Van Deerlin, V.M., et al., *TARDBP mutations in amyotrophic lateral sclerosis with TDP-43 neuropathology: a genetic and histopathological analysis*. The Lancet Neurology, 2008. **7**(5): p. 409-416.

145. Ling, S.-C., M. Polymenidou, and D.W. Cleveland, *Converging mechanisms in ALS and FTD: disrupted RNA and protein homeostasis*. Neuron, 2013. **79**(3): p. 416-438.
146. Zinszner, H., et al., *TLS (FUS) binds RNA in vivo and engages in nucleo-cytoplasmic shuttling*. Journal of Cell Science, 1997. **110**(15): p. 1741-1750.
147. Ayala, Y.M., et al., *Structural determinants of the cellular localization and shuttling of TDP-43*. Journal of cell science, 2008. **121**(22): p. 3778-3785.
148. Fujii, R. and T. Takumi, *TLS facilitates transport of mRNA encoding an actin-stabilizing protein to dendritic spines*. Journal of cell science, 2005. **118**(24): p. 5755-5765.
149. Arai, T., et al., *TDP-43 is a component of ubiquitin-positive tau-negative inclusions in frontotemporal lobar degeneration and amyotrophic lateral sclerosis*. Biochemical and biophysical research communications, 2006. **351**(3): p. 602-611.
150. Neumann, M., et al., *A new subtype of frontotemporal lobar degeneration with FUS pathology*. Brain, 2009. **132**(11): p. 2922-2931.
151. Mackenzie, I.R., et al., *Pathological TDP-43 distinguishes sporadic amyotrophic lateral sclerosis from amyotrophic lateral sclerosis with SOD1 mutations*. Annals of neurology, 2007. **61**(5): p. 427-434.
152. Tan, C.-F., et al., *TDP-43 immunoreactivity in neuronal inclusions in familial amyotrophic lateral sclerosis with or without SOD1 gene mutation*. Acta neuropathologica, 2007. **113**(5): p. 535-542.
153. Pamphlett, R., et al., *TDP-43 neuropathology is similar in sporadic amyotrophic lateral sclerosis with or without TDP-43 mutations*. Neuropathology and applied neurobiology, 2009. **35**(2): p. 222-225.
154. Lashley, T., et al., *A comparative clinical, pathological, biochemical and genetic study of fused in sarcoma proteinopathies*. Brain, 2011. **134**(9): p. 2548-2564.
155. Davidson, Y.S., et al., *Nuclear carrier and RNA-binding proteins in frontotemporal lobar degeneration associated with fused in sarcoma (FUS) pathological changes*. Neuropathology and applied neurobiology, 2013. **39**(2): p. 157-165.
156. Yamazaki, T., et al., *FUS-SMN protein interactions link the motor neuron diseases ALS and SMA*. Cell reports, 2012. **2**(4): p. 799-806.
157. Kabashi, E., et al., *FUS and TARDBP but not SOD1 interact in genetic models of amyotrophic lateral sclerosis*. PLoS genetics, 2011. **7**(8): p. e1002214.
158. Gurney, M.E., et al., *Motor neuron degeneration in mice that express a human Cu, Zn superoxide dismutase mutation*. Science, 1994. **264**(5166): p. 1772-1775.
159. McGoldrick, P., et al., *Rodent models of amyotrophic lateral sclerosis*. Biochimica et Biophysica Acta (BBA)-Molecular Basis of Disease, 2013. **1832**(9): p. 1421-1436.
160. Bergemalm, D., et al., *Overloading of stable and exclusion of unstable human superoxide dismutase-1 variants in mitochondria of murine amyotrophic lateral sclerosis models*. The Journal of neuroscience, 2006. **26**(16): p. 4147-4154.
161. Moser, J.M., P. Bigini, and T. Schmitt-John, *The wobbler mouse, an ALS animal model*. Molecular Genetics and Genomics, 2013. **288**(5-6): p. 207-229.
162. Kraemer, B.C., et al., *Loss of murine TDP-43 disrupts motor function and plays an essential role in embryogenesis*. Acta neuropathologica, 2010. **119**(4): p. 409-419.
163. Hicks, G.G., et al., *Fus deficiency in mice results in defective B-lymphocyte development and activation, high levels of chromosomal instability and perinatal death*. Nature genetics, 2000. **24**(2): p. 175-179.
164. Kuroda, M., et al., *Male sterility and enhanced radiation sensitivity in TLS-/- mice*. The EMBO journal, 2000. **19**(3): p. 453-462.

165. Arnold, E.S., et al., *ALS-linked TDP-43 mutations produce aberrant RNA splicing and adult-onset motor neuron disease without aggregation or loss of nuclear TDP-43*. Proceedings of the National Academy of Sciences, 2013. **110**(8): p. E736-E745.
166. Stallings, N.R., et al., *Progressive motor weakness in transgenic mice expressing human TDP-43*. Neurobiology of disease, 2010. **40**(2): p. 404-414.
167. Wegorzewska, I., et al., *TDP-43 mutant transgenic mice develop features of ALS and frontotemporal lobar degeneration*. Proceedings of the National Academy of Sciences, 2009. **106**(44): p. 18809-18814.
168. Wils, H., et al., *TDP-43 transgenic mice develop spastic paralysis and neuronal inclusions characteristic of ALS and frontotemporal lobar degeneration*. Proceedings of the National Academy of Sciences, 2010. **107**(8): p. 3858-3863.
169. Zhou, H., et al., *Transgenic rat model of neurodegeneration caused by mutation in the TDP gene*. PLoS genetics, 2010. **6**(3): p. e1000887.
170. Huang, C., et al., *Mutant TDP-43 in motor neurons promotes the onset and progression of ALS in rats*. The Journal of clinical investigation, 2012. **122**(1): p. 107.
171. Huang, C., et al., *FUS transgenic rats develop the phenotypes of amyotrophic lateral sclerosis and frontotemporal lobar degeneration*. PLoS genetics, 2011. **7**(3): p. e1002011.
172. Mitchell, J.C., et al., *Overexpression of human wild-type FUS causes progressive motor neuron degeneration in an age-and dose-dependent fashion*. Acta neuropathologica, 2013. **125**(2): p. 273-288.
173. Johnson, B.S., et al., *TDP-43 is intrinsically aggregation-prone, and amyotrophic lateral sclerosis-linked mutations accelerate aggregation and increase toxicity*. Journal of Biological Chemistry, 2009. **284**(30): p. 20329-20339.
174. Laird, A.S., et al., *Progranulin is neurotrophic in vivo and protects against a mutant TDP-43 induced axonopathy*. PLoS One, 2010. **5**(10): p. e13368.
175. Liachko, N.F., C.R. Guthrie, and B.C. Kraemer, *Phosphorylation promotes neurotoxicity in a Caenorhabditis elegans model of TDP-43 proteinopathy*. The Journal of Neuroscience, 2010. **30**(48): p. 16208-16219.
176. Vaccaro, A., et al., *Methylene blue protects against TDP-43 and FUS neuronal toxicity in C. elegans and D. rerio*. PLoS One, 2012. **7**(7): p. e42117.
177. Armstrong, G.A. and P. Drapeau, *Loss and gain of FUS function impair neuromuscular synaptic transmission in a genetic model of ALS*. Human molecular genetics, 2013. **22**(21): p. 4282-4292.
178. McGown, A., et al., *Early interneuron dysfunction in ALS: insights from a mutant sod1 zebrafish model*. Annals of neurology, 2013. **73**(2): p. 246-258.
179. Bosco, D.A., et al., *Mutant FUS proteins that cause amyotrophic lateral sclerosis incorporate into stress granules*. Human molecular genetics, 2010. **19**(21): p. 4160-4175.
180. Watson, M.R., et al., *A drosophila model for amyotrophic lateral sclerosis reveals motor neuron damage by human SOD1*. Journal of Biological Chemistry, 2008. **283**(36): p. 24972-24981.
181. Sakowski, S.A., et al., *Neuromuscular effects of G93A-SOD1 expression in zebrafish*. Molecular neurodegeneration, 2012. **7**(1): p. 1-15.
182. Robinson, R., *A yeast model for understanding ALS: fast, cheap, and easy to control*. PLoS biology, 2011. **9**(4): p. e1001053.
183. Babin, P.J., C. Goizet, and D. Raldúa, *Zebrafish models of human motor neuron diseases: Advantages and limitations*. Progress in neurobiology, 2014. **118**: p. 36-58.

184. Wen, X., et al., *Antisense Proline-Arginine RAN Dipeptides Linked to C9ORF72-ALS/FTD Form Toxic Nuclear Aggregates that Initiate In Vitro and In Vivo Neuronal Death*. *Neuron*, 2014. **84**(6): p. 1213-1225.
185. Stepto, A., et al., *Modelling C9ORF72 hexanucleotide repeat expansion in amyotrophic lateral sclerosis and frontotemporal dementia*. *Acta neuropathologica*, 2014. **127**(3): p. 377-389.
186. Takahashi, K., et al., *Induction of pluripotent stem cells from adult human fibroblasts by defined factors*. *cell*, 2007. **131**(5): p. 861-872.
187. Lagarkova, M.A., et al., *Induction of pluripotency in human endothelial cells resets epigenetic profile on genome scale*. *cell cycle*, 2010. **9**(5): p. 937-946.
188. Dimos, J.T., et al., *Induced pluripotent stem cells generated from patients with ALS can be differentiated into motor neurons*. *science*, 2008. **321**(5893): p. 1218-1221.
189. Niemitz, E., *iPSC models of ALS*. *Nature genetics*, 2014. **46**(6): p. 532-532.
190. Burkhardt, M.F., et al., *A cellular model for sporadic ALS using patient-derived induced pluripotent stem cells*. *Molecular and Cellular Neuroscience*, 2013. **56**: p. 355-364.
191. Chen, H., et al., *Modeling ALS with iPSCs reveals that mutant SOD1 misregulates neurofilament balance in motor neurons*. *Cell Stem Cell*, 2014. **14**(6): p. 796-809.
192. Kiskinis, E., et al., *Pathways disrupted in human ALS motor neurons identified through genetic correction of mutant SOD1*. *Cell Stem Cell*, 2014. **14**(6): p. 781-795.
193. Zhang, Z., et al., *Downregulation of microRNA-9 in iPSC-derived neurons of FTD/ALS patients with TDP-43 mutations*. *PloS one*, 2013. **8**(10): p. e76055.
194. Bilican, B., et al., *Mutant induced pluripotent stem cell lines recapitulate aspects of TDP-43 proteinopathies and reveal cell-specific vulnerability*. *Proceedings of the National Academy of Sciences*, 2012. **109**(15): p. 5803-5808.
195. Sareen, D., et al., *Targeting RNA foci in iPSC-derived motor neurons from ALS patients with a C9ORF72 repeat expansion*. *Science translational medicine*, 2013. **5**(208): p. 208ra149-208ra149.
196. Egawa, N., et al., *Drug screening for ALS using patient-specific induced pluripotent stem cells*. *Science translational medicine*, 2012. **4**(145): p. 145ra104-145ra104.
197. Cozzolino, M. and M.T. Carri, *Mitochondrial dysfunction in ALS*. *Progress in neurobiology*, 2012. **97**(2): p. 54-66.
198. Blokhuis, A.M., et al., *Protein aggregation in amyotrophic lateral sclerosis*. *Acta neuropathologica*, 2013. **125**(6): p. 777-794.
199. Walker, A.K. and J.D. Atkin, *Stress signaling from the endoplasmic reticulum: A central player in the pathogenesis of amyotrophic lateral sclerosis*. *IUBMB life*, 2011. **63**(9): p. 754-763.
200. Atkin, J.D., et al., *Mutant SOD1 inhibits ER-Golgi transport in amyotrophic lateral sclerosis*. *Journal of neurochemistry*, 2014. **129**(1): p. 190-204.
201. Preston, A., et al., *Reduced endoplasmic reticulum (ER)-to-Golgi protein trafficking contributes to ER stress in lipotoxic mouse beta cells by promoting protein overload*. *Diabetologia*, 2009. **52**(11): p. 2369-2373.
202. van Es, M.A., et al., *Genome-wide association study identifies 19p13. 3 (UNC13A) and 9p21. 2 as susceptibility loci for sporadic amyotrophic lateral sclerosis*. *Nature genetics*, 2009. **41**(10): p. 1083-1087.
203. Hollenbeck, P.J. and W.M. Saxton, *The axonal transport of mitochondria*. *Journal of cell science*, 2005. **118**(23): p. 5411-5419.
204. Otero, M.G., et al., *Fast axonal transport of the proteasome complex depends on membrane interaction and molecular motor function*. *Journal of cell science*, 2014. **127**(7): p. 1537-1549.

205. Ravikumar, B., et al., *Dynein mutations impair autophagic clearance of aggregate-prone proteins*. Nature genetics, 2005. **37**(7): p. 771-776.
206. Tumbarello, D.A., et al., *Autophagy receptors link myosin VI to autophagosomes to mediate Tom1-dependent autophagosome maturation and fusion with the lysosome*. Nature cell biology, 2012. **14**(10): p. 1024-1035.
207. Williamson, T.L. and D.W. Cleveland, *Slowing of axonal transport is a very early event in the toxicity of ALS-linked SOD1 mutants to motor neurons*. Nature neuroscience, 1999. **2**(1): p. 50-56.
208. LaMonte, B.H., et al., *Disruption of dynein/dynactin inhibits axonal transport in motor neurons causing late-onset progressive degeneration*. Neuron, 2002. **34**(5): p. 715-727.
209. Ross, C.A. and M.A. Poirier, *Protein aggregation and neurodegenerative disease*. 2004.
210. Wood, J., T. Beaujeux, and P. Shaw, *Protein aggregation in motor neurone disorders*. Neuropathology and applied neurobiology, 2003. **29**(6): p. 529-545.
211. Robinson, J.L., et al., *TDP-43 skeins show properties of amyloid in a subset of ALS cases*. Acta neuropathologica, 2013. **125**(1): p. 121-131.
212. Mizusawa, H., *Hyaline and Skein-like Inclusions in Amyotrophic Lateral Sclerosis*. Neuropathology, 1993. **13**(3): p. 201-208.
213. Polymenidou, M. and D.W. Cleveland, *Prion-like spread of protein aggregates in neurodegeneration*. The Journal of experimental medicine, 2012. **209**(5): p. 889-893.
214. Sundaramoorthy, V., et al., *Extracellular wildtype and mutant SOD1 induces ER-Golgi pathology characteristic of amyotrophic lateral sclerosis in neuronal cells*. Cellular and Molecular Life Sciences, 2013. **70**(21): p. 4181-4195.
215. Barmada, S.J., et al., *Cytoplasmic mislocalization of TDP-43 is toxic to neurons and enhanced by a mutation associated with familial amyotrophic lateral sclerosis*. The Journal of Neuroscience, 2010. **30**(2): p. 639-649.
216. Rotunno, M.S. and D.A. Bosco, *An emerging role for misfolded wild-type SOD1 in sporadic ALS pathogenesis*. Frontiers in cellular neuroscience, 2013. **7**.
217. Brotherton, T.E., et al., *Localization of a toxic form of superoxide dismutase 1 protein to pathologically affected tissues in familial ALS*. Proceedings of the National Academy of Sciences, 2012. **109**(14): p. 5505-5510.
218. Deng, H.X., et al., *FUS-immunoreactive inclusions are a common feature in sporadic and non-SOD1 familial amyotrophic lateral sclerosis*. Annals of neurology, 2010. **67**(6): p. 739-748.
219. Furukawa, Y., et al., *A seeding reaction recapitulates intracellular formation of Sarkosyl-insoluble transactivation response element (TAR) DNA-binding protein-43 inclusions*. Journal of Biological Chemistry, 2011. **286**(21): p. 18664-18672.
220. Deng, H.X., et al., *Differential involvement of optineurin in amyotrophic lateral sclerosis with or without SOD1 mutations*. Archives of neurology, 2011. **68**(8): p. 1057.
221. Osawa, T., et al., *Optineurin in neurodegenerative diseases*. Neuropathology, 2011. **31**(6): p. 569-574.
222. Mori, F., et al., *Optineurin immunoreactivity in neuronal nuclear inclusions of polyglutamine diseases (Huntington's, DRPLA, SCA2, SCA3) and intranuclear inclusion body disease*. Acta neuropathologica, 2012. **123**(5): p. 747-749.
223. Klionsky, D.J., *Autophagy: from phenomenology to molecular understanding in less than a decade*. Nature reviews Molecular cell biology, 2007. **8**(11): p. 931-937.
224. Mizushima, N., *Autophagy: process and function*. Genes & development, 2007. **21**(22): p. 2861-2873.
225. Chen, S., et al., *Autophagy dysregulation in amyotrophic lateral sclerosis*. Brain pathology, 2012. **22**(1): p. 110-116.

226. Boya, P., F. Reggiori, and P. Codogno, *Emerging regulation and functions of autophagy*. Nature cell biology, 2013. **15**(7): p. 713-720.
227. Yang, Z. and D.J. Klionsky, *Eaten alive: a history of macroautophagy*. Nature cell biology, 2010. **12**(9): p. 814-822.
228. Levine, B. and G. Kroemer, *Autophagy in the pathogenesis of disease*. Cell, 2008. **132**(1): p. 27-42.
229. Nixon, R.A., *The role of autophagy in neurodegenerative disease*. Nature medicine, 2013. **19**(8): p. 983-997.
230. Kroemer, G., G. Mariño, and B. Levine, *Autophagy and the integrated stress response*. Molecular cell, 2010. **40**(2): p. 280-293.
231. Yao, T.-P., *The role of ubiquitin in autophagy-dependent protein aggregate processing*. Genes & cancer, 2010. **1**(7): p. 779-786.
232. Xie, Z. and D.J. Klionsky, *Autophagosome formation: core machinery and adaptations*. Nature cell biology, 2007. **9**(10): p. 1102-1109.
233. Jin, M. and D.J. Klionsky, *The core molecular machinery of autophagosome formation*, in *Autophagy and Cancer*. 2013, Springer. p. 25-45.
234. Shang, L. and X. Wang, *AMPK and mTOR coordinate the regulation of Ulk1 and mammalian autophagy initiation*. Autophagy, 2011. **7**(8): p. 924-926.
235. Nakatogawa, H., *Two ubiquitin-like conjugation systems that mediate membrane formation during autophagy*. Essays in biochemistry, 2013. **55**(1): p. 39-50.
236. Jahreiss, L., F.M. Menzies, and D.C. Rubinsztein, *The itinerary of autophagosomes: from peripheral formation to kiss-and-run fusion with lysosomes*. Traffic, 2008. **9**(4): p. 574-587.
237. Monastyrska, I., et al., *Multiple roles of the cytoskeleton in autophagy*. Biological Reviews, 2009. **84**(3): p. 431-448.
238. Ao, X., L. Zou, and Y. Wu, *Regulation of autophagy by the Rab GTPase network*. Cell Death & Differentiation, 2014. **21**(3): p. 348-358.
239. Sasaki, S., *Autophagy in spinal cord motor neurons in sporadic amyotrophic lateral sclerosis*. Journal of Neuropathology and Experimental Neurology, 2011. **70**(5): p. 349-359.
240. Zhang, X., et al., *Rapamycin treatment augments motor neuron degeneration in SOD1(G93A) mouse model of amyotrophic lateral sclerosis*. Autophagy, 2011. **7**(4): p. 412-25.
241. Otomo, A., et al., *Defective relocalization of ALS2/alsin missense mutants to Rac1-induced macropinosomes accounts for loss of their cellular function and leads to disturbed amphisome formation*. FEBS Letters, 2011. **585**(5): p. 730-736.
242. Wang, I.-F., et al., *Autophagy activators rescue and alleviate pathogenesis of a mouse model with proteinopathies of the TAR DNA-binding protein 43*. Proceedings of the National Academy of Sciences, 2012. **109**(37): p. 15024-15029.
243. Zhang, X., et al., *MTOR-independent, autophagic enhancer trehalose prolongs motor neuron survival and ameliorates the autophagic flux defect in a mouse model of amyotrophic lateral sclerosis*. Autophagy, 2014. **10**(4): p. 22-36.
244. Castillo, K., et al., *Trehalose delays the progression of amyotrophic lateral sclerosis by enhancing autophagy in motoneurons*. Autophagy, 2013. **9**(9): p. 1308-1320.
245. Barmada, S.J., et al., *Autophagy induction enhances TDP43 turnover and survival in neuronal ALS models*. Nature chemical biology, 2014. **10**(8): p. 677-685.
246. Zhang, X., et al., *Rapamycin treatment augments motor neuron degeneration in SOD1G93A mouse model of amyotrophic lateral sclerosis*. Autophagy, 2011. **7**(4): p. 412-425.
247. Group, U.-L.S., *Lithium in patients with amyotrophic lateral sclerosis (LiCALS): a phase 3 multicentre, randomised, double-blind, placebo-controlled trial*. Lancet neurology, 2013. **12**(4): p. 339.

248. Shaw, P. and P. Ince, *Glutamate, excitotoxicity and amyotrophic lateral sclerosis*. Journal of neurology, 1997. **244**(2): p. S3-S14.
249. Kruman, I.I., et al., *ALS-linked Cu/Zn-SOD mutation increases vulnerability of motor neurons to excitotoxicity by a mechanism involving increased oxidative stress and perturbed calcium homeostasis*. Experimental neurology, 1999. **160**(1): p. 28-39.
250. Boill  e, S., C. Vande Velde, and D.W. Cleveland, *ALS: a disease of motor neurons and their nonneuronal neighbors*. Neuron, 2006. **52**(1): p. 39-59.
251. Rothstein, J.D., et al., *Selective loss of glial glutamate transporter GLT-1 in amyotrophic lateral sclerosis*. Annals of neurology, 1995. **38**(1): p. 73-84.
252. Guo, H., et al., *Increased expression of the glial glutamate transporter EAAT2 modulates excitotoxicity and delays the onset but not the outcome of ALS in mice*. Human molecular genetics, 2003. **12**(19): p. 2519-2532.
253. Spreux-Varoquaux, O., et al., *Glutamate levels in cerebrospinal fluid in amyotrophic lateral sclerosis: a reappraisal using a new HPLC method with coulometric detection in a large cohort of patients*. Journal of the neurological sciences, 2002. **193**(2): p. 73-78.
254. Yin, H.Z., D.T. Tang, and J.H. Weiss, *Intrathecal infusion of a Ca²⁺-permeable AMPA channel blocker slows loss of both motor neurons and of the astrocyte glutamate transporter, GLT-1 in a mutant SOD1 rat model of ALS*. Experimental neurology, 2007. **207**(2): p. 177-185.
255. Saxena, S., et al., *Neuroprotection through excitability and mTOR required in ALS motoneurons to delay disease and extend survival*. Neuron, 2013. **80**(1): p. 80-96.
256. Stranahan, A.M. and M.P. Mattson, *Recruiting adaptive cellular stress responses for successful brain ageing*. Nature Reviews Neuroscience, 2012. **13**(3): p. 209-216.
257. Mattson, M.P., *Excitation Bolsters Motor Neurons in ALS Mice*. Neuron, 2013. **80**(1): p. 1-3.
258. Sasaki, S. and M. Iwata, *Ultrastructural study of synapses in the anterior horn neurons of patients with amyotrophic lateral sclerosis*. Neuroscience letters, 1996. **204**(1): p. 53-56.
259. HIRANO, A., et al., *Fine structural study of neurofibrillary changes in a family with amyotrophic lateral sclerosis*. Journal of Neuropathology & Experimental Neurology, 1984. **43**(5): p. 471-480.
260. Siklos, L., et al., *Ultrastructural evidence for altered calcium in motor nerve terminals in amyotrophic lateral sclerosis*. Annals of neurology, 1996. **39**(2): p. 203-216.
261. Liu, J., et al., *Toxicity of familial ALS-linked SOD1 mutants from selective recruitment to spinal mitochondria*. Neuron, 2004. **43**(1): p. 5-17.
262. Sotelo-Silveira, J.R., et al., *Axonal mitochondrial clusters containing mutant SOD1 in transgenic models of ALS*. Antioxidants & redox signaling, 2009. **11**(7): p. 1535-1545.
263. Higgins, C.M., C. Jung, and Z. Xu, *ALS-associated mutant SOD1G93A causes mitochondrial vacuolation by expansion of the intermembrane space and by involvement of SOD1 aggregation and peroxisomes*. BMC neuroscience, 2003. **4**(1): p. 16.
264. Menzies, F.M., et al., *Mitochondrial dysfunction in a cell culture model of familial amyotrophic lateral sclerosis*. Brain, 2002. **125**(7): p. 1522-1533.
265. Carr  , M.T., et al., *Expression of a Cu, Zn superoxide dismutase typical of familial amyotrophic lateral sclerosis induces mitochondrial alteration and increase of cytosolic Ca²⁺ concentration in transfected neuroblastoma SH-SY5Y cells*. FEBS letters, 1997. **414**(2): p. 365-368.
266. Gu  gan, C., et al., *Recruitment of the mitochondrial-dependent apoptotic pathway in amyotrophic lateral sclerosis*. The Journal of Neuroscience, 2001. **21**(17): p. 6569-6576.

267. Martin, L.J., *Neuronal death in amyotrophic lateral sclerosis is apoptosis: possible contribution of a programmed cell death mechanism*. Journal of Neuropathology & Experimental Neurology, 1999. **58**(5): p. 459-471.
268. Soo, K.Y., et al., *Bim links ER stress and apoptosis in cells expressing mutant SOD1 associated with amyotrophic lateral sclerosis*. PloS one, 2012. **7**(4): p. e35413.
269. Braakman, I. and N.J. Bulleid, *Protein folding and modification in the mammalian endoplasmic reticulum*. Annual review of biochemistry, 2011. **80**: p. 71-99.
270. Ruddock, L.W. and M. Molinari, *N-glycan processing in ER quality control*. Journal of cell science, 2006. **119**(21): p. 4373-4380.
271. Ellgaard, L. and L.W. Ruddock, *The human protein disulphide isomerase family: substrate interactions and functional properties*. EMBO reports, 2005. **6**(1): p. 28-32.
272. Smith, M.J. and G. Koch, *Multiple zones in the sequence of calreticulin (CRP55, calregulin, HACBP), a major calcium binding ER/SR protein*. The EMBO journal, 1989. **8**(12): p. 3581.
273. Werstuck, G.H., et al., *Homocysteine-induced endoplasmic reticulum stress causes dysregulation of the cholesterol and triglyceride biosynthetic pathways*. The Journal of clinical investigation, 2001. **107**(10): p. 1263-1273.
274. Fu, S., et al., *Aberrant lipid metabolism disrupts calcium homeostasis causing liver endoplasmic reticulum stress in obesity*. Nature, 2011. **473**(7348): p. 528-531.
275. Rutkowski, D.T. and R.J. Kaufman, *A trip to the ER: coping with stress*. Trends in cell biology, 2004. **14**(1): p. 20-28.
276. Hetz, C. and B. Mollereau, *Disturbance of endoplasmic reticulum proteostasis in neurodegenerative diseases*. Nature Reviews Neuroscience, 2014. **15**(4): p. 233-249.
277. Høyer-Hansen, M. and M. Jäättelä, *Connecting endoplasmic reticulum stress to autophagy by unfolded protein response and calcium*. Cell Death & Differentiation, 2007. **14**(9): p. 1576-1582.
278. Hetz, C., et al., *The unfolded protein response: integrating stress signals through the stress sensor IRE1 α* . Physiological Reviews, 2011. **91**(4): p. 1219-1243.
279. Lee, A.-H., N.N. Iwakoshi, and L.H. Glimcher, *XBP-1 regulates a subset of endoplasmic reticulum resident chaperone genes in the unfolded protein response*. Molecular and cellular biology, 2003. **23**(21): p. 7448-7459.
280. Shaffer, A., et al., *XBP1, downstream of Blimp-1, expands the secretory apparatus and other organelles, and increases protein synthesis in plasma cell differentiation*. Immunity, 2004. **21**(1): p. 81-93.
281. Sriburi, R., et al., *Coordinate regulation of phospholipid biosynthesis and secretory pathway gene expression in XBP-1 (S)-induced endoplasmic reticulum biogenesis*. Journal of Biological Chemistry, 2007. **282**(10): p. 7024-7034.
282. Sriburi, R., et al., *XBP1 a link between the unfolded protein response, lipid biosynthesis, and biogenesis of the endoplasmic reticulum*. The Journal of cell biology, 2004. **167**(1): p. 35-41.
283. Nishitoh, H., et al., *ASK1 is essential for endoplasmic reticulum stress-induced neuronal cell death triggered by expanded polyglutamine repeats*. Genes & development, 2002. **16**(11): p. 1345-1355.
284. Nishitoh, H., et al., *ASK1 is essential for JNK/SAPK activation by TRAF2*. Molecular cell, 1998. **2**(3): p. 389-395.
285. Hollien, J. and J.S. Weissman, *Decay of endoplasmic reticulum-localized mRNAs during the unfolded protein response*. Science, 2006. **313**(5783): p. 104-107.
286. Shen, J., et al., *ER stress regulation of ATF6 localization by dissociation of BiP/GRP78 binding and unmasking of Golgi localization signals*. Developmental cell, 2002. **3**(1): p. 99-111.

287. Shoulders, M.D., et al., *Stress-independent activation of XBP1s and/or ATF6 reveals three functionally diverse ER proteostasis environments*. Cell reports, 2013. **3**(4): p. 1279-1292.
288. Rao, R., et al., *Coupling endoplasmic reticulum stress to the cell-death program: a novel HSP90-independent role for the small chaperone protein p23*. Cell Death & Differentiation, 2005. **13**(3): p. 415-425.
289. Scorrano, L., et al., *BAX and BAK regulation of endoplasmic reticulum Ca²⁺: a control point for apoptosis*. Science, 2003. **300**(5616): p. 135-139.
290. Lin, J.H., et al., *IRE1 signaling affects cell fate during the unfolded protein response*. science, 2007. **318**(5852): p. 944-949.
291. Walter, P. and D. Ron, *The unfolded protein response: from stress pathway to homeostatic regulation*. Science, 2011. **334**(6059): p. 1081-1086.
292. Puthalakath, H., et al., *ER stress triggers apoptosis by activating BH3-only protein Bim*. Cell, 2007. **129**(7): p. 1337-1349.
293. Galehdar, Z., et al., *Neuronal apoptosis induced by endoplasmic reticulum stress is regulated by ATF4-CHOP-mediated induction of the Bcl-2 homology 3-only member PUMA*. The Journal of Neuroscience, 2010. **30**(50): p. 16938-16948.
294. Marciniak, S.J., et al., *CHOP induces death by promoting protein synthesis and oxidation in the stressed endoplasmic reticulum*. Genes & development, 2004. **18**(24): p. 3066-3077.
295. Atkin, J.D., et al., *Induction of the unfolded protein response in familial amyotrophic lateral sclerosis and association of protein-disulfide isomerase with superoxide dismutase 1*. Journal of Biological Chemistry, 2006. **281**(40): p. 30152-30165.
296. Saxena, S., E. Cabuy, and P. Caroni, *A role for motoneuron subtype-selective ER stress in disease manifestations of FALS mice*. Nature neuroscience, 2009. **12**(5): p. 627-636.
297. Ferraiuolo, L., et al., *Microarray analysis of the cellular pathways involved in the adaptation to and progression of motor neuron injury in the SOD1 G93A mouse model of familial ALS*. The Journal of Neuroscience, 2007. **27**(34): p. 9201-9219.
298. Vaccaro, A., et al., *Pharmacological reduction of ER stress protects against TDP-43 neuronal toxicity< i> in vivo</i>*. Neurobiology of disease, 2013. **55**: p. 64-75.
299. Jiang, H.-Q., et al., *Guanabenz delays the onset of disease symptoms, extends lifespan, improves motor performance and attenuates motor neuron loss in the SOD1 G93A mouse model of amyotrophic lateral sclerosis*. Neuroscience, 2014.
300. Atkin, J.D., et al., *Endoplasmic reticulum stress and induction of the unfolded protein response in human sporadic amyotrophic lateral sclerosis*. Neurobiology of disease, 2008. **30**(3): p. 400-407.
301. Ilieva, E.V., et al., *Oxidative and endoplasmic reticulum stress interplay in sporadic amyotrophic lateral sclerosis*. Brain, 2007. **130**(12): p. 3111-3123.
302. Walker, A.K., et al., *Protein disulphide isomerase protects against protein aggregation and is S-nitrosylated in amyotrophic lateral sclerosis*. Brain, 2010. **133**(1): p. 105-116.
303. Oyanagi, K., et al., *Spinal anterior horn cells in sporadic amyotrophic lateral sclerosis show ribosomal detachment from, and cisternal distention of the rough endoplasmic reticulum*. Neuropathology and applied neurobiology, 2008. **34**(6): p. 650-658.
304. Sasaki, S., *Endoplasmic reticulum stress in motor neurons of the spinal cord in sporadic amyotrophic lateral sclerosis*. Journal of Neuropathology & Experimental Neurology, 2010. **69**(4): p. 346-355.
305. Oh, Y.K., et al., *Superoxide dismutase 1 mutants related to amyotrophic lateral sclerosis induce endoplasmic stress in neuro2a cells*. Journal of neurochemistry, 2008. **104**(4): p. 993-1005.

306. Farg, M.A., et al., *Mutant FUS induces endoplasmic reticulum stress in amyotrophic lateral sclerosis and interacts with protein disulfide-isomerase*. *Neurobiology of aging*, 2012. **33**(12): p. 2855-2868.
307. Walker, A.K., et al., *ALS-associated TDP-43 induces endoplasmic reticulum stress, which drives cytoplasmic TDP-43 accumulation and stress granule formation*. *PloS one*, 2013. **8**(11): p. e81170.
308. Kanekura, K., et al., *Characterization of amyotrophic lateral sclerosis-linked P56S mutation of vesicle-associated membrane protein-associated protein B (VAPB/ALS8)*. *Journal of Biological Chemistry*, 2006. **281**(40): p. 30223-30233.
309. Gkogkas, C., et al., *VAPB interacts with and modulates the activity of ATF6*. *Human molecular genetics*, 2008. **17**(11): p. 1517-1526.
310. Suzuki, H., et al., *ALS-linked P56S-VAPB, an aggregated loss-of-function mutant of VAPB, predisposes motor neurons to ER stress-related death by inducing aggregation of co-expressed wild-type VAPB*. *Journal of neurochemistry*, 2009. **108**(4): p. 973-985.
311. Ratnaparkhi, A., et al., *A Drosophila model of ALS: human ALS-associated mutation in VAP33A suggests a dominant negative mechanism*. *PLoS One*, 2008. **3**(6): p. e2334.
312. Zhang, Y.-J., et al., *Aggregation-prone c9FTD/ALS poly (GA) RAN-translated proteins cause neurotoxicity by inducing ER stress*. *Acta neuropathologica*, 2014. **128**(4): p. 505-524.
313. Colanzi, A., et al., *A specific activation of the mitogen-activated protein kinase kinase 1 (MEK1) is required for Golgi fragmentation during mitosis*. *The Journal of cell biology*, 2000. **149**(2): p. 331-340.
314. Hicks, S.W. and C.E. Machamer, *Golgi structure in stress sensing and apoptosis*. *Biochimica et Biophysica Acta (BBA)-Molecular Cell Research*, 2005. **1744**(3): p. 406-414.
315. Thayer, D.A., Y.N. Jan, and L.Y. Jan, *Increased neuronal activity fragments the Golgi complex*. *Proceedings of the National Academy of Sciences*, 2013. **110**(4): p. 1482-1487.
316. Zolov, S.N. and V.V. Lupashin, *Cog3p depletion blocks vesicle-mediated Golgi retrograde trafficking in HeLa cells*. *The Journal of cell biology*, 2005. **168**(5): p. 747-759.
317. Farber-Katz, S.E., et al., *DNA damage triggers golgi dispersal via DNA-PK and GOLPH3*. *Cell*, 2014. **156**(3): p. 413-427.
318. Nakagomi, S., et al., *A Golgi fragmentation pathway in neurodegeneration*. *Neurobiology of disease*, 2008. **29**(2): p. 221-231.
319. Sütterlin, C., et al., *Fragmentation and dispersal of the pericentriolar Golgi complex is required for entry into mitosis in mammalian cells*. *Cell*, 2002. **109**(3): p. 359-369.
320. Gonatas, N.K., A. Stieber, and J.O. Gonatas, *Fragmentation of the Golgi apparatus in neurodegenerative diseases and cell death*. *Journal of the neurological sciences*, 2006. **246**(1): p. 21-30.
321. Gonatas, N., et al., *Fragmentation of the Golgi apparatus of motor neurons in amyotrophic lateral sclerosis*. *The American journal of pathology*, 1992. **140**(3): p. 731.
322. Fujita, Y. and K. Okamoto, *Golgi apparatus of the motor neurons in patients with amyotrophic lateral sclerosis and in mice models of amyotrophic lateral sclerosis*. *Neuropathology*, 2005. **25**(4): p. 388-394.
323. van Dis, V., et al., *Golgi fragmentation precedes neuromuscular denervation and is associated with endosome abnormalities in SOD1-ALS mouse motor neurons*. *Acta neuropathologica communications*, 2014. **2**(1): p. 38.
324. Fujita, Y., et al., *Fragmentation of the Golgi apparatus of the anterior horn cells in patients with familial amyotrophic lateral sclerosis with SOD1 mutations and posterior column involvement*. *Journal of the neurological sciences*, 2000. **174**(2): p. 137-140.

325. Fujita, Y., et al., *Anterior horn cells with abnormal TDP-43 immunoreactivities show fragmentation of the Golgi apparatus in ALS*. Journal of the neurological sciences, 2008. **269**(1): p. 30-34.
326. Ito, H., et al., *Clinicopathologic study on an ALS family with a heterozygous E478G optineurin mutation*. Acta neuropathologica, 2011. **122**(2): p. 223-229.
327. Mourelatos, Z., et al., *The Golgi apparatus of spinal cord motor neurons in transgenic mice expressing mutant Cu, Zn superoxide dismutase becomes fragmented in early, preclinical stages of the disease*. Proceedings of the National Academy of Sciences, 1996. **93**(11): p. 5472-5477.
328. Stieber, A., et al., *Disruption of the structure of the Golgi apparatus and the function of the secretory pathway by mutants G93A and G85R of Cu, Zn superoxide dismutase (SOD1) of familial amyotrophic lateral sclerosis*. Journal of the neurological sciences, 2004. **219**(1): p. 45-53.
329. Teuling, E., et al., *Motor neuron disease-associated mutant vesicle-associated membrane protein-associated protein (VAP) B recruits wild-type VAPs into endoplasmic reticulum-derived tubular aggregates*. The Journal of Neuroscience, 2007. **27**(36): p. 9801-9815.
330. Farg, M.A., et al., *Ataxin-2 interacts with FUS and intermediate-length polyglutamine expansions enhance FUS-related pathology in amyotrophic lateral sclerosis*. Human molecular genetics, 2013. **22**(4): p. 717-728.
331. Rogelj, B., et al., *Widespread binding of FUS along nascent RNA regulates alternative splicing in the brain*. Scientific reports, 2012. **2**.
332. Fujii, R., et al., *The RNA binding protein TLS is translocated to dendritic spines by mGluR5 activation and regulates spine morphology*. Current Biology, 2005. **15**(6): p. 587-593.
333. Lagier-Tourenne, C., et al., *Divergent roles of ALS-linked proteins FUS/TLS and TDP-43 intersect in processing long pre-mRNAs*. Nature neuroscience, 2012. **15**(11): p. 1488-1497.
334. Lu, Y., J. Ferris, and F.-B. Gao, *Frontotemporal dementia and amyotrophic lateral sclerosis-associated disease protein TDP-43 promotes dendritic branching*. Mol Brain, 2009. **2**(30): p. 103.
335. Liu-Yesucevitz, L., et al., *Tar DNA binding protein-43 (TDP-43) associates with stress granules: analysis of cultured cells and pathological brain tissue*. PloS one, 2010. **5**(10): p. e13250.
336. Daigle, J.G., et al., *RNA-binding ability of FUS regulates neurodegeneration, cytoplasmic mislocalization and incorporation into stress granules associated with FUS carrying ALS-linked mutations*. Human molecular genetics, 2013. **22**(6): p. 1193-1205.
337. McDonald, K.K., et al., *TAR DNA-binding protein 43 (TDP-43) regulates stress granule dynamics via differential regulation of G3BP and TIA-1*. Human molecular genetics, 2011: p. ddr021.
338. Li, Y.R., et al., *Stress granules as crucibles of ALS pathogenesis*. The Journal of cell biology, 2013. **201**(3): p. 361-372.
339. Bentmann, E., C. Haass, and D. Dormann, *Stress granules in neurodegeneration—lessons learnt from TAR DNA binding protein of 43 kDa and fused in sarcoma*. FEBS Journal, 2013. **280**(18): p. 4348-4370.
340. Tollervey, J.R., et al., *Characterizing the RNA targets and position-dependent splicing regulation by TDP-43*. Nature neuroscience, 2011. **14**(4): p. 452-458.
341. Tibshirani, M., et al., *Cytoplasmic sequestration of FUS/TLS associated with ALS alters histone marks through loss of nuclear protein arginine methyltransferase 1*. Human molecular genetics, 2015. **24**(3): p. 773-786.

342. Haeusler, A.R., et al., *C9orf72 nucleotide repeat structures initiate molecular cascades of disease*. Nature, 2014. **507**(7491): p. 195-200.
343. Schroer, T.A., *Dynactin*. Annu. Rev. Cell Dev. Biol., 2004. **20**: p. 759-779.
344. Brown, M.E. and P.C. Bridgman, *Myosin function in nervous and sensory systems*. Journal of neurobiology, 2004. **58**(1): p. 118-130.
345. Grosshans, B.L., D. Ortiz, and P. Novick, *Rabs and their effectors: achieving specificity in membrane traffic*. Proceedings of the National Academy of Sciences, 2006. **103**(32): p. 11821-11827.
346. Farg, M.A., et al., *C9ORF72, implicated in amyotrophic lateral sclerosis and frontotemporal dementia, regulates endosomal trafficking*. Human molecular genetics, 2014. **13**(23): p. ddu068.
347. Alami, N.H., et al., *Axonal transport of TDP-43 mRNA granules is impaired by ALS-causing mutations*. Neuron, 2014. **81**(3): p. 536-543.
348. Laird, F.M., et al., *Motor neuron disease occurring in a mutant dynactin mouse model is characterized by defects in vesicular trafficking*. The Journal of Neuroscience, 2008. **28**(9): p. 1997-2005.
349. Levine, T.P., et al., *The product of C9orf72, a gene strongly implicated in neurodegeneration, is structurally related to DENN Rab-GEFs*. Bioinformatics, 2013. **29**(4): p. 499-503.
350. Zhang, D., et al., *Discovery of novel DENN proteins: implications for the evolution of eukaryotic intracellular membrane structures and human disease*. Frontiers in genetics, 2012. **3**.
351. Sahlender, D.A., et al., *Optineurin links myosin VI to the Golgi complex and is involved in Golgi organization and exocytosis*. The Journal of cell biology, 2005. **169**(2): p. 285-295.
352. Yi, P., et al., *Sorafenib-mediated targeting of the AAA+ ATPase p97/VCP leads to disruption of the secretory pathway, endoplasmic reticulum stress, and hepatocellular cancer cell death*. Molecular cancer therapeutics, 2012. **11**(12): p. 2610-2620.
353. Arita, M., T. Wakita, and H. Shimizu, *Valosin-containing protein (VCP/p97) is required for poliovirus replication and is involved in cellular protein secretion pathway in poliovirus infection*. Journal of virology, 2012. **86**(10): p. 5541-5553.
354. Ballar, P., A. Pabuccuoglu, and F.A. Kose, *Different p97/VCP complexes function in retrotranslocation step of mammalian ER-associated degradation (ERAD)*. The international journal of biochemistry & cell biology, 2011. **43**(4): p. 613-621.
355. Pantaloni, D. and M.-F. Carlier, *How profilin promotes actin filament assembly in the presence of thymosin β 4*. Cell, 1993. **75**(5): p. 1007-1014.
356. Kuijpers, M., et al., *The ALS8 protein VAPB interacts with the ER–Golgi recycling protein YIF1A and regulates membrane delivery into dendrites*. The EMBO journal, 2013. **32**(14): p. 2056-2072.
357. Skehel, P., R. Fabian-Fine, and E. Kandel, *Mouse VAP33 is associated with the endoplasmic reticulum and microtubules*. Proceedings of the National Academy of Sciences, 2000. **97**(3): p. 1101-1106.
358. Jiang, J., et al., *AMPA receptor trafficking and synaptic plasticity require SQSTM1/p62*. Hippocampus, 2009. **19**(4): p. 392-406.
359. Calderilla-Barbosa, L., et al., *Interaction of SQSTM1 with the motor protein dynein–SQSTM1 is required for normal dynein function and trafficking*. Journal of cell science, 2014. **127**(18): p. 4052-4063.
360. Otomo, A., et al., *ALS2, a novel guanine nucleotide exchange factor for the small GTPase Rab5, is implicated in endosomal dynamics*. Human molecular genetics, 2003. **12**(14): p. 1671-1687.

361. Topp, J.D., et al., *Alsin is a Rab5 and Rac1 guanine nucleotide exchange factor*. Journal of Biological Chemistry, 2004. **279**(23): p. 24612-24623.
362. Urwin, H., et al., *Disruption of endocytic trafficking in frontotemporal dementia with CHMP2B mutations*. Human molecular genetics, 2010: p. ddq100.
363. Ross, J.L., et al., *Kinesin and dynein-dynactin at intersecting microtubules: motor density affects dynein function*. Biophysical journal, 2008. **94**(8): p. 3115-3125.
364. Liu, Q., et al., *Neurofilament proteins in neurodegenerative diseases*. Cellular and Molecular Life Sciences CMLS, 2004. **61**(24): p. 3057-3075.
365. Oakley, B.R., *An abundance of tubulins*. Trends in cell biology, 2000. **10**(12): p. 537-542.
366. Oblinger, M.M., J. Wong, and L.M. Parysek, *Axotomy-induced changes in the expression of a type III neuronal intermediate filament gene*. The Journal of Neuroscience, 1989. **9**(11): p. 3766-3775.
367. Pérez-Brangulí, F., et al., *Dysfunction of spatacsin leads to axonal pathology in SPG11 linked hereditary spastic paraplegia*. Human molecular genetics, 2014: p. ddu200.
368. Ruscher, K. and T. Wieloch, *The involvement of the sigma-1 receptor in neurodegeneration and neurorestoration*. Journal of Pharmacological Sciences, 2014.
369. Pabba, M., et al., *NMDA receptors are upregulated and trafficked to the plasma membrane after Sigma-1 receptor activation in the rat hippocampus*. The Journal of Neuroscience, 2014. **34**(34): p. 11325-11338.
370. Gentil, B.J., M. Tibshirani, and H.D. Durham, *Neurofilament dynamics and involvement in neurological disorders*. Cell and tissue research, 2015: p. 1-12.
371. Stenmark, H. and V.M. Olkkonen, *The rab gtpase family*. Genome Biol, 2001. **2**(5): p. S3007.
372. Stenmark, H., *Rab GTPases as coordinators of vesicle traffic*. Nature reviews Molecular cell biology, 2009. **10**(8): p. 513-525.
373. Dejgaard, S.Y., et al., *Rab18 and Rab43 have key roles in ER-Golgi trafficking*. Journal of cell science, 2008. **121**(16): p. 2768-2781.
374. Barr, F.A. *Rab GTPase function in Golgi trafficking*. in *Seminars in cell & developmental biology*. 2009. Elsevier.
375. Plutner, H., et al., *Rab1b regulates vesicular transport between the endoplasmic reticulum and successive Golgi compartments*. The Journal of Cell Biology, 1991. **115**(1): p. 31-43.
376. Rodman, J.S. and A. Wandinger-Ness, *Rab GTPases coordinate endocytosis*. Journal of Cell Science, 2000. **113**(2): p. 183-192.
377. Cherfils, J. and M. Zeghouf, *Regulation of small GTPases by GEFs, GAPs, and GDIs*. Physiological Reviews, 2013. **93**(1): p. 269-309.
378. Shen, F. and M.C. Seabra, *Mechanism of Digeranylgeranylation of Rab Proteins FORMATION OF A COMPLEX BETWEEN MONOGERANYLGERANYL-Rab AND Rab ESCORT PROTEIN*. Journal of Biological Chemistry, 1996. **271**(7): p. 3692-3698.
379. Barr, F. and D.G. Lambright, *Rab GEFs and GAPs*. Current opinion in cell biology, 2010. **22**(4): p. 461-470.
380. Hadano, S., et al., *A gene encoding a putative GTPase regulator is mutated in familial amyotrophic lateral sclerosis 2*. Nature genetics, 2001. **29**(2): p. 166-173.
381. Eymard-Pierre, E., et al., *Infantile-onset ascending hereditary spastic paralysis is associated with mutations in the alsin gene*. The American Journal of Human Genetics, 2002. **71**(3): p. 518-527.
382. Hadano, S., et al., *Mice deficient in the Rab5 guanine nucleotide exchange factor ALS2/alsin exhibit age-dependent neurological deficits and altered endosome trafficking*. Human molecular genetics, 2006. **15**(2): p. 233-250.

383. Palmisano, R., et al., *Endosomal accumulation of APP in wobbler motor neurons reflects impaired vesicle trafficking: implications for human motor neuron disease*. BMC neuroscience, 2011. **12**(1): p. 24.
384. Kachaner, D., et al., *Toward an integrative view of Optineurin functions*. Cell Cycle, 2012. **11**(15): p. 2808-2818.
385. Hattula, K. and J. Peränen, *FIP-2, a coiled-coil protein, links Huntingtin to Rab8 and modulates cellular morphogenesis*. Current Biology, 2000. **10**(24): p. 1603-1606.
386. del Toro, D., et al., *Mutant huntingtin impairs post-Golgi trafficking to lysosomes by delocalizing optineurin/Rab8 complex from the Golgi apparatus*. Molecular biology of the cell, 2009. **20**(5): p. 1478-1492.
387. Phichith, D., et al., *Cargo binding induces dimerization of myosin VI*. Proceedings of the National Academy of Sciences, 2009. **106**(41): p. 17320-17324.
388. Chibalina, M.V., et al., *Rab8-Optineurin-Myosin VI: Analysis of Interactions and Functions in the Secretory Pathway*. Methods in enzymology, 2008. **438**: p. 11-24.
389. Bond, L.M., et al., *Myosin VI and its binding partner optineurin are involved in secretory vesicle fusion at the plasma membrane*. Molecular biology of the cell, 2011. **22**(1): p. 54-65.
390. Duden, R., *ER-to-Golgi transport: COP I and COP II function (review)*. Molecular membrane biology, 2003. **20**(3): p. 197-207.
391. Boslem, E., et al., *Alteration of endoplasmic reticulum lipid rafts contributes to lipotoxicity in pancreatic β -cells*. Journal of Biological Chemistry, 2013. **288**(37): p. 26569-26582.
392. Nassif, M., et al., *Amyotrophic lateral sclerosis pathogenesis: a journey through the secretory pathway*. Antioxidants & redox signaling, 2010. **13**(12): p. 1955-1989.
393. Lippincott-Schwartz, J., T.H. Roberts, and K. Hirschberg, *Secretory protein trafficking and organelle dynamics in living cells 1*. Annual review of cell and developmental biology, 2000. **16**(1): p. 557-589.
394. Storrie, B., et al., *Recycling of Golgi-resident glycosyltransferases through the ER reveals a novel pathway and provides an explanation for nocodazole-induced Golgi scattering*. The Journal of cell biology, 1998. **143**(6): p. 1505-1521.
395. Diekstra, F.P., et al., *UNC13A is a modifier of survival in amyotrophic lateral sclerosis*. Neurobiology of aging, 2012. **33**(3): p. 630. e3-630. e8.
396. Barlowe, C., et al., *COPII: a membrane coat formed by Sec proteins that drive vesicle budding from the endoplasmic reticulum*. Cell, 1994. **77**(6): p. 895-907.
397. Bickford, L.C., E. Mossessova, and J. Goldberg, *A structural view of the COPII vesicle coat*. Current opinion in structural biology, 2004. **14**(2): p. 147-153.
398. Jensen, D. and R. Schekman, *COPII-mediated vesicle formation at a glance*. Journal of cell science, 2011. **124**(1): p. 1-4.
399. Kirchhausen, T., *Making COPII coats*. Cell, 2007. **129**(7): p. 1251-1252.
400. Barlowe, C., *COPII and selective export from the endoplasmic reticulum*. Biochimica et Biophysica Acta (BBA)-Molecular Cell Research, 1998. **1404**(1): p. 67-76.
401. Martínez-Menárguez, J.A., et al., *Vesicular tubular clusters between the ER and Golgi mediate concentration of soluble secretory proteins by exclusion from COPI-coated vesicles*. Cell, 1999. **98**(1): p. 81-90.
402. Appenzeller-Herzog, C. and H.-P. Hauri, *The ER-Golgi intermediate compartment (ERGIC): in search of its identity and function*. Journal of Cell Science, 2006. **119**(11): p. 2173-2183.
403. Vaughan, K.T., *Microtubule plus ends, motors, and traffic of Golgi membranes*. Biochimica et Biophysica Acta (BBA)-Molecular Cell Research, 2005. **1744**(3): p. 316-324.
404. Watson, P., et al., *Coupling of ER exit to microtubules through direct interaction of COPII with dynactin*. Nature cell biology, 2005. **7**(1): p. 48-55.

405. Slavin, I., et al., *Role of Rab1b in COPII dynamics and function*. European journal of cell biology, 2011. **90**(4): p. 301-311.
406. Saraste, J., U. Lahtinen, and B. Goud, *Localization of the small GTP-binding protein rab1p to early compartments of the secretory pathway*. Journal of Cell Science, 1995. **108**(4): p. 1541-1552.
407. Levy, J.R., et al., *A motor neuron disease-associated mutation in p150Glued perturbs dynactin function and induces protein aggregation*. The Journal of cell biology, 2006. **172**(5): p. 733-745.
408. Zhang, F., et al., *Interaction between familial amyotrophic lateral sclerosis (ALS)-linked SOD1 mutants and the dynein complex*. Journal of Biological Chemistry, 2007. **282**(22): p. 16691-16699.
409. Kabuta, T., et al., *Familial amyotrophic lateral sclerosis-linked mutant SOD1 aberrantly interacts with tubulin*. Biochemical and biophysical research communications, 2009. **387**(1): p. 121-126.
410. Ho, K.-C., et al., *Brief Communication: Correlation of Neuronal Cell Body Size in Motor Cortex and Hippocampus with Body Height, Body Weight, and Axonal Length*. International journal of neuroscience, 1992. **65**(1-4): p. 147-153.
411. Liu-Yesucevitz, L., et al., *ALS-Linked Mutations Enlarge TDP-43-Enriched Neuronal RNA Granules in the Dendritic Arbor*. The Journal of Neuroscience, 2014. **34**(12): p. 4167-4174.
412. Chevalier-Larsen, E. and E.L. Holzbaur, *Axonal transport and neurodegenerative disease*. Biochimica et Biophysica Acta (BBA)-Molecular Basis of Disease, 2006. **1762**(11): p. 1094-1108.
413. Shi, P., et al., *Effects of ALS-related SOD1 mutants on dynein-and KIF5-mediated retrograde and anterograde axonal transport*. Biochimica et Biophysica Acta (BBA)-Molecular Basis of Disease, 2010. **1802**(9): p. 707-716.
414. Hirokawa, N. and R. Takemura, *Molecular motors and mechanisms of directional transport in neurons*. Nature Reviews Neuroscience, 2005. **6**(3): p. 201-214.
415. Collard, J.-F., F. Côté, and J.-P. Julien, *Defective axonal transport in a transgenic mouse model of amyotrophic lateral sclerosis*. Nature, 1995. **375**(6526): p. 61-64.
416. Tateno, M., et al., *Mutant SOD1 impairs axonal transport of choline acetyltransferase and acetylcholine release by sequestering KAP3*. Human molecular genetics, 2009. **18**(5): p. 942-955.
417. Morfini, G.A., et al., *Inhibition of fast axonal transport by pathogenic SOD1 involves activation of p38 MAP kinase*. PloS one, 2013. **8**(6): p. e65235.
418. Ligon, L.A., et al., *Mutant superoxide dismutase disrupts cytoplasmic dynein in motor neurons*. Neuroreport, 2005. **16**(6): p. 533-536.
419. Volkening, K., et al., *Tar DNA binding protein of 43 kDa (TDP-43), 14-3-3 proteins and copper/zinc superoxide dismutase (SOD1) interact to modulate NFL mRNA stability. Implications for altered RNA processing in amyotrophic lateral sclerosis (ALS)*. Brain research, 2009. **1305**: p. 168-182.
420. Groen, E.J., et al., *ALS-associated mutations in FUS disrupt the axonal distribution and function of SMN*. Human molecular genetics, 2013: p. ddt222.
421. Fallini, C., et al., *The survival of motor neuron (SMN) protein interacts with the mRNA-binding protein HuD and regulates localization of poly (A) mRNA in primary motor neuron axons*. The Journal of Neuroscience, 2011. **31**(10): p. 3914-3925.
422. Dombert, B., et al., *Presynaptic Localization of Smn and hnRNP R in Axon Terminals of Embryonic and Postnatal Mouse Motoneurons*. PloS one, 2014. **9**(10): p. e110846.

423. Diekstra, F.P., et al., *C9orf72 and UNC13A are shared risk loci for amyotrophic lateral sclerosis and frontotemporal dementia: A genome-wide meta-analysis*. Annals of neurology, 2014. **76**(1): p. 120-133.
424. Tong, J., et al., *XBP1 depletion precedes ubiquitin aggregation and Golgi fragmentation in TDP-43 transgenic rats*. Journal of neurochemistry, 2012. **123**(3): p. 406-416.
425. Lucocq, J., G. Warren, and J. Pryde, *Okadaic acid induces Golgi apparatus fragmentation and arrest of intracellular transport*. Journal of cell science, 1991. **100**(4): p. 753-759.
426. De Vos, K.J., et al., *Familial amyotrophic lateral sclerosis-linked SOD1 mutants perturb fast axonal transport to reduce axonal mitochondria content*. Human molecular genetics, 2007. **16**(22): p. 2720-2728.
427. Pathak, D., K.J. Sepp, and P.J. Hollenbeck, *Evidence that myosin activity opposes microtubule-based axonal transport of mitochondria*. The Journal of Neuroscience, 2010. **30**(26): p. 8984-8992.
428. Jokic, N., et al., *The neurite outgrowth inhibitor Nogo-A promotes denervation in an amyotrophic lateral sclerosis model*. EMBO reports, 2006. **7**(11): p. 1162-1167.
429. Shi, P., et al., *Mitochondrial dysfunction in amyotrophic lateral sclerosis*. Biochimica et Biophysica Acta (BBA)-Molecular Basis of Disease, 2010. **1802**(1): p. 45-51.
430. Smethurst, P., K.C. Sidle, and J. Hardy, *Prion-like mechanisms of TDP-43 in ALS*. Neuropathology and applied neurobiology, 2014.
431. Guo, J.L. and V.M. Lee, *Cell-to-cell transmission of pathogenic proteins in neurodegenerative diseases*. Nature medicine, 2014. **20**(2): p. 130-138.
432. Braak, H. and E. Braak, *Neuropathological staging of Alzheimer-related changes*. Acta neuropathologica, 1991. **82**(4): p. 239-259.
433. Braak, H., et al., *Staging of brain pathology related to sporadic Parkinson's disease*. Neurobiology of aging, 2003. **24**(2): p. 197-211.
434. Braak, H., et al., *Staging of the intracerebral inclusion body pathology associated with idiopathic Parkinson's disease (preclinical and clinical stages)*. Journal of neurology, 2002. **249**(3): p. iii1-iii5.
435. Kosaka, K., K. Tsuchiya, and M. Yoshimura, *Lewy body disease with and without dementia: a clinicopathological study of 35 cases*. Clinical neuropathology, 1987. **7**(6): p. 299-305.
436. Baleriola, J., et al., *Axonally synthesized ATF4 transmits a neurodegenerative signal across brain regions*. Cell, 2014. **158**(5): p. 1159-1172.
437. Glass, C.K., et al., *Mechanisms underlying inflammation in neurodegeneration*. Cell, 2010. **140**(6): p. 918-934.
438. Goedert, M., F. Clavaguera, and M. Tolnay, *The propagation of prion-like protein inclusions in neurodegenerative diseases*. Trends in neurosciences, 2010. **33**(7): p. 317-325.
439. Frost, B. and M.I. Diamond, *Prion-like mechanisms in neurodegenerative diseases*. Nature Reviews Neuroscience, 2009. **11**(3): p. 155-159.
440. Aguzzi, A., C. Sigurdson, and M. Heikenwaelder, *Molecular mechanisms of prion pathogenesis*. Annu. Rev. pathmechdis. Mech. Dis., 2008. **3**: p. 11-40.
441. Aguzzi, A. and L. Rajendran, *The transcellular spread of cytosolic amyloids, prions, and prionoids*. Neuron, 2009. **64**(6): p. 783-790.
442. Aguzzi, A., *Cell biology: Beyond the prion principle*. Nature, 2009. **459**(7249): p. 924-925.
443. Iba, M., et al., *Synthetic tau fibrils mediate transmission of neurofibrillary tangles in a transgenic mouse model of Alzheimer's-like tauopathy*. The Journal of Neuroscience, 2013. **33**(3): p. 1024-1037.

444. Luk, K.C., et al., *Intracerebral inoculation of pathological α -synuclein initiates a rapidly progressive neurodegenerative α -synucleinopathy in mice*. The Journal of experimental medicine, 2012. **209**(5): p. 975-986.
445. Masuda-Suzukake, M., et al., *Prion-like spreading of pathological α -synuclein in brain*. Brain, 2013: p. awt037.
446. Stöhr, J., et al., *Purified and synthetic Alzheimer's amyloid beta (A β) prions*. Proceedings of the National Academy of Sciences, 2012. **109**(27): p. 11025-11030.
447. de Calignon, A., et al., *Propagation of tau pathology in a model of early Alzheimer's disease*. Neuron, 2012. **73**(4): p. 685-697.
448. Nonaka, T., et al., *Seeded Aggregation and Toxicity of α -Synuclein and Tau* CELLULAR MODELS OF NEURODEGENERATIVE DISEASES. Journal of Biological Chemistry, 2010. **285**(45): p. 34885-34898.
449. Frost, B., R.L. Jacks, and M.I. Diamond, *Propagation of tau misfolding from the outside to the inside of a cell*. Journal of Biological Chemistry, 2009. **284**(19): p. 12845-12852.
450. Luk, K.C., et al., *Exogenous α -synuclein fibrils seed the formation of Lewy body-like intracellular inclusions in cultured cells*. Proceedings of the National Academy of Sciences, 2009. **106**(47): p. 20051-20056.
451. Kordower, J.H., et al., *Lewy body-like pathology in long-term embryonic nigral transplants in Parkinson's disease*. Nature medicine, 2008. **14**(5): p. 504-506.
452. Li, J.-Y., et al., *Lewy bodies in grafted neurons in subjects with Parkinson's disease suggest host-to-graft disease propagation*. Nature medicine, 2008. **14**(5): p. 501-503.
453. Münch, C., J. O'Brien, and A. Bertolotti, *Prion-like propagation of mutant superoxide dismutase-1 misfolding in neuronal cells*. Proceedings of the National Academy of Sciences, 2011. **108**(9): p. 3548-3553.
454. Alberti, S., et al., *A systematic survey identifies prions and illuminates sequence features of prionogenic proteins*. Cell, 2009. **137**(1): p. 146-158.
455. King, O.D., A.D. Gitler, and J. Shorter, *The tip of the iceberg: RNA-binding proteins with prion-like domains in neurodegenerative disease*. Brain research, 2012. **1462**: p. 61-80.
456. Cushman, M., et al., *Prion-like disorders: blurring the divide between transmissibility and infectivity*. Journal of Cell Science, 2010. **123**(8): p. 1191-1201.
457. Nomura, T., et al., *Intranuclear aggregation of mutant FUS/TLS as a molecular pathomechanism of amyotrophic lateral sclerosis*. Journal of Biological Chemistry, 2014. **289**(2): p. 1192-1202.
458. Bai, C., R. Richman, and S.J. Elledge, *Human cyclin F*. The EMBO journal, 1994. **13**(24): p. 6087.
459. Hershko, A., *Roles of ubiquitin-mediated proteolysis in cell cycle control*. Current opinion in cell biology, 1997. **9**(6): p. 788-799.
460. Pines, J., *Cyclins and cyclin-dependent kinases: take your partners*. Trends in biochemical sciences, 1993. **18**(6): p. 195-197.
461. D'Angiolella, V., M. Esencay, and M. Pagano, *A cyclin without cyclin-dependent kinases: cyclin F controls genome stability through ubiquitin-mediated proteolysis*. Trends in cell biology, 2013. **23**(3): p. 135-140.
462. Cenciarelli, C., et al., *Identification of a family of human F-box proteins*. Current biology, 1999. **9**(20): p. 1177-S3.
463. Bai, C., et al., *SKP1 connects cell cycle regulators to the ubiquitin proteolysis machinery through a novel motif, the F-box*. Cell, 1996. **86**(2): p. 263-274.
464. Lim, S. and P. Kaldis, *Cdks, cyclins and CKIs: roles beyond cell cycle regulation*. Development, 2013. **140**(15): p. 3079-3093.

465. Kong, M., et al., *Cyclin F regulates the nuclear localization of cyclin B1 through a cyclin–cyclin interaction*. The EMBO journal, 2000. **19**(6): p. 1378-1388.
466. Rechsteiner, M. and S.W. Rogers, *PEST sequences and regulation by proteolysis*. Trends in biochemical sciences, 1996. **21**(7): p. 267-271.
467. Fung, T.K., et al., *Cyclin F is degraded during G2-M by mechanisms fundamentally different from other cyclins*. Journal of Biological Chemistry, 2002. **277**(38): p. 35140-35149.
468. Lemus, L. and V. Goder, *Regulation of endoplasmic reticulum-associated protein degradation (ERAD) by ubiquitin*. Cells, 2014. **3**(3): p. 824-847.
469. Meusser, B., et al., *ERAD: the long road to destruction*. Nature cell biology, 2005. **7**(8): p. 766-772.
470. Yoshida, Y., et al., *E3 ubiquitin ligase that recognizes sugar chains*. Nature, 2002. **418**(6896): p. 438-442.
471. Yoshida, Y., et al., *Fbs2 is a new member of the E3 ubiquitin ligase family that recognizes sugar chains*. Journal of Biological Chemistry, 2003. **278**(44): p. 43877-43884.
472. Otoda, T., et al., *Proteasome dysfunction mediates obesity-induced endoplasmic reticulum stress and insulin resistance in the liver*. Diabetes, 2013. **62**(3): p. 811-824.
473. Kotani, T., et al., *Cyclin B1 mRNA translation is temporally controlled through formation and disassembly of RNA granules*. The Journal of cell biology, 2013. **202**(7): p. 1041-1055.
474. Heck, M.V., et al., *Dysregulated expression of lipid storage and membrane dynamics factors in Tia1 knockout mouse nervous tissue*. neurogenetics, 2014. **15**(2): p. 135-144.
475. Williams, K.L., et al., *UBQLN2/ubiquilin 2 mutation and pathology in familial amyotrophic lateral sclerosis*. Neurobiology of Aging, 2012. **33**(10): p. 2527. e3-2527. e10.
476. Fecto, F. and T. Siddique, *UBQLN2/P62 cellular recycling pathways in amyotrophic lateral sclerosis and frontotemporal dementia*. Muscle & nerve, 2012. **45**(2): p. 157-162.
477. Xia, Y., et al., *Pathogenic mutation of UBQLN2 impairs its interaction with UBXD8 and disrupts endoplasmic reticulum-associated protein degradation*. Journal of neurochemistry, 2014. **129**(1): p. 99-106.
478. Weihl, C.C., et al., *Inclusion body myopathy-associated mutations in p97/VCP impair endoplasmic reticulum-associated degradation*. Human molecular genetics, 2006. **15**(2): p. 189-199.
479. Liang, C.-J., et al., *Derlin-1 Regulates Mutant VCP-Linked Pathogenesis and Endoplasmic Reticulum Stress-Induced Apoptosis*. PLoS genetics, 2014. **10**(9): p. e1004675.
480. Di Fonzo, A., et al., *FBXO7 mutations cause autosomal recessive, early-onset parkinsonian-pyramidal syndrome*. Neurology, 2009. **72**(3): p. 240-245.
481. Zhao, T., et al., *Loss of nuclear activity of the FBXO7 protein in patients with parkinsonian-pyramidal syndrome (PARK15)*. PloS one, 2011. **6**(2): p. e16983.
482. Sandebring, A. and A. Cedazo-Mínguez, *Parkin-An E3 Ubiquitin Ligase with Multiple Substrates*. J Alzheimers Dis Parkinsonism S, 2012. **10**: p. 2161-0460.
483. Shimura, H., et al., *Familial Parkinson disease gene product, parkin, is a ubiquitin-protein ligase*. Nature genetics, 2000. **25**(3): p. 302-305.
484. Dawson, T.M. and V.L. Dawson, *Molecular pathways of neurodegeneration in Parkinson's disease*. Science, 2003. **302**(5646): p. 819-822.
485. Bandopadhyay, R. and J. de Belleruche, *Pathogenesis of Parkinson's disease: emerging role of molecular chaperones*. Trends in molecular medicine, 2010. **16**(1): p. 27-36.
486. Emanuele, M.J., et al., *Global identification of modular cullin-RING ligase substrates*. Cell, 2011. **147**(2): p. 459-474.
487. D'Angiolella, V., et al., *Cyclin F-mediated degradation of ribonucleotide reductase M2 controls genome integrity and DNA repair*. Cell, 2012. **149**(5): p. 1023-1034.

488. Wang, W., et al., *Neural cell cycle dysregulation and central nervous system diseases*. Progress in neurobiology, 2009. **89**(1): p. 1-17.
489. Vincent, I., et al., *Aberrant expression of mitotic cdc2/cyclin B1 kinase in degenerating neurons of Alzheimer's disease brain*. The Journal of Neuroscience, 1997. **17**(10): p. 3588-3598.
490. Gijssels, I., et al., *A C9orf72 promoter repeat expansion in a Flanders-Belgian cohort with disorders of the frontotemporal lobar degeneration-amyotrophic lateral sclerosis spectrum: a gene identification study*. The Lancet Neurology, 2012. **11**(1): p. 54-65.
491. Pfeffer, S. and D. Aivazian, *Targeting Rab GTPases to distinct membrane compartments*. Nature reviews Molecular cell biology, 2004. **5**(11): p. 886-896.
492. Korolchuk, V.I., F.M. Menzies, and D.C. Rubinsztein, *Mechanisms of cross-talk between the ubiquitin-proteasome and autophagy-lysosome systems*. FEBS letters, 2010. **584**(7): p. 1393-1398.
493. Fornai, F., et al., *Autophagy and amyotrophic lateral sclerosis: The multiple roles of lithium*. Autophagy, 2008. **4**(4): p. 527-530.
494. Fuchs, E., et al., *Specific Rab GTPase-activating proteins define the Shiga toxin and epidermal growth factor uptake pathways*. The Journal of cell biology, 2007. **177**(6): p. 1133-1143.
495. Chen, Z.-Y., et al., *A novel endocytic recycling signal distinguishes biological responses of Trk neurotrophin receptors*. Molecular biology of the cell, 2005. **16**(12): p. 5761-5772.
496. Rajagopal, R., et al., *Transactivation of Trk neurotrophin receptors by G-protein-coupled receptor ligands occurs on intracellular membranes*. The Journal of Neuroscience, 2004. **24**(30): p. 6650-6658.
497. Kittler, J.T. and S.J. Moss, *The dynamic synapse: molecular methods in ionotropic receptor biology*. 2006: CRC Press.
498. Manders, E., F. Verbeek, and J. Aten, *Measurement of co-localization of objects in dual-colour confocal images*. Journal of microscopy, 1993. **169**(3): p. 375-382.
499. Longatti, A. and S.A. Tooze, *Recycling endosomes contribute to autophagosome formation*. Autophagy, 2012. **8**(11): p. 1682-1683.
500. Lamb, C.A., H.C. Dooley, and S.A. Tooze, *Endocytosis and autophagy: Shared machinery for degradation*. Bioessays, 2013. **35**(1): p. 34-45.
501. Frasa, M.A., et al., *Illuminating the functional and structural repertoire of human TBC/RABGAPs*. Nature Reviews Molecular Cell Biology, 2012. **13**(2): p. 67-73.
502. Carlos Martín Zoppino, F., et al., *Autophagosome formation depends on the small GTPase Rab1 and functional ER exit sites*. Traffic, 2010. **11**(9): p. 1246-1261.
503. Bucci, C., et al., *The small GTPase rab5 functions as a regulatory factor in the early endocytic pathway*. Cell, 1992. **70**(5): p. 715-728.
504. Vitelli, R., et al., *Role of the small GTPase Rab7 in the late endocytic pathway*. Journal of Biological Chemistry, 1997. **272**(7): p. 4391-4397.
505. Bucci, C., et al., *Rab7: a key to lysosome biogenesis*. Molecular biology of the cell, 2000. **11**(2): p. 467-480.
506. Jäger, S., et al., *Role for Rab7 in maturation of late autophagic vacuoles*. Journal of cell science, 2004. **117**(20): p. 4837-4848.
507. Fader, C.M., et al., *Induction of autophagy promotes fusion of multivesicular bodies with autophagic vacuoles in k562 cells*. Traffic, 2008. **9**(2): p. 230-250.
508. Aguilera, M.O., W. Berón, and M.I. Colombo, *The actin cytoskeleton participates in the early events of autophagosome formation upon starvation induced autophagy*. Autophagy, 2012. **8**(11): p. 1590-1603.

509. Lee, J.Y., et al., *HDAC6 controls autophagosome maturation essential for ubiquitin-selective quality-control autophagy*. The EMBO journal, 2010. **29**(5): p. 969-980.
510. Eberth, A. and M.R. Ahmadian, *In vitro GEF and GAP assays*. Current Protocols in Cell Biology, 2009: p. 14.9. 1-14.9. 25.
511. Meggouh, F., et al., *Charcot-Marie-Tooth disease due to a de novo mutation of the RAB7 gene*. Neurology, 2006. **67**(8): p. 1476-1478.
512. Kimura, N., et al., *Dynein Dysfunction Induces Endocytic Pathology Accompanied by an Increase in Rab GTPases A POTENTIAL MECHANISM UNDERLYING AGE-DEPENDENT ENDOCYTIC DYSFUNCTION*. Journal of Biological Chemistry, 2009. **284**(45): p. 31291-31302.
513. Winslow, A.R., et al., *α -Synuclein impairs macroautophagy: implications for Parkinson's disease*. The Journal of cell biology, 2010. **190**(6): p. 1023-1037.
514. Ravikumar, B., et al., *Rab5 modulates aggregation and toxicity of mutant huntingtin through macroautophagy in cell and fly models of Huntington disease*. Journal of cell science, 2008. **121**(10): p. 1649-1660.
515. Thomas, M., J. Alegre-Abarategui, and R. Wade-Martins, *RNA dysfunction and aggregate at the centre of an amyotrophic lateral sclerosis/frontotemporal dementia disease continuum*. Brain, 2013: p. awt030.
516. Buchan, J.R., et al., *Eukaryotic stress granules are cleared by autophagy and Cdc48/VCP function*. Cell, 2013. **153**(7): p. 1461-1474.
517. Bennett, E.J., et al., *Global impairment of the ubiquitin-proteasome system by nuclear or cytoplasmic protein aggregates precedes inclusion body formation*. Molecular cell, 2005. **17**(3): p. 351-365.
518. Hutt, D.M. and W.E. Balch, *Expanding proteostasis by membrane trafficking networks*. Cold Spring Harbor perspectives in biology, 2013. **5**(7): p. a013383.
519. Orsi, A., H.E. Polson, and S.A. Tooze, *Membrane trafficking events that partake in autophagy*. Current opinion in cell biology, 2010. **22**(2): p. 150-156.
520. Figley, M.D., et al., *Profilin 1 associates with stress granules and ALS-linked mutations alter stress granule dynamics*. The Journal of Neuroscience, 2014. **34**(24): p. 8083-8097.
521. Ezzi, S.A., M. Urushitani, and J.P. Julien, *Wild-type superoxide dismutase acquires binding and toxic properties of ALS-linked mutant forms through oxidation*. Journal of neurochemistry, 2007. **102**(1): p. 170-178.
522. Estévez, A.G., et al., *Induction of Nitric Oxide--Dependent Apoptosis in Motor Neurons by Zinc-Deficient Superoxide Dismutase*. Science, 1999. **286**(5449): p. 2498-2500.
523. Pokrishevsky, E., et al., *Aberrant localization of FUS and TDP43 is associated with misfolding of SOD1 in amyotrophic lateral sclerosis*. PloS one, 2012. **7**(4): p. e35050.
524. Ayers, J.I., et al., *Experimental transmissibility of mutant SOD1 motor neuron disease*. Acta neuropathologica, 2014. **128**(6): p. 791-803.
525. Forsberg, K., et al., *Novel antibodies reveal inclusions containing non-native SOD1 in sporadic ALS patients*. PloS one, 2010. **5**(7): p. e11552.
526. Liu, H.N., et al., *Lack of evidence of monomer/misfolded superoxide dismutase-1 in sporadic amyotrophic lateral sclerosis*. Annals of neurology, 2009. **66**(1): p. 75-80.
527. Rakhit, R., et al., *An immunological epitope selective for pathological monomer-misfolded SOD1 in ALS*. Nature medicine, 2007. **13**(6): p. 754-759.
528. Cashman, N.R., et al. *Active and passive immunization of superoxide dismutase-1 disease-specific epitopes in a mouse model of amyotrophic lateral sclerosis*. in ANNALS OF NEUROLOGY. 2007. WILEY-LISS DIV JOHN WILEY & SONS INC, 111 RIVER ST, HOBOKEN, NJ 07030 USA.

529. Velde, C.V., et al., *Selective association of misfolded ALS-linked mutant SOD1 with the cytoplasmic face of mitochondria*. Proceedings of the National Academy of Sciences, 2008. **105**(10): p. 4022-4027.
530. Kabashi, E., et al., *TARDBP mutations in individuals with sporadic and familial amyotrophic lateral sclerosis*. Nature genetics, 2008. **40**(5): p. 572-574.
531. Bigio, E.H., et al., *Inclusions in frontotemporal lobar degeneration with TDP-43 proteinopathy (FTLD-TDP) and amyotrophic lateral sclerosis (ALS), but not FTLD with FUS proteinopathy (FTLD-FUS), have properties of amyloid*. Acta neuropathologica, 2013. **125**(3): p. 463-465.
532. Arai, T., et al., *Phosphorylated and cleaved TDP-43 in ALS, FTLD and other neurodegenerative disorders and in cellular models of TDP-43 proteinopathy*. Neuropathology, 2010. **30**(2): p. 170-181.
533. Hasegawa, M., et al., *Phosphorylated TDP-43 in frontotemporal lobar degeneration and amyotrophic lateral sclerosis*. Annals of neurology, 2008. **64**(1): p. 60-70.
534. Guo, W., et al., *An ALS-associated mutation affecting TDP-43 enhances protein aggregation, fibril formation and neurotoxicity*. Nature structural & molecular biology, 2011. **18**(7): p. 822-830.
535. Liu, G.C.-H., et al., *Delineating the membrane-disrupting and seeding properties of the TDP-43 amyloidogenic core*. Chemical communications, 2013. **49**(95): p. 11212-11214.
536. Nonaka, T., et al., *Prion-like properties of pathological TDP-43 aggregates from diseased brains*. Cell reports, 2013. **4**(1): p. 124-134.
537. Ahmed, Z., et al., *A novel in vivo model of tau propagation with rapid and progressive neurofibrillary tangle pathology: the pattern of spread is determined by connectivity, not proximity*. Acta neuropathologica, 2014. **127**(5): p. 667-683.
538. Liu, L., et al., *Trans-synaptic spread of tau pathology in vivo*. PloS one, 2012. **7**(2): p. e31302.
539. Freundt, E.C., et al., *Neuron-to-neuron transmission of α -synuclein fibrils through axonal transport*. Annals of neurology, 2012. **72**(4): p. 517-524.
540. Ulusoy, A., et al., *Caudo-rostral brain spreading of α -synuclein through vagal connections*. EMBO molecular medicine, 2013. **5**(7): p. 1119-1127.
541. Chia, R., et al., *Superoxide dismutase 1 and tgSOD1G93A mouse spinal cord seed fibrils, suggesting a propagative cell death mechanism in amyotrophic lateral sclerosis*. PloS one, 2010. **5**(5): p. e10627.
542. Grad, L.I., S. Fernando, and N.R. Cashman, *From molecule to molecule and cell to cell: Prion-like mechanisms in amyotrophic lateral sclerosis*. Neurobiology of Disease, 2015.
543. Pramatarova, A., et al., *Neuron-specific expression of mutant superoxide dismutase 1 in transgenic mice does not lead to motor impairment*. The Journal of Neuroscience, 2001. **21**(10): p. 3369-3374.
544. Urushitani, M., et al., *Chromogranin-mediated secretion of mutant superoxide dismutase proteins linked to amyotrophic lateral sclerosis*. Nature neuroscience, 2006. **9**(1): p. 108-118.
545. Zhao, W., et al., *Extracellular mutant SOD1 induces microglial-mediated motoneuron injury*. Glia, 2010. **58**(2): p. 231-243.
546. Roberts, K., et al., *Extracellular aggregated Cu/Zn superoxide dismutase activates microglia to give a cytotoxic phenotype*. Glia, 2013. **61**(3): p. 409-419.
547. Kato, S., et al., *Pathological characterization of astrocytic hyaline inclusions in familial amyotrophic lateral sclerosis*. The American journal of pathology, 1997. **151**(2): p. 611.
548. Kato, S., et al., *New consensus research on neuropathological aspects of familial amyotrophic lateral sclerosis with superoxide dismutase 1 (SOD1) gene mutations: inclusions containing SOD1 in neurons and astrocytes*. Amyotrophic Lateral Sclerosis, 2000. **1**(3): p. 163-184.

-
549. Tran, H.T., et al., *α -Synuclein immunotherapy blocks uptake and templated propagation of misfolded α -synuclein and neurodegeneration*. Cell reports, 2014. **7**(6): p. 2054-2065.
550. Urushitani, M., S.A. Ezzi, and J.-P. Julien, *Therapeutic effects of immunization with mutant superoxide dismutase in mice models of amyotrophic lateral sclerosis*. Proceedings of the National Academy of Sciences, 2007. **104**(7): p. 2495-2500.
551. Liu, H.-N., et al., *Targeting of monomer/misfolded SOD1 as a therapeutic strategy for amyotrophic lateral sclerosis*. The Journal of Neuroscience, 2012. **32**(26): p. 8791-8799.
552. Gros-Louis, F., et al., *Intracerebroventricular infusion of monoclonal antibody or its derived Fab fragment against misfolded forms of SOD1 mutant delays mortality in a mouse model of ALS*. Journal of neurochemistry, 2010. **113**(5): p. 1188-1199.
553. Cooper, A.A., et al., *α -Synuclein blocks ER-Golgi traffic and Rab1 rescues neuron loss in Parkinson's models*. Science, 2006. **313**(5785): p. 324-328.
554. Haas, A.K., et al., *Analysis of GTPase-activating proteins: Rab1 and Rab43 are key Rabs required to maintain a functional Golgi complex in human cells*. Journal of cell science, 2007. **120**(17): p. 2997-3010.
555. Willis, D., et al., *Differential transport and local translation of cytoskeletal, injury-response, and neurodegeneration protein mRNAs in axons*. The Journal of neuroscience, 2005. **25**(4): p. 778-791.
556. Maday, S., K.E. Wallace, and E.L. Holzbaur, *Autophagosomes initiate distally and mature during transport toward the cell soma in primary neurons*. The Journal of cell biology, 2012. **196**(4): p. 407-417.

9. Appendix

Appendix 1

***CCNF* mutations in amyotrophic lateral sclerosis and frontotemporal dementia**

Kelly L. Williams^{1,2,3}, Shu Yang^{1,2}, Jennifer A. Fifita^{1,2}, Bradley Smith⁴, Simon Topp⁴, Sadaf T. Warraich¹, Katharine Y. Zhang¹, Natalie Farrawell⁵, Caroline Vance⁴, Xun Hu⁴, Alessandra Chesi⁶, Claire S. Leblond^{7,8}, Vinod Sundaramoorthy^{1,9}, Carol Dobson-Stone^{10,11}, Albert Lee^{1,12}, Stephanie L. Rayner¹, Mark P. Molloy^{1,12}, Marka van Blitterswijk¹³, Dennis W. Dickson¹³, Ronald C. Petersen¹⁴, Neill R. Graff-Radford¹⁵, Bradley F. Boeve¹⁴, Melissa E. Murray¹³, Cyril Pottier¹³, Emily Don¹, Claire Winnick¹, Andrew P. Badrock¹, Emily P. McCann¹, Alison Hogan¹, Hussein Daoud^{7,8}, Annie Levert^{7,8}, Patrick A. Dion^{7,8}, Jun Mitsui¹⁶, Hiroyuki Ishiura¹⁶, Yuji Takahashi¹⁶, Jun Goto¹⁶, Jason Kost^{17,18}, Cinzia Gellera¹⁹, Athina Soragia Gkazi⁴, Jack Miller⁴, Joanne Stockton²⁰, William S. Brooks¹⁰, Karyn Boundy²¹, Meraida Polak²², José Luis Muñoz-Blanco²³, Jesús Esteban-Pérez²⁴, Alberto Rábano²⁵, Orla Hardiman²⁶, Karen E. Morrison^{20,27}, Nicola Ticozzi^{28,29}, Vincenzo Silani^{28,29}, Jonathan D. Glass²², John B. J. Kwok^{10,11}, Gilles J. Guillemin¹, Roger S. Chung¹, Shoji Tsuji^{16,30}, Robert H. Brown Jr¹⁸, Alberto García-Redondo²⁴, Rosa Rademakers¹³, John E. Landers¹⁸, Aaron D. Gitler⁶, Guy A Rouleau^{7,8}, Nicholas J. Cole^{1,3}, Justin J. Yerbury⁵, Julie D. Atkin^{1,9}, Christopher E. Shaw⁴, Garth A. Nicholson^{1,2,3,31} & Ian P. Blair^{1,2}

¹ Australian School of Advanced Medicine, Macquarie University, Sydney, NSW 2109, Australia.

² Northcott Neuroscience Laboratory, ANZAC Research Institute, Sydney, NSW 2139, Australia.

³ Sydney Medical School, University of Sydney, NSW 2006, Australia.

⁴ Medical Research Council Centre for Neurodegeneration Research, King's College London, Department of Clinical Neuroscience, Institute of Psychiatry, London SE5 8AF, UK.

⁵ Illawarra Health and Medical Research Institute/School of Biological Sciences, University of Wollongong, Wollongong, NSW 2522, Australia.

⁶ Department of Genetics, Stanford University School of Medicine, Stanford, CA 94305, USA.

⁷ Montreal Neurological Institute and Hospital, Department of Neurology and Neurosurgery, McGill University, Montreal QC H3A 2B4, Canada.

⁸ Pathology and Cellular Biology Department, Montreal University, Montreal QC, Canada

⁹ Department of Biochemistry, La Trobe University, Melbourne, VIC 3086, Australia.

¹⁰ Neuroscience Research Australia, Randwick, Sydney, NSW 2031, Australia.

¹¹ School of Medical Sciences, University of New South Wales, Kensington, Sydney, NSW 2052, Australia

¹² Australian Proteome Analysis Facility, Macquarie University, Sydney, NSW 2109, Australia.

¹³ Department of Neuroscience, Mayo Clinic Florida, Jacksonville, FL 32224, USA.

¹⁴ Department of Neurology, Mayo Clinic Rochester, Rochester, MN 55905, USA.

¹⁵ Department of Neurology, Mayo Clinic Florida, Jacksonville, FL 32224, USA.

¹⁶ Medical Genome Center, The University of Tokyo Hospital, The University of Tokyo, Tokyo 113-8655, Japan

¹⁷ Worcester Polytechnic Institute, Worcester, MA 01609, USA.

¹⁸ Department of Neurology, University of Massachusetts Medical School, Worcester, Massachusetts 01605, USA.

¹⁹ Unit of Genetics of Neurodegenerative and Metabolic Diseases, Fondazione IRCCS Istituto Neurologico ‘Carlo Besta’, Milan 20133, Italy

²⁰ School of Clinical and Experimental Medicine, College of Medical and Dental Sciences, University of Birmingham, UK.

²¹ The Queen Elizabeth Hospital, Woodville South, SA 5011 Australia.

²² Department of Neurology, Emory University, Atlanta, GA 30322, USA.

²³ Unidad de ELA, Instituto de Investigación Hospital Gregorio Marañón de Madrid, SERMAS, Spain.

²⁴ Unidad de ELA, Instituto de Investigación Hospital 12 de Octubre de Madrid, SERMAS, and Centro de Investigación Biomédica en Red de Enfermedades Raras (CIBERER U-723), Madrid, Spain.

²⁵ Banco de Tejidos, Centro Alzheimer – Fundación Reina Sofia, Fundación CIEN, Madrid, Spain.

²⁶ Academic Unit of Neurology, Trinity Biomedical Sciences Institute, Trinity College Dublin, Dublin, Republic of Ireland.

²⁷ Queen Elizabeth Hospital, University Hospitals Birmingham NHS Foundation Trust UK.

²⁸ Department of Neurology and Laboratory of Neuroscience, IRCCS Istituto Auxologico Italiano, Milan 20149, Italy.

²⁹ Department of Pathophysiology and Transplantation, 'Dino Ferrari' Center - Università degli Studi di Milano, Milan 20122 Italy.

³⁰ Department of Neurology, Graduate School of Medicine, The University of Tokyo, Tokyo 113-8655, Japan.

³¹ Molecular Medicine Laboratory, Concord Hospital, NSW 2139, Australia.

Correspondence should be addressed I.P.B. (ian.blair@mq.edu.au).

Amyotrophic lateral sclerosis (ALS) and frontotemporal dementia (FTD) are overlapping, fatal neurodegenerative disorders in which the molecular and pathogenic basis remains poorly understood. Ubiquitinated protein aggregates, of which TDP-43 is a major component, are a characteristic pathological feature of most ALS and FTD patients. We have identified *CCNF* missense mutations in cohorts of familial and sporadic ALS and FTD cases from diverse geographic populations including Australia, Canada, Spain, Italy, Japan, the UK and USA. *CCNF* encodes cyclin F, a component of an E3 ubiquitin-protein ligase complex ($\text{SCF}^{\text{Cyclin F}}$). Expression of mutant *CCNF* in neuronal cells caused abnormal ubiquitination and led to accumulation of ubiquitinated proteins, including TDP-43 and a known $\text{SCF}^{\text{Cyclin F}}$ substrate. Mutations in *CCNF* cause ALS and FTD, and appear to further implicate common mechanisms, linked to protein homeostasis, underlying neuronal degeneration.

Amyotrophic lateral sclerosis (ALS) is a late-onset fatal disorder characterised by the progressive degeneration of upper and lower motor neurons. Approximately 10% of ALS cases have a positive family history (familial ALS) and appear clinically indistinguishable from sporadic ALS cases. Mutations in several genes including *SOD1*, *TARDBP*, *FUS*, *UBQLN2*, *PFN1*, *OPTN*, and *C9ORF72* account for approximately two-thirds of familial ALS and 5% of sporadic ALS cases¹⁻⁸. Other ALS families are not linked to known loci and the cause of most sporadic ALS also remains unknown. Up to 15% of ALS patients are also diagnosed with frontotemporal dementia (FTD) and segregation of both ALS and FTD may be seen within families, particularly those with mutations in *C9ORF72*^{7,8}.

A hallmark pathological feature of most ALS and FTD cases is the presence of abnormally ubiquitinated proteins, particularly TDP-43, in neuronal cytoplasmic inclusions⁹. The etiology of ALS remains poorly understood but recent ALS gene discoveries are providing insight into pathological disease mechanisms and are critical to the development of *in vitro* and *in vivo* models

to study pathogenesis. Coupling linkage analysis with next-generation sequencing provides a powerful approach for the identification of novel ALS genes. We have used this approach to discover a pathogenic *CCNF* mutation in a large ALS-FTD family. We showed that *CCNF* mutations are also present in diverse international ALS and FTD cohorts at a similar prevalence to that seen for other critical ALS genes, *TARDBP* (which encodes TDP-43) and *FUS*. We demonstrated that ALS/FTD mutations in *CCNF* resulted in abnormal ubiquitination and accumulation of ubiquitinated proteins, including TDP-43.

RESULTS

Linkage mapping implicates a novel ALS locus on chromosome 16

To identify novel ALS loci, we performed two independent genome-wide scans for linkage in a multi-generational family (FALS10) comprising 10 individuals with ALS and/or FTD (Fig. 1a). The family displays autosomal dominant inheritance of disease and mutations in all known ALS genes were excluded. The first genome-wide scan for linkage, which used 10K Affymetrix SNP arrays, identified three candidate linkage regions with maximum multipoint LOD scores > 1.9 on chromosomes 11p15.4-p14.3, 16p13.3-p12.3 and 20p13-p12.2 respectively. The second genome-wide scan for linkage, which used 539 microsatellite markers, generated LOD scores > 3.0 at a single candidate region on chromosome 16 (maximum genome-wide two-point LOD score of 3.16, $\theta=0$, at D16S3065) that overlapped the chromosome 16 interval identified by the initial, SNP-based, linkage scan. Fine mapping and recombinant haplotype analysis using a dense coverage of microsatellite markers spanning the chromosome 16 interval refined the minimal candidate region to 10 Mb on chromosome 16p13.3 flanked by D16S521 and D16S3126 (Supplementary Table 1, Supplementary Fig. 1).

A missense mutation in *CCNF* causes ALS and FTD

Two family members with ALS (FALS10, individuals II:13 and III:1) and with the greatest familial separation were chosen for whole exome sequencing. The mean read depth for these patients was 50.3X and 36.2X respectively, with an average of 5.4×10^9 base pairs sequenced per individual (Supplementary Table 2). To identify candidate mutations, exome sequence variants were annotated and filtered (Supplementary Table 3) using the following criteria: the variant was present in both affected family members, resulted in altered amino acid sequence, and was absent from public SNP databases including dbSNP134, the 1000 Genomes Project (<0.001 frequency, Nov 2010 release) and the NHLBI Exome Sequencing Project (ESP) exome variant server (6503 sequenced human exomes). Of the 179 variants that remained following filtering, only one was located within the linked region on chromosome 16p13.3. This variant lies in the *CCNF* gene, leads to an A to G substitution at position 1861 of the coding DNA (c.1861A>G) and results in an amino acid substitution of serine with glycine at codon 621 at the protein level (p.S621G). Sanger sequencing of 29 family members demonstrated segregation of the mutation in all affected family members for whom DNA was available (three ALS and one FTD) and indicated its presence in a further three family members diagnosed with ALS for whom DNA was unavailable (obligate carriers, Fig. 1a, b). The mutation was also present in five at-risk family members ranging in age from 22 to 59 years. This variant was absent from 1831 control individuals recruited from the same population.

***CCNF* mutations are present in familial and sporadic ALS and FTD cases from diverse geographic populations**

To determine whether mutations in *CCNF* are present in other ALS and FTD patients, we used targeted sequencing, whole exome sequencing, or whole genome sequencing in the following cohorts: index cases from 75 Australian ALS families, 159 UK ALS families, 108 USA ALS families, 100 Canadian ALS families, 99 Italian ALS families, 32 Japanese ALS families, 30

Spanish ALS families, 16 Irish ALS families, 283 Japanese sporadic ALS cases, 168 French-Canadian sporadic ALS cases, 26 USA sporadic ALS cases, 49 USA ALS trios, 99 USA FTD (FTLD-TDP) cases, 43 Australian FTD families, and 29 Australian sporadic FTD cases. Nine additional novel missense variants in *CCNF* were identified and confirmed by Sanger sequencing. Most substituted amino acids are highly conserved across species (Fig. 1d). Variants were examined in large control cohorts and datasets including: dbSNP; NHLBI ESP Exome Variant Server, 1000 Genomes Project, the Japanese Human Genetic Variation Database, and 967 Australian control exomes (of European ancestry). Selected variants were also tested in population-specific control cohorts from the UK, USA, Canada, and Japan. None of the variants were present in genotyped controls and were absent from the public databases (Table 1). ALS/FTD mutations in *CCNF* were present in the overall cohorts from these diverse geographic populations at frequencies ranging from 0.6 to 3.3%, which is comparable to the frequency of mutations in *TARDBP* (which encodes TDP-43) and *FUS* that have been reported in familial ALS cohorts¹⁰.

The average ages of disease onset in familial and sporadic ALS cases with a *CCNF* mutation were 54.5 ± 8.1 and 64.8 ± 19.7 respectively (Supplementary Table 4). Detailed clinical descriptions are provided in the Supplementary Information. Using immunohistochemistry (IHC), we observed ubiquitin- and TDP-43-positive protein aggregates, a characteristic pathological feature of most ALS and FTD patients, in post mortem brain and spinal cord tissue from ALS and FTD patients with *CCNF* mutations (Supplementary Fig. 2). No evidence of abnormal cyclin F pathology was seen in these tissues, nor that from other ALS patients (Supplementary Fig. 3).

Cyclin F mutations result in UPS dysfunction and ubiquitination of TDP-43

CCNF (also called *FBXO1*) encodes the 786 amino acid cyclin F protein (Fig. 1c). Cyclin F is a member of the cyclin protein family, but unlike most cyclins, it does not bind or activate a cyclin dependent kinase (CDK)¹¹. Cyclin F is also a member of the F-box protein family characterized by

an F-box motif that binds directly to SKP1, which in turn recruits CUL1 to form a SCF (SKP1-CUL1-F-box protein) E3 ubiquitin-protein ligase complex (SCF^{Cyclin F})^{12,13}. E3s mediate the ubiquitination and proteasomal degradation of target proteins and are an integral component of the ubiquitin proteasome system (UPS).

Aberrant misfolded proteins are targeted for disposal by protein degradation pathways including the UPS and autophagic-lysosomal system, both of which are components of the complex network that maintains protein homeostasis (proteostasis). The accumulation of neuronal protein aggregates in ALS patients implicates dysfunction of the proteostasis network through inappropriate or inadequate response to aberrant proteins¹⁴. As a ubiquitin-protein ligase, cyclin F catalyses the transfer of activated ubiquitin to target proteins¹². To investigate whether ALS- and FTD-linked cyclin F mutations lead to proteostasis dysfunction, we used the UPS reporter, GFP^u, that consists of a 16 amino acid degron (CL1, a specific substrate for the UPS), fused to the carboxyl terminus of GFP¹⁵. The degron sequence ensures rapid degradation of the GFP fusion through ubiquitin mediated pathways, and the accumulation of this GFP reporter indicates UPS impairment. We confirmed that GFP^u signal correlates with UPS function in a motor neuron-like cell line (NSC-34) by inhibiting proteasome function using either the chemical inhibitor MG132, or expression of a mutant huntingtin exon 1 fragment containing an expanded polyQ sequence previously shown to inhibit the proteasome¹⁶ (Supplementary Fig. 4). Next, we co-transfected the NSC-34 cell line with GFP^u and either mutant cyclin F, wild type cyclin F, or cyclin F with SNPs identified in ALS/FTD patients, including those in public databases (Supplementary Table 5). Significantly higher levels of GFP^u fluorescence were observed for cyclin F with ALS/FTD mutations, indicating UPS dysfunction (Fig. 2a). This effect was independent of cyclin F expression levels (Fig. 2b). To examine whether the significant accumulation of GFP^u arose from the loss of proteasome activity or occurred upstream of the proteasome, we used two separate ubiquitin-independent small peptide 20S proteasome activity assays. These demonstrated that the UPS dysfunction was not due to altered proteolysis in the proteasome (Supplementary Fig. 5), consistent instead with the

dysfunction stemming from abnormal ubiquitination or transport to the proteasome, mechanisms that are mediated, in part, by cyclin F. Consistent with these observations, western blotting confirmed the presence of significantly more ubiquitinated proteins in neuronal cell lines expressing mutant cyclin F (Fig. 3a,b). Collectively our data suggest that mutations in *CCNF* modify the activity of SCF^{Cyclin F} resulting in over-accumulation of ubiquitinated proteins. To specifically demonstrate this, we found higher levels of the known SCF^{Cyclin F} target, RRM2 (Fig. 3a,b), including higher levels of ubiquitinated RRM2 (Fig. 3c), in neuronal cells expressing mutant cyclin F. Notably, we also observed substantially elevated levels of ubiquitinated TDP-43 in neuronal cells expressing mutant cyclin F (Fig. 3c), in accordance with the presence of ubiquitinated TDP-43 inclusions in cyclin F patient tissue (Supplementary Fig. 2).

DISCUSSION

We performed whole-genome linkage analysis and whole exome sequencing in one of the largest ALS-FTD pedigrees to be described in recent years to identify a pathogenic *CCNF* mutation. We also extended mutation analysis, to identify additional *CCNF* mutations in diverse geographic populations, most of European ancestry.

Neuronal accumulations of ubiquitinated TDP-43 are a major pathological feature of almost all ALS cases, and the majority of FTD cases. However, the mechanisms responsible for TDP-43 ubiquitination are poorly understood. We demonstrated that ALS/FTD mutations in *CCNF* are responsible for abnormal increases in ubiquitination of TDP-43 and may to be responsible for wider changes in protein homeostasis.

Abnormal protein homeostasis has been hypothesized to play a role in ALS pathogenesis. Convincing genetic linkage to familial ALS has also been shown for *UBQLN2*, which encodes ubiquilin 2, a protein that physically associates with ubiquitin ligases and proteasomes to mediate protein degradation⁴. Ubiquilin 2 positive neuronal inclusions are seen in affected motor neurons of

some ALS and ALS/FTD patients, and ALS-linked mutations in ubiquitin 2 have also been shown to impair protein degradation mediated by the UPS^{4,17}. Several other molecules that are functionally linked with cellular protein degradation pathways have also been associated with ALS (reviewed by Ling *et al.*¹⁴). Putative ALS-associated variants have been described in *SQSTM1*/p62, a ubiquitin binding protein with roles in protein degradation via the proteasome and autophagy. Interestingly, one of these *SQSTM1*/p62 variants and two cyclin F mutations described here, lie in a PEST sequence, a domain that is thought to act as a signal peptide for protein degradation¹⁸. ALS mutations have also been described in OPTN, an autophagic adaptor protein that binds substrates targeted for degradation and delivers them to autophagosomes⁶. OPTN-linked pathogenic mechanisms remain to be determined. A *VCP* mutation linked to inclusion body myopathy with Paget's disease of the bone and frontotemporal dementia (IBMPFD) impairs ER-associated degradation of ubiquitinated proteins from the ER¹⁹. *VCP* mutations have also been described in ALS cases but the mechanisms by which these lead to motor neuron degeneration remain unclear²⁰. There is also evidence that defects in molecules functionally related to cyclin F play a role in other neurodegenerative diseases. Mutations in the related F-box only protein 7 gene (*FBXO7*) cause autosomal recessive, early-onset, parkinsonian-pyramidal syndrome and lead to decreased stability of the *FBXO7* protein²¹. Similar to cyclin F, the F-box motif of *FBXO7* interacts directly with Skp1 to form the SCF E3 ubiquitin-protein ligase complex¹². Furthermore, around 10% of early onset Parkinson's disease cases are caused by mutations in *PARK2*, which encodes Parkin, an E3-ubiquitin ligase. Parkin mutations impair degradation of its substrates, leading to accumulation of toxic products and eventually cell death²².

Further resequencing of *CCNF* is warranted in other ALS and FTD cohorts, particularly those of European ancestry. Our data suggest that mutation of the encoded E3 ubiquitin ligase caused abnormal ubiquitination, implicating that common mechanisms, linked to protein homeostasis, underlie motor neuron degeneration. Additional functional studies, including animal models, can now commence to assess the pathogenic mechanism, and identify the targets of the

mutant SCF^{Cyclin F} complex. These target molecules may, in turn, be considered candidate ALS genes.

METHODS

Participants and samples

Patients, family members and unrelated controls were recruited under informed written consent as approved by the institutional review boards of the participating institutions. Patients were diagnosed with definite or probable ALS according to El Escorial criteria²³. Patients had previously been screened for mutations/expansions in known ALS genes including *TARDBP*, *SOD1*, *FUS*, *UBQLN2*, *OPTN*, *VCP*, *PFN1*, and *C9ORF72*. Formalin-fixed, paraffin-embedded cervical spinal cord sections from Australian patients and neurologically normal controls were provided by New South Wales Tissue Resource Centre (Sydney, Australia).

Genetic linkage analysis

Genomic DNA was extracted from peripheral blood using standard protocols. For SNP based genetic linkage analysis, genotyping was undertaken using the Affymetrix GeneChip® Mapping 10Kv2.0 XbaI Array containing 10,204 SNP markers following the manufacturer's instructions and apparatus (Affymetrix, Santa Clara, CA, USA). The raw microarray feature intensities were processed using the Affymetrix Genotyping Tools software package (GCOS/GTYPE) to derive SNP genotypes, marker order and linear chromosomal location. Parametric multipoint linkage analysis of SNP data was performed using Merlin v1.1 with intermarker distances obtained from the Marshfield (<http://research.marshfieldclinic.org/>) and deCODE (<http://www.decode.com/>) sex-averaged SNP linkage maps.

For microsatellite based genetic linkage analysis, genotyping was performed by deCODE genetics using 539 microsatellite markers spaced at an average of 8cM. Two-point linkage analysis was performed using the FASTLINK v4.1 program of the easyLINKAGE v5.08 package^{24,25}. All available family members were used for analysis. Parameters for linkage analysis included autosomal dominant inheritance, age-dependent penetrance (0-30 years, 1%; 31-40 years, 30%; 41-

50 years, 50%; 51-60 years, 70%; 61-70 years, 85%, >70 years, 90%), a disease allele frequency of 0.0001, equal male and female recombination, and equal marker allele frequencies.

Whole exome sequencing and mutation analysis

Exomes were captured using TruSeq Exome Enrichment kit or Agilent SureSelectXT Human All Exon V4. Paired-end sequencing was performed using the Illumina HiSeq2000 instrument.

Validation and analysis of the *CCNF* mutations was performed by direct DNA sequencing following PCR amplification of coding exons (NM_001761). PCR products were Sanger sequenced using Big-Dye terminator sequencing and an ABI 3730XL DNA analyser (Applied Biosystems).

SNP genotyping in control individuals was performed using a custom TaqMan SNP genotyping assay according to the manufacturer's instructions (Life Technologies) and analysed using a Viia 7 real time PCR system (Life Technologies).

Control exome data from 967 healthy Australian individuals of European ancestry was obtained from the Diamantina Institute, University of Queensland (Diamantina Australian Control Collection).

Bioinformatics

Sequencing reads generated by the Illumina platform were aligned to the hg19 human genome assembly using BWA v0.6.1²⁶, variants were called using SAMtools v0.1.16²⁷ and annotated using both the Sequence Variant Analyzer (SVA)²⁸ and ANNOVAR²⁹. SVA generated a list of candidate variants present in two affected individuals from family FALS10. ANNOVAR generated a variant report files for each individual sample. Variants were compared among affected family members and controls using the Galaxy Browser (<https://main.g2.bx.psu.edu/>). Filtering of variants was performed using dbSNP (releases 131, 132, 134 and 137; <https://www.ncbi.nlm.nih.gov/SNP/>), 1000 Genomes Project (Nov 2010 release; <http://www.1000genomes.org/>) and the NHLBI Exome

Sequencing Project (ESP) exome variant server (ESP6500 data release; <http://evs.gs.washington.edu/EVS/>).

Conservation of cyclin F orthologues was examined by aligning sequences from a variety of species (Entrez protein database; <http://ncbi.nlm.nih.gov>) using Clustal Omega (<http://www.ebi.ac.uk/Tools/msa/clustalo/>).

Plasmids and cloning

Expression constructs comprising wild type and mutant *CCNF* cDNA fused with an N-terminal mCherry were developed using pmCherry-C1-*CCNF* (Addgene) and Q5® Site-Directed Mutagenesis Kit (NEB) according to the manufacturer's protocol. All constructs were verified by DNA sequencing. A plasmid map is shown in Supplementary Figure 6.

Antibodies

The following primary antibodies were used in this study: rabbit polyclonal anti-cyclin F (cat # sc-952, Santa Cruz Biotechnology), rabbit polyclonal anti-cyclin F (cat # NB100-91730, Novus Biologicals), mouse monoclonal anti-TDP-43 antibody (cat # H00023435-M01, Abnova), rabbit polyclonal anti-ubiquitin (Dako), mouse monoclonal anti-RRM2 (cat # ab57653, Abcam), anti- β actin (cat # A5441 [AC-15], Sigma-Aldrich).

Cell lines

Mouse NSC-34 (neuroblastoma/motor neuron-enriched primary spinal cord hybrid) cells were provided by Prof Neil Cashman, University of Toronto. Mouse neuroblastoma Neuro-2a cells, and human neuroblastoma SH-SY5Y cells were from the ATCC repository (ATCC Product Nos. CCL-131 and CRL-2266).

Confocal microscopy

Confocal fluorescence imaging was performed using a Leica DM6000 upright laser scanning confocal microscope with Leica application suite advanced fluorescence software. Images were acquired with a 63x (1.4 numerical aperture) oil immersion objective. Images were acquired using sequential mode to avoid crosstalk between two dyes. Immunohistochemistry imaging was performed with a Zeiss Axio Imager 2 with ZEN pro program, using a 40x objective.

Immunohistochemistry of post mortem tissue

Immunostaining was performed on 5 µm thick paraffin-embedded spinal cord sections from control or ALS patients. Sections were deparaffinized using xylene, followed by rehydration in a series of descending ethanol concentrations. Antigen retrieval was carried out by heating sections in 10 mM citrate buffer (pH 6.0). Endogenous peroxidase activity was quenched using 3% hydrogen peroxidase in methanol for sections used in immunohistochemical analyses. Non-specific background was blocked using 3% goat serum (Vector Laboratories, Inc.). For immunohistochemistry studies, sections were incubated overnight at 4°C with rabbit polyclonal anti-cyclin F (1:200), followed by incubation with biotinylated goat anti-rabbit IgG (Vector Laboratories, Inc.) for 1 h at room temperature. The immunoreactive signal was detected using the avidin-biotin complex detection system (Vector Laboratories, Inc) with 3,3'-diaminobenzidine as the chromogen. Slides were counterstained with hematoxylin (Sigma-Aldrich) and coverslipped using DPX (Sigma-Aldrich) mounting media.

Cell culture and transfection for UPS assays

NSC-34 cells were maintained in Dulbecco's modified Eagle's medium (Sigma Aldrich) containing 100 U/ml penicillin, 100 mg/ml streptomycin and 10% (v/v) heat-inactivated fetal bovine serum (Sigma Aldrich). Cells were maintained in a humidified 37°C incubator with 5% CO₂. For the UPS assay and Enzo proteasome assay, NSC-34 cells were plated at a density of 50,000 cells/well in 6-well plate. For the Abcam proteasome assay, NSC-34 cells were plated at a density of 2,000 cells/well in 96-plate well plate. Transfections were carried out using Lipofectamine LTX (Life

Technologies) according to manufacturer's protocol. Transfections included 2.5 µg DNA for the UPS assay, 5 µg DNA for the Enzo proteasome assay, or 0.1 µg DNA for the Abcam proteasome assay.

Ubiquitinated protein immunoprecipitation

Co-transfected Neuro-2a cells were lysed and total protein was extracted with sonication (10 s, Setting 3, Branson Sonifier 450) in extraction buffer (1% (v/v) Nonidet P-40 in TBS (50 mM Tris-HCl, pH 7.5, 150 mM NaCl) with protease inhibitor cocktail). Cellular debris was pelleted at 18,000×g (30 min at 4°C). Protein concentration was estimated using the BCA Protein Assay Reagent (Pierce Biotechnology). Typically, 3 µg of anti-ubiquitin (Dako) per 500 µg of protein extract was used for immunoprecipitations. Protein A/G magnetic beads (Pierce Biotechnology) were used to capture the antibody:protein complex. Immunoprecipitates were washed with TBS + 1% (v/v) NP-40 (3x) to remove non-specifically bound proteins, and then resuspended in 1x LDS buffer with 50 mM DTT, and heated at 95°C for 10 min.

UPS reporter assay and 20S proteasome activity assay

For the UPS reporter assay, NSC34 cells were cultured in 6-well plates for 24 h, followed by co-transfection with a UPS-specific degron GFP^u and cyclin F constructs. The GFP^u reporter contains a CL1 sequence which signals ubiquitination and degradation by the proteasome^{15,30}. The resulting GFP signal is a reporter for rate of protein degradation in the cell. Cells were collected 48 h post-transfection by trypsin and resuspended in PBS (Sigma-Aldrich). In order to show the sensitivity of GFP^u construct, cells were either transfected with GFP^u for 24 h followed by MG132 (Calbiochem) treatment at various doses for a further 24 h, or co-transfected with GFP^u and mCherry with or without MG132, or lastly co-transfected with GFP^u and either Httex125Q or Httex146Q and incubated for 48 h. The fluorescent intensity GFP in harvested cells was analysed using flow cytometry Becton Dickinson LSR II. At least 50,000 cells per treatment were collected. Data was gated on mCherry positive cells with an excitation at 541 nm and an emission at 575 nm. The

geometric mean of the GFP signal from this population was collected with an excitation at 488 nm and an emission at 520 nm. Data were from three independent experiments.

The proteasome enzymatic activity of cyclin F was measured using either a 20S proteasome assay kit from Enzo Life Sciences or Abcam following the manufacturer's instructions. For the Enzo Life Sciences proteasome activity kit, NSC-34 cells were transfected wild type pmCherry-C1-CCNF or mutant pmCherry-C1-CCNF in 6-well plates and protein extract was generated by freeze-thaw lysis 48 h post-transfection. Protein concentration was measured by BCA protein assay (Thermo Scientific) and equal amount of protein was used in the assay. The proteasome activity was measured by hydrolysis of a fluorogenic peptide substrate Suc-Leu-Leu-Val-Tyr-AMC (AMC: 7-amino-4-methylcoumarin). The substrate is cleaved by the 20S proteasome and the release of free AMC fluorophore is used as an indication of proteolytic activity. The fluorescent signal was measured by FLUOstar OPTIMA fluorescence plate reader (BMG Labtech) with an excitation at 360 nm and an emission at 460 nm. The data was collected at 2 min interval for 50 min. For the Abcam proteasome activity kit, NSC-34 cells were transfected with wild type pmCherry-C1-CCNF or mutant pmCherry-C1-CCNF in 96-well plates for 48 h. A proteasome substrate Leu-Leu-Val-Tyr-R110 was added directly to the cells and incubated at 37 °C for 1 h. The substrate is cleaved by the 20S proteasome and the fluorescent signal generated from the cleavage is used as an indication of proteolytic activity. The fluorescent signal was measured by FLUOstar OPTIMA fluorescence plate reader (BMG Labtech) with an excitation at 490 nm and an emission at 525 nm.

Statistical analysis

All statistical analyses were performed using GraphPad Prism Software. Fisher's exact test was used to determine whether novel non-synonymous variants were overrepresented in patients when compared with controls. One-way ANOVA with Tukey's multiple comparison tests (adjusted $p < 0.05$) were used for grouped GFP^u data (wild type, cyclin F-SNP, cyclin F mutation). One-way ANOVA with Dunnett's multiple comparison tests were used for comparison of GFP^u levels in the

presence of cyclin F variants, with wild type. Statistical analyses of other in vitro assays were performed using two-tail unpaired Student's t-tests ($p < 0.05$). All values were mean \pm s.e.m. Variance was similar between groups. Sample size was chosen based on results from pilot studies.

References

1. Rosen, D. R. *et al.* Mutations in Cu/Zn superoxide dismutase gene are associated with familial amyotrophic lateral sclerosis. *Nature* **362**, 59-62 (1993).
2. Sreedharan, J. *et al.* TDP-43 mutations in familial and sporadic amyotrophic lateral sclerosis. *Science* **319**, 1668-1672 (2008).
3. Vance, C. *et al.* Mutations in FUS, an RNA processing protein, cause familial amyotrophic lateral sclerosis type 6. *Science* **323**, 1208-1211 (2009).
4. Deng, H. X. *et al.* Mutations in UBQLN2 cause dominant X-linked juvenile and adult-onset ALS and ALS/dementia. *Nature* **477**, 211-215 (2011).
5. Wu, C. H. *et al.* Mutations in the profilin 1 gene cause familial amyotrophic lateral sclerosis. *Nature* **488**, 499-503 (2012).
6. Maruyama, H. *et al.* Mutations of optineurin in amyotrophic lateral sclerosis. *Nature* **465**, 223-226 (2010).
7. DeJesus-Hernandez, M. *et al.* Expanded GGGGCC hexanucleotide repeat in noncoding region of C9ORF72 causes chromosome 9p-linked FTD and ALS. *Neuron* **72**, 245-256 (2011).
8. Renton, A. E. *et al.* A hexanucleotide repeat expansion in C9ORF72 is the cause of chromosome 9p21-linked ALS-FTD. *Neuron* **72**, 257-268 (2011).
9. Neumann, M. *et al.* Ubiquitinated TDP-43 in frontotemporal lobar degeneration and amyotrophic lateral sclerosis. *Science* **314**, 130-133 (2006).
10. Robberecht, W., Philips, T. The changing scene of amyotrophic lateral sclerosis. *Nat. Rev. Neurosci.* **14**, 248-264 (2013).

11. D'Angiolella, V. *et al.* SCF(Cyclin F) controls centrosome homeostasis and mitotic fidelity through CP110 degradation. *Nature* **466**, 138-142 (2010).
12. Bai, C. *et al.* SKP1 connects cell cycle regulators to the ubiquitin proteolysis machinery through a novel motif, the F-box. *Cell* **86**, 263-274 (1996).
13. D'Angiolella, V., Esencay, M., Pagano, M. A cyclin without cyclin-dependent kinases: cyclin F controls genome stability through ubiquitin-mediated proteolysis. *Trends Cell Biol.* **23**,135-140 (2013).
14. Ling, S. C., Polymenidou, M. & Cleveland, D. W. Converging Mechanisms in ALS and FTD: Disrupted RNA and Protein Homeostasis. *Neuron* **79**, 416-438 (2013).
15. Bence, N. F., Sampat, R. M., Kopito, R. R. Impairment of the ubiquitin-proteasome system by protein aggregation. *Science* **292**: 1552-1555 (2001).
16. Duennwald, M. L. & Lindquist, S. Impaired ERAD and ER stress are early and specific events in polyglutamine toxicity. *Genes Dev.* **22**, 3308-3319 (2008).
17. Williams, K. L. *et al.* UBQLN2/ubiquilin 2 mutation and pathology in familial amyotrophic lateral sclerosis. *Neurobiol. Aging* **33**, 2527 e2523-2527 (2012).
18. Fecto, F. *et al.* SQSTM1 mutations in familial and sporadic amyotrophic lateral sclerosis. *Arch. Neurol.* **68**,1440-1446 (2011).
19. Weihl, C. C. Valosin containing protein associated fronto-temporal lobar degeneration: clinical presentation, pathologic features and pathogenesis. *Curr. Alzheimer Res.* **8**, 252-260 (2011).
20. Johnson, J. O. *et al.* Exome Sequencing Reveals VCP Mutations as a Cause of Familial ALS. *Neuron* **68**, 857-864 (2010).
21. Zhao, T. *et al.* Loss of nuclear activity of the FBXO7 protein in patients with parkinsonian-pyramidal syndrome (PARK15). *PLOS One* **6**, e16983 (2011).
22. Bandopadhyay, R. & de Belleruche, J. Pathogenesis of Parkinson's disease: emerging role of molecular chaperones. *Trends Mol. Med.* **16**, 27-36 (2010).

23. Brooks, B. R., Miller, R. G., Swash, M. & Munsat, T. L. El Escorial revisited: revised criteria for the diagnosis of amyotrophic lateral sclerosis. *Amyotroph. Lateral Scler. Other Motor Neuron Disord.* **1**, 293-299 (2000).
24. Lathrop, G. M. & Lalouel, J. M. Easy calculations of lod scores and genetic risks on small computers. *Am. J. Hum. Genet.* **36**, 460-465 (1984).
25. Lindner, T. H. & Hoffmann, K. easyLINKAGE: a PERL script for easy and automated two-/multi-point linkage analyses. *Bioinformatics* **21**, 405-407 (2005).
26. Li, H. & Durbin, R. Fast and accurate short read alignment with Burrows-Wheeler transform. *Bioinformatics* **25**, 1754-1760 (2009).
27. Li, H. *et al.* The Sequence Alignment/Map format and SAMtools. *Bioinformatics* **25**, 2078-2079 (2009).
28. Ge, D. *et al.* SVA: software for annotating and visualizing sequenced human genomes. *Bioinformatics* **27**, 1998-2000 (2011).
29. Wang, K., Li, M. & Hakonarson, H. ANNOVAR: functional annotation of genetic variants from high-throughput sequencing data. *Nucleic Acids Res.* **38**, e164 (2010).
30. Bence, N. F., Bennett, E. J. & Kopito, R. R. Application and analysis of the GFPu family of ubiquitin-proteasome system reporters. *Methods Enzymol.* **399**, 481-490 (2005).

Acknowledgments

We thank C. Cecere and M. Edwards for their assistance in compiling family information, J. S. de Belleruche for providing ALS0057 pedigree information, Paul Leo, Emma Duncan and Matthew Brown for access to exome data from the Diamantina Australian Control Collection, Michael Simpson for the assembling and variant calling of the UK exome data, and M. Hallupp for technical assistance. This work was funded by the Motor Neurone Disease Research Institute of Australia (grants to I.P.B. and J.D.A. and a Bill Gole fellowship to K.L.W.), National Health and Medical Research Council of Australia (1004670, 1003032, 1034816, 1006141, 1030513 & 630428), The

Snow Foundation, European Community's Seventh Framework programme (FP7/2007-2013) under the grant agreement number 259867, Medical Research Council, Motor Neuron Disease Association (UK), Heaton-Ellis Trust, NIH/NINDS (1DP2OD0044171, R01 NS065317, P50 AG016574, R01 NS076471, R01 AG026251, P50 NS72187, P01 AG03949, R01NS073873, 1R01NS050557 and RC2-NS070-342), ALS Therapy Alliance, ALS Association, the Milton Safenowitz Post-Doctoral Fellowship for ALS research from the ALS Association (to M.v B.), the Mangurian Foundation, CurePSP, Project ALS, P2ALS, Angel Fund, Pierre L. de Bourgnecht ALS Research Foundation, Al-Athel ALS Research Foundation, CIHR (208973), MDA (153959), ARC Discovery Early Career Award (DE120102840), Fondo de Investigación Sanitaria of Spain (EC08/00049; PI10/00092), FUNDELA (Spanish foundation for the development of ALS research), Mireia Barneda project “No llores, no te rindas”, Midlands Neuroscience Teaching and Research Fund, and AriSLA (co-financed with support of '5x1000' - Healthcare research of the Ministry of Health, grants EXOMEFALS 2009, NOVALS 2012).

Author contributions

K.L.W., S.Y., X.H., V.S., A.G-R., N.J.C., J.J.Y., J.D.A. and I.P.B designed research. K.L.W., S.Y., X.H., V.S., J.A.F., S.T.W., K.Y.Z., N.F., B.S., A.C., C.S.L., C.D-S., C.W., E.D., and M.vB performed the experiments. W.S.B., K.B., J.D.G., N.T., V.S., A.G-R., O.H., K.M., S.T., R.H.B., G.A.R., C.E.S., and G.A.N collected clinical information and samples. All authors contributed to data analysis. K.L.W. and I.P.B. wrote the manuscript with input from all of the authors.

Competing financial interests

The authors declare no competing financial interests.

Table 1. ALS and/or FTD mutations in *CCNF*.

Amino acid change	Nucleotide change	Exon	Cohort	Control samples (Sanger and exome)	Public database MAF
p.S3G	7A>G	1	1/99 US FTLD-ALS	0/1038 US controls 0/657 AU controls 0/967 AU control exomes	Absent
p.K97R	290A>G	4	1/159 UK FALS	0/897 UK controls 0/967 AU control exomes	Absent
p.T181I	542C>T	6	1/283 JA SALS	0/514 JA controls 0/967 AU control exomes	Absent
p.S195R	585T>G	6	1/99 IT FALS	0/967 AU control exomes	Absent
p.R392T	1175G>C	11	1/99 US FTLD	0/1038 US controls 0/967 AU control exomes	Absent
p.S509P	1525T>C	13	1/30 SP FALS 1/168 CA SALS	0/361 CA controls 0/967 AU control exomes	Absent
p.T543I	1628C>T	15	1/283 JA SALS	0/514 JA controls 0/967 AU control exomes	Absent
p.S621G	1861A>G	16	1/75 AU FALS	0/864 AU Sanger controls 0/967 AU control exomes	Absent
p.E624K	1870G>A	16	1/49 US SALS trios	0/801 AU Sanger controls 0/967 AU control exomes	Absent
p.I772T	2315T>C	17	1/159 UK FALS	0/897 UK controls 0/967 AU control exomes	Absent

CCNF accession NM_001761. AU, Australian; SP, Spanish; IT, Italian; CA, Canadian; JA, Japanese; UK, United Kingdom; US, USA; MAF, minor allele frequency. Data was mined from whole exome or genome sequence data and validated by Sanger sequencing.

Figure legends

Figure 1. *CCNF* mutations in ALS-FTD identified following genetic linkage analysis and

exome sequencing. (a) Pedigree of family FALS10. All family members from whom DNA was available for genotyping are indicated by either wild type ('WT') for *CCNF*, or by mutation in *CCNF* ('S621G'). Individuals with ALS are represented by a black filled symbol, individuals with FTD by a grey filled symbol. Arrows indicate samples used for exome sequencing. (b) Sequence traces of WT and c.1861A>G mutation identified in family FALS10. (c) Diagrammatic representation of cyclin F protein and the location of mutations. Cyclin F contains three functional modules within its protein structure. The F-box domain forms a 'pseudocatalytic' module, the two cyclin domains form the substrate recruitment module and the C-terminus contains both a nuclear localisation signal (NLS) and a PEST sequence (short stretch of amino acids enriched in proline, glutamic acid, serine and threonine) that form the regulatory module¹³. (d) Multiple sequence alignment of cyclin F across species showing evolutionary conservation of the substituted amino acid residues (indicated by arrows). Sequences include NP_001752.2 (human), NP_001252844.1 (chimpanzee), NP_031660.3 (mouse), NP_001093944.1 (rat), NP_001092340.1 (cow), NP_001079901.1 (frog) and NP_996931.1 (zebrafish).

Figure 2. Mutant cyclin F impairs ubiquitin-mediated proteasomal degradation. NSC-34 cells were co-transfected with GFP^u and either wild type or mutant cyclin F or cyclin F with SNPs (identified in ALS/FTD patients including those in public databases), tagged with mCherry. GFP^u fluorescence intensity was analysed by flow cytometry 48 h post transfection. (a) Plot of GFP^u fluorescence intensity following flow cytometry. A significantly higher level of GFP^u fluorescence was observed in cells expressing cyclin F mutations when compared to those expressing wt *CCNF* or *CCNF* SNPs. (b) The higher level of GFP^u fluorescence was independent of the level of cyclin F

as quantified using mCherry signal - R-squared = 0.03. Data represent mean, Error bars, \pm s.e.m. $n = 3$; * $P < 0.05$; ** $P < 0.01$; *** $P < 0.001$.

Figure 3. Increased ubiquitinated proteins in neuronal cell lines expressing mutant cyclin F.

NSC-34 and Neuro-2a cells were transfected with wild-type or mutant cyclin F (p.S621G) expression constructs, and cells were harvested after twenty four hours. **(a, b)** Cells transfected with mutant cyclin F (p.S621G) show increased levels (normalized to transfected cyclin F-mCherry) of ubiquitinated proteins and a known cyclin F-SCF complex target, RRM2. **(c)** Immunoprecipitation (IP) of ubiquitinated proteins from transfected Neuro-2a cells (wild-type and mutant cyclin F [p.S621G]) show elevated levels of ubiquitinated RRM2 and TDP-43 in neuronal cells expressing mutant cyclin F. Data represent mean \pm s.e.m. $n=3$; * $P < 0.05$.

SUPPLEMENTARY INFORMATION

Supplementary Tables

Supplementary Table 1. Two-point LOD scores for microsatellite markers from the chromosome 16 minimum candidate disease interval.

Marker	cM	LOD (theta=0)
D16S521	1.14	1.791
D16S3401	1.143	2.3626
D16S3024	5.27	1.8288
D16S3082	9.09	3.0844
D16S475	9.83	2.7667
D16S2622	9.831	2.8871
D16S3065	9.832	3.1604
D16S3134	12.51	1.8828
D16S423	14.05	0.7926
D16S3088	18.34	0.5967
D16S418	19.59	-1.7817
D16S768	22.44	0.5554
D16S404	24.89	-0.3148
D16S3126	25.11	-3.0896

Significant LOD scores are indicated in bold.

Supplementary Table 2. Exome sequencing data summary.

Sample	III:1	II:13
Total reads	44,483,548	61,515,712
Total yield (bp)	4,492,838,348	6,213,086,912
Average read length (bp)	101	101
Mappable reads (=reads mapped to human genome)	39,864,586	55,184,515
Mappable yield (bp)	3,805,291,572	5,246,419,907
% Mappable reads (out of total reads)	89.6%	89.7%
On-target reads (=reads mapped to target regions)	28,906,171	40,199,320
On-target yield (bp)	2,245,981,955	3,120,667,747
% On-target reads (out of mappable reads)	72.5%	72.8%
% On-target reads (out of total reads)	65.0%	65.3%
Target regions (bp)	62,085,286	62,085,286
% Coverage of target regions (more than 1X)	91.4%	92.6%
Number of on-target genotypes (more than 1X)	56,755,078	57,510,293
% Coverage of target regions (more than 10X)	73.0%	80.4%
Number of on-target genotypes (more than 10X)	45,295,674	49,904,527
Median read depth of target regions	28.0X	43.0X
Mean read depth of target regions	36.2X	50.3X
Number of SNPs	56,583	62,581
Number of coding SNPs	16,898	18,499
Number of Indels	11,945	12,824
Number of coding Indels	623	562

Supplementary Table 3. Filtering steps to identify causative gene mutation in ALS family FALS10.

Filter	Variants
Total variants identified	143,933
Present in both affected	46,794
Alters amino acid sequence	5,976
Novel variants	179 (dbSNP and EVS)
Within linkage region chr16p13.3*	1

* No novel variants were identified in linkage regions on chromosomes 11 and 20.

Supplementary Table 4. Characteristics of individuals with *CCNF* mutations.

Family #	Amino acid change	Origin	Diagnosis	Sex	Age of onset (years)	Duration (months)	Site of Onset	Cognitive impairment
FALS10; III:1	S621G	Australia	ALS	M	54	12	Bulbar	
FALS10; II:14	S621G	Australia	ALS	F	61	60	Limb	
FALS10; II:13	S621G	Australia	ALS	F	Died at 81	unknown	Bulbar	
FALS10; II:10	S621G	Australia	FTD	F	Died at 72	unknown		FTD
FALS10; III:15	S621G	Australia	ALS	M	58	>6	Limb	
FALS10; III:4*	S621G	Australia	ALS	M	42	44	Limb	
FALS10; II:2*	S621G	Australia	ALS	F	Died at 74	unknown	unknown	Multiple strokes, dementia
FALS10; II:6*	S621G	Australia	ALS	M	Died at 68	unknown	Limb	
NA09-350	S3G	USA	FTLD-ALS	M	66	14	unknown	FTD
ALS0057	K97R	UK	ALS	F	44	>20	Limb	
ALS0084	I772T	UK	PLS	F	62	unknown	Limb	
SP-37	S195R	Spain	ALS	F	54	21	unknown	
IT	S509P	Italian	ALS	M	57	unknown	Limb	
Sporadic								
	T181I	Japanese	ALS	F	81	unknown	Bulbar	
NA10-205	R392T	USA	FTLD-TDP	M	86	64		FTD
	S509P	French-Canadian	ALS	M	65	unknown	Spinal	unknown
	T543I	Japanese	ALS	F	54	unknown	Bulbar	
	E624K	USA	ALS	F	38	>156	Limb	

*Variant could not be confirmed through sequencing as no DNA was available, however segregation analysis confirmed the presence of the mutation.

Supplementary Table 5. *CCNF* SNPs identified in ALS and/or FTD cohorts.

Amino acid change	Nucleotide change	rs ID	ALS/FTD MAF (population)	Control MAF (n>950)	Public database MAF
p.H69Y [§]	205C>T	Novel	0.002976 (CA SALS)	0	Absent
p.A74T	220G>A	rs4589553	0.006667 (AU FALS)	0	NA (dbSNP)
p.G161R	481G>A	rs148159882	0.019231 (US SALS)	0	NA (dbSNP) 0.000077 (ESP)
p.V318G	953T>G	rs201540325	0.006667 (AU FALS)	0.074744	NA (dbSNP)
p.R344K	1031G>A	rs371050277	0.015152 (JA FALS)	0	NA (dbSNP) 0.000077 (ESP)
p.L372fs [#]	1114_1115insC	Novel	0.006667 (AU FALS)	0	Absent
p.R406Q	1217G>A	rs146438723	0.005051 (US FTLD-MND)	0.002068	NA (dbSNP) 0.001616 (ESP)
p.E528Q	1582G>C	Novel	0.001767 (JA SALS)	0	0.002743 (HGVD)
p.L531R	1592T>C	rs372723774	0.003155 (JA FALS & JA SALS)	0	NA (dbSNP) 0.001667 (HGVD)
p.R574Q	1721G>A	rs369730776	0.002976 (CA SALS)	0	NA (dbSNP) 0.000231 (ESP)
p.F604I	1810T>A	rs118131564	0.012367 (JA SALS)	0.004785	0.000693 (ESP) 0.020202 (1000 genomes) 0.014602 (HGVD)
p.Q669*	2005C>T	rs145521789	0.005051 (US FTLD-MND)	0	NA (dbSNP) 0.000077 (ESP)
p.R691Q	2072G>A	rs148419125	0.001767 (JA SALS)	0	0.000308 (ESP) 0.000459 (1000 genomes) 0.002060 (HGVD)
p.T698M	2093C>T	rs201460257	0.006944 (AU sporadic FTD)	0	0.000 (dbSNP) 0.000459 (1000 genomes)
p.V714M	2140G>A	rs61755288	0.017606 (AU FALS & CA SALS)	0.013220	0.010619 (ESP) 0.005510 (1000 genomes)

CCNF accession NM_001761. AU, Australian; CA, Canadian; JA, Japanese; UK, United Kingdom; US, USA; HGVD, Human Genetic Variation Database (Japanese; <http://www.genome.med.kyoto-u.ac.jp/SnpDB>); NA, not available. §H69Y is listed here because other variants at the H69 codon are present in dbSNP, (including p.H69D, rs369245530). #Variant does not segregate with disease.

Supplementary clinical notes: Additional clinical information for ALS/FTD cases with *CCNF* mutations.

Family FALS10 In the linked ALS/FTD family FALS10, the average age of onset was 53.8 ± 8.3 years (range 42 – 61) and the average duration of disease was 38.7 ± 24.4 months (range 12 – 60 months). Including age information from four at-risk carriers, the age-dependent penetrance in family FALS10 is estimated to be 50% by age 56 and 100% by 61.

FALS10, III:4 The patient started to show symptoms of ALS at age 43 with weakness of movement of right thumb, tiredness, weakness of legs, twitches in muscles, cramping of calves and slurring of speech. No swallowing or breathing difficulty was observed. Examination revealed a mild slurring. There was mild weakness of the palate and pharyngeal muscles. Upper limb weakness was confined to the hands. Wasting was present in the right thenar region and in the abductor digiti minimi. Also weak were the adductor pollicis on the right and the extensor pollicis longus and brevis on both sides, but more on the right. In the lower limbs weakness was confined to the muscles below the knee with the left side more affected. Tibialis anterior, toe extensors and the peronei were considerably affected on both sides. The right tibialis posterior was only mildly affected. No obvious wasting was present in the lower limbs. Widespread occasional fasciculations were noted in all limbs. Sensory examination was normal.

FALS10, II:13 This patient presented with a history of progressive dysarthria with weakness in the arms and legs for several months. Upon examination, the patient had dysarthria, but no tongue fasciculations or weakness. The jaw jerk was present and brisk and cranial nerves were intact. There was some reduction of facial expressions and bradykinesia with mild increased tone in the neck and extremities. The patient had grade 4/5 strength (MRC grading) for shoulder abduction and small muscles of the hands. Proximal leg weakness was also observed. Fasciculation was noted generally in the upper limbs and the right quadriceps. Ankle tendon reflexes were reduced. EMG showed wide spread denervation including the tongue. Nerve conduction studies did not indicate a neuropathy. No dementia is present, but the patient has mild parkinsonian features.

FALS10, III:1 The first symptom observed in this patient was the inability to move the tongue properly. Upon examination, the patient had localized tongue fasciculations that were confirmed by EMG and nerve conduction studies. No other fasciculations were evident, however the patient had extensor planters. There was no evidence of nerve conduction failure. During disease progression, the patient had significant speech problems and fasciculation were evident in the arms and legs.

FALS10, II:4 This patient had asymmetrical muscular atrophy more marked in the right upper limb progressing to the left upper limb. There was bilateral weakness of dorsiflexion of the feet. The disease progressed distally rather than proximally with no convincing upper motor neurone features.

SP-37 Age at onset was about 54.3 years with a duration of illness about 20.5 months. Her father had dementia plus parkinsonism. Her grandmother had generalized weakness (dysphagia and dysarthria) and died at age 75.

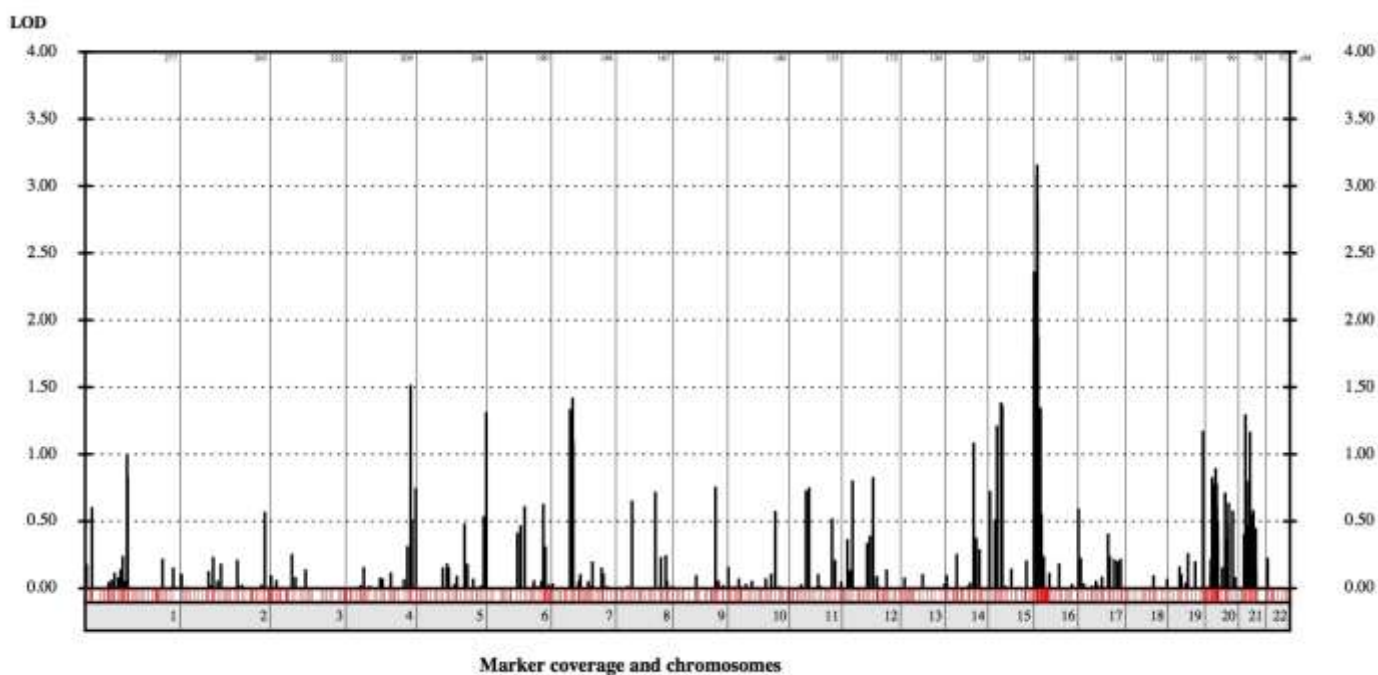
SALS-E624K This woman developed leg weakness at age 38, manifested by difficulty going down stairs. Over the next two years she developed bilateral foot drop along with weakness and atrophy of the left hand and arm. At first examination, 2 years into the illness, she showed spasticity in bilateral lower extremities, as well as significant weakness in the lower extremities and the left hand. Sensory examination was normal and reflexes were pathologically brisk. Her EMG was consistent with diffuse denervating disease. Thirteen years after onset the patient is still alive though severely disabled. No trach or vent. Parents are in their mid-70's and still healthy. The *CCNF* p.E624K variant was also present in the unaffected father, who remains healthy in his mid 70s. No new cases of ALS or other neurodegenerative disease in family.

IT Male, onset at age 57 in his left leg, classic ALS with UMN and LMN signs, no dementia. His mother and a sister of his maternal grandmother had ALS; his maternal grandmother had dementia, while a maternal aunt had PD.

NA09-350 Male, Caucasian. Clinical and pathological diagnosis of FTLN-MND with TDP-43 type 1 pathology. Age at onset was 66.3 years, age at death was 67.5 years. Balance disturbances with falls and personality change (angry, irritable, apathetic, withdrawn). Re: family history of dementia in first degree relative, relevant for mother with Alzheimer disease diagnosed when she was 76 years of age, passing away when she was 86 years of age.

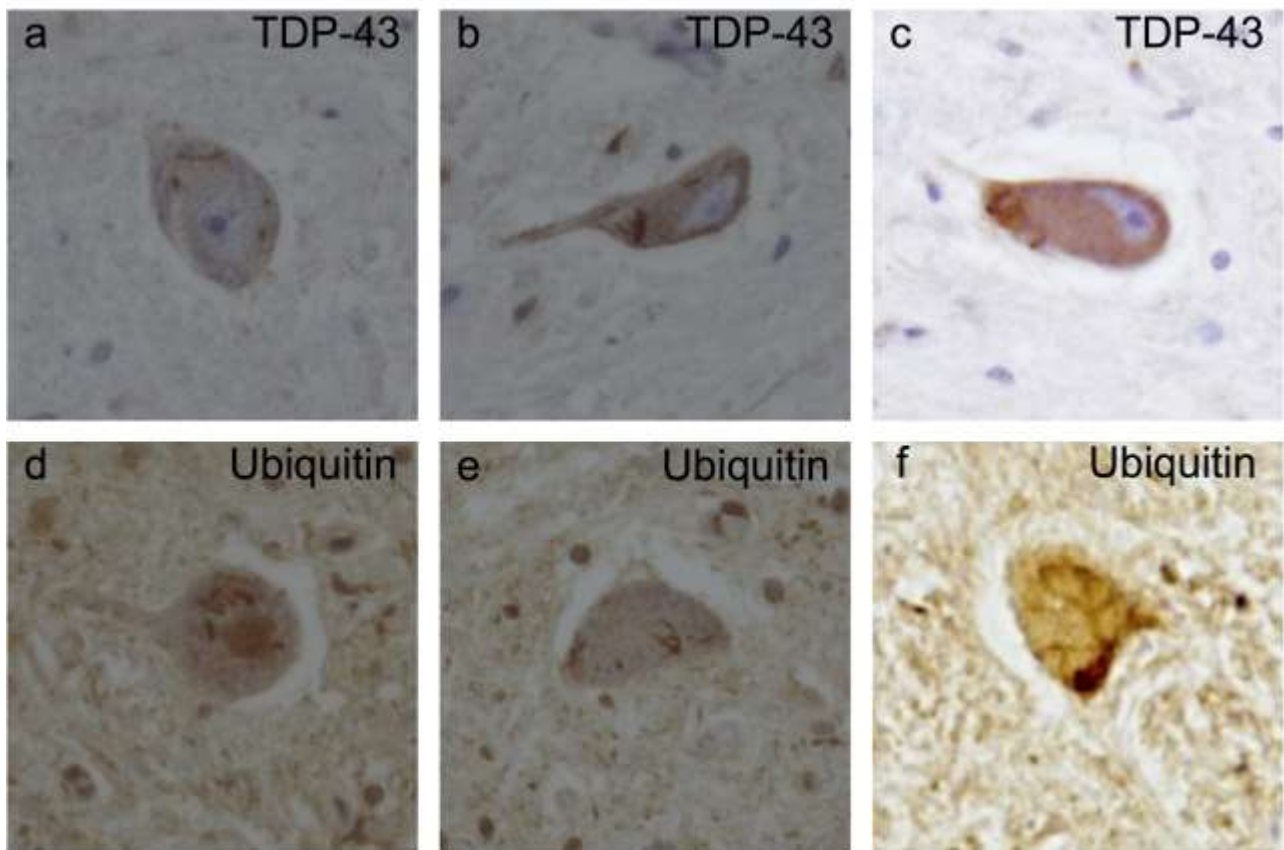
NA10-205 Male, Caucasian. Clinical and pathological diagnosis of FTLN with TDP-43 type 1 pathology. Age at onset was 86.3 years, age at death was 91.7 years. 2005 gait abnormality; lower left heel pain; 2006 memory impairment.

Supplementary Figures

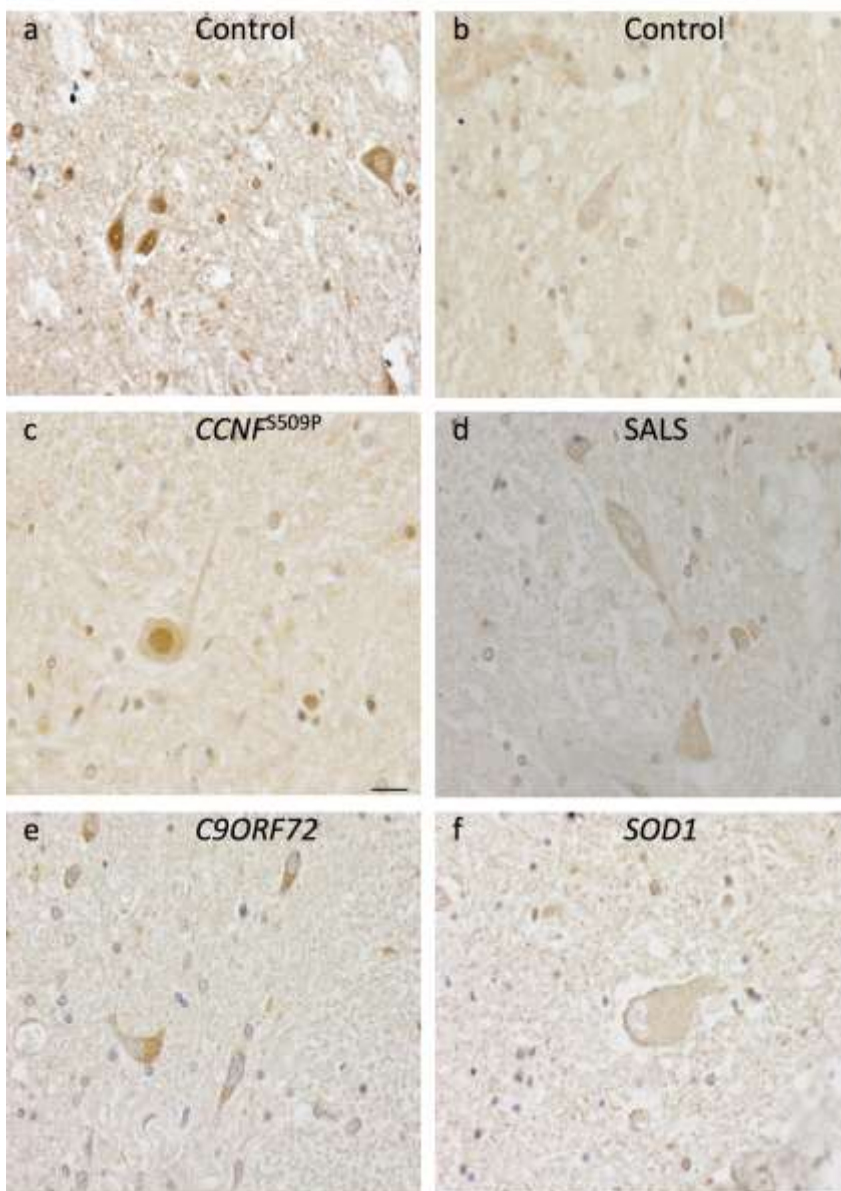


Supplementary Figure 1. Summary of data from genome-wide linkage analysis in family

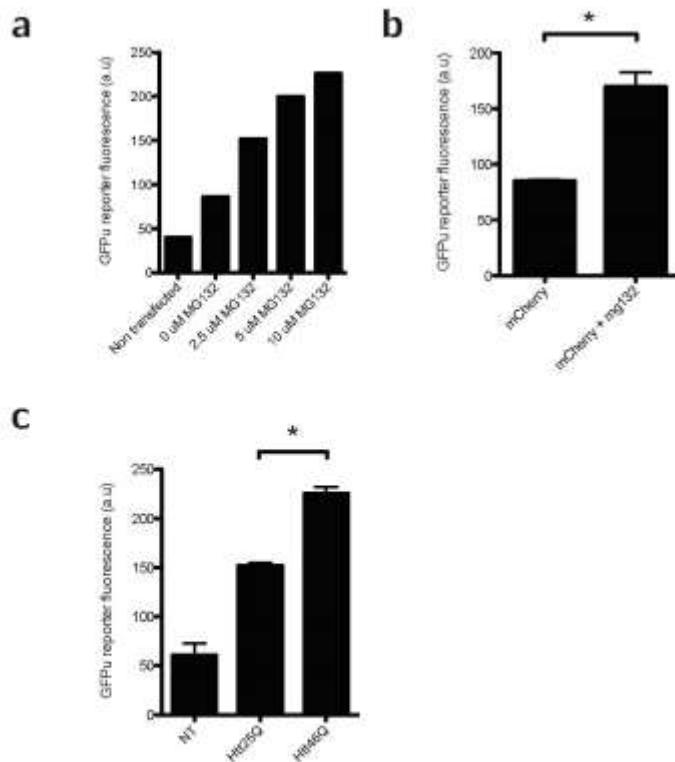
FALS 10. Black vertical lines indicate positive LOD scores. Red vertical lines indicate the microsatellite markers that were genotyped in the family. No X-chromosome marker generated a LOD score > 0 , hence they are not shown.



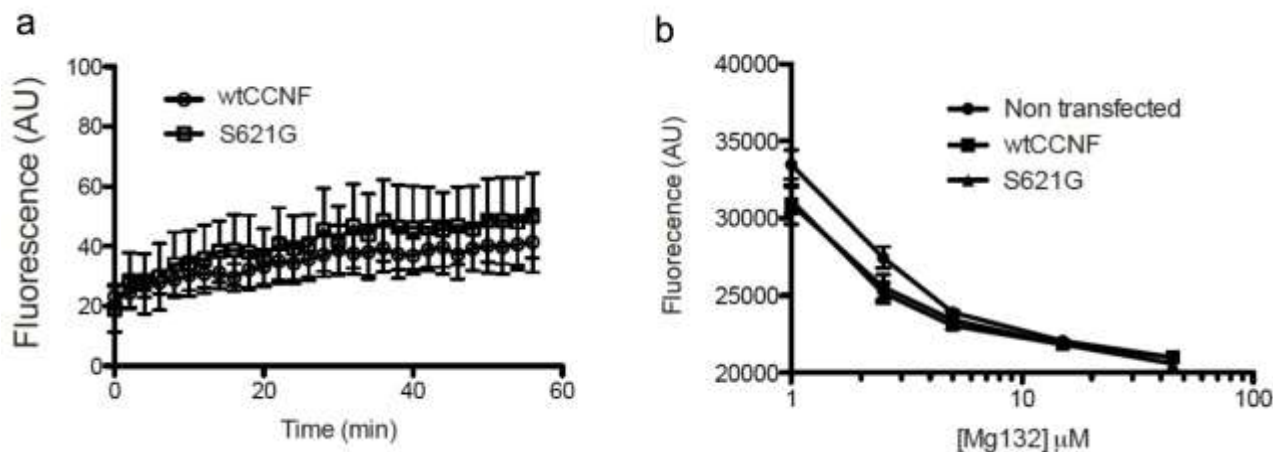
Supplementary Figure 2. TDP-43- and ubiquitin-immunoreactive inclusions in the spinal cord from a patient with a *CCNF*^{S509P} mutation. Sections were analyzed by immunohistochemistry and confocal microscopy using polyclonal antibodies against TDP-43 and ubiquitin. Normal TDP-43 is a predominantly nuclear protein, but in affected neurons of most ALS and FTD patients, TDP-43 is redistributed to the cytoplasm and sequestered as ubiquitinated insoluble inclusions. **(a-c)** Mislocalisation of TDP-43 from the nucleus to the cytoplasm and formation of inclusions. **(d-f)** Ubiquitin-immunoreactive inclusions.



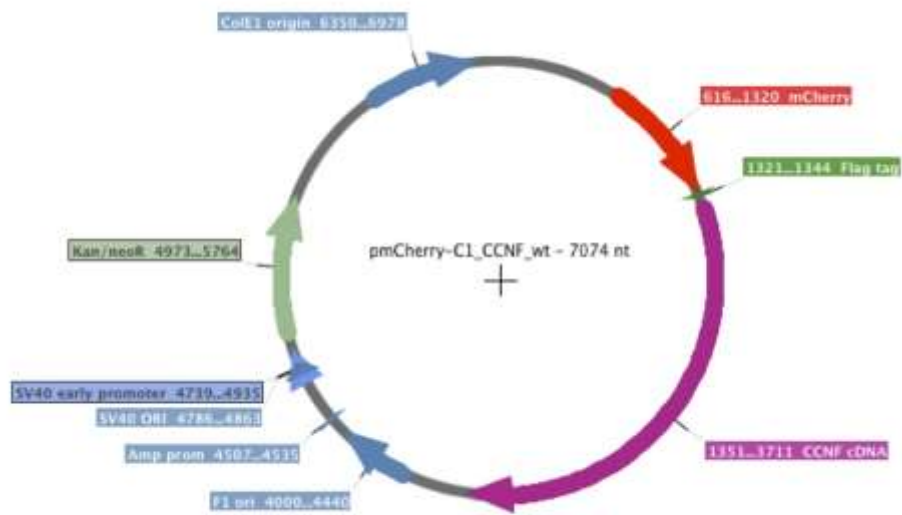
Supplementary Figure 3. Representative immunohistochemical staining of cyclin F in spinal motor neurons. Cyclin F was detected using a polyclonal cyclin F antibody. In contrast to non-neuronal cells, which showed normal nuclear labeling in a variety of tissues, particularly dividing cells, motor neurons showed weaker, mixed nuclear and cytoplasmic staining. No abnormal cyclin F pathology was observed in ALS cases relative to control tissue (**a, b**). Cases included (**c**) ALS patient with CCNF mutation, (**d**) sporadic ALS, (**e**) ALS patient with C9ORF72 repeat expansion, and (**f**) SOD1 mutation. SALS, sporadic ALS.



Supplementary Figure 4. GFP^u signal correlates with UPS function. NSC-34 cells were transfected with GFP^u. The fluorescence intensity of GFP^u was analyzed with flow cytometry. **(a)** Cells were treated with various doses of MG132 at 24 h post-transfection and incubated for a further 24 h before analysis. A dose-dependent increase of GFP^u fluorescence was observed when proteasome function was inhibited by MG132. **(b)** NSC-34 cells were co-transfected with GFP^u and empty pmCherry vector. After 24 h, cells were treated with 5 μ g/ml MG132 and incubated for a further 24 h before analysis. A significant accumulation of GFP^u fluorescence was found, indicating that co-transfection with pmCherry did not affect proteostasis of GFP^u. **(c)** NSC-34 cells were co-transfected with Huntingtin exon1 fragments containing an expanded polyQ (Htt25Q and Htt46Q). The fluorescence was measured 48 h post-transfection. Htt25Q and Htt46Q have been previously shown to inhibit the proteasome. A significant increase of GFP^u fluorescence was observed. Data are mean \pm s.e.m. $n = 3$; * $P < 0.05$.



Supplementary Figure 5. Dysfunction of ubiquitin-mediated degradation was not due to altered proteasome activity. NSC-34 cells were transfected with either wild type or mutant *CCNF* tagged with mCherry. Proteasome enzymatic activity was measured by fluorogenic proteasome assays 48 h post-transfection. **(a)** Protein lysate was generated from transfected NSC-34 cells and the kinetics of 20S proteasome chymotrypsin-like protease activity was measured using the Suc-LLVY-AMC fluorogenic peptide substrate (Enzo Life Sciences). Fluorescence changes were measured at 2 min intervals for 50 min. No significant difference was found between wild type and mutant cyclin F. **(b)** Proteasome activity was measured in intact NSC-34 cells using a cell permeable proteasome substrate (Abcam). No significance difference was found between wild type and mutant cyclin F. Data represent mean \pm s.e.m. $n = 3$.



Supplementary Figure 6. Plasmid map of cyclin F expression construct.

Figure 1 (Blair)

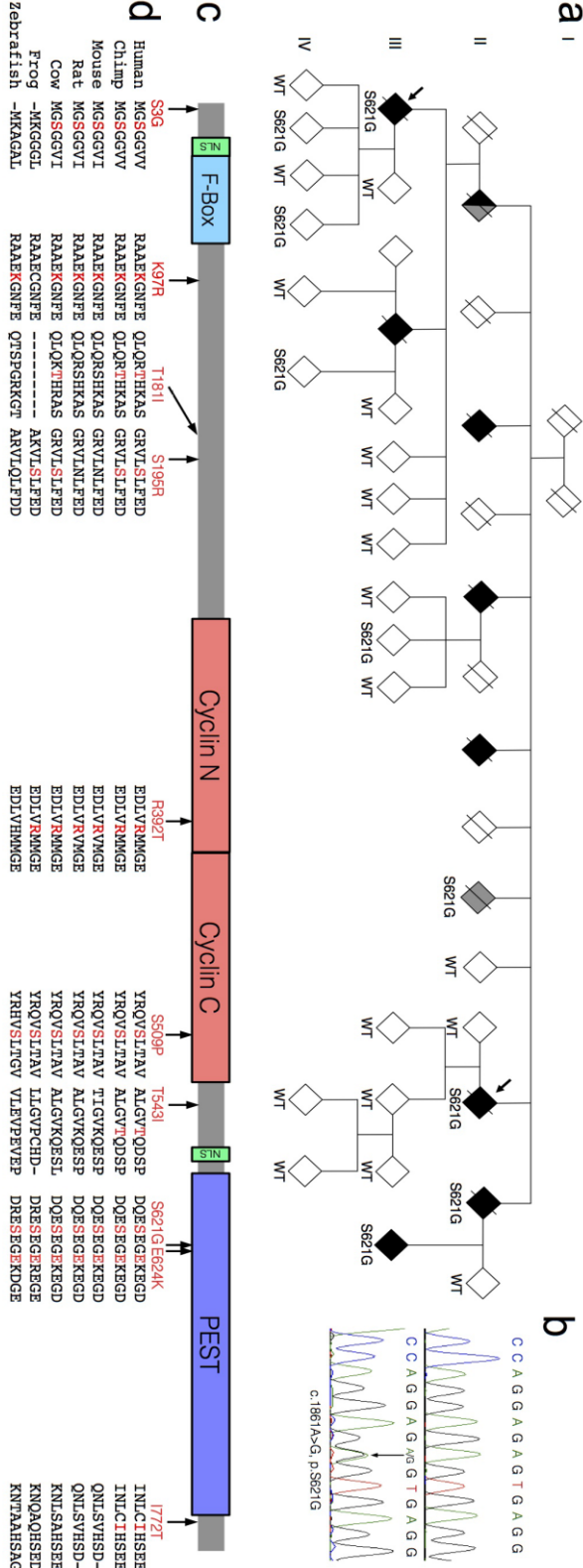


Figure 2 (Blair)

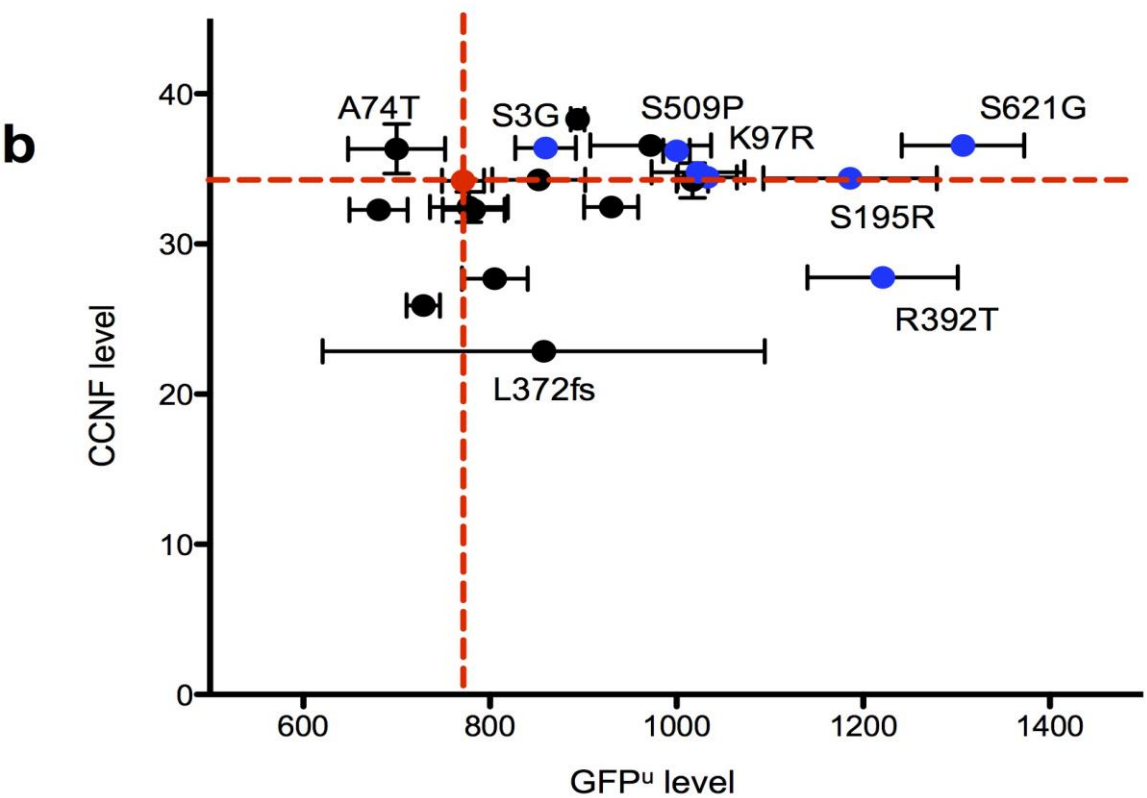
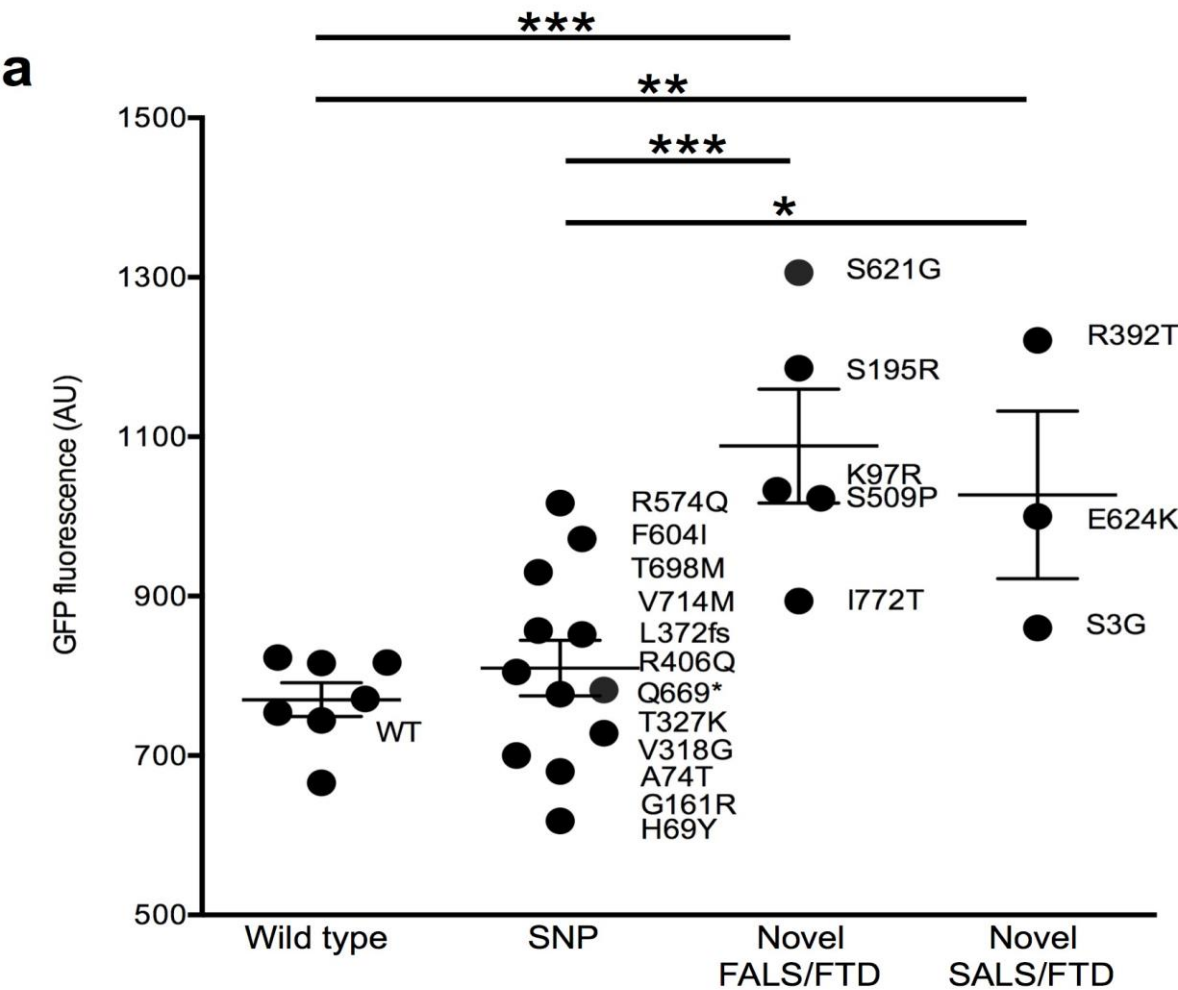
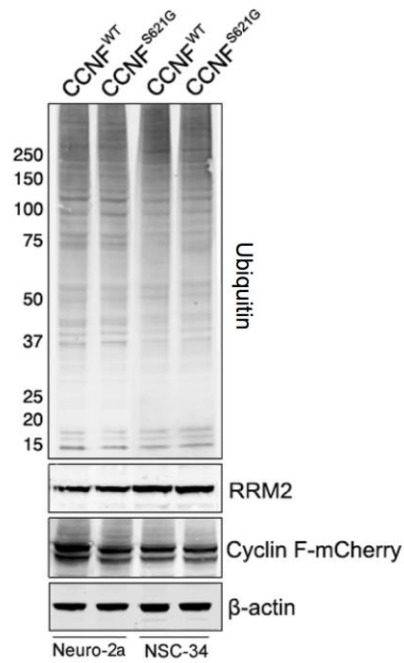
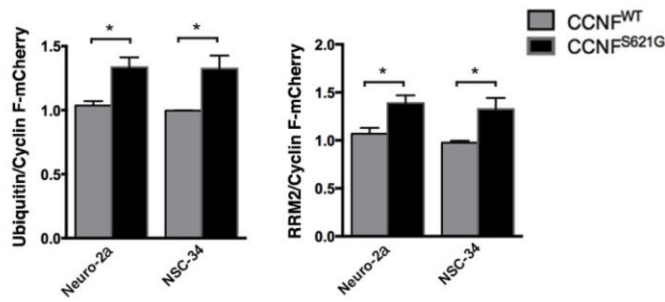


Figure 3 (Blair)

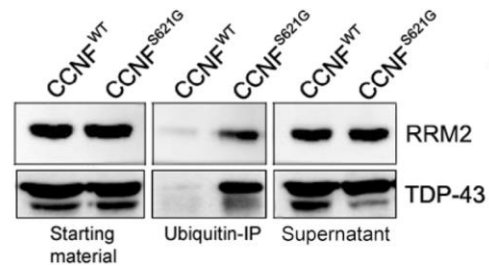
a



b



c



Appendix 2

C9ORF72, implicated in amyotrophic lateral sclerosis and frontotemporal dementia, regulates endosomal trafficking

Manal A. Farg¹, Vinod Sundaramoorthy¹, Jessica M. Sultana¹, Shu Yang³, Rachel A.K. Atkinson⁵, Vita Levina¹, Mark A. Halloran², Paul A. Gleeson⁴, Ian P. Blair³, Kai Y. Soo¹, Anna E. King⁵ and Julie D. Atkin^{1,*}

¹Department of Biochemistry, ²Department of Neuroscience, School of Psychological Science, La Trobe University, Victoria, Australia, ³Australian School of Advanced Medicine, Macquarie University, Sydney, NSW, Australia, ⁴Department of Biochemistry and Molecular Biology, Bio21 Molecular Science and Biotechnology Institute, The University of Melbourne, Victoria, Australia, and ⁵Wicking Dementia Research and Education Centre, University of Tasmania, Hobart, Tasmania, Australia

Received October 14, 2013; Revised January 13, 2014; Accepted February 10, 2014

Intronic expansion of a hexanucleotide GGGGCC repeat in the chromosome 9 open reading frame 72 (C9ORF72) gene is the major cause of familial amyotrophic lateral sclerosis (ALS) and frontotemporal dementia. However, the cellular function of the C9ORF72 protein remains unknown. Here, we demonstrate that C9ORF72 regulates endosomal trafficking. C9ORF72 colocalized with Rab proteins implicated in autophagy and endocytic transport: Rab1, Rab5, Rab7 and Rab11 in neuronal cell lines, primary cortical neurons and human spinal cord motor neurons, consistent with previous predictions that C9ORF72 bears Rab guanine exchange factor activity. Consistent with this notion, C9ORF72 was present in the extracellular space and as cytoplasmic vesicles. Depletion of C9ORF72 using siRNA inhibited transport of Shiga toxin from the plasma membrane to Golgi apparatus, internalization of TrkB receptor and altered the ratio of autophagosome marker light chain 3 (LC3) II:LC3I, indicating that C9ORF72 regulates endocytosis and autophagy. C9ORF72 also colocalized with ubiquitin-2 and LC3-positive vesicles, and co-migrated with lysosome-stained vesicles in neuronal cell lines, providing further evidence that C9ORF72 regulates autophagy. Investigation of proteins interacting with C9ORF72 using mass spectrometry identified other proteins implicated in ALS; ubiquitin-2 and heterogeneous nuclear ribonucleoproteins, hnRNP A2/B1 and hnRNP A1, and actin. Treatment of cells overexpressing C9ORF72 with proteasome inhibitors induced the formation of stress granules positive for hnRNP A1 and hnRNP A2/B1. Immunohistochemistry of C9ORF72 ALS patient motor neurons revealed increased colocalization between C9ORF72 and Rab7 and Rab11 compared with controls, suggesting possible dysregulation of trafficking in patients bearing the C9ORF72 repeat expansion. Hence, this study identifies a role for C9ORF72 in Rab-mediated cellular trafficking.

INTRODUCTION

Amyotrophic lateral sclerosis (ALS) is characterized by degeneration of upper and lower motor neurons in the brain, brainstem and spinal cord, leading to progressive paralysis. Frontotemporal dementia (FTD) is the second most common cause of pre-senile dementia (1) and increasing evidence suggests that ALS

and FTD overlap, occupying two opposite poles of disease continuum (2–4). Hexanucleotide (GGGGCC) repeat expansions in a non-coding region of chromosome 9 open reading frame 72 (C9ORF72) are the major cause of familial ALS (~33%) and FTD (~25%) worldwide and are present in 8% of sporadic ALS cases, highlighting a major role for C9ORF72 in neurodegeneration (5–7). The normal cellular function of C9ORF72

* To whom correspondence should be addressed at: Dr Julie Atkin, La Trobe Institute for Molecular Science, Department of Biochemistry, School of Molecular Sciences, La Trobe University Bundoora. Tel: +03 9479 5480; Fax: +03 9479 2467; Email: j.atkin@latrobe.edu.au

remains unknown but it is highly conserved and expressed in many tissues, including the cerebellum, cortex and spinal cord. Similarly, it remains unclear how C9ORF72 repeat expansions trigger ALS pathology, although haploinsufficiency due to impaired transcription/splicing, leading to reduced C9ORF72 protein expression (up to 50%) (8), RNA dysfunction, and unconventional translation of the repeat to generate insoluble polypeptides, are possible mechanisms (9,10).

Rab GTPases regulate membrane trafficking events and efficient intracellular trafficking is essential for cellular viability (11). Rab GTPases are master regulators of nearly all membrane traffic through their interactions with vesicular coat components, motor proteins and SNARE proteins. In humans, there are >60 members of the Rab family that are localized to distinct intracellular membranes. Rabs alternate between two conformational states: the activated guanosine tri-phosphate (GTP)-bound form and the guanosine di-phosphate (GDP)-bound inactive form. Exchange of GDP with GTP is catalyzed by Rab guanine nucleotide exchange factors (GEFs) that act at specific membranes and facilitate GDP release, thus locally activating their targets. DENN (differentially expressed in normal and neoplastic cells) domain-containing proteins are RabGEFs that activate mostly endocytotic Rabs (12). Two recent bioinformatics studies predicted that C9ORF72 possesses DENN domains (13,14), raising the possibility that it regulates Rab-dependent intracellular trafficking (12). The endosomal system is necessary for regulating, sorting and degrading proteins via autophagy or the ubiquitin–proteasome system (UPS) (15). Multiple Rabs have been implicated in autophagy including Rab1, Rab5, Rab7 and Rab11 (16–18).

Defects in protein degradation are increasingly implicated in ALS pathogenesis (19) and mutations in ubiquilin-2 (20), which regulates autophagy and the UPS by binding/transport of protein cargo (21), also cause ALS/FTD. Inhibition of the proteasome induces the formation of stress granules (SGs) (22), a cellular hallmark of ALS (23). Recently, mutations in heterogeneous nuclear ribonucleoproteins hnRNP2/B1 and hnRNP1 were identified in ALS patients (24). hnRNPs granules are major components of SGs that mediate nucleocytoplasmic trafficking of mRNA and RNA metabolism (25). Inhibition of the proteasome triggers alternative splicing of hnRNPs and mRNA-bound hnRNP1 is recruited to cytoplasmic SGs (26).

Elucidation of the function of C9ORF72 is essential to understand its role in ALS/FTD. Here, we demonstrate a role for C9ORF72 in endosomal trafficking. C9ORF72 colocalized with ubiquilin-2 and Rab proteins implicated in autophagy, and co-migrated with lysosome-positive vesicles. Depletion of C9ORF72 using siRNA dysregulated autophagy and inhibited endocytosis. Mass spectrometry identified other proteins linked to ALS as interacting partners of C9ORF72: hnRNP1, hnRNP2/B1, ubiquilin-2 and actin. Proteasome inhibition and C9ORF72 overexpression led to the formation of nuclear C9ORF72 aggregates and cytoplasmic SGs positive for hnRNP1 and hnRNP2/B1. Hence, this study defines novel functions for C9ORF72 in cellular trafficking and protein degradation.

RESULTS

C9ORF72 colocalizes and interact with Rabs in neuronal cell lines

To characterize C9ORF72, we examined expression of endogenous C9ORF72 in neuronal cell lines; murine neuro2a and human

SH-SY5Y. Immunofluorescence was present diffuse in the nucleus and as cytoplasmic vesicles (Fig. 1A and B). Similarly, in cells transfected with a construct-encoding GFP-tagged C9ORF72 (Fig. 1C), both nuclear protein and cytoplasmic vesicles were observed (Fig. 1C). The cellular distribution of endogenous C9ORF72 was investigated further using subcellular fractionation of SH-SY5Y cell lysates. Using immunoblotting, we detected that significantly more C9ORF72 was present in the nucleus compared with the cytoplasm (Fig. 1D and E); 64%, $P < 0.05$). C9ORF72 in the nuclear fraction was present as the 50 kDa isoform; however, in the cytoplasmic fraction, lower molecular weight bands were present in addition to the 50 kDa band, possibly representing the 25 kDa isoform (Fig. 1D). We also detected C9ORF72 in conditioned medium, suggesting active secretion (Fig. 1F), presumably via non-classical means because bioinformatics analysis predicted that a signal leader peptide was not present in C9ORF72 (Secretome P) (27). This was confirmed by immunoblotting of human CSF (Fig. 1G).

C9ORF72 expression in vesicles suggests a possible role in cellular trafficking, consistent with RabGEF function. This was investigated using immunocytochemistry for Rab proteins. C9ORF72 colocalized strongly with Rabs implicated in autophagy and endosomal transport: Rab1, Rab7, Rab5 and Rab11 (Fig. 2A). Similarly, C9ORF72 co-immunoprecipitated with Rab1, Rab7 and Rab11 (Fig. 2B); control immunoprecipitations using isotype-matched antibodies were negative. This was confirmed by precipitations using GFP-Trap in the reverse direction, with cell lysates transfected with Rab-GFP constructs (Supplementary Material, Fig. S1). Similarly, C9ORF72 was precipitated using GFP-Trap from cells transfected with Rab5-GFP, although we could not determine if Rab5 precipitated with C9ORF72 antibodies due to species cross-reactivity with the available antibodies. However, these findings suggest a physical interaction between C9ORF72 and Rab proteins, consistent with predictions that C9ORF72 is a RabGEF.

We examined the expression of C9ORF72 further in primary cortical neurons obtained from C57Bl/6 mice. C9ORF72 was present both in the nucleus and in vesicles, similar to its expression in neuronal cell lines (Fig. 3A). Immunocytochemistry using Rab5, Rab7 and Rab11 antibodies revealed that C9ORF72-positive vesicles frequently colocalized with Rab5, Rab7 and Rab11 (Fig. 3B). Interestingly, we detected colocalization of C9ORF72 with Rab7 in the axon and the cell body. These data provide further evidence that C9ORF72 has a role in protein trafficking with multiple Rab proteins (Fig. 3A and B). To further validate the interaction between Rab proteins and C9ORF72, C9ORF72-GFP was expressed in neuro2a cells and immunostaining with Rab5 was performed. Rab5 and GFP-tagged fluorescent C9ORF72 vesicles were clearly colocalized in these cells (Supplementary Material, Fig. S2).

Rab7 and Rab11 colocalize in C9ORF72 human spinal cord motor neurons

These findings were investigated further using immunohistochemistry of human spinal cord sections. Quantitative analysis of 30+ motor neurons in control patients revealed that C9ORF72 colocalized with Rab5 (60%), Rab7 (70%) and Rab11 (60%), consistent with the findings obtained from cell

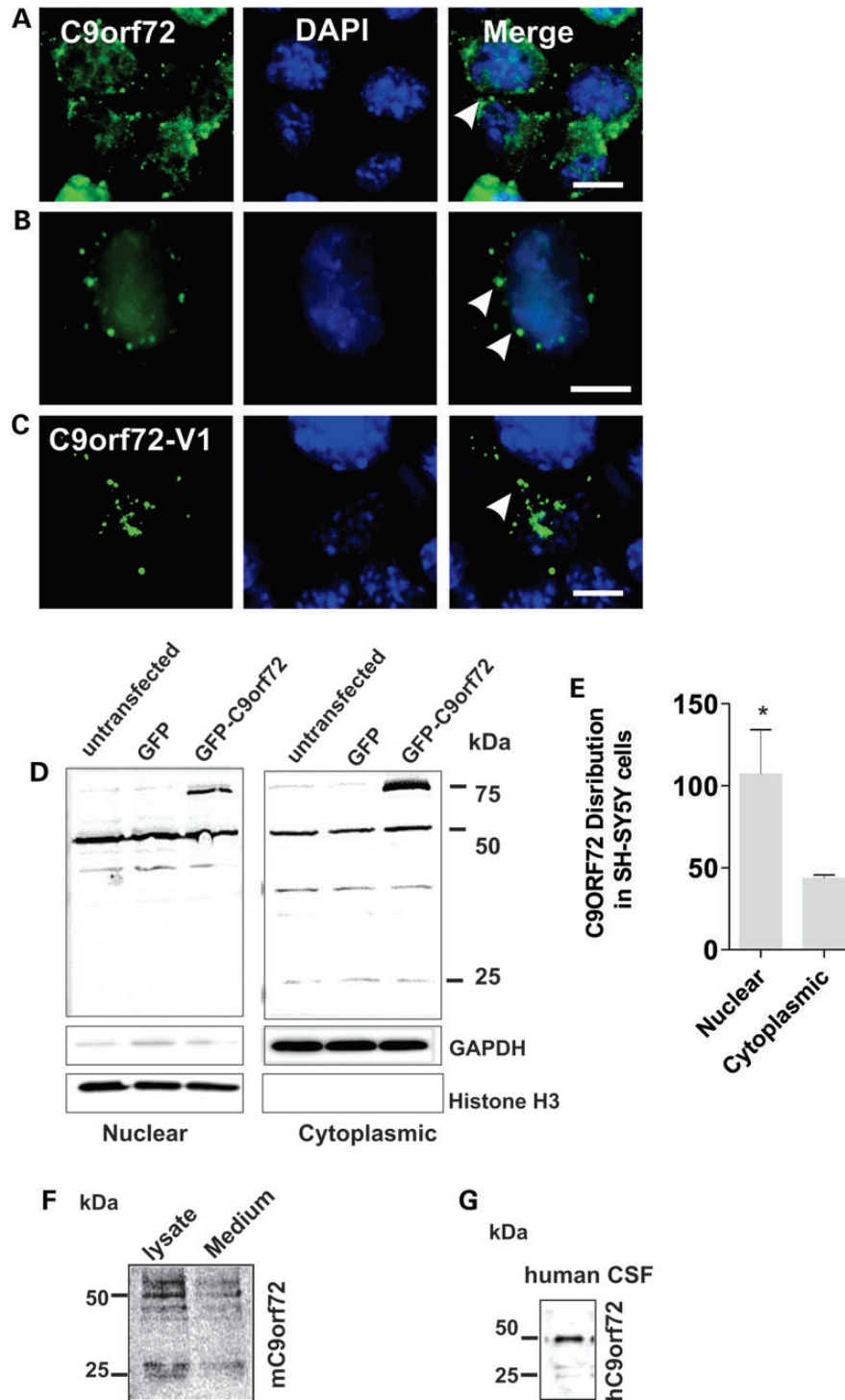


Figure 1. C9ORF72 expression and secretion in neuronal cell lines. (A) Murine Neuro2a cells were fixed and immunostained with anti-C9ORF72 antibodies (green) and DAPI (blue); scale bar: 10 μ m. White arrows indicate C9ORF72-positive vesicular-type structures present in the cytoplasm; expression of C9ORF72 is diffuse in the nucleus. (B) Human SH-SY5Y cells were fixed and immunostained with anti-C9ORF72 antibodies (green) and DAPI (blue), expression of C9ORF72 is similar to (A). Scale bar: 10 μ m. White arrows indicate C9ORF72-positive vesicular-type structures present in the cytoplasm. (C) Overexpression of C9ORF72-Variant 1 tagged with GFP in SH-SY5Y cells forms cytoplasmic vesicles. (D) Subcellular fractionation of human SH-SY5Y neuroblastoma cells; immunoblotting of nuclear and cytoplasmic fractions. Histone H3 and GAPDH were used as subcellular markers and loading controls for nucleus and cytoplasm, respectively. C9ORF72 is expressed primarily as the 50 kDa isoform in the nucleus, additional bands are present in the cytoplasmic fraction at 25 and 36 kDa. (E) Quantification of endogenous C9ORF72 present in the nuclear and cytoplasmic fraction by densitometry of immunoblots. Data are represented as mean \pm SEM; $^*P < 0.05$, $n = 3$ nuclear versus cytoplasmic by unpaired t -test. (F) C9ORF72 isoforms (50 and 25 kDa) are present in conditioned medium of Neuro2a cells immunoprecipitated using an anti-C9ORF72 antibody; cell lysate fraction shown as a control. (G) C9ORF72 is secreted in human CSF. Immunoblotting with C9ORF72 antibody detects both C9ORF72 isoforms, corresponding to 50 and 25 kDa proteins.

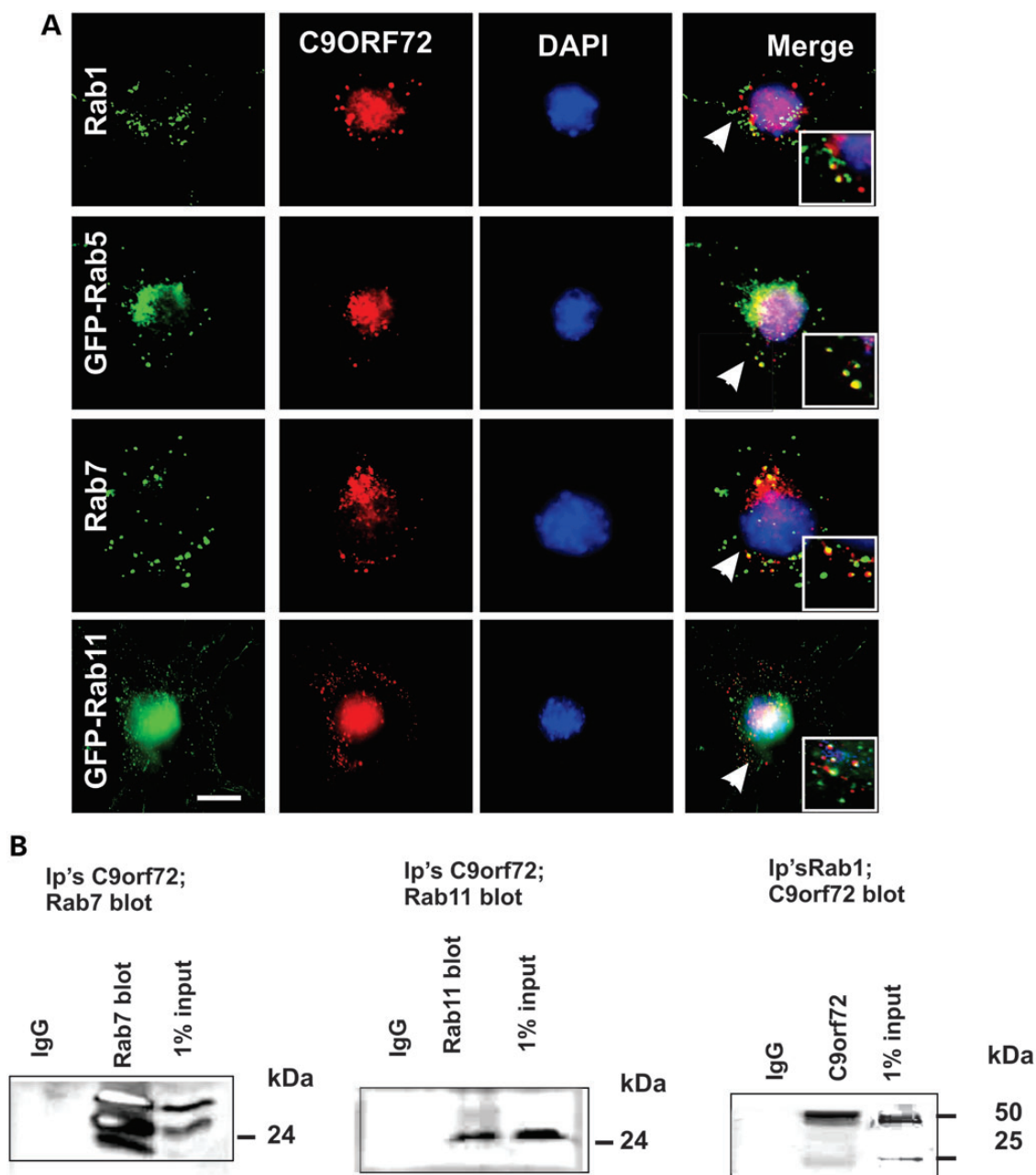


Figure 2. C9ORF72 colocalizes with endosomal Rabs; Rab1, Rab5, Rab7 and Rab11 in neuronal cell lines. **(A)** Neuro2a cells were fixed and immunostained with anti-C9ORF72 antibodies (red) and either anti-Rab7 or anti-Rab1 antibodies (green), or transfected with constructs encoding either GFP-Rab5 or GFP-Rab11 for 48 h, followed by DAPI staining (blue). The white arrows indicate regions of colocalization between C9ORF72 and the respective Rabs. Scale bar: 10 μ m, applied to all fields. Insets demonstrate higher magnification ($\times 100$) of the areas highlighted to illustrate colocalization with vesicular structures. **(B)** Co-immunoprecipitation followed by western blotting revealed that Rab7 and Rab11 are pulled down using anti-C9ORF72 antibodies, and that C9ORF72 is pulled down using anti-Rab1 antibodies. Control immunoprecipitations using an isotype-matched, irrelevant IgG antibody were negative, indicating no cross-reactivity with the antibodies used. 1% input also shown.

lines (Fig. 4A and B), confirming that C9ORF72 colocalizes with Rab proteins. Quantitation of motor neurons from an ALS patient with the C9ORF72 hexanucleotide repeat expansion revealed an increased proportion of cells with colocalization of C9ORF72 with Rab7 or Rab11 compared with controls ($P < 0.05$) (Fig. 4B). These data suggest possible dysregulation of endosomal trafficking in ALS patients with the C9ORF72 hexanucleotide repeat expansion.

C9ORF72 regulates endocytosis in neuronal cell lines

Next, to examine if C9ORF72 regulates endocytosis, human neuronal SH-SY5Y cells were treated with short interfering RNA (siRNA) duplexes to silence human C9ORF72 expression. Using immunoblotting, C9ORF72 levels were depleted by 30%, i.e. to 70% of the original expression level, without obvious off-target effects, as indicated by no change in the levels of

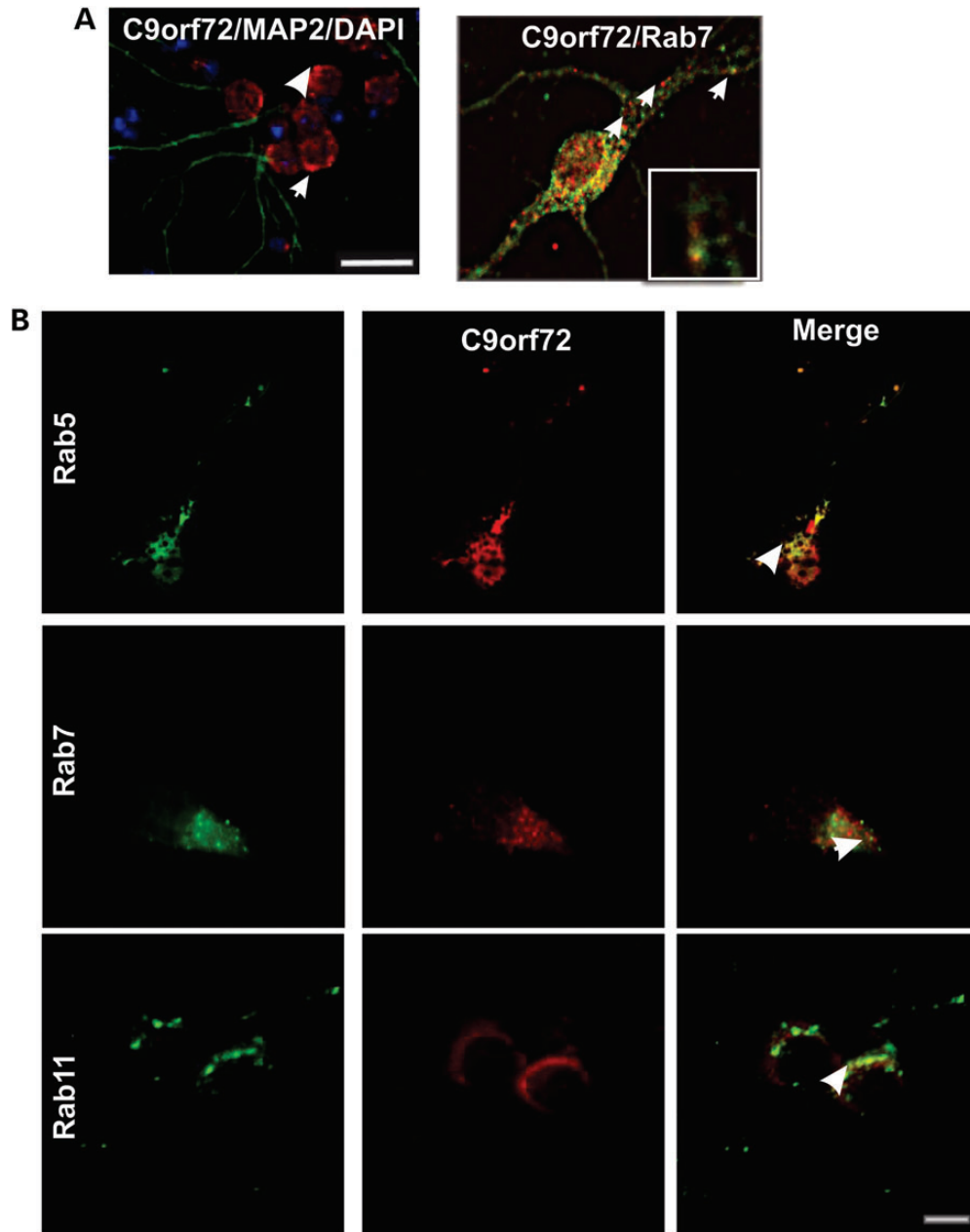


Figure 3. C9ORF72 colocalizes with Rab5, Rab7 and Rab11 in primary neurons. Primary cortical neuronal cells were obtained from the cerebrum of C56/Bl6 mice at E15.5; cortical tissue was dissected from E15.5 mouse embryos and dissociated using 0.0125% trypsin. Tissue was washed in cell plating media, and cells were plated onto poly-L-lysine-coated 12 mm coverslips in 24-well plates at a concentration of 30 000 cells per coverslip. (A) Cells were fixed and immunostained with anti-C9ORF72 antibodies (red), neuronal marker microtubule-associated protein 2 (MAP2) (green), and DAPI (blue). Scale bar: 10 μm. White arrows indicate C9ORF72-positive vesicular structures present in the cytoplasm and axons. (B) Cells were fixed and immunostained with anti-C9ORF72 antibodies (red) and either anti-Rab5 or anti-Rab7 or anti-Rab11 antibodies (green), the white arrows indicate regions of C9ORF72 and the respective Rab immunoreactivity. Scale bar: 10 μm, applied to all fields.

β-actin (Fig. 5A). Endocytosis was examined using Shiga toxin subunit B (STxB), an endocytosis marker, conjugated to Cy3, which traffics from the plasma membrane to Golgi network (28). Mander's overlap coefficient (29) was calculated to quantify colocalization between STxB and cis-Golgi marker GM130, detected immunocytochemically. In cells depleted of C9ORF72, transport of STxB-Cy3 to the Golgi apparatus was inhibited by 18% (Fig. 5B and C; $P < 0.01$) compared with cells treated

with control siRNA. Hence, C9ORF72 regulates an endocytotic pathway used by Shiga toxin to reach the cis-Golgi network. To confirm this finding, we also examined endocytosis of TrkB receptor by cell surface biotinylation in SH-SY5Y cells depleted of C9ORF72 by 80% using two successive siRNA transfections (Fig. 5D). C9ORF72 depleted cells expressing FLAG-tagged TrkB were biotinylated for 30 min at 4°C. Endocytosis of biotinylated TrkB receptor was then induced by incubation with

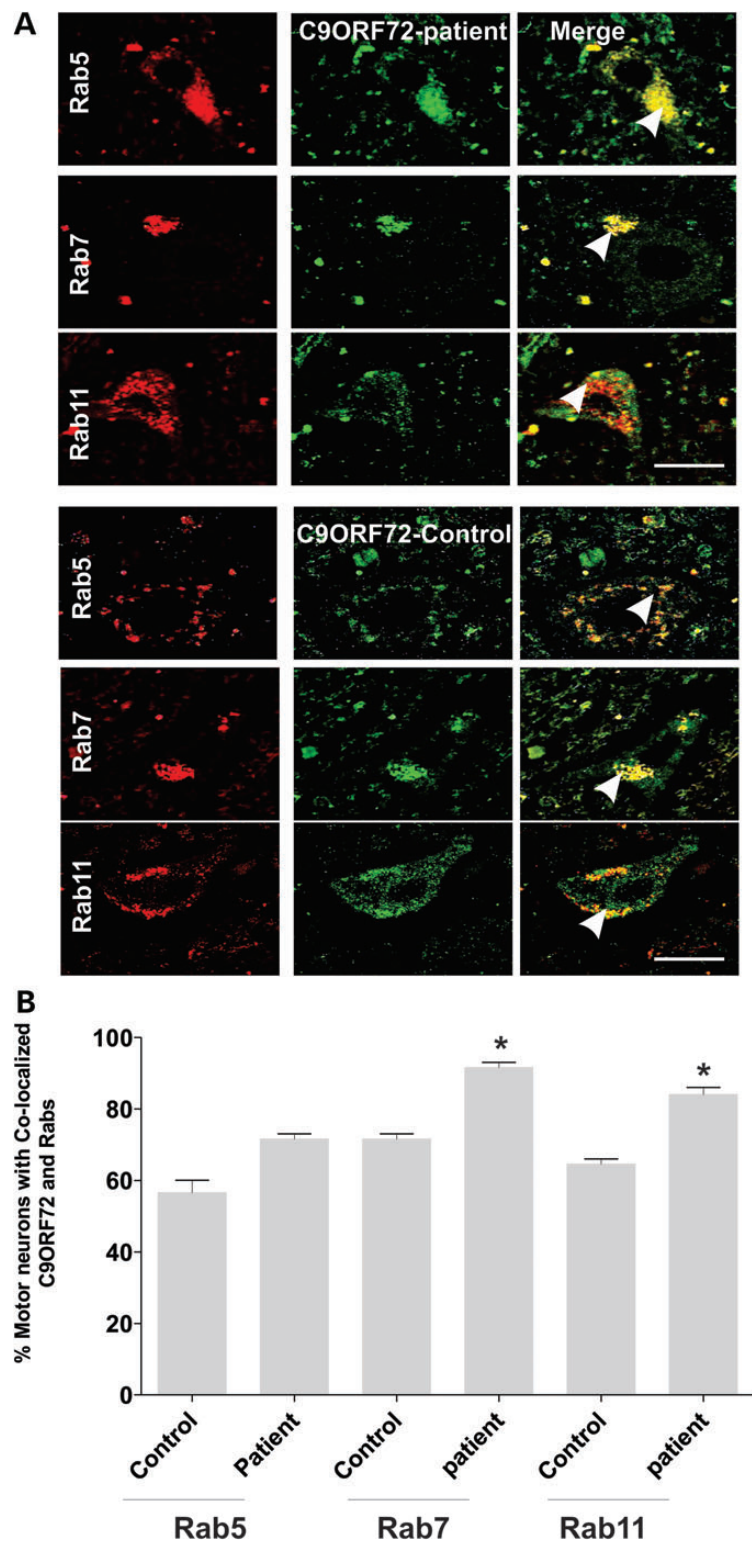


Figure 4. Colocalization of Rab 5, Rab 7 and Rab 11 in human spinal cord motor neurons in an ALS patient with C9ORF72-intronic repeat expansion mutation. **(A)** Immunohistochemistry of human postmortem spinal cord sections from a control individual without neurological disorders and a human ALS patient bearing C9ORF72-intronic mutation. Human postmortem spinal cord sections (5 μ m) were immunostained with anti-Rab11, anti-Rab5 or anti-Rab7 (first column) antibodies and anti-C9ORF72 antibodies (second column). Merge (third column) indicates overlays of the fluorescent confocal images of C9ORF72 and each Rab. White arrow indicates areas of colocalization between C9ORF72 and Rabs in both control and ALS patient tissues. Scale bar: 20 μ m, applied to all fields. **(B)** Quantification of motor neurons containing colocalized C9ORF72 and Rabs reveals an increased proportion of motor neurons in which C9ORF72 colocalized with Rab11 or Rab7 in tissues from an ALS patient bearing the C9ORF72 repeat expansion compared with a control patient. Fifty motor neuron cells were scored for each population. Data are represented as mean \pm SEM; * P < 0.05, ALS versus control by unpaired t -test.

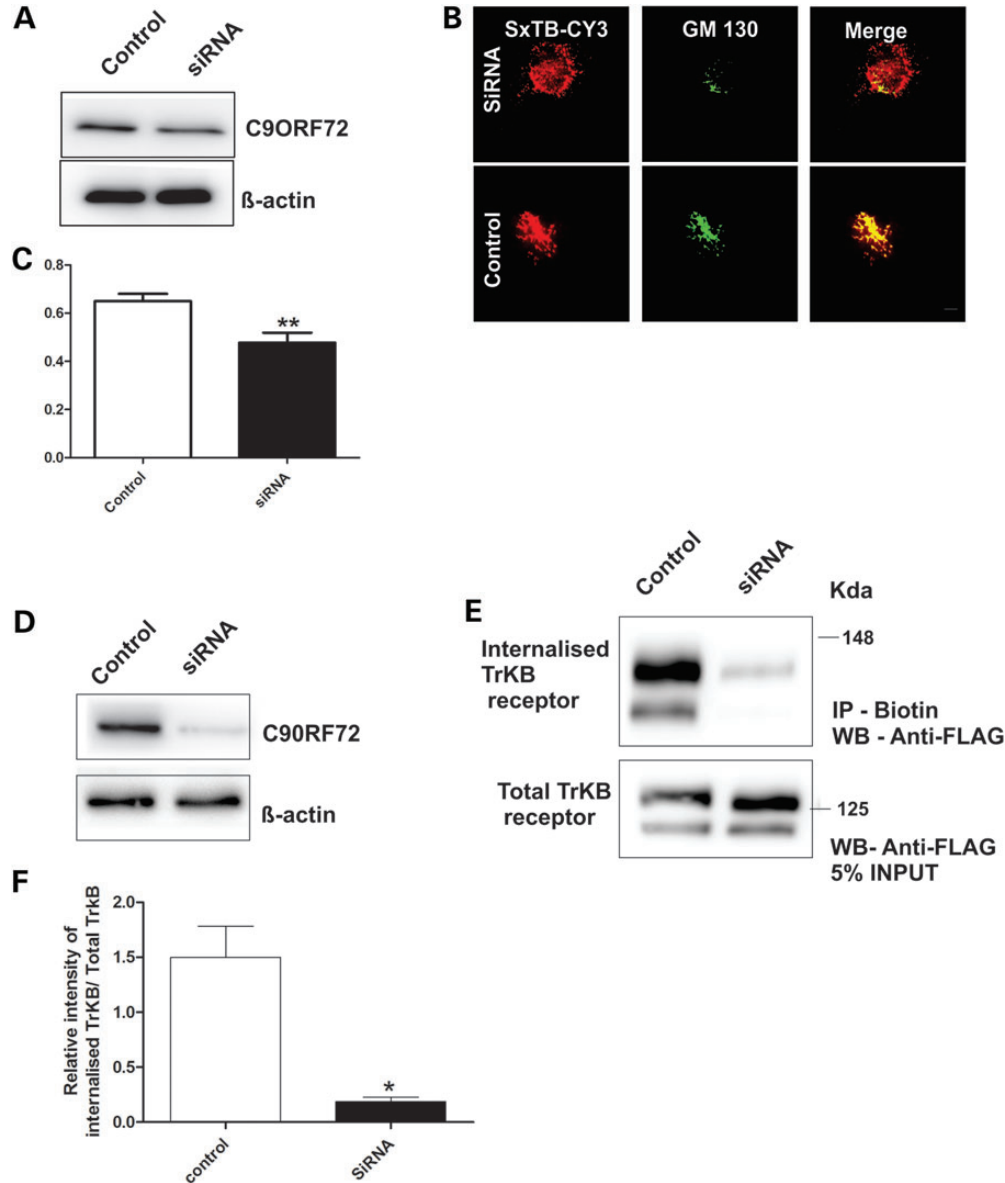


Figure 5. C9ORF72 mediates endocytosis of Shiga toxin-CY3 and TrkB receptor. (A) SH-SY5Y cells were transfected with C9ORF72-targeted siRNA and control siRNA for 72 h. Cell lysates were harvested and immunoblotting followed by densitometry quantification revealed that C9ORF72 expression was reduced by 30% in cells treated with C9ORF72 siRNA compared with control siRNA-treated cells. (B) Purified Shiga toxin conjugated to CY3 (SxTB-CY3) (red) was added to the medium of cells treated with C9ORF72 and control siRNA for 30 min. Endocytosis was examined after 60 min using immunocytochemistry for Golgi marker GM130 (green). (C) The colocalization between C9ORF72 and GM130 was quantified using Mander's coefficient, revealing 18% inhibition of endocytosis of Shiga toxin in C9ORF72-siRNA-treated cells. For each of two replicate experiments, 50 cells were scored for each population. Data are represented as mean \pm SEM; ** $P < 0.001$, using unpaired t -test. (D) SH-SY5Y cells were transfected with C9ORF72-targeted siRNA and control siRNA followed by a second transfection 24 h later. Cell lysates were harvested and immunoblotting followed by densitometry quantification revealed that C9ORF72 expression was reduced by 80% compared with control siRNA-treated cells. (E) C9ORF72 depleted and control cells expressing FLAG-tagged TrkB receptor were treated with biotin NHS at 4°C to biotinylate cell surface proteins. The cells were then incubated at 37°C and medium containing BDNF was added to induce endocytosis of TrkB receptor. The rate of TrkB receptor endocytosis was examined after 2 h by precipitating biotinylated and internalized TrkB receptor from cell lysates with streptavidin beads and immunoblotting with an anti-FLAG antibody. (F) Densitometric quantification of immunoblots reveals inhibition of endocytosis of TrkB receptor by 87% in cells depleted of C9ORF72 compared with control cells. Biotin precipitation and immunoblotting were performed in triplicate. Data are represented as mean \pm SEM; * $P < 0.05$, using unpaired t -tests.

BDNF ligand. Internalized TrkB receptor was precipitated with streptavidin beads and quantified by immunoblotting with an anti-FLAG antibody. In cells 80% depleted of C9ORF72, endocytosis of TrkB was inhibited by 87% compared with control cells, confirming that C9ORF72 regulates endocytosis (Fig. 5E and F).

C9ORF72 regulates autophagy in neuronal cell lines

To examine if C9ORF72 regulates autophagy, cells were cotransfected with constructs-encoding C9ORF72-GFP and DsRed-tagged microtubule-associated protein 1 light chain 3 (LC3), a marker for autophagosomes, in neuro2a cells. The

appearance of C9ORF72 as punctate structures that colocalized with DsRed-LC3 in 23% of cells (counted from at least 100 cells), suggested that C9ORF72 associates with autophagosome-like structures under basal conditions (Fig. 6A). Blockage of autophagosome fusion to the lysosome by bafilomycin yielded a significantly increased proportion of cells with LC3-positive structures, suggestive of autophagosomes (73%, $P < 0.01$), providing further evidence that C9ORF72 associates with autophagosomes (Fig. 6B–D). Immunoblotting for LC3I relative to its phosphatidylethanolamine-modified product, LC3II, was investigated in human SH-SY5Y cells depleted of C9ORF72 by 75% using siRNA (Fig. 6E). The LC3II:LC3I ratio was increased by 45% ($P < 0.001$) in siRNA-treated cells, indicating dysregulated autophagosome formation. In contrast, there was no change in LC3II:LC3I ratio in cells treated with control siRNA (Fig. 6F) compared with untreated cells. Similarly, in the presence of bafilomycin, LC3II levels increased in SH-SY5Y cells, indicating efficient autophagic flux in this cell line (Fig. 6D), thus confirming the specificity of the findings with C9ORF72 depletion. C9ORF72-positive vesicles also colocalized with Lyso-tracker, a marker of lysosomes, in every cell examined (Fig. 6G), and co-migrated with Lyso-tracker-stained vesicles in live cells, indicating that C9ORF72 was present in acidic vesicles of the endolysosomal system (Supplementary Material, Fig. S2). Hence, taken together, these data suggest that C9ORF72 regulates autophagy-mediated trafficking.

Endogenous C9ORF72 interacts with ubiquitin-2, hnRNPA1 and hnRNPA2/B1

To gain further insight into the function of C9ORF72, we used mass spectrometry to identify novel proteins that interact with C9ORF72 in immunoprecipitated cell lysates. These studies identified five additional interacting partners of C9ORF72; ubiquitin-1, ubiquitin-2, hnRNA1, hnRNA2/B1 and actin (cytoplasmic), with Mascot scores 284.78, 579.71, 155.58, 185.47 and 621.91, respectively (Supplementary Material, Table S1). The interaction between C9ORF72 and ubiquitin-2 was investigated further using immunocytochemistry and immunoprecipitation. Immunocytochemistry and subsequent quantification revealed that C9ORF72 and ubiquitin-2 colocalized in 25% of neuro2a cells (Fig. 7A and C) under basal conditions. Also, ubiquitin-2 was coprecipitated from neuro2a cell lysates using C9ORF72 antibodies: control reactions containing buffer only or an isotype-matched control antibody were negative (Fig. 7D). The autophagy and proteasome systems are closely linked; therefore, we treated cells with an inhibitor of the 26S proteasome, lactacystin, to increase autophagic flux (Fig. 7B). This treatment significantly increased the proportion of cells with ubiquitin-2 and C9ORF72 colocalization (Fig. 7B; $P < 0.001$). Hence these data suggest that C9ORF72 and ubiquitin-2 interact, and hence may function together in autophagy.

Using immunocytochemistry, C9ORF72 also colocalized with both hnRNPA1 and hnRNPA2/B1 in SH-SY5Y cells (Fig. 7E), and C9ORF72 was co-immunoprecipitated using hnRNA1 and hnRNA2/B1 antibodies in cell lysates, confirming the mass spectrometry findings (Fig. 7F). Similarly, immunocytochemistry revealed that C9ORF72 colocalized with actin (Fig. 7G) thus providing further evidence linking C9ORF72 to cellular trafficking pathways.

Inhibition of the proteasome in cells overexpressing C9ORF72 induces the formation of SGs

We next transfected neuro2a cells with a construct-encoding C9ORF72 tagged with GFP. The distribution appeared similar to endogenous C9ORF72, primarily nuclear with cytoplasmic vesicles. However, we also observed the presence of fluorescent aggregate structures containing C9ORF72 in the nucleus in 40% of cells (Fig. 8A), suggesting possible disturbance to protein degradation pathways in cells overexpressing C9ORF72. This was investigated further using lactacystin treatment to inhibit the 26S proteasome; the proportion of cells overexpressing C9ORF72 with nuclear C9ORF72 aggregates significantly increased to 74% (Fig. 8B; $P < 0.001$) and the number of nuclear aggregates per cell significantly increased in treated cells (Fig. 8C; $P < 0.001$). Hence, the nuclear aggregates are linked to proteasome function, indicating possible cellular stress. This was investigated by examining the formation of cytoplasmic SGs using immunocytochemistry for hnRNPA1 and hnRNPA2/B1 as SG markers. SGs were not present in untransfected cells or control GFP cells with or without lactacystin treatment. However, in cells overexpressing C9ORF72, cytoplasmic SGs were present, identified by hnRNPA1 (12% cells) and hnRNPA2/B1 (7% cells) staining, respectively (Fig. 8D), and the proportion of SGs stained by hnRNPA2/B1 was significantly increased with proteasome inhibition (Fig. 8E; $P < 0.05$). Hence, proteasome inhibition promotes the formation of nuclear C9ORF72-aggregates and cytoplasmic SGs in cells overexpressing C9ORF72.

DISCUSSION

Despite the importance of C9ORF72 in neurodegeneration, its normal cellular function remains undefined. Clearly, understanding this function is necessary for elucidating its role in disease. In this study, we demonstrate that C9ORF72 regulates intracellular trafficking processes in the endosomal and autophagy-lysosomal compartments. We observed that depletion of C9ORF72 using siRNA inhibited endocytosis and increased the ratio of LC3II:LC3I, suggesting dysregulation of autophagosome formation. C9ORF72 also colocalized with autophagosomes, lysosomes and ubiquitin-2, implicating C9ORF72 in trafficking essential for autophagy.

Rabs function as molecular switches that alternate between two conformational states: the activated GTP-bound form and the GDP-bound inactive form. Exchange of GDP with GTP is catalyzed by RabGEFs which facilitate GDP release and thus activate Rabs. One would expect that C9ORF72 would colocalize with Rabs in the appropriate compartments and to physically interact with Rab proteins if C9ORF72 possesses RabGEF activity. Consistent with this hypothesis, we observed colocalization and coprecipitation of C9ORF72 with four Rab proteins implicated in endolysosomal trafficking in both neuronal cell lines and primary cortical neurons: Rab1, Rab5, Rab7 and Rab11. Hence, this study is consistent with previous bioinformatics studies that reported the presence of a DENN domain in C9ORF72, part of a hitherto undetected group of DENN proteins that mediate autophagy and vascular-vesicle interactions (13,14). This raises the possibility that C9ORF72 functions as a RabGEF that

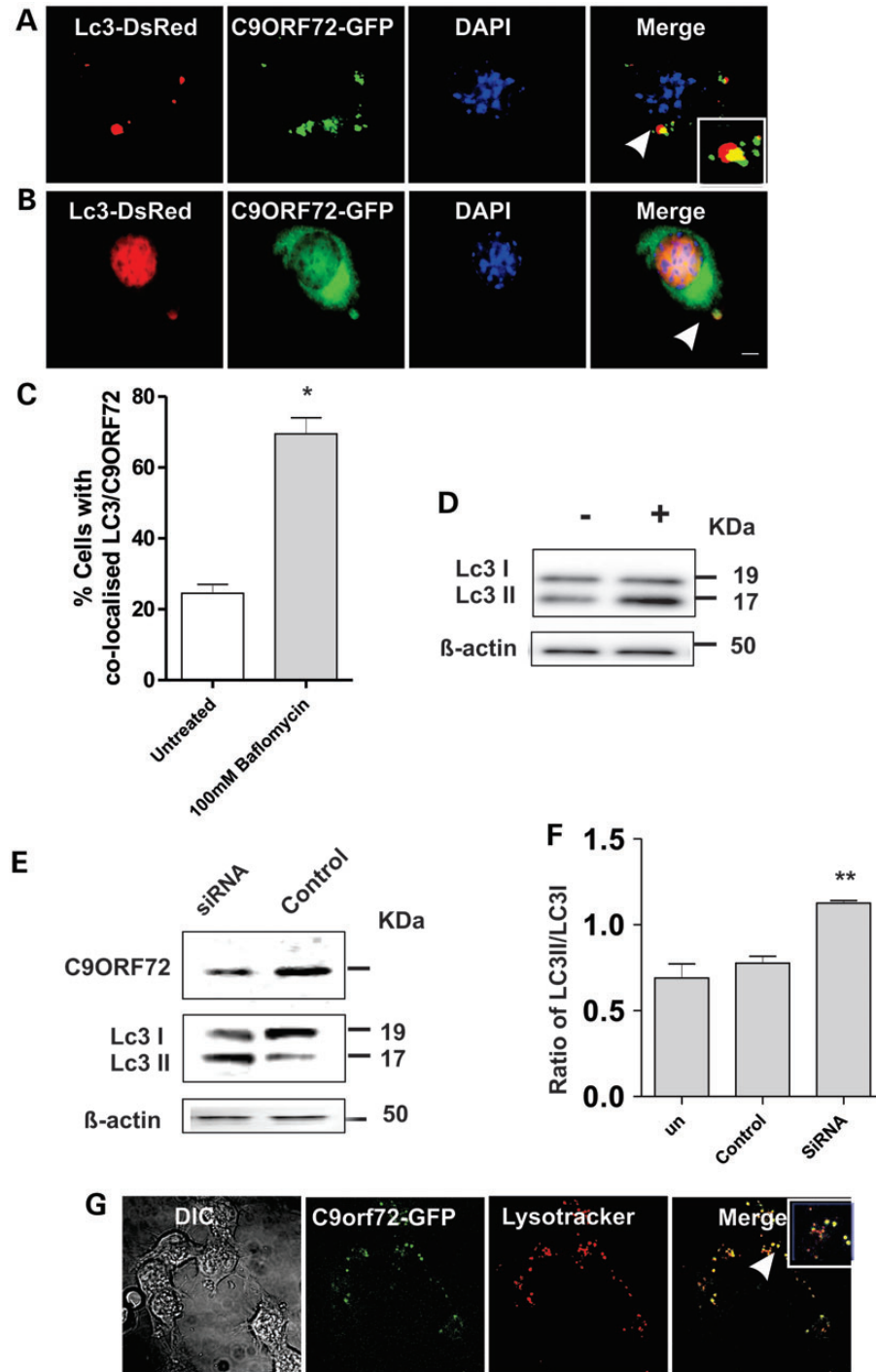


Figure 6. C9ORF72 regulates autophagy in neuronal cell lines. (A) Neuro2a cells were cotransfected with DsRed-LC3 for 48 h. Fluorescence microscopy revealed that C9ORF72 appeared as punctate structures that colocalized with DsRed-LC3, indicating autophagosomes, inset demonstrates higher magnification ($\times 100$) of the areas highlighted to illustrate autophagosomes, Scale bar: 10 μ m. (B) Cells were treated with 100 nM bafilomycin for 4 h to inhibit fusion of autophagosomes to the lysosome. White arrow represents C9ORF72 colocalization with autophagosomes. Scale bar: 10 μ m. (C) Quantification of the percentage of cells in which C9ORF72 colocalized with DsRed-LC3 revealed elevation in the numbers of LC3-positive structures, indicating autophagosomes, colocalizing with C9ORF72 in bafilomycin treated cells. Data are represented as mean \pm SEM; * $P < 0.05$ versus untreated cells by unpaired t -test, 50 cells were scored, $n = 2$. (D) Human SH-SY5Y cells were treated with 100 nM bafilomycin for 4 h to test examine autophagic flux by LC3 immunoblotting. (E) Human SH-SY5Y cells were transfected with human C9ORF72-targeting or control siRNA for 72 h. Immunoblotting revealed depletion of C9ORF72 by 75% compared with control siRNA-treated cells. Immunoblotting for LC3 was performed on lysates harvested from cells treated with control or C9ORF72-targeted siRNA, indicating the formation of autophagosomes. (F) Quantification of the ratio of phosphatidylethanolamine-modified product of LC3II, relative to LC3I by densitometry of immunoblots, demonstrated a reduction in this ratio by 45% in C9ORF72-siRNA-treated cells, whereas there was no change in control siRNA-treated cells compared with untreated cells. Data are represented as mean \pm SEM; ** $P < 0.001$ versus untreated cells by unpaired t -test, $n = 3$. (G) C9ORF72 is associated with lysosomes in Neuro 2A cells. Cells were transfected with C9ORF72-GFP and treated with Lysotracker for 20 min, Scale bar: 10 μ m.

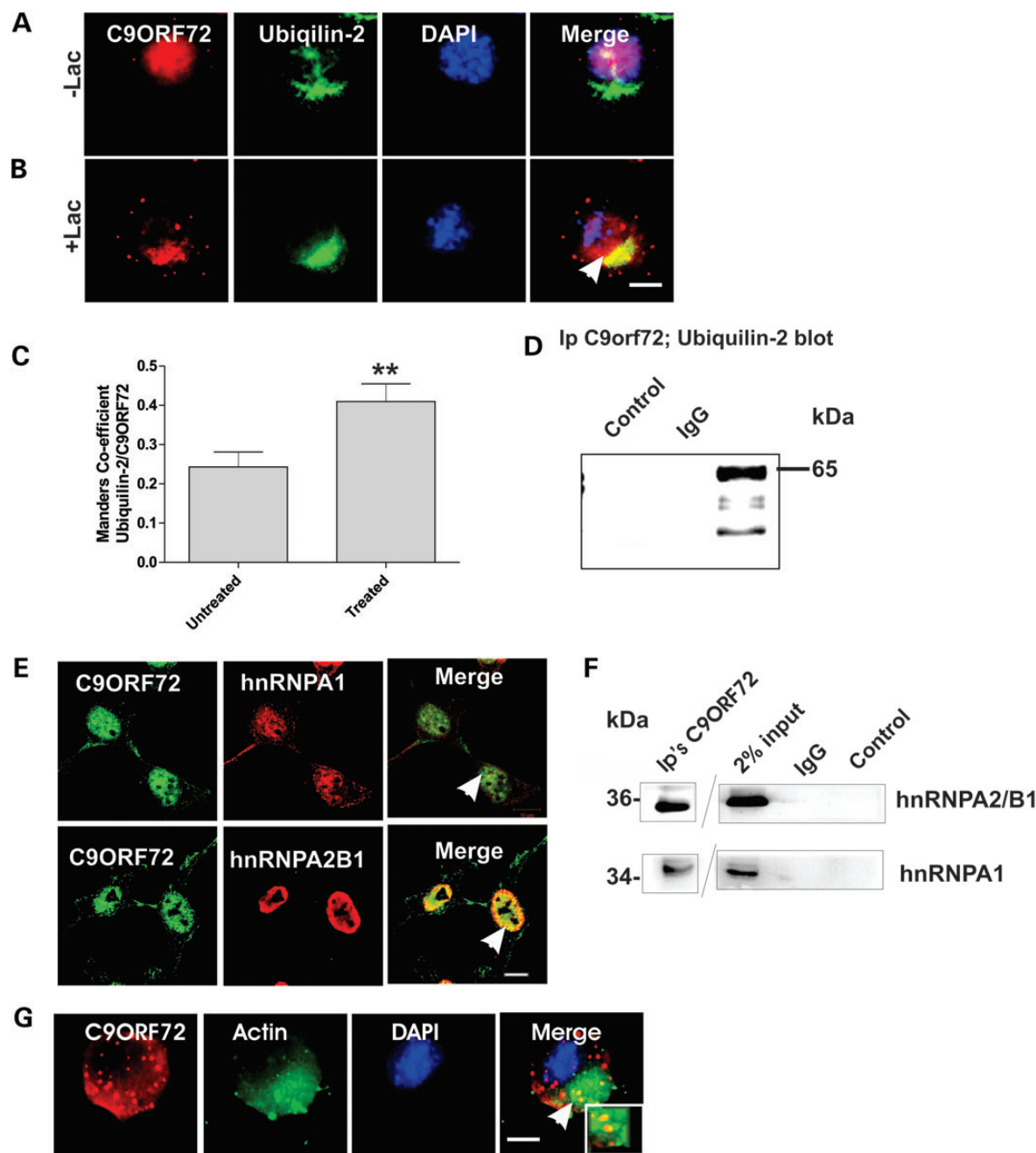


Figure 7. C9ORF72 colocalizes with hnRNP A1, hnRNP A2/B1, ubiquitin-2 and actin. (A) Neuro2a cells were treated with 10 μ M lactacystin for 16 h. Both treated and untreated cells were immunostained with anti-C9ORF72 (red) and anti-ubiquitin-2 antibodies (green) and stained with DAPI to locate the nucleus (blue). White arrow in the merge image shows areas of colocalization of ubiquitin-2 and C9ORF72. Scale bar: 10 μ m, applied to all fields. Lac, lactacystin. (B) Inhibition of the proteasome by lactacystin promotes the colocalization of C9ORF72 and ubiquitin-2. Manders coefficient was used to calculate the degree of colocalization between C9ORF72 and ubiquitin-2. Data are represented as mean \pm SEM; $**P < 0.001$ versus untreated cells by unpaired *t*-test. (C) Ubiquitin-2 coprecipitates using anti-C9ORF72 antibodies in Neuro2a cells, revealed by immunoblotting for ubiquitin-2. Control immunoprecipitations using buffer only or irrelevant, isotype-matched control IgG antibody indicates there is no non-specific cross-reactivity. (D) Immunocytochemistry of SH-SY5Y cells using anti-C9ORF72 antibodies (green), anti-hnRNP A1 or anti-hnRNP A2/B1 antibodies (red). White arrow indicates the colocalization between C9ORF72 and hnRNP A2/B1 and hnRNP A1; scale bar: 10 μ m. (E) hnRNPs coprecipitate using anti-C9ORF72 antibodies in SH-SY5Y cells, revealed by immunoblotting with anti-hnRNP A1 or anti-hnRNP A2/B1 antibodies. Control immunoprecipitations using buffer only or irrelevant, isotype-matched control IgG antibody indicate there is no non-specific cross-reactivity. (F) Colocalization of C9ORF72 (red) and actin (green) in neuro 2a cells and stained with DAPI to locate the nucleus (blue), white arrows indicate areas of colocalization. Inset demonstrates higher magnification ($\times 100$) of the areas highlighted to illustrate colocalization. Scale bar: 10 μ m.

regulates Rab-dependent intracellular trafficking. This study therefore provides the first experimental evidence to support this notion.

Each of the Rab proteins we investigated has a specific function in endocytosis and/or autophagy. Endocytic cargo is initially present in Rab5-containing early endosomes that undergo

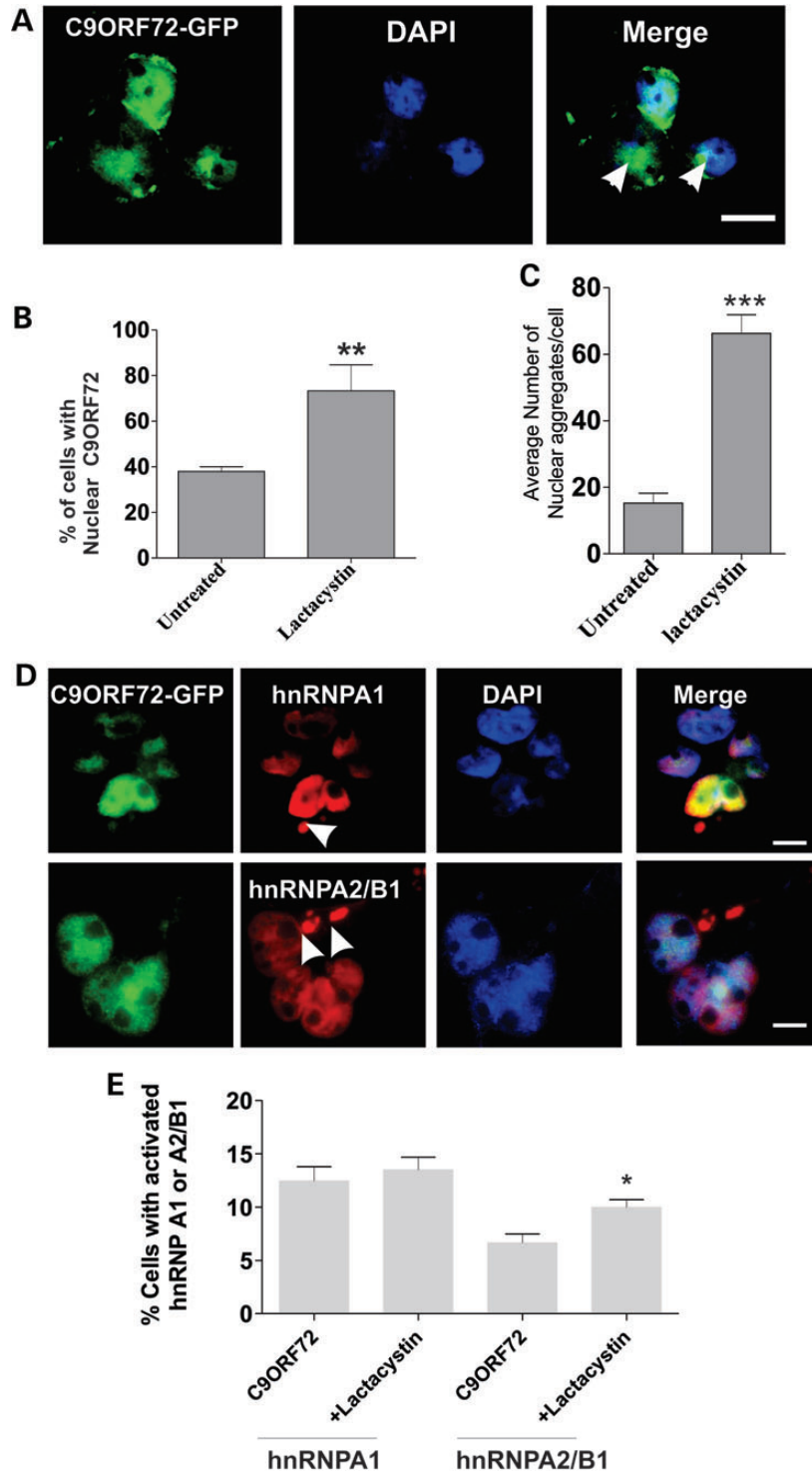


Figure 8. Inhibition of the proteasome in cells overexpressing C9ORF72 promotes the formation of nuclear aggregates and cytoplasmic SG's. (A) Neuro2a cells were transfected with C9ORF72-GFP for 48 h, followed by 10 μ M lactacystin treatment for 16 h and DAPI staining to locate the nucleus. C9ORF72-positive nuclear aggregate structures are present in the nucleus, with and without lactacystin treatment. Scale bar: 10 μ m. (B) Quantification demonstrates that lactacystin increased the percentage of cells bearing nuclear C9ORF72 aggregates from 37% to 70%. Data are represented as mean \pm SEM; ** P < 0.001, n = 2 treated versus untreated by unpaired t -test. (C) The number of nuclear aggregates per cell increased by 60% in lactacystin treated versus untreated cells. For each of three replicate experiments, 50 cells were scored for each population. Data are represented as mean \pm SEM; * P < 0.005 versus untreated by one-way unpaired t -test. (D) SH-SY5Y cells were transfected with C9ORF72-EGFP and immunostained using either hnRNPA1 or hnRNPA2/B1 antibodies (red) and DAPI (blue) to locate the nucleus. Arrows indicate hnRNPs-positive SGs formed in the cytoplasm. Scale bar: 10 μ m. (E) The percentage of cells displaying hnRNPA1 or hnRNPA2/B1-positive SGs was quantified, for each of two replicate experiments, 50 cells were scored for each population. Cytoplasmic SGs positive for hnRNPA1 (12%) and hnRNPA2/B1 (7%) were present in C9ORF72-expressing cells. This was significantly increased in the proportion of hnRNPA2/B1-positive SGs treated by proteasome inhibition, lactacystin. Data are represented as mean \pm SEM; * P < 0.005 versus untreated by unpaired t -test.

maturation to become Rab7-containing late endosomes (18). Rab7 is a critical regulatory component that regulates transport from early-to-late endosomes, biogenesis of lysosomes and maturation of autophagosomes (30–33). Similarly, Rab1 is necessary for the formation of the autophagosome (18), and Rab11 regulates recycling of endocytosed proteins via recycling endosomes and promotes autophagy by providing the autophagosome membrane (17). Hence, association with these four Rab proteins suggests that C9ORF72 may have a broad function in facilitating endocytic trafficking events. Our study is therefore consistent with previous reports that Rab effectors exhibit broad specificity for Rab proteins and interact with multiple Rab isoforms (34). However, whilst our findings support the notion that C9ORF72 is a RabGEF, more specific studies are required to determine this conclusively.

Ubiquitin-2 is part of a family of ubiquitin-like proteins involved in protein degradation that bind and transport ubiquitinated cargo to the proteasome and autophagosome (35). Mass spectrometry, immunoprecipitation and immunocytochemistry identified ubiquitin-2 as an interacting partner of C9ORF72, and this interaction was enhanced by proteasome inhibition, thus providing further evidence that the function of C9ORF72 is linked to protein degradation. These data therefore imply that C9ORF72 mediates trafficking of cargo to the autophagosome and/or proteasome in conjunction with ubiquitin-2. Consistent with this notion, ALS patients with the C9ORF72 repeat expansion also possess p62/ubiquitin-positive pathology (20,36,37).

It remains unclear how the hexanucleotide repeat expansions in C9ORF72 are linked to ALS, although reduced levels of C9ORF72 have been reported in C9ORF72-patient motor neurons (19). Our finding that endocytosis and autophagy are inhibited in cells depleted of C9ORF72 therefore identifies cellular processes affected by reduction in C9ORF72 expression. Membrane trafficking processes are vital for cellular maintenance and viability, hence inhibition of these events would significantly impact on cellular functions. In addition, motor neurons may be particularly vulnerable to disruption in cellular transport due to their large size and long axons. We also found that in motor neurons in tissue obtained from ALS patients bearing the C9ORF72 GGGGCC mutation, the association of C9ORF72 with Rab7 and Rab11 was increased, implying possible dysregulation of endosomal trafficking in C9ORF72-ALS. Defects in Rab-mediated trafficking are previously described in diseases affecting motor neurons. Mutations in Rab7 cause Charcot-Marie-Tooth disease type 2B (38), and Rab7-positive endosome abnormalities impair trafficking in Wobbler mice (39). Mutations in Alsln, a RabGEF for Rab5, cause juvenile onset ALS and primary lateral sclerosis (40) and enlarged Rab5-positive endosomes are present in spinal ALS motor neurons (41). Dysfunction in dynein, which powers endocytic trafficking, has been described in ALS (42) and depletion of dynein also results in endocytic Rab accumulation and endosomal pathology (43). We also recently demonstrated that mutant SOD1 induces dysfunction in the trafficking between the ER and Golgi compartments, another trafficking process regulated by Rab1 (44).

Similarly, disturbance to protein degradation pathways, including autophagy, are increasingly implicated in ALS (19). Autophagosomes accumulate in the spinal cord of sporadic ALS patients (45) and enhancement of autophagy and decrease

in autophagic flux is present in ALS mouse and cell lines expressing mutant SOD1 (46). Multiple ALS causative or associated genes are also linked to autophagy: SQSTM1, DCTN1, VCP, FIG4 and Rab7A (47). We also identified actin as an interacting partner of C9ORF72 by mass spectrometry, another vesicular trafficking protein that provides the structural unit of microfilaments. Moreover, actin plays a role at the early stage of autophagosome formation (48), and autophagosomes are surrounded by an actin filament network that is required for autophagosome/lysosome fusion (49), providing additional evidence for a role for C9ORF72 in autophagy. Furthermore, mutations in profilin, which regulates actin polymerization, were also recently linked to ALS (50). We also provide evidence that C9ORF72 is present extracellularly in neuronal cell lines, human CSF and within the axons of primary neurons. Similarly, C9ORF72 is highly concentrated in synaptic terminals in brains of ALS/FTD patients (51). Hence together, these data imply a possible role for C9ORF72 in synaptic vesicle trafficking.

In this study, we also demonstrate a relationship between C9ORF72 and hnRNP A1 and hnRNP A2B1. Whereas a recent report found that C9ORF72 RNA with the repeat expansion bound to three different hnRNPs, hnRNP A1, hnRNP A2/B1 and hnRNP A3 (10), here we show that wild-type C9ORF72 also interacts with hnRNPs. Hence, this interaction is independent of the presence of the C9ORF72 GGGGCC mutation. hnRNPs shuttle continuously between the nucleus and cytoplasm and during cellular stress they accumulate in cytoplasmic SGs (52). Hence, it is possible that C9ORF72 may facilitate the transport of hnRNPs between the nucleus and cytoplasm, although we did not examine nuclear-cytoplasmic transport in this study. Alternatively, another intriguing possibility is that C9ORF72 may have a functional role with hnRNPs, as an RNA-binding protein with possible roles in RNA metabolism or stability, as proteasome inhibition modifies RNA splicing (26).

The UPS plays an active role in the nucleus at the quality control and transcriptional levels. We observed that expression of C9ORF72 induces cytoplasmic SG's, and this was enhanced by proteasome inhibition, suggesting that wild-type C9ORF72 may induce cellular stress. This may occur via a direct effect on C9ORF72 misfolding or indirectly via other cellular proteins or pathways. Elevated expression of wild-type versions of other proteins linked to ALS, SOD1 and TDP-43, trigger ALS-like pathology (53–55). Targets of the nuclear proteasome form nuclear aggregates reminiscent of aggresomes when the proteasome is inhibited (56). We also identified the presence of nuclear aggregate structures in cells expressing C9ORF72, although these aggregates remain to be characterized. However, TDP-43 and FUS form nuclear foci and also interact with hnRNPs (57), TDP-43-positive pathology is present in C9ORF72 patients (58), and sequestration of nuclear RNA-binding proteins leads to cytoplasmic TDP-43 aggregates in ALS patients with the C9ORF72 mutation (59).

Hence, we show in this study that C9ORF72 is involved in intracellular trafficking pathways linked to protein degradation. We summarize a hypothetical scenario to illustrate convergence of C9ORF72 function in protein degradation (Fig. 9). C9ORF72 normally mediates endocytic trafficking to facilitate both autophagy and endosomal transport, at least partially in conjunction with ubiquitin-2. C9ORF72 also mediates shuttling of hnRNP A2/B1 and hnRNP A1 between the nucleus and cytoplasm, and may

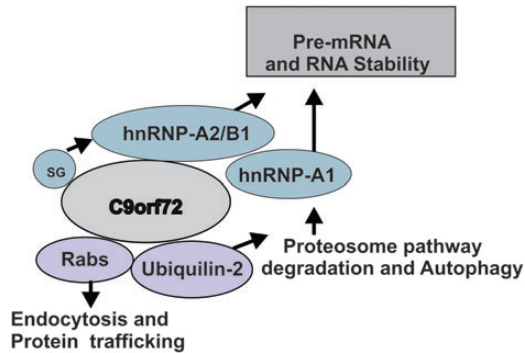


Figure 9. Possible functions of C9ORF72. C9ORF72 mediates endocytic trafficking to facilitate autophagy and proteasome function, at least partially with ubiquilin-2. However, during conditions of cellular stress and SGs, C9ORF72 interacts with hnRNP A2/B1 and hnRNP A1 that regulate splicing and RNA metabolism and may cause RNA instability in ALS.

also be linked to RNA metabolism. Further experiments in this area are necessary as understanding the normal cellular function of C9ORF72 is an important step in understanding how dysregulation of this function may lead to both ALS and FTD.

MATERIALS AND METHODS

Constructs

A construct C9ORF72-Variant 1 tagged with AC-GFP-tagged (NM_018325) was obtained from OriGene, encoding the full length of human C9ORF72 cDNA and constructs-encoding GFP-tagged Rab5, Rab7, Rab11 and DsRed-LC3, were as previously described (60,61). FLAG-tagged TrkB receptor was a kind gift from Drs Junhua Xiao and Simon Murray from the Department of Anatomy and Cell Biology, University of Melbourne.

Cell culture and transfection

Neuro2a or SH-SY5Y neuroblastoma cells were subcultured in 24-well plates at a density of 2×10^4 cells/well and were transfected transiently with plasmids (1 μ g DNA per well) using lipofectamine reagent. Cells were examined with an inverted fluorescent microscope (Olympus, NSW, Australia) 72 h after transfection unless otherwise stated. Cells were transfected with C9ORF72-Variant 2 and DsRed-LC3 (61) using lipofectamine 2000 (Invitrogen/Life Technologies) according to the manufacturer's instructions. For proteosomal inhibition, cells were treated with lactacystin (Sigma, L6785) for 16 h before analysis. Fixed cells were immunostained with DAPI to visualize the nucleus, and at least 50 cells were analyzed in each category. To knockdown endogenous human C9ORF72 expression, human SH-SY5Y cells were transfected with C9ORF72 siRNA (Dharma; L-013341-01), following the manufacturers instruction's.

Subcellular fractionation

Subcellular fractionation of SH-SY5Y neuroblastoma cells was performed after lysis of cells using 500 μ l of fractionation buffer (250 mM sucrose, 20 mM HEPES (7.4), 10 mM KCl, 1.5 mM $MgCl_2$, 1 mM EDTA, 1 mM EGTA with protease inhibitors).

Cell lysates were passed through a 25 G needle 10 times and left on ice for 20 min. Homogenates were centrifuged at 720 g for 5 min to isolate the nuclear fraction, and washed by adding 500 μ l of fractionation buffer. The pellet was passed through a 25 G needle 10 times and centrifuged at 720 g for 10 min. After washing, the pellet was resuspended in standard TN lysis buffer and stored as the nuclear fraction. The supernatant was spun at 100 000 g at 4°C, to obtain the cytosolic fraction. Protein measurements of the obtained fractions were determined and analyzed by immunoblotting, as described.

Primary cells from the central nervous system

Primary neurons were harvested from the cells from the cortex of C57BL/6 mouse embryos at embryonic (E) day 15.5. The procedure for the culture of primary neurons was as described previously (62,63). Briefly, cortical tissue was dissected from E15.5 mouse embryos and dissociated using 0.0125% trypsin (5 min at 37°C). Tissue was washed in cell plating media (consisting of NeurobasalTM medium (Gibco), 2% B27 supplement, 10% fetal calf serum (Gibco), 0.5 mM glutamine, 25 μ M glutamate and 1% antibiotic/antimycotic (Gibco), followed by mechanical titration using a 1 ml pipette. Cell viability and density were assessed using a trypan blue exclusion assay. Cells were plated onto poly-L-lysine-coated 12 mm coverslips (Marienfeld) in 24-well plates at a concentration of 30 000 cell per coverslip. The following day, media were changed to cell maintenance media consisting of plating media without the fetal calf serum and glutamate. Cells were grown in 5% CO₂ at 37°C. All animal experiments were performed under the approval of the University of Tasmania animal ethics committee (Ethics # A12780). The purity of primary cortical neurons was confirmed by immunostaining using specific antibodies: neuronal marker microtubule-associated protein 2, MAP2 (Millipore, MAB3418 clone AP20, 1:1000). Immunocytochemistry staining was performed to show the colocalization of C9ORF72 and Rabs by using anti-C9ORF antibody and anti-Rabs antibodies using standard methods as described below.

Immunocytochemistry and endocytosis

Neuro2a or SH-SY5Y neuroblastoma cells were grown on coverslips, washed with PBS and fixed with 4% paraformaldehyde in PBS for 10 min. Cells were permeabilized in 0.1% Triton X-100 in PBS for 2 min, blocked for 30 min with 1% BSA in PBS, and incubated with primary anti-C9ORF72 (1:100, Santa-Cruz, sc-138763), anti-Rab 1 (1:100, SantaCruz sc-28566), anti-Rab 7, (Abcam, ab50533, 1:50), anti-hnPNP-A1 (Sigma, R4528) or anti hnRNP-A2/B1 (Sigma, R4653), for 16 h at 4°C. Secondary AlexaFluor-594 conjugated anti-mouse or anti-rabbit antibodies (1:200, Molecular Probes) were then incubated for 1 h at room temperature, and cells were counter-stained with DAPI and mounted. Images were acquired using an Olympus inverted confocal laser-scanning microscope or an Olympus inverted fluorescence microscope. To examine endocytosis, purified Shiga toxin conjugated to CY3 (SxTB-CY3) as previously described (28) was added to the medium of cells treated with C9ORF72 and control siRNA for 30 min. Shiga toxin was added for 30 min, and then examined after 60 min by immunocytochemistry for Golgi marker GM130. Endocytosis was

confirmed by quantifying the internalization of TrkB receptor by cell surface biotinylation as described previously (64–66). Briefly, SH-SY5Y cells were transfected with C9ORF72 siRNA, and 24 h later transfected again with siRNA to increase the efficiency of knockdown. The C9ORF72 depleted cells were then transfected with a construct-encoding FLAG-tagged TrkB receptor for 48 h. Cells were then washed twice with ice-cold PBS, and incubated with 0.5 mg/ml biotin NHS (Thermo Scientific) in PBS for 30 min at 4°C to biotinylate all cell surface proteins. Unreacted biotin was quenched and removed with 50 mM NH₄Cl for 5 min. Biotinylated cells were then transferred to pre-warmed medium containing 50 ng/ml BDNF (Millipore) for 2 h to induce endocytosis of TrkB receptor, and the cells were immediately lysed in TN buffer with 0.1% SDS. Internalized biotinylated TrkB receptor was then precipitated from cell lysates with 10 µl of streptavidin-agarose beads (Cell signaling) and quantified by immunoblotting with anti-FLAG antibody (Sigma).

Live cell imaging

Neuro 2A cells transfected with C9ORF72-GFP were stained for 20 min with 1 µM LysoTracker (L7528, Molecular Probes) and the movement of C9ORF72 vesicles was examined by time-lapse imaging. Images were acquired every 7 s for 15 min using a Zeiss LSM 510 confocal microscope.

Protein extraction

Cells were lysed in Tris–NaCl (TN) buffer (50 mM Tris–HCl, pH 7.5, 150 mM NaCl) with 0.1% (v/v) NP-40, 0.1% (w/v) SDS and 1% (v/v) protease inhibitor mixture (Sigma) for 10 min on ice. Cellular lysates were clarified by centrifugation at 16g for 10 min. Proteins were quantified using the BCA assay kit (Pierce).

Immunoprecipitation and immunoblotting

For immunoprecipitation, cell lysates were incubated with anti-C9ORF72 antibody, and 30 µl of 50% (w/v) protein A-Sepharose CL-4B (Amersham Biosciences) in Tris buffer [50 mM Tris–HCl, pH 7.5, 0.02% (w/v) NaN₃] on a rotating wheel overnight at 4°C. Proteins eluted from the beads were separated on 10% tris–glycine polyacrylamide gels. For western blotting, protein measurements of all obtained fractions were determined by BCA assay. Between 10 and 20 µg of protein was loaded and separated in 8–15% SDS–PAGE gels. Proteins were then electrophoretically transferred onto nitrocellulose membranes (Bio-Rad). These membranes were subsequently blocked with 5% (w/v) non-fat milk powder in Tris-buffered saline (TBS) or with 3% bovine serum albumin (BSA) in TBS containing 0.1% Tween 20 (TBS-T) at room temperature for 1 h, followed by incubation with the primary antibodies diluted in 1% BSA/TBS-T overnight at 4°C with shaking. C9ORF72 (1:500, SantaCruz sc-138763), or Rab 5 (1:500, Abcam ab50523), or Rab 11 (1:500, BD Transduction Labs, 610657), or Rab 7 (1:500, ab50533), or LC3 antibody (1:1000, Novus Biologicals; NB100–2220), ubiquilin-2 antibody (1:700, Abnova, H00029978), mouse anti-glyceraldehyde-3-phosphate dehydrogenase (GAPDH, 1:10,000, Ambion AM4300), Histone H3 96C10, Cell Signalling, 36385) and

β-actin (1:5000, Sigma). Membranes were washed with TBS-T and then incubated for 1 h at room temperature with secondary antibodies (1:4000, HRP-conjugated goat anti-rabbit or goat anti-mouse antibodies, Chemicon). Protein bands were detected by using enhanced chemiluminescence reagents (Roche), as described by the manufacturer.

Immunohistochemistry

Human postmortem cervical spinal cord sections (5 µm) from a male fALS patients carrying the hexanucleotide GGGGCC repeat expansion was obtained. This patient developed limb onset ALS at 74 years old, with a disease duration of 13 months. He was not diagnosed with FTD, but deterioration of memory was reported. A sex and age matched neurologically normal individual was used as a control. Formalin-fixed, paraffin-embedded spinal cord tissues deparaffinised with xylene, and rehydrated with a descending series of diluted ethanol and water. Antigen retrieval was conducted by boiling the sections for 20 mins in 10 mM citric buffer (pH 6.0). Sections were blocked using 3% goat serum/0.3% Tween 20 for 1 h and then immunostained with different Rabs (1:50) and C9ORF72 (1:100) antibodies and left overnight at 4°C. Sections were washed twice in PBS Tween 20 (0.1%) and secondary antibodies were added; anti-rabbit/mouse Alexa Fluor (1:200, Molecular Probes, Invitrogen, VIC, Australia), for 1 h at RT. Sections were again washed twice in PBS Tween 20 and then a cover slip was applied using Prolong Gold antifade reagent (Invitrogen, VIC, Australia). Images were acquired using an Leica confocal laser-scanning microscope.

Mass spectrometry

Untransfected Neuro 2A cell lysates (500 µg) were immunoprecipitated using anti-C9ORF72 antibody (SantaCruz, sc-138763) and 30 µl of 50% (w/v) protein A-Sepharose CL-4B (Amersham Biosciences), on a rotating wheel overnight at 4°C. Samples were centrifuged at 15 800 g for 1 min, and Sepharose pellets were washed twice in Tris buffer for 10 min each. Protein samples for mass spectrometry were eluted from the beads by heating for 5 min, followed by centrifugation to remove cellular debris, then separated on 10% SDS–PAGE gel, and stained using Coomassie blue. Gel lanes were cut into slices, reduced, alkylated and digested with trypsin: only the five most abundant protein bands were excised. The resulting peptides were injected onto a trapping column (Dionex Acclaim Pepmap100, Nano trap 100 µm × 2 cm, C18, 5 µm, 100 Å) using A-buffer (2% acetonitrile in 0.1% formic acid (aqueous); Sigma-Aldrich). Following a 6 min wash, the sample was transferred onto a resolving column (Dionex Acclaim Pepmap RSLC, 75 µm × 15 cm, C18, 5 µm, 100 Å) and eluted with a gradient of B-buffer (98% acetonitrile in A-buffer) over 70 min. The eluent from the column was directly electrosprayed into the microTof-Q-MS instrument (Bruker-Daltonics, Germany). Mass data were continuously acquired and for each MS spectrum three MS/MS were recorded of the most intense peaks. The score for each protein reflects the combined scores of all observed peptide mass spectra that can be matched to the amino acid sequences within that protein. The peptide score reflects the probability of matching the experimental spectra to the

swiss data base. The data were annotated and deconvoluted using the Data Analysis program (Bruker-Daltonics). The acquired MS/MS spectra of peptides were searched protein database from SwissProt (ExPASy, <http://www.expasy.org/proteomics>) using the Mascot search engine (Matrix Science, London, UK).

Statistical analysis

All analyses were performed using GraphPad Prism 5 software. Statistical significance was calculated using one-way ANOVA followed by Tukey's post-test or two-tailed 'unpaired *t*-test', from two or three independent experiments. *P* < 0.05 was considered significant. Data are presented as mean ± SEM.

SUPPLEMENTARY MATERIAL

Supplementary Material is available at *HMG* online.

ACKNOWLEDGEMENTS

The C9ORF72 construct was kindly provided by Dr Justin Yerbury, University of Wollongong, and the human CSF was kindly provided by Professor Malcolm Horne, Florey Institute of Neuroscience and Mental Health. We thanks Prof. Gleeson for providing all the GFP-Rab constructs, and Dr Xiao and Dr Murray for providing Flag-tagged TrkB-FL. We also thank Dr Gert Hoy Talbo, Head of the mass spectrometry facility at La Trobe University.

Conflict of Interest statement. None declared.

FUNDING

This work was supported by funding from National Health and Medical Research Council of Australia (project grants 1006141, 1004670 and 1030513), MND Research Institute of Australia and Bethlehem Griffiths Research Council. Funding to pay the Open Access publication charges for this article was provided by LaTrobe University.

REFERENCES

- Josephs, K.A., Hodges, J.R., Snowden, J.S., Mackenzie, I.R., Neumann, M., Mann, D.M. and Dickson, D.W. (2011) Neuropathological background of phenotypical variability in frontotemporal dementia. *Acta Neuropathol.*, **122**, 137–153.
- Dobson-Stone, C., Hallupp, M., Bartley, L., Shepherd, C.E., Halliday, G.M., Schofield, P.R., Hodges, J.R. and Kwok, J.B.J. (2012) C9ORF72 repeat expansion in clinical and neuropathologic frontotemporal dementia cohorts. *Neurology*, **79**, 995–1001.
- Sha, S.J., Takada, L.T., Rankin, K.P., Yokoyama, J.S., Rutherford, N.J., Fong, J.C., Khan, B., Karydas, A., Baker, M.C., DeJesus-Hernandez, M. *et al.* (2012) Frontotemporal dementia due to C9ORF72 mutations: clinical and imaging features. *Neurology*, **79**, 1002–1011.
- van Swieten, J.C. and Grossman, M. (2012) FTD/ALS families are no longer orphaned: the C9ORF72 story. *Neurology*, **79**, 962–964.
- Renton, A.E., Majounie, E., Waite, A., Simon-Sanchez, J., Rollinson, S., Gibbs, J.R., Schymick, J.C., Laaksovirta, H., van Swieten, J.C., Myllykangas, L. *et al.* (2011) A hexanucleotide repeat expansion in C9ORF72 is the cause of chromosome 9p21-linked ALS-FTD. *Neuron*, **72**, 257–268.
- DeJesus-Hernandez, M., Mackenzie, I.R., Boeve, B.F., Boxer, A.L., Baker, M., Rutherford, N.J., Nicholson, A.M., Finch, N.A., Flynn, H., Adamson, J. *et al.* (2011) Expanded GGGGCC hexanucleotide repeat in noncoding region of C9ORF72 causes chromosome 9p-linked FTD and ALS. *Neuron*, **72**, 245–256.
- Majounie, E., Renton, A.E., Mok, K., Dopper, E.G., Waite, A., Rollinson, S., Chio, A., Restagno, G., Nicolaou, N., Simon-Sanchez, J. *et al.* (2012) Frequency of the C9orf72 hexanucleotide repeat expansion in patients with amyotrophic lateral sclerosis and frontotemporal dementia: a cross-sectional study. *Lancet Neurol.*, **11**, 323–330.
- Fratta, P., Mizielinska, S., Nicoll, A.J., Zloh, M., Fisher, E.M., Parkinson, G. and Isaacs, A.M. (2012) C9orf72 hexanucleotide repeat associated with amyotrophic lateral sclerosis and frontotemporal dementia forms RNA G-quadruplexes. *Sci. Rep.*, **2**, 1016.
- Ash, P.E., Bieniek, K.F., Gendron, T.F., Caulfield, T., Lin, W.L., DeJesus-Hernandez, M., van Blitterswijk, M.M., Jansen-West, K., Paul, J.W. III, Rademakers, R. *et al.* (2013) Unconventional translation of C9ORF72 GGGGCC expansion generates insoluble polypeptides specific to c9FTD/ALS. *Neuron*, **77**, 639–646.
- Mori, K., Weng, S.M., Arzberger, T., May, S., Rentzsch, K., Kremmer, E., Schmid, B., Kretzschmar, H.A., Cruts, M., Van Broeckhoven, C. *et al.* (2013) The C9orf72 GGGGCC repeat is translated into aggregating dipeptide-repeat proteins in FTL/ALS. *Science*, **339**, 1335–1338.
- Pfeffer, S. and Aivazian, D. (2004) Targeting Rab GTPases to distinct membrane compartments. *Nat. Rev. Mol. Cell Biol.*, **5**, 886–896.
- Cherfils, J. and Zeghouf, M. (2013) Regulation of small GTPases by GEFs, GAPs, and GDIs. *Physiol. Rev.*, **93**, 269–309.
- Levine, T.P., Daniels, R.D., Gatta, A.T., Wong, L.H. and Hayes, M.J. (2013) The product of C9orf72, a gene strongly implicated in neurodegeneration, is structurally related to DENN Rab-GEFs. *Bioinformatics*, **29**, 499–503.
- Zhang, D., Iyer, L.M., He, F. and Aravind, L. (2012) Discovery of novel DENN proteins: implications for the evolution of eukaryotic intracellular membrane structures and human disease. *Front. Genet.*, **3**, 283.
- Korolchuk, V.I., Menzies, F.M. and Rubinshtein, D.C. (2010) Mechanisms of cross-talk between the ubiquitin-proteasome and autophagy-lysosome systems. *FEBS Lett.*, **584**, 1393–1398.
- Nishida, Y., Arakawa, S., Fujitani, K., Yamaguchi, H., Mizuta, T., Kanaseki, T., Komatsu, M., Otsu, K., Tsujimoto, Y. and Shimizu, S. (2009) Discovery of Atg5/Atg7-independent alternative macroautophagy. *Nature*, **461**, 654–U699.
- Longatti, A., Lamb, C.A., Razi, M., Yoshimura, S., Barr, F.A. and Tooze, S.A. (2012) TBC1D14 regulates autophagosome formation via Rab11 and ULK1-positive recycling endosomes. *J. Cell Biol.*, **197**, 659–675.
- Zoppino, F.C., Militello, R.D., Slavin, I., Alvarez, C. and Colombo, M.I. (2010) Autophagosome formation depends on the small GTPase Rab1 and functional ER exit sites. *Traffic*, **11**, 1246–1261.
- Thomas, M., Alegre-Abarrategui, J. and Wade-Martins, R. (2013) RNA dysfunction and aggregopathy at the centre of an amyotrophic lateral sclerosis/frontotemporal dementia disease continuum. *Brain*, **136**, 1345–1360.
- Deng, H.X., Chen, W., Hong, S.T., Boycott, K.M., Gorrie, G.H., Siddique, N., Yang, Y., Fecto, F., Shi, Y., Zhai, H. *et al.* (2011) Mutations in UBQLN2 cause dominant X-linked juvenile and adult-onset ALS and ALS/dementia. *Nature*, **477**, 211–215.
- Rothenberg, C. and Monteiro, M.J. (2010) Ubiquitin at a crossroads in protein degradation pathways. *Autophagy*, **6**, 979–980.
- Bennett, E.J., Bence, N.F., Jayakumar, R. and Kopito, R.R. (2005) Global impairment of the ubiquitin-proteasome system by nuclear or cytoplasmic protein aggregates precedes inclusion body formation. *Mol. Cell*, **17**, 351–365.
- Li, Y.R., King, O.D., Shorter, J. and Gitler, A.D. (2013) Stress granules as crucibles of ALS pathogenesis. *J. Cell Biol.*, **201**, 361–372.
- Kim, H.J., Kim, N.C., Wang, Y.D., Scarborough, E.A., Moore, J., Diaz, Z., Maclea, K.S., Freibaum, B., Li, S., Molliex, A. *et al.* (2013) Mutations in prion-like domains in hnRNPA2B1 and hnRNPA1 cause multisystem proteinopathy and ALS. *Nature*, **495**, 467–473.
- Bekenstein, U. and Soreq, H. (2013) Heterogeneous nuclear ribonucleoprotein A1 in health and neurodegenerative disease: from

- structural insights to post-transcriptional regulatory roles. *Mol. Cell. Neurosci.*, **56**, 436–446.
26. Bieler, S., Hammer, E., Gesell-Salazar, M., Volker, U., Stangl, K. and Meiners, S. (2012) Low dose proteasome inhibition affects alternative splicing. *J. Proteome Res.*, **11**, 3947–3954.
 27. Bendtsen, J.D., Jensen, L.J., Blom, N., Von Heijne, G. and Brunak, S. (2004) Feature-based prediction of non-classical and leaderless protein secretion. *Protein Eng. Des. Sel.*, **17**, 349–356.
 28. Fuchs, E., Haas, A.K., Spooner, R.A., Yoshimura, S., Lord, J.M. and Barr, F.A. (2007) Specific Rab GTPase-activating proteins define the Shiga toxin and epidermal growth factor uptake pathways. *J. Cell Biol.*, **177**, 1133–1143.
 29. Manders, E.M.M., Verbeek, F.J. and Aten, J.A. (1993) Measurement of colocalization of objects in dual-color confocal images. *J. Microsc.-Oxford*, **169**, 375–382.
 30. Harrison, R.E., Bucci, C., Vieira, O.V., Schroer, T.A. and Grinstein, S. (2003) Phagosomes fuse with late endosomes and/or lysosomes by extension of membrane protrusions along microtubules: role of Rab7 and RILP. *Mol. Cell. Biol.*, **23**, 6494–6506.
 31. Jager, S., Bucci, C., Tanida, I., Ueno, T., Kominami, E., Saftig, P. and Eskelinen, E.L. (2004) Role for Rab7 in maturation of late autophagic vacuoles. *J. Cell Sci.*, **117**, 4837–4848.
 32. Gutierrez, M.G., Munafo, D.B., Beron, W. and Colombo, M.I. (2004) Rab7 is required for the normal progression of the autophagic pathway in mammalian cells. *J. Cell Sci.*, **117**, 2687–2697.
 33. Bucci, C., Thomsen, P., Nicoziani, P., McCarthy, J. and van Deurs, B. (2000) Rab7: a key to lysosome biogenesis. *Mol. Biol. Cell*, **11**, 467–480.
 34. Fukuda, M., Kanno, E., Ishibashi, K. and Itoh, T. (2008) Large scale screening for novel rab effectors reveals unexpected broad Rab binding specificity. *Mol. Cell. Proteomics*, **7**, 1031–1042.
 35. Rothenberg, C., Srinivasan, D., Mah, L., Kaushik, S., Peterhoff, C.M., Ugelino, J., Fang, S., Cuervo, A.M., Nixon, R.A. and Monteiro, M.J. (2010) Ubiquitin functions in autophagy and is degraded by chaperone-mediated autophagy. *Hum. Mol. Genet.*, **19**, 3219–3232.
 36. Brettschneider, J., Van Deerlin, V.M., Robinson, J.L., Kwong, L., Lee, E.B., Ali, Y.O., Safren, N., Monteiro, M.J., Toledo, J.B., Elman, L. *et al.* (2012) Pattern of ubiquitin pathology in ALS and FTL indicates presence of C9ORF72 hexanucleotide expansion. *Acta Neuropathol.*, **123**, 825–839.
 37. Troakes, C., Maekawa, S., Wijesekera, L., Rogelj, B., Siklos, L., Bell, C., Smith, B., Newhouse, S., Vance, C., Johnson, L. *et al.* (2012) An MND/ALS phenotype associated with C9orf72 repeat expansion: abundant p62-positive, TDP-43-negative inclusions in cerebral cortex, hippocampus and cerebellum but without associated cognitive decline. *Neuropathology*, **32**, 505–514.
 38. Meggouh, F., Bienfait, H.M.E., Weterman, M.A.J., de Visser, M. and Baas, F. (2006) Charcot-Marie-Tooth disease due to a de novo mutation of the RAB7 gene. *Neurology*, **67**, 1476–1478.
 39. Palmisano, R., Golfi, P., Heimann, P., Shaw, C., Troakes, C., Schmitt-John, T. and Bartsch, J.W. (2011) Endosomal accumulation of APP in wobbler motor neurons reflects impaired vesicle trafficking: implications for human motor neuron disease. *BMC Neurosci.*, **12**, 24.
 40. Topp, J.D., Gray, N.W., Gerard, R.D. and Horadzovsky, B.F. (2004) Alsin is a Rab5 and Rac1 guanine nucleotide exchange factor. *J. Biol. Chem.*, **279**, 24612–24623.
 41. Hadano, S., Benn, S.C., Kakuta, S., Otomo, A., Sudo, K., Kunita, R., Suzuki-Utsunomiya, K., Mizumura, H., Shefner, J.M., Cox, G.A. *et al.* (2006) Mice deficient in the Rab5 guanine nucleotide exchange factor ALS2/alsin exhibit age-dependent neurological deficits and altered endosome trafficking. *Hum. Mol. Genet.*, **15**, 233–250.
 42. LaMonte, B.H., Wallace, K.E., Holloway, B.A., Shelly, S.S., Ascano, J., Tokito, M., Van Winkle, T., Howland, D.S. and Holzbaur, E.L.F. (2002) Disruption of dynein/dynactin inhibits axonal transport in motor neurons causing late-onset progressive degeneration. *Neuron*, **34**, 715–727.
 43. Kimura, N., Inoue, M., Okabayashi, S., Ono, F. and Negishi, T. (2009) Dynein dysfunction induces endocytic pathology accompanied by an increase in Rab GTPases: a potential mechanism underlying age-dependent endocytic dysfunction. *J. Biol. Chem.*, **284**, 31291–31302.
 44. Sundaramoorthy, V., Walker, A.K., Yerbury, J., Soo, K.Y., Farg, M.A., Hoang, V., Zeineddine, R., Spencer, D. and Atkin, J.D. (2013) Extracellular wildtype and mutant SOD1 induces ER-Golgi pathology characteristic of amyotrophic lateral sclerosis in neuronal cells. *Cell. Mol. Life Sci.*, **70**, 4181–4195.
 45. Sasaki, S. (2011) Autophagy in spinal cord motor neurons in sporadic amyotrophic lateral sclerosis. *J. Neuropathol. Exp. Neurol.*, **70**, 349–359.
 46. Ferraiuolo, L., Kirby, J., Grierson, A.J., Sendtner, M. and Shaw, P.J. (2011) Molecular pathways of motor neuron injury in amyotrophic lateral sclerosis. *Nat. Rev. Neurol.*, **7**, 616–630.
 47. Otomo, A., Pan, L. and Hadano, S. (2012) Dysregulation of the autophagy-endolysosomal system in amyotrophic lateral sclerosis and related motor neuron diseases. *Neurol. Res. Int.*, **2012**, 498428.
 48. Aguilera, M.O., Beron, W. and Colombo, M.I. (2012) The actin cytoskeleton participates in the early events of autophagosome formation upon starvation induced autophagy. *Autophagy*, **8**, 1590–1603.
 49. Lee, J.Y., Koga, H., Kawaguchi, Y., Tang, W., Wong, E., Gao, Y.S., Pandey, U.B., Kaushik, S., Tresse, E., Lu, J. *et al.* (2010) HDAC6 controls autophagosome maturation essential for ubiquitin-selective quality-control autophagy. *EMBO J.*, **29**, 969–980.
 50. Wu, C.H., Fallini, C., Ticozzi, N., Keagle, P.J., Sapp, P.C., Piotrowska, K., Lowe, P., Koppers, M., McKenna-Yasek, D., Baron, D.M. *et al.* (2012) Mutations in the profilin 1 gene cause familial amyotrophic lateral sclerosis. *Nature*, **488**, 499–503.
 51. Snowden, J.S., Rollinson, S., Thompson, J.C., Harris, J.M., Stopford, C.L., Richardson, A.M., Jones, M., Gerhard, A., Davidson, Y.S., Robinson, A. *et al.* (2012) Distinct clinical and pathological characteristics of frontotemporal dementia associated with C9ORF72 mutations. *Brain*, **135**, 693–708.
 52. Guil, S., Long, J.C. and Caceres, J.F. (2006) hnRNP A1 relocalization to the stress granules reflects a role in the stress response. *Mol. Cell. Biol.*, **26**, 5744–5758.
 53. Bosco, D.A., Morfini, G., Karabacak, N.M., Song, Y., Gros-Louis, F., Pasinelli, P., Goolsby, H., Fontaine, B.A., Lemay, N., McKenna-Yasek, D. *et al.* (2010) Wild-type and mutant SOD1 share an aberrant conformation and a common pathogenic pathway in ALS. *Nat. Neurosci.*, **13**, 1396–1403.
 54. Janssens, J., Wils, H., Kleinberger, G., Joris, G., Cuij, I., Ceuterick-de Groote, C., Van Broeckhoven, C. and Kumar-Singh, S. (2013) Overexpression of ALS-associated P.M337V human TDP-43 in mice worsens disease features compared to wild-type human TDP-43 mice. *Mol. Neurobiol.*, **48**, 22–35.
 55. Armakola, M., Higgins, M.J., Figley, M.D., Barmada, S.J., Scarborough, E.A., Diaz, Z., Fang, X., Shorter, J., Krogan, N.J., Finkbeiner, S. *et al.* (2012) Inhibition of RNA lariat debranching enzyme suppresses TDP-43 toxicity in ALS disease models. *Nat. Genet.*, **44**, 1302–1309.
 56. Latonen, L., Moore, H.M., Bai, B., Jaamaa, S. and Laiho, M. (2011) Proteasome inhibitors induce nucleolar aggregation of proteasome target proteins and polyadenylated RNA by altering ubiquitin availability. *Oncogene*, **30**, 790–805.
 57. Tsuji, H., Iguchi, Y., Furuya, A., Kataoka, A., Hatsuta, H., Atsuta, N., Tanaka, F., Hashizume, Y., Akatsu, H., Murayama, S. *et al.* (2013) Spliceosome integrity is defective in the motor neuron diseases ALS and SMA. *EMBO Mol. Med.*, **5**, 221–234.
 58. Boeve, B.F., Boylan, K.B., Graff-Radford, N.R., DeJesus-Hernandez, M., Knopman, D.S., Pedraza, O., Vemuri, P., Jones, D., Lowe, V., Murray, M.E. *et al.* (2012) Characterization of frontotemporal dementia and/or amyotrophic lateral sclerosis associated with the GGGGCC repeat expansion in C9ORF72. *Brain*, **135**, 765–783.
 59. Hsiung, G.Y., DeJesus-Hernandez, M., Feldman, H.H., Sengdy, P., Bouchard-Kerr, P., Dwosh, E., Butler, R., Leung, B., Fok, A., Rutherford, N.J. *et al.* (2012) Clinical and pathological features of familial frontotemporal dementia caused by C9ORF72 mutation on chromosome 9p. *Brain*, **135**, 709–722.
 60. Derby, M.C., Lieu, Z.Z., Brown, D., Stow, J.L., Goud, B. and Gleeson, P.A. (2007) The trans-Golgi network golgin, GCC185, is required for endosome-to-Golgi transport and maintenance of Golgi structure. *Traffic*, **8**, 758–773.
 61. Tung, Y.T., Hsu, W.M., Lee, H., Huang, W.P. and Liao, Y.F. (2010) The evolutionarily conserved interaction between LC3 and p62 selectively mediates autophagy-dependent degradation of mutant huntingtin. *Cell. Mol. Neurobiol.*, **30**, 795–806.
 62. Hosie, K.A., King, A.E., Blizzard, C.A., Vickers, J.C. and Dickson, T.C. (2012) Chronic excitotoxin-induced axon degeneration in a compartmented neuronal culture model. *ASN Neuro.*, **4**, pii: e00076.

63. King, A.E., Chung, R.S., Vickers, J.C. and Dickson, T.C. (2006) Localization of glutamate receptors in developing cortical neurons in culture and relationship to susceptibility to excitotoxicity. *J. Comp. Neurol.*, **498**, 277–294.
64. Chen, Z.Y., Ieraci, A., Tanowitz, M. and Lee, F.S. (2005) A novel endocytic recycling signal distinguishes biological responses of Trk neurotrophin receptors. *Mol. Biol. Cell*, **16**, 5761–5772.
65. Rajagopal, R., Chen, Z.Y., Lee, F.S. and Chao, M.V. (2004) Transactivation of Trk neurotrophin receptors by G-protein-coupled receptor ligands occurs on intracellular membranes. *J. Neurosci.*, **24**, 6650–6658.
66. Arancibia-Carcamo, I.L., Fairfax, B.P., Moss, S.J. and Kittler, J.T. (2006) Chapter 6. *Frontiers in Neuroscience* Kittler, J.T. and Moss, S.J. (eds), In *The Dynamic Synapse: Molecular Methods in Ionotropic Receptor Biology*, Boca Raton, FL, CRC Press.